

https://dspace.org/

An experimental and modelling study of fires in ventilated passages.

Comitis, Spiros, Costas.

1994
http://hdl.handle.net/10539/22932

Downloaded from a DSpace repository. https://dspace.org/

AN EXPERIMENTAL AND MODELLING STUDY OF FIRES IN VENTILATED PASSAGES

Spiros Costas Comitis

A thesis submitted to the Faculty of Engineering, University of the Witwatersrand, Johannesburg, in fulfilment of the requirements for the degree of Doctor of Philosophy.

Johannesburg, 1994

DECLARATION

I declare that this thesis is my own, unaided work. It is being submitted for the Degree of Doctor of Philosophy in the University of the Witwatersrand, Johannesburg. It has not been submitted before for any degree or examination in any other University.

S. Lomitis.

(Signature of candidate)

9th day of JUNE 1994

ABSTRACT

A theoretical and experimental treatment of fire processes in fuel-lined, ventilated passages is presented. Initially a radially well mixed axial flow condition is considered. Experiments are first performed in non-stratified flow conditions where fire propagation and gas temperature histories are acquired from liquid and solid fuelled fires. Theory and experiment display transient fire propagation for typical duct fire scenarios where initial fuel mass loading is constant with respect to duct length. The phenomenon observed, as predicted by theory, is an initial jump of the fully developed combustion process followed by convergence to a steady-state constant fire propagation speed. Fuel mass distributions are found to play a key role in these analyses. The model is also able to predict measured fuel mass distributions. The theory is in all important aspects able to quantitatively model fires in non-stratified conditions. A brief fire growth analysis is also used to assess the concept of an ignition temperature as a controlling mechanism for growth.

A simplified approach to the study of fires in ventilated passages with fire induced stratification is also presented. In conjunction with small scale experiments on liquid fuelled fires it is shown that a one dimensional model, requiring minimal computational effort, may be used to describe propagation as well as the dominant features of the flow process. Extreme stratification results in separation of the gas flow stream into a hot and cold layer, whereas flow systems with higher Froude and Reynolds numbers result in no evident layering. Mixing may still control in such cases. Identification of the two types of flow scenario is found important in the application of the model to such fires. A new correlation for stratification using fuel/duct properties and air velocity is also presented as a means of predicting stratification conditions. The model is found to operate well in the extremely stratified regime and, to a lesser extent, in a regime where the flow is neither close to well mixed nor layered. Fire propagation along the passage is also well described by the model under such flow conditions.

ACKNOWLEDGEMENTS

I should like to express my gratitude to my supervisor, Professor David Glasser, and to Dr Bruce D. Young, for their interest and encouragement during the course of this work.

The workshop staff were of great assistance in the building of experimental apparatus.

The Chemical Engineering department of the University of the Witwatersrand in Johannesburg provided the financial support for this work.

CONTENTS PAGE

CONTENTS	Page
DECLARATION	ii
ABSTRACT	iii
ACKNOWLEDGEMENTS	iv
CONTENTS	v
LIST OF FIGURES	viii
LIST OF TABLES	xiii
NOMENCLATURE	xv
1 OVERVIEW OF PASSAGE FIRES AND RELATED PROBLEMS	1
1.1 Introduction	1
1.2 Relevant Literature	3
1.2.1 Flame spread over solid materials	5
1.2.2 Duct fire studies	14
2 THEORETICAL TREATMENT AND ANALYSIS OF PROBLEM	20
2.1 Gas-Phase Equations	22
2.1.1 Modelling the combustion zone	26
2.1.2 Modelling the excess fuel zone	28
2.1.3 Modelling the preheating zone	31
2.1.4 Defining a fire propagation rate	32
2.2 Condensed-Phase Analysis	36
2.2.1 Equations of change	36
2.3 Application of Model Equations	39
2.3.1 Typical model output	45
2.4 Dimensional and Sensitivity Analysis of Model Equations	52
2.4.1 Sensitivity analysis of model	54
2.5 Effect of Heat Loss due to Thermal Radiation	62

3	LIQUID FUELLED FIRES IN NON-STRATIFIED FLOW	64
3.1	Apparatus for Non-Stratified Conditions	65
3.2	Experimental Procedure	69
3.3	Results	69
3.4	Discussion	80
3.5	Conclusion	84
4	SOLID FUELLED FIRES	87
4.1	Experimental	88
4.2	Results	90
4.2.1	Polymethylmethacrylate (PMMA)	90
4.2.2	Char-coal	99
4.3	Discussion	100
4.3.1	Fire propagation	100
4.3.2	Fire growth	104
4.3.3	Char-coal	106
4.4	Conclusion	107
5	FIRE-INDUCED STRATIFICATION EFFECTS	109
5.1	Experimental	109
5.2	Results	112
5.2.1	Modelling	117
5.3	Discussion	131
5.3.1	A proposed simple correlation for stratification	133
5.4	Conclusion	136
6	CONCLUSIONS AND RECOMMENDATIONS	139
6.1	Summary and Conclusion	139
6.1.1	Duct fires in well mixed flow	139
6.1.2	Duct fires with stratification	142
6.1.3	Concluding remarks	144

6.2 Recommendations for Future Work 144

APPENDIX A PROGRAMS TO SOLVE MODEL EQUATIONS 148
APPENDIX B DATA AND FILE LISTING FOR RETRIEVAL 165
APPENDIX C GAS TEMPERATURE MEASUREMENT 174
APPENDIX D DRAWINGS OF APPARATUS 182
APPENDIX E HOT AND COLD LAYER ANALYSIS (STRATIFICATION) 183
APPENDIX F COPY OF JOURNAL PUBLICATION ON LIQUID FUELLED FIRES 186

REFERENCES 201

LIST OF FIGURES

Figure		Page
1.1	Schematic of theoretical models used up to date. Also shown are some important system variables used in model descriptions.	11
2.1.	Schematic of proposed duct fire model zones.	21
2.2.	Schematic representation of control volume.	23
2.3.	Simplified diagram of a diffusion flame hanging over the surface of a solid combustible inside a ventilated duct.	34
2.4.	Fire propagation through a duct.	37
2.5.	Propagation sequence showing effect on fuel loading.	41
2.6.	Effect of migrating fire zones on fuel loading.	43
2.7.	Gas temperature profile inside duct is shown in the lagrangian coordinate system.	48
2.8.	Transient model solution of fuel distribution along the duct length.	49
2.9.	Fire-front history inside the duct.	50
2.10.	Steady-state fuel profile achieved after a long time. Shown in the eulerian coordinate system.	51
2.11.	Effect of h_f.	57

2.12.	Effect of U_d.	58
2.13.	Effect of γ.	59
2.14.	Effect of β.	60
3.1.	Schematic representation of equipment used for fire experiments.	68
3.2.	Gas temperature profiles from run 5 showing the stationary fire soon after ignition (*) and the moving fire 750 seconds (□) and 1200 seconds (x) after ignition. Proposed model fits (——) are also shown.	70
3.3.	Fire-front history along the duct for run 4 (x), run 5 (*) and run 8 (Δ). Run 8 was repeated (o) to test for the quality of reproduction of the experiment. Proposed model fits (——) are also shown.	71
3.4(a).	Graphic display of experimental data acquired from run 5. The surface shows the gas temperature profile evolving with time.	73
3.4(b).	Contour plot of the time evolving temperature profile inside the duct for run 5.	73
3.5.	Comparison of gas temperature profiles from run 1 (□) and run 5 (*) with proposed model (——). Combustion zone model solved with the radiation term is also shown (----).	78
3.6.	Air flow effect on combustion zone length for isooctane fuelled fires in non-stratified flow.	83
4.1.	Fire growth from point ignition source to fully developed size over a PMMA sheet 6 mm thick, 30 mm wide, lying flat on fuel tray	92

floor. Gas temperature profiles shown at 2 minute intervals.

4.2. Fire growth data. 93

4.3. Gas stream temperature profiles for two typical fully developed duct fires supported by PMMA (run 3 (x) and 5 (□)). Proposed model fit is also shown in each case with radiative (----) or without (——) radiative model. 94

4.4 Progressive motion of the combustion zone represented as fire-front propagation $\chi_f(t)$ for three duct fires (run 2 (*), 5 (o) and 7 (x)). Proposed model is also shown (——). 95

4.5. Contour diagram of time evolving gas temperature profile inside the duct for run 2 (PMMA). 95

4.6. Measured fuel mass distributions for run 1 (□), 2 (*), 3 (o), and 4 (+) after sufficient time has evolved to allow relatively constant fire propagation speeds. Model prediction (——) is compared in each case. 98

4.7. Effect of air mass flowrate supplied to the duct and solid fuel mass loading on steady fire propagation speed. 99

5.1. Fire tunnel apparatus used for stratified flow experiments. G_f=0.06 m, G_d=0.75 m. 111

5.2. Contour plots of 2-D gas temperature profile inside duct for (a) run 1 (isooctane), (b) run 2 (isooctane), (c) run 7 (ethanol) and (d) run 11 (ethylene glycol). 113-114

5.3. A comparison between the correlation (———) developed by Newman (1984) to predict fire induced stratification and present results. Isooctane (*), Ethanol (□), and Ethylene Glycol (o) results. 116

5.4. Flow pattern expected from severely stratified flow inside a flaming tunnel. 118

5.5. Model fit to plume of run 1. Temperature profiles at three different heights are shown (0.05m (*), 0.147m (o), and 0.25m (Δ) above floor). First the floor (———) and then the ceiling (----) section of the plume are followed with the one dimensional model. 121

5.6. Fraction of cross-sectional area α occupied by hot gas layer as a function of bypass mass fraction B_{pl}. 123

5.7. Fire-front history of an isooctane fire (run ?) measured from the floor and from the center-line gas temperature probes. Model fit is also shown. 125

5.8. Floor temperature profile (*;———) and ceiling profile (o) of run 5 meet with no discontinuity. Average gas temperature profile (Δ) and model fit (-----) are also shown. 127

5.9. Effect of increasing air velocity on the model fit to data when the average gas temperature is used to describe the gas phase process. 129

5.10. Observed effect of air ventilation rate (total) $\dot{m}_a$ and fuel mass loading on fire propagation speed for ethanol (*) and isooctane (o) fires. 131

5.11.	Stratification correlated with fuel properties.	135
B.1.	Steady-state propagation rate data from PMMA flakes experiments.	168
C.1.	Circuit diagram of thermocouple connections showing how the switches are multiplexed to read the emf of 34 thermocouples individually. At this instant thermocouple 20 is connected to the voltmeter.	175
C.2.	Effect of radiation on a thermocouple probe 1.018 m along the larger tunnel during a fire spread situation using paraffin lamp oil as the fuel.	177
D.1.	Details of small tunnel construction (non-stratified).	182
D.2.	Details of large tunnel construction (stratified).	182
E.1.	Simplification of mixing zone showing hot plume stream exchanging mass with cold bypass.	183

LIST OF TABLES

Table		Page
2.1.	Specific heat capacities of some gases	24
2.2(a)	Duct Geometry Parameters.	46
2.2(b)	Fuel Parameters.	47
2.2(c)	Flow Stream Parameters.	47
2.3	Gas-Phase Model Parameters	53
2.4(a)	Fuel Properties.	55
2.4(b)	Fire conditions.	56
2.5	Duct fire features from sensitivity analysis.	61
3.1	Model parameter listing for all experiments. Also shown is h_i the duct inside film heat transfer coefficient as estimated from correlations for air flowing in conduits.	74
3.2	Combustion zone parameters where thermal radiation is included as an important pathway for heat losses.	79
3.3(a)	Parameters known for each run.	79
3.3(b)	Fuel parameters.	79
4.1	Duct fire conditions and estimated model parameters for all experiments. Also shown is h_i the duct inside film heat transfer coefficient as estimated from correlations for air flowing in conduits.	96

4.2	Duct wall emissivities estimated from model fit. Some fire characteristics determined from the model are also shown.	97
5.1	Listing of experiments performed together with results obtained from flow analysis.	112
5.2.	Comparison between measured burning rates $\gamma_{(measured)}$ and averaged values ($\gamma_{(model)}$) from table 5.1 and non-stratified fires (table 3.1 and 4.2) in chapter 3 and 4.	120
5.3	Parameters estimated from fire propagation analysis where the average gas temperature is used to describe the gas phase process.	130
B.1.	Data files of liquid fuelled fires in small duct.	165
B.2	Data files of PMMA fuelled fires in small duct, including the fire growth run of chapter 4.	165
B.3	Data files of liquid fuelled fires in stratified flow (chapter 5).	166
B.4	PMMA flake experiment data files for V_{ss} versus ($\dot{m}_a/\lambda$) data.	166
B.5	Fuel mass loading data from PMMA strips experiments (steady-state).	167

NOMENCLATURE

English

A, B, C, D, E, p, q	constants
B_{p1}	fraction of air that bypasses the fire, calculated from floor gas temperature profile
B_{p2}	fraction of air that bypasses fire, calculated from average gas temperature profile
C_d	perimeter of duct wall cross-section (m)
$C_{d(est)}$	estimated average perimeter of duct wall cross-section used by hot plume layer (m)
C_f	exposed perimeter of fuel-lining cross-section (m)
$\hat{C}_p$	mean specific heat capacity of flow stream (J/kgK)
Fr	Froude number
g	acceleration due to gravity (m/s^2)
h_i	duct inside film heat transfer coefficient estimated from correlation (W/m^2K)
h_f	gas stream-to-fuel surface film heat transfer coefficient determined from model (W/m^2K)
H	duct height (m)
$\Delta\hat{H}_r$	gaseous enthalpy of combustion per unit mass of oxygen reacted at ambient temperature (J/kg oxygen)
$\hat{H}_{vap}$	latent heat of vaporization or sublimation of fuel (J/kg)
I(x)	temperature integral variable (m.K)
$\dot{m}_a$	mass flowrate of air (kg/s)
$\dot{m}_v$	mass flowrate of fuel vapour (kg/s)
m(x,t)	transient fuel loading profile inside duct (kg/m^2)
$m^\circ(x)$	initial fuel loading profile inside duct (kg/m^2)
$\dot{q}$	rate of heat loss through the duct walls

	(J/s)
t	time variable (s)
t_{res}	fire residing time before jump (s)
$T(x)$	gas stream temperature in the lagrangian coordinate system (°C)
$T(\chi,t)$	transient gas temperature in the eulerian coordinate system (°C)
T_o	ambient gas temperature (°C)
T_{avg}	average gas temperature (°C)
T_{vap}	fuel vaporization or sublimation temperature (°C)
ΔT_{cf}	gas temperature difference between ceiling and floor (°C)
ΔT_h	ceiling gas temperature rise above ambient . C)
ΔT_{avg}	average gas temperature rise above ambient (°C)
U_d	overall heat transfer coefficient of combustion zone duct walls (W/m^2K)
U_{d2}	overall heat transfer coefficient of excess fuel and preheating zone duct walls (W/m^2K)
U_o	overall heat transfer coefficient for duct calculated from correlations (W/m^2K)
V_∞	air ventilation average velocity (m/s)
V_{avg}	average gas velocity at gas temperature (m/s)
$V(t)$	fire propagation speed using the passage walls as the frame of reference (m/s)
V_{ss}	steady state fire propagation speed (m/s)
x	lagrangian distance coordinate (m)
$X_{lbz} = x_1$	length of combustion zone (m)
x_2	length of excess fuel and combustion zone (m)
$X_{efz} = x_2 - x_1$	length of excess fuel zone (m)
y	oxygen mole fraction in air
Y_{ox}	oxygen mass fraction in air

Greek

α	fraction of duct cross-section used by hot ceiling gas layer
α_1	percentage of heat generated by combustion that is fed back to the solid fuel up to the end of the combustion zone
α_2	percentage of heat generated by combustion that is fed back to the solid fuel up to the end of the excess fuel zone
β	combustion stoichiometric coefficient, mass of fuel reacted per unit mass of oxygen
γ	fuel burning rate (kg/m^2s)
δ	incremental change
ϵ	duct wall emissivity
θ	gas temperature above ambient, $T-T_o$, (°C)
λ	constant fuel loading (kg/m^2)
σ	Stefan-Boltzmann constant (W/m^2T^4)
$\bar{v}$	fire propagation rate (m/s)
ν_f	molar fuel stoichiometric coefficient for combustion reaction
χ	eulerian distance coordinate (m)
$\chi^*(t)$	start of combustion zone (m)
$\chi_f(t)$	fire front positior (end of combustion zone) on the stationary coordinate system (m)

1. OVERVIEW OF PASSAGE FIRES AND RELATED PROBLEMS

1.1 Introduction

Confined fires present an awesome example of the complex interactions occurring between natural phenomena. Gravitation, fluid dynamics, mass and heat transfer, and chemical reaction kinetics interact to produce the complex behaviour observed in fires. Understanding such behaviour is of immediate concern to the fire safety industry. The application of deterministic models of fires spreading within confined spaces is useful in assessing the fire safety value of various geometries such as ventilated rooms, building corridors, and mine tunnels or shafts. This work is restricted to studies involving one representative type of geometry, namely a horizontal ventilated fuel-lined duct or tunnel arrangement. The fuel source is considered to be in its condensed form (solid or liquid) and the fire results from diffusion-type flames burning over the condensed fuel surface.

Enclosed fires are sometimes referred to as being fuel rich (Roberts and Clough, 1967; de Ris, 1970). This represents the case where any oxygen entering the enclosed space is completely consumed by the fire process. The result is that large amounts of fuel vapour, volatilized due to preheating by hot combustion gases, remain unreacted in the flowing gas stream. Although this class of fire appears to be similar in description to open fires, the difference is significant when fire spread rates are under consideration. This is attributed to the magnitude and mechanism through which heat is transferred from the burning process to areas of virgin fuel.

Fires propagate by virtue of heat being transferred from the flaming region to unburnt condensed (solid or liquid) fuel. Consequently the fuel undergoes vaporization and pyrolysis which supplies the fire with gasified fuel for further combustion and generation of heat. In turn a portion of this generated heat is transferred back to the condensed fuel. This completes the

feedback cycle and forms the mechanism through which a fire can propagate. In open fires a large proportion of the generated heat is lost to the surrounding atmosphere and whatever heat is transferred to the condensed fuel is only transferred to regions near the fire. Initially confined fires propagate in the same way. If conditions favour propagation then the heat generated by the combustion reactions will be greater than that required to sustain the burning flames. In which case the fire auto-thermally grows to a maximum size determined by the rate of oxygen supplied to the fire. That is, if the flow is well mixed the fire size is ultimately determined by the ventilation rate supplied to the confined space. At this stage the entire gas stream becomes involved, causing its temperature and composition to be markedly affected by the combustion process. Having the gas stream temperature raised to magnitudes comparable to flame temperatures provides a new vehicle for heat transfer from the flames to unburnt fuel far ahead of the flaming zone.

A comprehensive discussion on fire propagation inside fuel-lined passages is given by Roberts and Clough (1967), where they propose a simple mathematical model based on thermophysical properties of duct systems. Experiments performed in a small scale passage were then used to assess the assumptions in their model. It is also demonstrated that the same model can be used to identify the conditions necessary for fuel rich or oxygen rich fires to prevail. Hunter and Favin (1981) and de Ris (1970) used the same experimental results to assess their modelling. More detail on the relevant literature will appear in the following section.

The aim of this work is to obtain a quantitative description of the fire dynamics inside the duct. Attention will be focused on ducts with thermally thin walls and where heat transfer is important only in the outward direction, and there is assumed to be no accumulation in the walls. The assumption of thin walls should not affect the general form of the fire process and mathematical formulation describing the fire inside the duct. Ultimately the use of good mathematical descriptions of such fire processes may be incorporated into designs of fire

prevention and control strategies for potentially hazardous environments such as mine roadways or tunnels. Accurate estimates of certain fire characteristics such as propagation rate and combustion gas production rates become critical variables in the design of optimally sized life support systems for mine tunnel occupants. Also, duct fire models can be used to interpret results from small scale tests, revealing important information relating geometrical, chemical and physical properties of materials to their fire safety value (de Ris, 1970). These aspects are of immediate concern to the fire safety industry.

After reviewing some of the relevant literature a mathematical model will be formulated from what is currently understood of the literature. Such a formulation should provide a basic viewpoint from which to study and analyze this class of fires. The many simplifying assumptions will not only reduce the mathematical complexity to the form of a simple model but also provide a means of gaining better insight into the mechanisms controlling the various processes. Such insight is best gained when the model is used as a tool to study real fires in the form of small scale experiments in ducts. Hence a rigorous experimental study of small scale duct fires will follow the theoretical treatment. Fluid-flow is important in this type of combustion problem and the study will encompass a wide range of possible flow scenarios, from well mixed to severely stratified flow. Fire spread and propagation along passages are equally important dynamics and will receive as much attention in this experimental and modelling study. In the end it is expected that such a treatment of the problem should provide a unified analysis of this class of fires. An improved understanding of this problem should also prove useful in developing more sophisticated and accurate models or simulations of this phenomenon.

1.2 Relevant Literature

Fire growth and fire propagation phenomena are constituent

processes of fires supported by condensed fuels. Most studies tend to examine one phenomenon in isolation from the other or even not distinguish between the two. This is probably because most classes of fire tend to be controlled, at least in part, by common mechanisms whether in their growth or propagation stage. In the context of this thesis propagation implies the motion or migration of the fully-developed fire as opposed to its growth or spread from an ignition source. In this section some of the fundamental approaches used to understand such fire processes will be introduced with the aid of various experimental and modelling studies that have been performed over the past few decades. Eventually the literature cited here will be narrowed down to studies specifically involving duct fires and closely related problems. Results of the many studies presented in this section will provide a useful source of improving ones understanding of fire phenomena. Hence, this provides a suitable starting point for the analyses that follow in later sections.

Before delving into the following sections it is well worth noting the publication by Williams (1976). The author provides a broad overview of work already performed, specifically in the area of establishing descriptions of the fire spread rate for a broad class of fires. It is clear from the cited literature that fire spread rate is a variable of immediate concern because of its direct impact on fire safety. A general framework is presented, providing a theoretical approach for determining the dominant mechanism(s) that control(s) flame spread or propagation for a broad variety of fire spread modes, e.g., horizontal flame spread over solids or liquids, vertical flame spread over solids, flame propagation in premixed gaseous fuels, etc.

Some of the concepts and equations are written in very general terms so as to accommodate the various classes of fire being studied in the cited literature. For instance the boundary between burning and non-burning combustible is defined as the *surface of fire inception*. It is this surface across which heat is transferred in order to raise and maintain the fuel temperature at its ignition temperature. In the case where fuel

and oxidizer are not premixed this is also the boundary across which fuel vapour must be transferred and brought into contact with the oxidizer. A fundamental equation of fire spread is used to describe the dependence of spread rate on heat transfer from burning to unburnt fuel. This equation is based on energy conservation considerations over a portion of unburnt fuel adjacent to the *surface of fire inception*. In general, the rate of spread depends on the time required to raise a portion of fuel, already in contact with oxidizer, to its ignition temperature.

Although this publication is not very recent, reference is made to research in the many classes of fire. It therefore provides a useful starting point for those wishing to work in this field.

1.2.1 Flame spread over solid materials

Experimental analyses of controlling mechanisms

From experimental studies of flow assisted flame spread over polymethylmethacrylate (PMMA) sheets performed by Loh and Fernandez-Pello (1984) it seems that spread rate data are correlated very well if heat-transfer models are used to determine the spread rate. Thus it was deduced that for this flame spread situation, heat-transfer from the flame to condensed fuel is the dominant mechanism controlling the spread process, and that finite chemical kinetic and mass-transfer effects are negligible. Most theoretical models of flame spread in a concurrent forced oxidizer flow are based on heat transfer mechanisms such as that by Fernandez-Pello (1979) who shows that the flame spread rate is proportional to the air stream velocity,

$$V_p \sim \frac{\rho_g C_p \lambda_g (T_f - T_v)^2}{\rho C \lambda (T_v - T_o)^2} V_\infty \qquad (1.1)$$

The linear dependence of flame spread rate V_p on air velocity

V_∞ is observed in wind tunnel experiments. Flame spread rate V_p is taken to be the time rate of change of the flame-front position dx_f/dt. Although good model correlation for experimental data is accomplished with analyses that consider laminar flow and do not include thermal radiation, it is noted that the scale of experiments performed were small enough for these conditions to prevail. For larger fires it is expected that one should include radiation and turbulence as important processes if models are to correlate experimental data.

A comprehensive review on advances made in experimental studies of mechanisms controlling the spread of flames over the surface of combustible solids is presented by Fernandez-Pello and Hirano (1983). The summary covers both modes of flame spread, where the oxidizer flows in the same direction of spread and for the case where it flows against the direction of spread. It is apparent that heat transfer or gas-phase chemical kinetics are important mechanisms for the concurrent or the opposed flow modes of flame spread respectively. The basic condition for flame spread is common to most cited literature. If flame spread is to be achieved, for either mode of spread, the temperature of the solid combustible has to increase to its pyrolysis or vaporization temperature. This requires heat transfer from the already pyrolysing and burning region to the virgin fuel. The rate at which heat is transferred to virgin material will determine the rate of temperature increase and consequently the rate of spread of the pyrolysis or ignition temperature front.

For the concurrent mode, heat transfer from the flame to unburnt fuel appears to be the primary controlling mechanism of flame spread. Although gas-phase chemical kinetics is unimportant in the spreading of flames in this mode, it does play a role in the establishment and degree of extension of the diffusion flame ahead of the pyrolysis front over virgin fuel. Extension of the flame plume over unburnt fuel, driven by the gas flow, is partly the reason for heat transfer being so important in this mode of fire spread. Not only is the fuel-to-flame view factor favourable for enhancing absorption of heat, virgin fuel is also exposed to hot combustion gases flowing over its surface.

According to Fernandez-Pello and Hirano (1983) large scale experiments performed with thick vertical PMMA sheets (Orloff *et al*, 1975) indicate that when the upward spread of flames and air flow are laminar in nature, heat transfer from flame to fuel is primarily by convection. As the flame grows and becomes turbulent, thermal radiation displays its importance. For flame heights of around 1 meter flame radiation becomes responsible for about 80 percent of the total heat transferred. Flame height and pyrolysis front are found to accelerate under these conditions when the fire spreads up vertical fuel surfaces in a natural convective environment.

For fires spreading in a forced air flow moving in the direction of spread, such as on horizontal fuel-linings, the spread rate is found to remain constant for a given flow velocity (Fernandez-Pello, 1979). In this particular study this observation is striking since the length of the flame is observed to increase as the pyrolysis front progressed, and a consequent enhancement of heat transfer from flame to fuel is expected. It is argued that this is because the heat flux from the flame to the solid combustible is reduced as the pyrolysis front progresses, because the extended flame stands further away from the fuel surface as the flame increases in size. The overall effect of lengthening the heated region and decreasing the heat flux, due to a standing plume, presumably counteract each other resulting in a constant spread rate.

Theoretical models of flame spread

Experimental studies reveal that a great deal is understood about mechanisms that control the flame spread phenomenon. Unfortunately the various mechanisms involved are found to interact in complicated ways, and formulation of complete deterministic models with analytic solutions is almost impossible. An extensive survey of different theoretical models for flame spread over solid combustibles in opposed and concurrent oxidizing flows has been presented by Fernandez-Pello

(1984). This survey finds that some of the more refined and detailed models, which include processes such as flame radiation, finite rate kinetics, and aerodynamics in the flame region, can only be solved numerically with the aid of a computer. On the other hand simpler models can be solved analytically at the expense of assuming *a priori* boundary conditions at the solid-gas interface and by neglecting some important transport phenomena. However, both these approaches are found useful in qualitative predictions and for gaining insight into the underlying mechanisms.

Formulation of rigorous mathematical models involves differential conservation equations (mass, energy and momentum) for the reacting gas-phase coupled to the condensed-phase process equations with appropriate boundary conditions at the solid-gas interface. There appears to be a deficiency in dealing with important phenomena such as the rigorous treatment of flow fields, flame radiation, and gas-phase chemistry. So far, flame radiation has been simulated through an empirical approach which assumes a functional form for the fraction of radiant heat absorbed by the solid fuel, that is a function of distance from the pyrolysis front. This avoids having to characterize the precise radiative properties of the flame such as emissivity, surface area, view factor, and even temperature. An opposed oxidizer flow mode of flame spread is modelled by de Ris (1969) using one such empirical simulation for radiation.

The effects of artificially irradiating fuel surfaces and of humidity on the propagation of a line fire through beds of homogeneous fuels were studied experimentally by Hottel *et al* (1965) in order to test four different heat transfer models of fire spread. Radiation from the "flame" (actually from the artificial radiation source) was modelled as a vertical black plane surface. The results showed rapid increases of spread with increasing radiation to the fuel surface, and for higher air humidities the flame spread was slower. Hottel *et al* (1971) modelled fuel preheating in steady-state, two-dimensional fires. Experimental results from a 4.5 ft diameter by 12 ft long wind tunnel were used to compare model predictions. Because the

fires under study were small, flame-to-fuel radiation was enhanced by using artificially applied radiation from heating wires. So in this case "flame"-to-fuel radiation was modelled as equally spaced vertical line sources at known temperature with known emissivity. Both of the above studies show how the task of characterising flame radiation may be avoided when studying its effect on fire spread.

Weber (1989) constructed a physical model on the basis that fuel preheating occurred purely from flame thermal radiation. Heat losses from the fuel surface were allowed through a linear dependence on surface temperature (conductive/convective heat losses). The differential energy equation for an element of solid fuel uses a functional form for fuel surface-to-flame view factor V as a function of position x along the fuel surface. This value is not only position but also time dependent due to a moving flame front. A useful analogy that flame propagation can be envisaged as a travelling wave-front is introduced and an equivalent "wave equation" is used to describe the flame front velocity.

Energy equation: "Wave equation of motion":

$$\rho C \frac{\partial \tau}{\partial t} = AV(x,R(t)) - B\tau \qquad \frac{\partial \tau}{\partial t} + \dot{R} \frac{\partial \tau}{\partial x} = 0 \qquad (1.2)$$

Here ρ and C are the fuel density and specific heat respectively, A is the product of the fuel surface absorption coefficient and flame radiation intensity, B is a convective cooling coefficient multiplied by the fuel surface area to volume ratio, τ is the temperature above ambient, and R is the fire front position. It is shown that the system of equations can be solved analytically.

The above analysis clearly shows the importance of fire front geometry on the fire spread process if radiative heat transfer controls. For a planar fire front the rate of spread is time independent and is proportional to the difference between flame heat output and heat lost by cooling, and inversely proportional to the energy required to heat the fuel up to ignition. In the

case of a fire starting at a point source where the fire front is non-planar the spread rate is initially very rapid. The effect of this view factor, from the fuel surface to a non-planar fire-front (circular front), is that the fire-front has a maximum acceleration at the start which dies down to zero as time evolves. That is the rate of spread reaches a constant value as the circular flame front approaches planar geometry.

Wind-aided flame spread

Intuition suggests that convective heat transfer is of primary importance to this mode of flame spread under experimental conditions which show a direct influence of forced air flow on spread rates (Fernandez-Pello, 1979; Apte *et al*, 1991; Wolff *et al*, 1991). One would also suspect that radiative heating of unburnt fuel is likely to become important in larger scale fires because of the enhanced view factor.

The diagram below shows some of the physical features of models presented in the literature for the concurrent mode of flame spread.

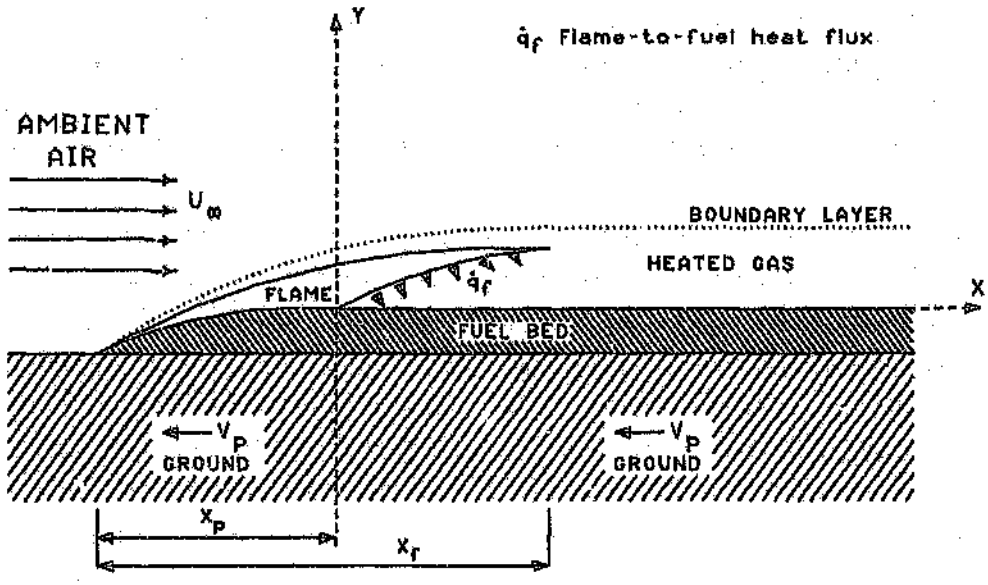


FIGURE 1.1 Schematic of theoretical models used up to date. Also shown are some important system variables used in model descriptions.

One of the earlier publications on modelling of flame propagation over a solid fuel in a laminar forced flow is that of Fernandez-Pello (1979). The flame is believed to propagate within a laminar boundary layer and the flame-front is assumed to progress when fuel ahead of the pyrolysis (burning) front reaches the fuel ignition temperature. Gas-phase conservation equations are uncoupled from the solid-phase equations (by specifying the gas-solid interface boundary conditions) and analytic expressions for the spread process were obtained. These results were in good quantitative agreement with experiments that showed a constant spread rate that is directly proportional to the gas flow velocity. Simplifying assumptions, such as fuel vaporization and pyrolysis occurring only in the flaming zone, infinite gas phase reaction (flame sheet approximation), and that the fuel has a surface temperature gradient ranging from

the fuel vaporization temperature at the pyrolysis front (flame-front) to the initial gas temperature at the flame tip, contribute to the achievement of an analytic solution. Although the problem is a transient one, the gas-phase process was taken to be at steady state because its characteristic process time is much smaller than that for the solid-phase process.

Fleeter *et al* (1984) emphasize the hazardous potential of wind-aided fire spread by way of example of numerous modern day urban fires. Experimental work was performed on beds composed of discrete fuel elements inside a specially designed wind tunnel. The tunnel is constructed to allow development of an unimpeded convective fire plume for the study of interactions between fire plume convection and cross-wind forced convection. A simplistic model is sought, revealing fire propagation (or spread) response to the dynamics of fire plume convection and crossflow interactions. To simulate fire plume convection the simplifying Boussinesq approximation was introduced to the set of 2-dimensio .al conservation equations.

An experimental study on turbulent wind-aided flame spread over flat horizontal surfaces on a scale where radiation is significant was performed by Apte *et al* (1991). Two successive modes of spread are observed. Initially the flame is confined within a boundary layer and is termed the boundary layer mode. The second mode, occurring some time later, is characterized by a rapid increase in pyrolysis flux resulting from a standing buoyant flame plume. Two mechanisms have been considered to contribute to flame-to-fuel heat flux, namely convection and radiation. An expression for flame spread rate, adopted from Quintiere *et al* (1988), was used to compare results from a 5.4 meter wide, 2.4 meter high fire gallery. This expression can be written as follows:

$$\frac{dx_p}{dt} = \frac{\left(x_f - x_p\right) \dot{q}_f^2}{(\pi/4)\, k_s\, \rho_s\, C_s \left(T_g - T_\infty\right)^2} = \frac{\left(x_f - x_p\right)}{\tau} \qquad (1.3)$$

τ is a characteristic ignition time, and

$\dot{q}_f$ is the total flame-to-fuel surface heat flux.

The total flame-to-fuel heat flux was equated to the sum of flame radiation flux and flame convective flux, which is equal to the energy flux required to pyrolyse a known (measured) mass of fuel plus the heat loss due to radiation from the fuel surface. Fuel surface radiative heat flux was simulated by assuming an ignition temperature along the fuel surface while using the Stefan-Boltzmann equation. Then the total flame-to-fuel heat flux was experimentally determined from measured rates of fuel mass loss data. Flame surface radiation was calculated using a thin flame-sheet approximation which provides an estimate for flame surface area.

Experiment showed that a transition from the boundary layer to the buoyant mode of spread is characterized by the flame tending to stand up. At this transition a change in slope is observed when flame length x_f is plotted against Froude number. Flame heat flux in pure forced convective combustion has a direct dependence on flow velocity. Experimental heat flux data in this case suggested an inverse dependence on flow velocity. This observation was explained from the increased radiative heat flux when buoyancy controls flame spread, and hence radiation was concluded to be dominant at this stage of fire spread. The reasoning for this conclusion is that increasing the air velocity tends to force the flame plume down and radiative fluxes are reduced through a reduction of flame height and hence view factor.

In a publication on wind-aided fire spread across arrays of discrete fuel elements, it was demonstrated that dimensional analysis can be used to successfully correlate flame spread velocities under varied conditions of air flow and fuel loading (Carrier *et al*, 1991). The relationship concentrates on the

effects of ambient wind speed and fuel loading since these are the most commonly varied conditions in experiments and natural fires. The analysis is performed for two possible cases, one where convective/conductive heat transfer dominates and the other when radiation is dominant. For the first case it is found that the resulting relationship $V_p \alpha (U_\infty/m)^{0.5}$ agrees very well with experiments performed (Wolff *et al*, 1991). On the other hand when radiative heat transfer is considered the expected relationship $V_p \alpha (U_\infty/m)^{1.5}$ is not confirmed with these experiments.

A detailed two-dimensional transient model for flame spread over thermally thick fuels has been solved with the aid of a computer and numerical techniques (Di Blasi *et al*, 1989). This is one of the few mathematical analyses that considers finite gas-phase combustion kinetics and pyrolysis kinetics which results in a microscopic description of the flame structure in terms of temperature, reaction rate, and flame species composition. An almost linear dependence of spread rate on air flow is found for situations where the velocity of spread is allowed to reach steady-state. Neglecting finite rate kinetics is shown to be a useful and valid assumption if one examines the model flame structure in terms of reaction rates. Reaction rates are found to be much greater than vaporization rates except within regions of the flame tip and leading edge of the flame where reaction rates are relatively small due to low temperatures or concentrations of reactants.

1.2.2 Duct fire studies

Duct fire experiments are usually performed at much smaller scales than realistic tunnel fires (Roberts and Clough, 1967) because they are favourable from an economic stand point, easier to control and permit more accurate measurement. Full scale passage fires also present the problem of inducing severely stratified flow, an added complication, if low or moderate air velocities are used or if the width to height ratio is small. Typically stratified flow would complicate the fire process to

such an extent that the familiar slug flow assumption held in most duct fire models (Roberts and Clough, 1967; de Ris, 1970; Hunter and Favin, 1981) would have to be replaced by a complex description of the flow process. This added complexity is usually avoided so as to study the role heat transfer and reaction kinetics play in the fire process prior to studying the coupled effects of fluid dynamics. Despite the persistence of this flow problem Newman and Tewarson (1983) have shown that calculated average gas temperatures of large passage fires with stratified flow can be used to successfully describe the overall fire process.

A significant contribution and comprehensive analysis of fire propagation inside fuel-lined passages is presented by Roberts and Clough (1967). Important differences between open and confined fires are highlighted and described with the aid of experiments and a mathematical analysis. To summarize, confined fuel-rich fire propagation is controlled by heat transfer of a greater order of magnitude than that of open fires. If conditions inside the passage are fuel-rich heat released during combustion is controlled by the amount of air supplied to the duct and the entire gas inventory becomes involved in transferring the generated heat to fresh regions of unburnt fuel. Open fires transfer heat only from the flaming region to local fuel surfaces but not through the surrounding air inventory to regions far from the fire. A simplified one-dimensional mathematical model for fuel-rich fires is developed where the fire propagation rate and gas-phase temperature profile are related to the tunnel system thermophysical properties. The analysis identifies three distinct zones developed in a fuel-rich steadily burning fire. The first is a combustion zone in which all the available oxygen is consumed and a sharp rise in gas temperature occurs with respect to tunnel distance. The second is an excess fuel zone where no oxygen is left over for reaction but fuel is still being volatilized due to heat transfer from flowing hot combustion gases. And the third is a preheating zone where all that happens is the cooling down of the gas stream due to duct-wall heat losses and sensible heating of solid fuel.

From energy conservation considerations over each zone, analytic expressions for the gas-phase temperature distribution are developed. Achievement of such analytic solutions is attributed mainly to the following simplifying assumptions:

i) Constant duct overall heat transfer coefficient and vaporization rate along the combustion and excess fuel zones (but these may vary at the boundary between the two zones).

ii) Perfect mixing in the radial direction and infinite gas-phase reaction rate.

iii) Radiative heat transfer from duct to surroundings or from fire to fuel surface is ignored.

An important parameter R is identified in Roberts and Clough's (1967) model equations as being the ratio of fuel vaporized to oxygen consumed in the tunnel. R is normalized so that for values greater than 1 the fire process is fuel-rich and less than 1 is oxygen rich. This parameter analysis goes further to characterize conditions where stable fuel-rich fire propagation may occur or when unstable oxygen-rich scenarios may prevail. That is, conditions leading to extinction or growth of a fire to a stable fuel-rich state.

Experiments performed in a 30 cm diameter duct show a linear spread rate dependence on air speed. Their mathematical model for fuel-rich fires is in good agreement with some fire characteristics observed if the gas flow Reynolds number is greater than 10^4. It is suggested that for lower values of Re fuel-air mixing may become important. Stratification would further aggravate the effect of poor mixing.

Following the pioneering work of Roberts and Clough (1967) on fuel-rich duct fires de Ris (1970) developed a theoretical analysis which also considers downstream condensation of volatilized fuel in the preheating zone. Results show a small effect on propagation speeds especially for fuels with low vaporization temperatures. Heat losses through the tunnel walls

are modelled in detail by setting up heat transfer equations of conduction from the inner surface of the tunnel through an infinite slab of homogeneous surrounding rock. Model solutions from this analysis were compared to experiments performed by Roberts *et al* (1966) and general agreement is found with the gas temperature decay of the reheating zone, although this data is not displayed graphically. Satisfactory predictions of the vaporization zone length was also obtained, but again this data is not shown or displayed. Observed linear relationships between measured steady fire propagation speed and inlet air mass flowrate also confirmed the valid use of the slug (plug) flow assumption under these flow conditions. All duct fire models to date are developed for slug flow conditions. In the present thesis duct fires in a wide range of possible flow conditions, from radially well mixed flow to severely stratified, will be modelled.

What is striking of both these cited duct fire analyses is that the fuel vaporization flux is assumed position independent in the excess fuel zone. Fuel vaporizes in this zone because of heat transfer from hot combustion gases to the solid fuel lining. Furthermore, convective heat transfer is assumed to be the dominant pathway for heat losses in this zone. Clearly then fuel vaporization rates will depend on the local gas temperature at the position of interest. That is, a position dependent fuel vaporization rate will result. A physical consequence of constant fuel vaporization flux in the excess fuel zone would not correspond to the achievement of a steady fire propagation speed as these authors have assumed. In a later section a more realistic fuel loss mechanism will be considered. Experimental evidence will be used to elaborate on the line of reasoning that their assumptions of fuel loss rate are not realistic enough to describe propagation. So far all duct fire propagation models have also assumed steady-state constant propagation. Steady-state constant propagation is not only incompatible with currently assumed fuel loss rate mechanisms but is often untrue in many typical duct fire scenarios, as it will be shown later. The dynamic effects resulting in transient fire propagation will be treated rigorously in the following chapter.

Fire induced buoyancy forces often result in stratified flow if crossflow ventilation currents are not strong enough. Roberts and Glough (1967) concluded that their slug flow assumption works well if Re > 10^4 inside their duct. Mixing controlled flow is suspected to prevail below this value of Reynolds number. Even if Re > 2000 (outside the typical laminar regime) well mixed flow may be prevented if fire induced buoyancy aggravates the flow.

Newman (1984) developed a correlation for quantifying the degree of fire-induced stratification downstream of a passage fire. The technique is based on the Froude number (Fr) which is used to characterize the degree of flow stratification (gas temperature and composition).

$$\frac{\Delta T}{\Delta T_{avg}} = f(Fr) = f\left\{\frac{V_{avg}}{\left(\frac{\Delta T}{\Delta T_{avg}} gH\right)^{1/2}}\right\} \qquad (1.4)$$

Here ΔT is a temperature difference associated with stratification; ΔT_{avg} is the average gas temperature rise above ambient; V_{avg} is the average gas velocity; and H is the height of the duct. Three regimes are delineated by the correlation each associated with different degrees of stratification. Extreme stratification is characterised with low Froude numbers since buoyancy forces almost completely dominate the flow. Mixing controlled flow with moderate Froude numbers is characterised by strong interactions between crossflow and buoyancy forces. Finally a third regime is identified where crossflow forces are strong enough to dominate the flow so that insignificant vertical temperature and composition gradients are observed. This analysis seems to be devoid of Reynolds number considerations. It would of course be useful to also know what combination of Froude and Reynold number will result in no vertical temperature or composition gradients. Clearly not only crossflow forces in laminar flow will suppress development of vertical temperature gradients but so will the achievement of fully developed turbulence.

A useful result that may be used for experimental work where fire plume backflow is undesirable is that the ratio $\Delta\rho gD/\rho V_a^2$ should be less than unity (de Ris,1970). For values greater than or equal to unity backflow (sometimes called reverse stratified flow) has been observed. In the above ratio D is duct height, g is acceleration due to gravity, ρ ambient gas density, V_a ventilation velocity, and $\Delta\rho$ the change in gas density of the fire plume. This dimensionless constant relates the buoyancy force of the hot fire plume to the forced air flow in the duct. Most fuel-rich fires that display little stratification are likely to have this ratio less than unity. Reverse stratified flow phenomena in duct fires has been studied in more detail by Hwang *et al* (1977).

Finally, on the issue of full-scale phenomena the paper by de Ris *et al* (1973) is relevant. Large scale fires can be modelled with small scale fire experiments if the product of the pressure-squared times characteristic length-cubed (P^2L^3) remains constant. Theoretical and experimental studies have shown this pressure modelling technique to be valid under certain conditions. The conditions are that chemical reaction kinetics must be infinitely fast compared to mass transfer rates or mixing; and fire radiation must either be unimportant or proportional to the rate of combustion. Fires that burn in the form of diffusion flames will satisfy the first condition though the second condition may be problematic. Not much information is known about fire radiation properties in general though the empirical approaches described earlier may be adequate if the required proportionality exists. If the above conditions are met the authors have shown that the complete set of Navier-Stokes combustion equations are satisfied equally on both size scales.

2. THEORETICAL TREATMENT AND ANALYSIS OF PROBLEM

Although part of this analysis is an adaptation of that presented by de Ris (1970), a fundamental difference will emerge when the concept of fire propagation speed is in question. Moreover, the model presented by de Ris (1970) is a steady state one, whereas this work will extend the analysis to include the non-steady motion of the fire in the duct. Also, in the first instance the flow is assumed to be well mixed. Later it will be shown how the analysis can be extended to include cases with mixing controlled and stratified flow. The conceptual understanding provided here should prove helpful in interpreting results from duct fire experiments.

Fuel burning is assumed to be controlled by the rate of vaporization of volatile components, rather than subsequent combustion reactions that follow. The rate of fuel vaporization is in turn controlled by heat transfer from the fire to the fuel surface. Chemical reaction kinetics would be much faster than vaporization rates because of the strong temperature dependence that the Arrhenius expression would display near flame temperatures. Evaporation-rate controlled burning leads to the assumption of a fuel-rich fire. Furthermore, vaporization is assumed to occur at a specific temperature termed the vaporization or pyrolysis temperature. For a pure substance this would be the boiling or sublimation temperature.

Three distinct zones, the lengths of which remain unknown prior to solving the model equations, are identified in the formulation of this duct fire model. Figure 2.1 depicts the relative position of each zone on a system of axes that moves along the duct at the fire propagation speed V. The value of V remains to be solved. Because no steady-state restriction is placed on V this variable will be written as time dependent V(t).

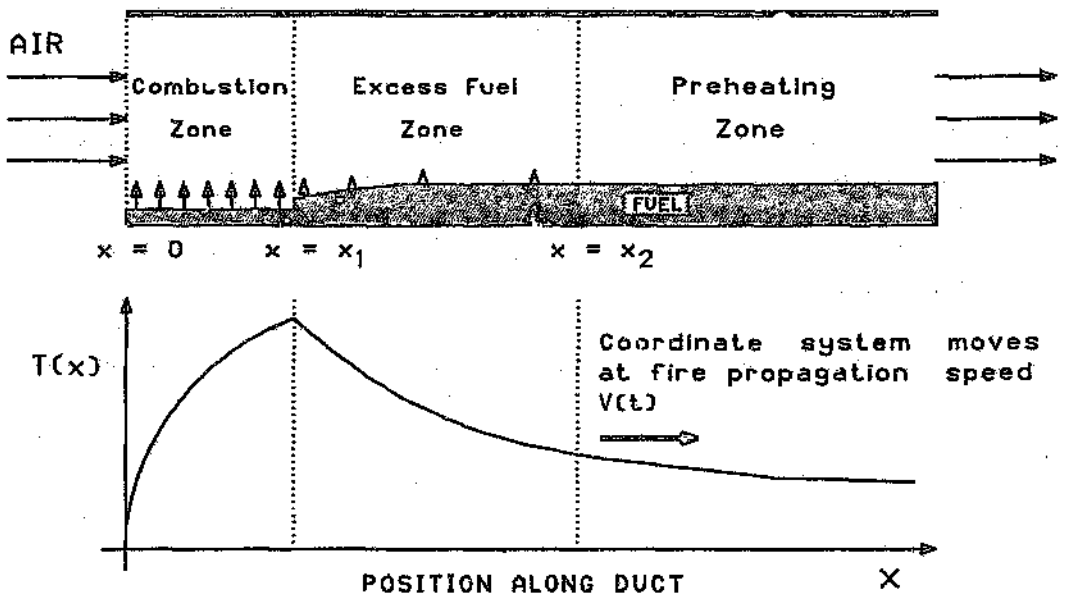


FIGURE 2.1. Schematic of proposed duct fire model zones.

As the ventilation air stream crosses the boundary $x = 0$ it encounters a combustion zone where the oxygen is consumed by the combustion reactions. In this zone the fuel volatilizes and is then assumed to instantaneously react with inflowing oxygen. By the time the gas stream crosses $x = x_1$ the entire oxygen inventory is depleted and the heated gas stream enters the second of these zones, namely the excess fuel zone. Here the gas temperature is above the fuel vaporization or pyrolysis temperature. The fluid stream cools down as a consequence of heat losses to the duct walls and to vaporization of condensed fuel lining the duct. It is assumed that the condensed fuel will vaporize at a fixed temperature termed the vaporization temperature. This will be valid for single component stable liquid fuels. Vaporization continues up to $x = x_2$ where the flowing gas stream has cooled down to the fuel vaporization temperature. This marks the start of the preheating zone. Beyond this region the gas stream cools down to ambient temperature as

it loses heat to the duct walls. Recondensation of fuel vapour will be ignored in this zone. de Ris (1970) shows this effect to be small. In any case this would only be relevant to fuels which do not pyrolyse to non-condensable materials.

As a result of progressive consumption of fuel the fire will propagate or migrate at some speed V(t) along the duct, which may or may not be constant with respect to time. Consequently the three zones mentioned above will propagate along the duct with this same speed. The model is written in the lagrangian coordinate system where the coordinate system is moving at the fire propagation speed. Care should be taken when considering the rate of air being supplied into the combustion zone. The air flow crossing the boundary of the combustion zone (x=0) is moving past this boundary at a velocity equivalent to the induced constant air velocity V_∞ minus the fire propagation speed V(t). In most fires of this type, because of the large difference in molar density between the condensed fuel phase and the oxygen in the air (about a thousand times), V(t) is small in comparison with V_∞, and is therefore neglected in this analysis. Hunter and Favin (1981) have also shown this. This same logic implies that, relative to the axial speed of the fire-front, the gas-phase temperature is rapidly achieved. This allows the assumption of a pseudo-steady-state in the gas-phase energy balance if a continuous fuel lining exists inside the passage. Later it will be shown that discontinuities in the fuel lining could result in very rapid propagation.

The analysis that follows is based on developing conservation equations for the two phases that constitute the heterogeneous system described above. Parts of section 2.1 are adapted from portions of the Young and Glasser (1990) steady state model which is a variation of the original Roberts and Clough (1967) and de Ris (1970) steady state fire propagation models. The present transient model and application of the gas-phase analysis of section 2.1 to model transient fire propagation is, however, new.

2.1 Gas-Phase Equations

An energy balance is considered over a control volume which starts at x = 0, the moving position at which the fire begins, and extends to an arbitrary value x. This control volume envelopes only the gas phase inside the duct and is represented

schematically in Figure 2.2. Using the lagrangian coordinate system x = 0 is always at the start of the combustion zone.

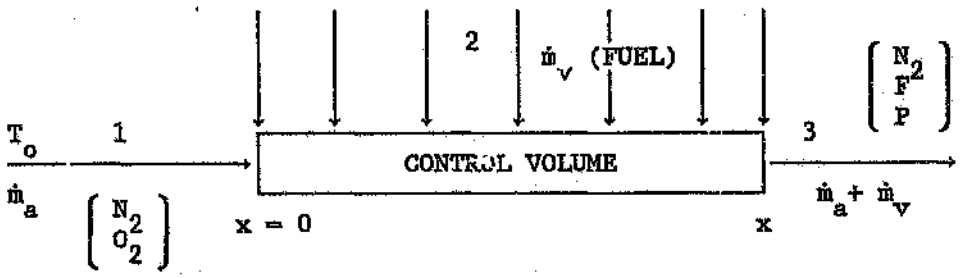


FIGURE 2.2. Schematic representation of control volume.

At x = 0 a certain constant mass flowrate $\dot{m}_a$ of air enters the control volume. This air is at temperature T_o which is invariant with time. This may not necessarily be ambient temperature as the air will be in contact with heated duct walls prior to entering the combustion zone. The oxygen reacts in the gas phase with fuel vapour which has vaporized from the fuel surface. Because the control volume considers only the gas phase, a mass flowrate $\dot{m}_v$ of fuel vapour is added to the control volume. This represents the total amount of fuel which has vaporized up to a point x, and changes along the length of the duct. A single equation is used to account for all possible combustion reactions occurring inside the combustion zone. Fuel vapour is presumed to react with oxygen according to

$$\nu_f F + O_2 \rightarrow \text{Products} \qquad (2.1)$$

One mole of oxygen molecules reacts with ν_f moles of fuel F and forms products of which there may be many. A radially perfectly mixed flow stream is considered, where the above reaction occurs as fuel vaporizes from the condensed state into the reactive gas stream. The stream leaving the control volume may contain nitrogen, oxygen, unburnt fuel, and product gases. A steady state assumption is made when considering the gas-phase process so that the flowing streams 1, 2, and 3 are constant with respect to time even though the control volume moves at some

transient velocity V(t). Because the flow streams entering and leaving the control volume are assumed constant, the size of the three zones mentioned above will also be constant throughout the propagation history. For reasons discussed earlier it is assumed that the characteristic evolution time for the gas-phase process is much smaller than that for the condensed-phase. Therefore the gas-phase process should not be disturbed by changes originating in the condensed-phase, such as progressive consumption of fuel lining. Fernández-Pello (1979) made a similar assumption with flame spread studies.

In order to simplify the mathematics it is assumed that the specific heat capacity of the gas $\hat{C}_p$ is independent of composition. Although this is not strictly true it is a reasonable approximation. In order to justify this, heat capacities of some typical gases that would be encountered are tabulated in table 2.1 for 25 and 1000 °C.

GAS	$\hat{C}_p$ at 25 °C J/(kgK)	$\hat{C}_p$ at 1000 °C J/(kgK)
O_2	815	1109
N_2	1016	1162
CO_2	853	1305
CO	1040	1218
H_2O	1941	2461

TABLE 2.1. Specific heat capacities of some gases

There may also be fuel vapour and $\hat{C}_p$ will depend on the type of fuel. It can be seen that all the $\hat{C}_p$ values are relatively similar apart from water vapour. Since it is expected that the mass fraction of water vapour will never be particularly large this should not have a strong impact. It may therefore be expected that the average specific heat capacity of the gas will be in the range 1100-1400 J/kgK.

An energy conservation equation for the control volume can be written using the lagrangian coordinate system where x=0 is always at the start of the combustion zone. The overall energy equation can be written

$$(\hat{\Delta H}_r/\beta)(d\dot{m}_v/dx) = \theta \hat{C}_p(d\dot{m}_v/dx) + \hat{C}_p(\dot{m}_a + \dot{m}_v)(d\theta/dx) + d\dot{q}/dx + \hat{H}_{vap}(d\dot{m}_v/dx), \quad (2.2)$$

where $\hat{\Delta H}_r$ is the gaseous heat of combustion per unit mass of oxygen consumed at temperature T_o, β the mass stoichiometric ratio of fuel consumed per unit mass of oxygen reacted, and $\hat{H}_{vap}$ the fuel latent heat of vaporization or pyrolysis. θ is the gas stream temperature above ambient ($T-T_o$) and $\dot{q}$ is the rate of heat loss to the duct walls. Equation (2.2) simply states that all the heat generated through combustion goes into heating the gas stream, vaporizing fuel, and losses to the duct walls. Inherent in this equation is the assumption that the gas-phase process is operating at steady state even though the fire is propagating along the duct at some speed V(t). That is, the length of each zone and the flow streams involved are time independent. Hence, only total derivatives with respect to x need be used. Equation (2.2) also neglects the sensible heating required to raise the condensed fuel temperature from ambient to its vaporization temperature. Only the latent heat term is considered to be important. Sensible heating of condensed fuel is found to be smaller than the latent heat term in the energy balance especially for fuels with low vaporization temperatures. It will be shown later, through a sensitivity analysis, that even the latent heat term has a very small effect on the gas-phase energy balance. Inclusion of sensible heating of condensed fuel is therefore not warranted especially if it complicates the model equations significantly.

The term on the L.H.S of equation (2.2) represents the "energy released" by the reaction. In the combustion zone the amount of energy released by the reaction increases with x. Once the end of the combustion zone has been reached and all the oxygen is consumed no more energy is released. The total amount of energy

released in the combustion zone is therefore easily calculated from the total amount of oxygen supplied to the duct. Bearing in mind that the control volume starts at $x = 0$ and therefore always includes the combustion zone, the amount of energy generated by the reaction is constant in the excess fuel and preheating zones. In the excess fuel zone the proportion of total heat generated that goes into heating the gas decreases as the gas cools (or as x increases in this zone). In order to balance this the proportion of the total heat generated that goes into heat losses to the duct walls and to vaporize fuel increases (more heat lost and more fuel vaporized as x increases). In the preheating zone no more fuel is vaporized and the energy lost by the gas, as it cools, goes into heat losses to the duct walls. Ultimately if the duct is long enough the gas cools down to ambient temperature and all the energy generated by reaction goes into heat losses to the duct walls and energy required to vaporize fuel.

Equation (2.2) forms the basis of further modelling of the gas-phase process.

2.1.1 Modelling the combustion zone

Figure 2.1 shows this zone to be in the region $0 \leq x \leq x_1$. It is assumed that in this zone the fuel vaporization rate γ is constant with respect to distance along the duct. This is surmised to be due to the existence of a fire over the entire length of fuel in this zone so that the heat flux at the fuel surface is approximately the same everywhere in this zone. Because the fuel burning rate is controlled by the rate of vaporization, which is controlled by heat transfer to the fuel surface, the constant burning rate assumption is reasonable. It is therefore presumed that the fuel burns at some rate γ (mass of fuel consumed per unit platform area of fuel lining per unit time) which is a property of the fuel. de Ris (1970) worked with this same assumption. Estimates of γ for various fuels may be obtained from de Ris *et al* (1973). Fuel vaporization (burning) in the combustion zone will therefore be described as

$$\frac{d\dot{m}_v}{dx} = C_f \gamma, \qquad \text{for } 0 \leq x \leq x_1. \qquad (2.3)$$

C_f is the perimeter of fuel cross-section (m) and γ is the fuel burning rate (kg/m^2s). Because of the thin duct wall assumption heat losses will be modelled with an overall heat transfer coefficient. A heat transfer coefficient U_d will represent the overall resistance to heat transfer, by conduction and convection, from the inside gas stream to the surrounding atmosphere. The driving force for heat transfer being the difference between the duct inside gas temperature and the outside ambient temperature. This is a significantly simpler model than that used by de Ris (1970) who took into account conduction through the surrounding rock of an underground tunnel. The present use of an overall heat transfer coefficient provides an adequate simple model and should display the correct type of behaviour. Values of heat transfer coefficients can be estimated from existing correlations.

For duct fires inside thin walled passages, it is expected that thermal radiation may become a formidable candidate for heat loss outside the duct walls. In which case the overall heat transfer coefficient for the duct walls will appear to be excessively large in comparison to expected values. In later sections radiation will be quantitatively accounted for. This mode of heat transfer is in the first instance neglected in order to preserve mathematical simplicity. This difference should in the first instance only affect the magnitude of the heat transfer coefficients by a predictable amount and probably have less influence on the general form of the gas temperature profile inside the duct. Because of the strong dependence of the duct heat transfer coefficient on temperature (via radiation), two overall heat transfer coefficients will be used in the model. The first, U_d, will be applied to the combustion zone which represents the hottest portion of the duct, and the second, U_{d2}, for the cooler excess fuel and preheating zones. Heat losses can therefore be modelled as

$$\frac{d\dot{q}}{dx} = C_d U_w (T - T_o), \qquad \text{for } x \geq 0, \tag{2.4}$$

where C_d is the perimeter of tunnel wall through which heat is being transferred (thin wall assumption), U_w is the overall heat transfer coefficient and may take on the value U_d or U_{d2}. Under these assumptions and using the boundary condition that at x=0, $T=T_o$, it can be shown that equation (2.2) may be solved to give the gas phase temperature profile in the combustion zone

$$\Delta T = \Delta T_{max}(1 - [1 + \psi x]^{-(1 + h_c)}) \tag{2.5}$$

where $\Delta T = T - T_o$

$$\psi = \frac{\gamma C_f}{\dot{m}_o}$$

$$\Delta T_{max} = \frac{\left[\frac{(-\Delta \hat{H}_r)\gamma C_f}{\beta} - \gamma C_f \hat{H}_{vap} \right]}{\gamma C_f C_p + C_d U_d}$$

$$h_c = \frac{C_d U_d}{\gamma C_f \hat{C}_p}$$

This is a very simple result for the gas temperature profile in the combustion zone. Heat losses from the combustion zone may be calculated from

$$\dot{q} = C_d U_d \int_0^{x_1} \Delta T \, dx \tag{2.6}$$

2.1.2 Modelling the excess fuel zone

In the excess fuel zone ($x_1 \leq x \leq x_2$ in figure 2.1) there is no oxygen left for reaction. Fuel is presumed to vaporize at a rate that is controlled by convective heat transfer from the hot

flow stream to condensed fuel in this zone. This is a more sophisticated mechanism than that proposed by de Ris (1970), who assumed a constant vaporization rate throughout the excess fuel zone. The implications of these two different assumptions will become apparent at a later stage when the model equations are solved and experiments are performed. The rate of loss of fuel lining can therefore be written as

$$\frac{d\dot{m}_v}{dx} = \frac{C_f h_f}{\hat{H}_{vap}} (\Delta T - \Delta T_{vap}), \qquad \text{for } x_1 \le x \le x_2. \qquad (2.7)$$

h_f is a convective film heat transfer coefficient between the gas stream and fuel surface, and $\Delta T_{vap} = (T_{vap} - T_o)$. Integrating (2.7) gives

$$\dot{m}_v = \dot{m}_{vf} + \frac{C_f h_f}{\hat{H}_{vap}} \int_{x_1}^{x} (\Delta T - \Delta T_{vap})\, dx, \quad \text{for } x_1 \le x \le x_2. \quad (2.8)$$

The constant $\dot{m}_{vf}$ is equal to the total mass of fuel flowing into the control volume up to $x=x_1$, and is easily obtained by integrating equation (2.3). Substituting equations (2.4) and (2.7) into equation (2.2) and introducing a new variable I(x) defined as

$$I(x) = \int_0^x \theta\, dx' \qquad \text{or} \qquad \frac{dI}{dx} = \theta \qquad (2.9)$$

yields the following differential equation describing the gas temperature profile inside the excess fuel zone:

$$(C_1 + C_2\Delta I - C_3\Delta x)(d\Delta I/d\Delta x) + C_4\Delta I - C_5\Delta x + C_6 = 0, \quad \text{for } 0 \le \Delta x \le (x_2 - x_1); \quad (2.10)$$

where $C_1 = (\dot{m}_o + \dot{m}_{vf})\hat{C}_p$

$$C_2 = \frac{C_f h_f \hat{C}_p}{\hat{H}_{vap}}$$

$$C_3 = \frac{C_f h_f \hat{C}_p \Delta T_{vap}}{\hat{H}_{vap}}$$

$$C_4 = C_d U_{d2} + C_f h_f$$

$$C_5 = C_f h_f \Delta T_{vap}$$

$$C_6 = C_d U_d I_1 + \dot{m}_{vf} \hat{H}_{vap} - \frac{(-\Delta \hat{H}_x)\dot{m}_{vf}}{\beta}$$

$$\Delta I = I - I_1 = I - I(x_1)$$

$$\Delta x = x - x_1$$

The boundary condition for equation (2.10) is simply $\Delta I=0$ when $\Delta x=0$.

Equation (2.10) may be solved analytically to produce the following non-linear equation relating ΔI to Δx implicitly:

$$\frac{\Delta x'}{\beta} = a_1^{a_4} \left(\frac{2C_2 v' + a_2}{2C_2 v' + a_3} \right)^{a_4} \left(\frac{C_2 v' + (C_4 - C_3)v' - C_5}{C_2 \frac{\alpha}{\beta^2} + (C_4 - C_3)\frac{\alpha}{\beta} - C_5} \right)^{-\frac{1}{2}} \qquad (2.11)$$

where $v' = \frac{\Delta I'}{\Delta x'}$

$$\Delta x' = \Delta x + \beta$$

$$\Delta I' = \Delta I + \alpha$$

$$\alpha = \frac{C_3 C_6 - C_1 C_5}{C_4 C_3 - C_2 C_5}$$

$$\beta = \frac{C_6 C_5 - C_1 C_5}{C_4 C_3 - C_2 C_5}$$

$$q = (C_4 - C_3)^2 + 4C_2 C_5$$

$$a_1 = \frac{2C_2\frac{\alpha}{\beta} - C_3 + C_4 + \sqrt{q}}{2C_2\frac{\alpha}{\beta} - C_3 + C_4 - \sqrt{q}}$$

$$a_2 = C_4 - C_3 - \sqrt{q}$$

$$a_3 = C_4 - C_3 + \sqrt{q}$$

$$a_4 = \frac{C_4 + C_3}{2\sqrt{q}}$$

Although equation (2.11) is an analytic solution to equation (2.10) it is a very unwieldy form requiring numerical root searching in order to obtain ΔI as an explicit function of Δx. Equation (2.10) may also be solved numerically with relatively little effort. This will be done using the standard fourth order Runge-Kutta technique. Both the analytic and numerical solutions produced the same answer when the non-trivial roots of equation (2.11) are sought.

Once ΔI is known the temperature profile and heat loss are easily calculated using equation (2.9)

$$\dot{q} = C_d U_{d2} \int_{x_1}^{x_2} \Delta T \, dx = C_d U_{d2} \left[I(x_2) - I(x_1) \right]$$

2.1.3 Modelling the preheating zone

In the preheating zone ($x \geq x_2$ in figure 2.1) the gas has cooled to below the fuel vaporization or pyrolysis temperature and no more fuel can vaporize. Furthermore, as suggested by de Ris (1970), no recondensation of fuel from the cooling gas stream is considered. The only process considered here is heat transfer to the duct walls. The heat transfer coefficient used in the excess fuel zone will be used in the preheating zone model. This results in an exponential temperature decay back to ambient temperature. Using equation (2.4) in equation (2.2) and

the fact that $d\dot{m}_v/dx=0$ for $x \geq x_2$ the following equation describing the preheating zone gas temperature profile is obtained:

$$(-\hat{\Delta H}_r)\frac{\dot{m}_{vf}}{\beta} = (\dot{m}_a + \dot{m}_{vu})\hat{C}_p \frac{d\Delta I''}{d\Delta x''} + C_d U_w (I_2 + \Delta I'') + \dot{m}_{vu}\hat{H}_{vap},$$

$$\text{for } 0 \leq \Delta x'' < \infty, \qquad (2.12)$$

where $\Delta I'' = I - I_2 = I - I(x_2)$

$\Delta x'' = x - x_2$.

Using the boundary condition $\Delta I''=0$ when $\Delta x''=0$ equation (2.12) has the following solution:

$$\Delta I'' = \epsilon(1 - \exp(-\nu\Delta x'')), \qquad \text{for } 0 \leq \Delta x'' < \infty, \qquad (2.13)$$

where $$\epsilon = \frac{(-\hat{\Delta H}_r)\frac{\dot{m}_{vf}}{\beta}}{C_d U_{d2}} \cdot I_2 - \frac{\dot{m}_{vu}\hat{H}_{vap}}{C_d U_{d2}} - I_1\left(\frac{U_d}{U_{d2}} - 1\right)$$

$$\nu = \frac{C_d U_{d2}}{(\dot{m}_o + \dot{m}_{vu})\hat{C}_p}$$

The new constant $\dot{m}_{vu}$ is equivalent to the total mass of fuel vapour flowing into the control volume up to $x=x_2$. Total heat losses in the preheating zone can be calculated as

$$\dot{q} = (\dot{m}_a + \dot{m}_{vu})\hat{C}_p(T(x_2) - T_o) \qquad (2.14)$$

Equation (2.14) simply states that all the heat lost from the gas stream is lost through the duct walls.

2.1.4 Defining a fire propagation rate

If an energy balance is performed between $x = 0$ and $x \to \infty$, over

the gas-phase only, a very simple relationship results:

$$(-\hat{\Delta H}_r)\,\frac{\dot{m}_{vf}}{\beta} = \dot{q} + \dot{m}_{vu}\hat{H}_{vap} \qquad (2.15)$$

Equation (2.15) is essentially the non-diferential form of equation (2.2) with the terms multiplied by θ being equal to zero because $\theta \to 0$ as $x \to \infty$. Since all the solid fuel is either burnt or vaporized it is possible to deduce a relationship between equation (2.15) and the condensed fuel lining inside the duct. If, for simplicity, it is assumed that the duct is uniformly lined with fuel, so that the duct fuel loading λ (mass of fuel per unit platform area of lining) is constant with respect to x then

$$\dot{m}_{vu} = \lambda C_f \bar{\nu}, \qquad (2.16)$$

The quantity $\bar{\nu}$ has units of speed and is defined as the fire propagation rate. Sometimes it is referred to as the average surface regression rate in the literature (Sibulkin and Lee, 1974). Substituting equation (2.16) into equation (2.15) results in an expression relating $\bar{\nu}$ to the thermophysical properties of the fuel-lined duct system.

$$\bar{\nu} = \frac{(-\hat{\Delta H}_r)\,\dot{m}_{vf}/\beta - \dot{q}}{\lambda C_f \hat{H}_{vap}} \qquad (2.17)$$

At this stage the reader is cautioned into not confusing the fire propagation rate $\bar{\nu}$, defined in (2.16), with the fire propagation speed V(t). Making a clear distinction between these two terms is crucial to the development of an accurate description of fire propagation along a passage. The next paragraph is devoted to a semi-qualitative discussion on the fundamental difference between these two concepts.

Consider a solid slab of homogeneous fuel lining a duct floor as shown in figure 2.3.

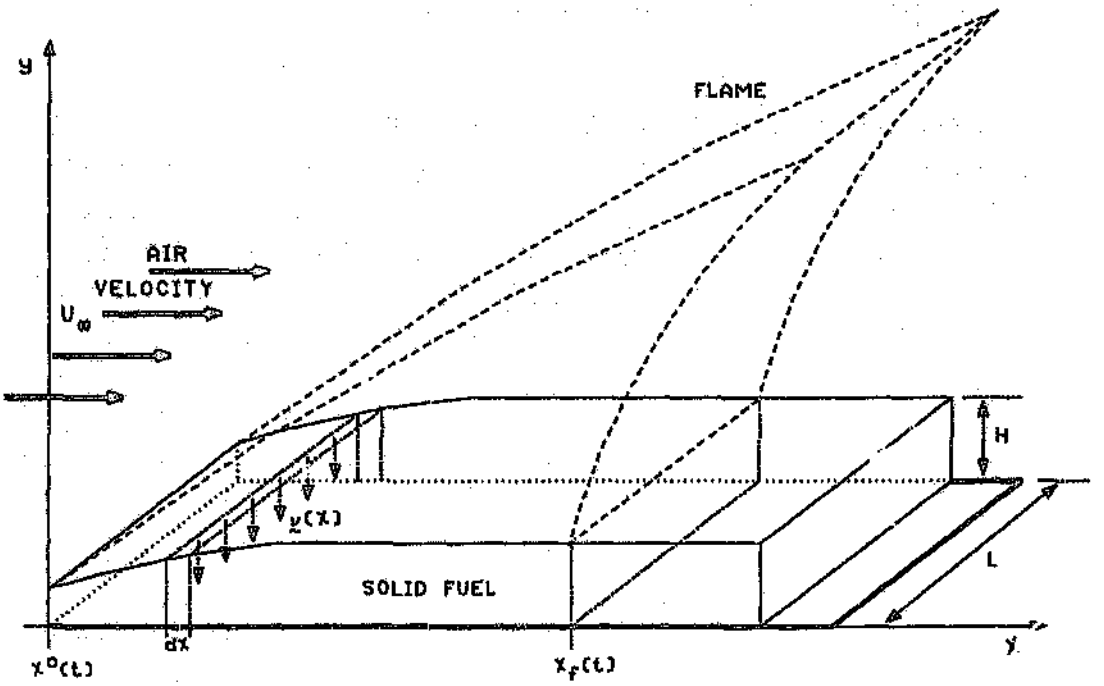


FIGURE 2.3. Simplified diagram of a diffusion flame hanging over the surface of a solid combustible inside a ventilated duct.

Ignoring vaporization ahead of the flame, the fuel surface under the flame moves in a direction away from the flame. This is because fuel is being volatilized from the outer fuel surface. The velocity $\underset{\sim}{\nu}$ at which the surface moves away from the flame may be a function of position χ, and points in a direction perpendicular to the tangent of the surface at the point of interest. The distance coordinate used is χ since, in this case, a coordinate system that is stationary with respect to the duct walls is adopted (eulerian distance coordinate). The variable $\underset{\sim}{\nu}(\chi)$ will be referred to as the surface regression rate vector. Although this variable is a vector, only its magnitude is important when computing the mass of fuel leaving the surface. Consider the differential rate of fuel $\dot{dm}_v$ leaving the solid fuel surface bounded by the region from χ to $\chi+d\chi$.

$$d\dot{m}_v = \rho L |\underline{v}(\chi)| d\chi, \qquad (2.18)$$

where ρ is the solid fuel density (kg/m^3) and L is the width of the fuel slab (m). Integrating equation (2.18) an expression is obtained for the total mass flow of fuel leaving the solid surface due to vaporization (burning). Using equation (2.16) and the result of integrating equation (2.18) the relationship between $\bar{v}$ and $|\underline{v}(\chi)|$ becomes clear,

$$\bar{v} = \frac{\rho}{\lambda} \int_{\chi^o}^{\chi_f} L |\underline{v}(\chi)| \, d\chi \qquad (2.19)$$

The integral in equation (2.19) is equal to the volumetric rate of disappearance of solid fuel $\dot{m}_v/\rho$ is the cross-sectional area H x L shown in figure 2.3. That is, $\bar{v}$ is a mean superficial velocity representing the rate at which the vaporizing fuel surface is regressing. This number is dependent on fire size ($\chi_f - \chi^o$), type of fuel and the properties described in equation (2.17), but is not related to the shape or profile of fuel lining inside the duct.

Now consider how the burning region from χ^o to χ_f would move along the duct length in the positive χ direction as solid fuel is consumed. Assuming the fire has reached its maximum size, which is controlled by the rate of air entering the duct for fuel-rich fires, the fire propagation speed along the duct is simply ($d\chi^o/dt$) (or $d\chi_f/dt$). In this case the coordinate system is stationary with respect to the duct walls and χ^o marks the point on the χ-axis where the continuous fuel loading begins. Clearly, from the diagram shown in figure 2.3 the value of $d\chi^o/dt$ will be zero until the fuel surface at χ^o meets the duct floor at y = 0. However, the fire propagation rate $\bar{v}$ will always assume the constant value given by equation (2.17), regardless of the value of the fire propagation speed V(t) = ($d\chi^o/dt$). Section 2.2 deals with the solid-phase analysis, where the exact relationship between fire propagation speed V(t) and fuel loading profile is shown to be quite simple.

2.2 Condensed-Phase Analysis

This section deals with deriving equations that describe the condensed-phase process. It is important to note that if the condensed-phase is liquid then only the case where the fuel is not permitted to flow is considered. So far the governing equations inherently assume the gas-phase process to be steady-state. The only source of transient behaviour comes from changes occurring in the solid or condensed-phase. Also, any changes that the solid-phase experiences will come as a consequence of gas-phase dynamics. Once again the lagrangian coordinate system is adopted, where the frame of reference is the propagating fire.

2.2.1 Equations of change

Consider a tunnel lined with a condensed fuel that vaporizes and reacts with a well-mixed gas phase that flows at constant velocity V_∞. The combustion reaction takes place in the gas-phase and is assumed to be infinitely fast in comparison to the fuel vaporization rate. Suppose that the duct houses a continuous distribution of fuel described by the continuous function $m(x,t)$ (mass of fuel per unit platform area of fuel surface), which is initially $m^\circ(x)$. A schematic of this system is shown in figure 2.4.

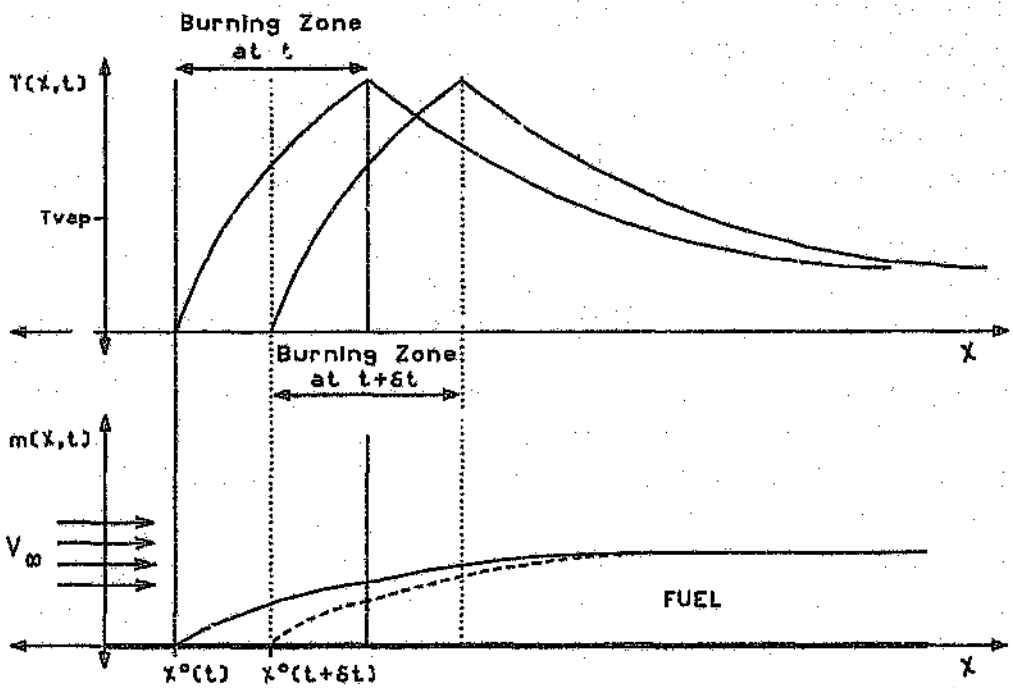


FIGURE 2.4. Fire propagation along a duct.

When considering the gas-phase, a reaction occurs only when the condensed-phase is present in that region of the duct. Hence, the position along the duct that represents the point where the fuel loading begins (i.e., where m = 0) is the start of the combustion zone and therefore the origin (x=0) of the lagrangian coordinate system. At some point $x \geq 0$ a time evolving material balance on the condensed fuel shows that

$$\partial m(x,t)/\partial t = \begin{cases} -\gamma & \text{if } 0 \leq x \leq x_1 \\ \dfrac{-h_f}{H_{vap}} (T - T_{vap}) & \text{if } x_1 \leq x \leq x_2 \\ 0 & \text{if } x > x_2. \end{cases} \qquad (2.20)$$

Now consider the eulerian coordinate system which has the fire propagating away from its origin (χ=0) in the positive χ

direction, χ being the eulerian distance coordinate. Relating the motion of the lagrangian coordinate system to the eulerian is one way of establishing a relationship for V(t). Fuel loading in the duct changes as time progresses. It also varies with respect to distance. In differential form this can be written as

$$dm = \left(\frac{\partial m}{\partial t}\right)^{t\chi} dt + \left(\frac{\partial m}{\partial \chi}\right)^{t\chi} d\chi \qquad (2.21)$$

Notice the use of the variable χ, which is the distance coordinate in the eulerian system. Now consider the moving point χ°, which lies on top of and follows the point x = 0 in lagrangian coordinates. The mass of fuel is zero at this point so that dm=0 (at $\chi^\circ(t)$). Note this always assumes the fuel loading tends to zero with a well defined slope at x=0. The implications of not assuming this will be apparent at a later stage. Bearing in mind that $d\chi = dx + V(t)dt$ it is simple to show that $(d\chi/dt)\big|_{x=0} = V(t)$. Equation (2.21) can be written for the condition where x=0 (which is the point $\chi=\chi^\circ(t)$). This results in an expression for the fire propagation speed V(t) where the frame of reference is the duct walls.

$$(d\chi/dt)\Big|_{x=0} = V(t) = \left.\frac{-(\partial m/\partial t)^{t\chi}}{(\partial m/\partial \chi)^{t\chi}}\right|_{\chi^\circ(t)} = \gamma/(\partial m/\partial \chi)\big|_{\chi^\circ(t)}, \qquad (2.22)$$

Clearly, if the fire is to propagate at a constant speed, the fuel profile inside the duct must be in a specific form so that $(\partial m/\partial \chi)\big|_{\chi^\circ(t)}$ remains constant as time evolves. If a solid homogeneous fuel is used then V(t) is inversely proportional to the physical slope of the fuel surface at x = 0 (or $\chi^\circ(t)$). In which case $(\partial m/\partial \chi)\big|_{\chi^\circ(t)}$ can take on a large range of values (from infinity to zero) throughout the propagation history. Of course, the governing equations have been derived only for cases where $V(t) \ll V_\infty$. The situation where V(t) is close to V_∞ is not considered in the gas-phase analysis.

The most important feature of the solid-phase transient analysis is that the only source of transient behaviour comes from changes in the condensed fuel loading profile. The gas phase is

modelled as if it were a steady state process and no accumulation of mass or energy is involved with that part of the mathematical formulation (as described in section 2.1). This may be valid if the fire moves at speeds much smaller than the gas velocity. If, however, the fire moves rapidly it will be shown later that this will happen over a very short time and not influence the propagation process significantly. This will be discussed later in more detail and will be apparent with the aid of experimental results.

2.3 Application of Model Equations

So far, the model equations describing the gas phase process have been solved or presented in a form whereby it is simple to evaluate the gas temperature profile. Because the condensed-phase equations are dependent on the gas-phase process it will not be possible to solve the former set without first solving the gas-phase. An algorithm for solving a typical case study will be presented. This method of solution or algorithm can be used to solve a variety of cases and can be easily used to program a personal computer. The model equations will be solved using a Turbo Pascal computer program that is based on this algorithm. Appendix A contains the program code.

(a) Brief description of the case study

Consider a typical case where fuel loading is constant along the tunnel length, such as a flat slab of solid homogeneous fuel. Although the description that follows will consider the case where the excess fuel zone is longer than the combustion zone it is not difficult to apply the same algorithm for the opposite case. Before delving into this algorithm it is important to note that in the context of this thesis fire propagation implies the motion or migration of the fully-developed fire along a duct or passage. This is quite different from the concept of fire spread which implies the growth of a fire from its ignition source and not necessarily migration of the entire fire system.

After ignition the fire achieves its fully developed size at the start of the tunnel lining, and because the burning rate is constant the solid fuel is consumed evenly in the combustion zone. The combustion zone remains constant in length and burning continues in this region until the flat fuel profile vanishes. Equation (2.22) confirms that $V(t) = 0$ throughout the course of this uniform fuel consumption because the fuel loading has an initial square edge, i.e., $(\partial m/\partial x)\big|_{x=0} \rightarrow \infty$.

Throughout this time fuel ahead of the combustion zone vaporizes according to equation (2.20), due to the presence of the excess fuel zone. This is shown schematically in figure 2.5(a). As soon as fuel in the combustion zone is depleted the fire will "jump" one combustion zone length along the tunnel (figure 2.5(b)). That is, if conditions ahead of the fire are volatile enough for the fire to propagate, in the form of a "jump" or deflagration, from its original position to its new location forward in the passage. Uniform fuel consumption occurs over the new combustion zone location until the fuel loading at $x = 0$ reaches a zero value (at time t_{v1}). At that moment the combustion zone begins to migrate at some speed according to equation (2.22). Throughout this time condensed fuel ahead of the combustion zone is also consumed by the vaporization process due to hot combustion gases leaving the combustion zone. The vaporization process occurs due to the initially stationary excess fuel zone (figure 2.5(b)) followed by the moving combustion and excess fuel zones when the fire begins its motion (figure 2.5(c)). Then, the fire stops moving again when the start of the combustion zone reaches the new fuel loading step (figure 2.5(d)). Clearly this process will repeat, each time resulting in a newly shaped fuel profile, and the fire may or may not reach some steady propagation speed.

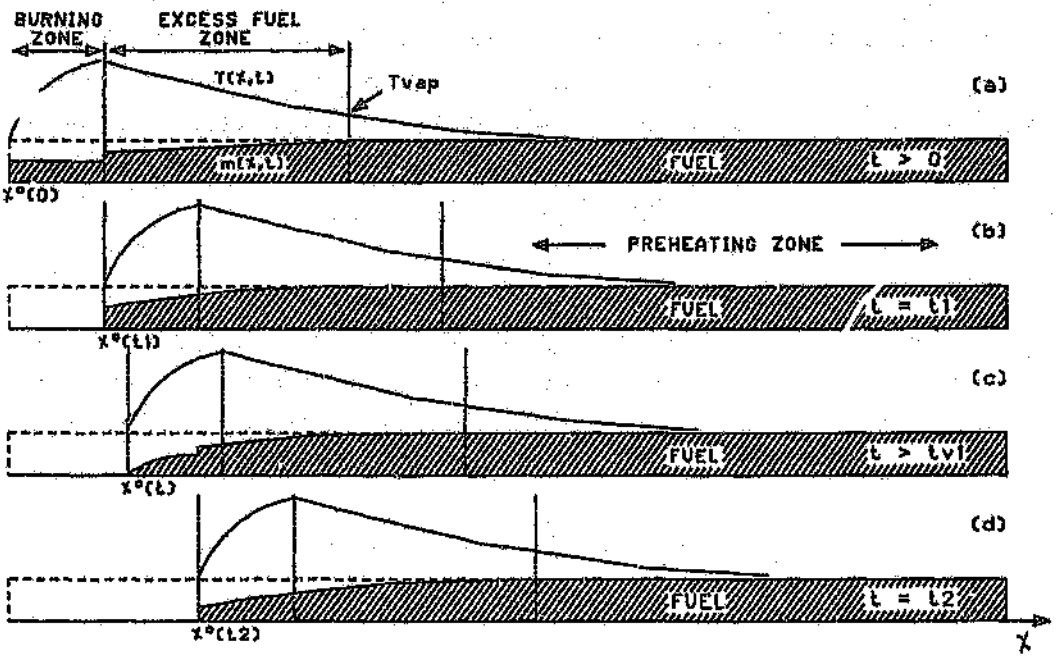


FIGURE 2.5. Propagation sequence showing effect on fuel loading.

(b) An iterative method for simulating fire propagation

The equations describing the gas temperature profile can be solved analytically to give temperature as an explicit function of distance, except for equation (2.10) which can only be expressed as an implicit function of T and x (eqn. 2.11). To find a value of T for any x ($x_1 \leq x \leq x_2$) a root searching technique must be employed which leads to problems of selecting the non-trivial root. In this case it is convenient to use a standard fourth order Runge-Kutta algorithm to solve equation (2.10) instead of using equation (2.11). The analytic equations (2.5) and (2.13) together with the numerical solution of equation (2.10) give the complete gas temperature profile prior to any knowledge of the condensed-phase equations. The gas temperature profile is then used when solving the condensed-phase equations. The condensed-phase system of equations will be solved numerically for $\chi^{\circ}(t)$ and m(x,t), because this system of equations depends on the numerical

solution of equation (2.10).

Working in the lagrangian coordinate system, the calculation procedure for simulating fire propagation would be initiated by calculating the time t_1 taken before the first "jump" occurs, using equation (2.20):

Step 1: *(Figure 2.5(a)→(b))* $t_1 = m(x=0,t=0)/\gamma$

Step 2: *(Figure 2.5(a)→(b))* Evaluate the new fuel profi . due to vaporization in the excess fuel zone occurring over time t_1, using eqn. (2.20):

$$m(x,t_1) = m(x,0) - t_1 \frac{h_f}{H_{vap}} (T(x,0) - T_{vap}),$$

for $X_{1bz} \leq x \leq (X_{1bz}+X_{efz})$;

where X_{1bz} is the combustion zone length and X_{efz} ⁻e excess fuel zone length.

Step 3: Calculate the time taken for the fuel mass loading at x=0 to reach zero:

$$t_{v1} = m(0,t)/\gamma + t_1$$

Step 4: *(Figure 2.5(b)→(c))* During the period of time from t_1 to t_{v1} the fire remains stationary and fuel vaporizes from the excess fuel zone. The resulting fuel profile in the excess fuel zone is given by:

$$m(x,t_{v1}) = m(x,t_1) - (t_{v1}-t_1) \frac{h_f}{H_{vap}} \left[T(x,t_1) - T_{vap}\right],$$

for $X_{1bz} \leq x \leq (X_{1bz}+X_{efz})$.

Step 5: After time t_{v1} the fire will migrate along the tunnel at some velocity V(t). So $\chi^\circ(t)$ (or χ° vs t) is calculated in the interval $\chi^\circ(t_1) \leq \chi^\circ \leq (\chi^\circ(t_1)+X_{1bz})$ by ⁻ing values of χ° within the specified interval and computing t from equation

(2.20). Bearing in mind that $\chi^{\circ}(t)$ is always the point x=0

$$t = m(\chi^{\circ}, t_{v1})/\gamma + t_{v1}$$

is used to describe the fire motion (χ° versus t) shown in figure 2.5(c).

Step 6: The previous step takes the fire to a position represented by figure 2.5(d), and all that is left is to calculate the form of the fuel profile at this stage of the sequence. The latest update of the fuel profile comes from the result of STEP 4 where the fuel loading at time t_{v1} is calculated. Since this moment in time, the fuel has undergone further vaporization and consumption due to the migrating fire system which took place from time t_{v1} to time t_2. This calculation will be done with the aid of figure 2.6 in order to obtain a visual representation of the physical processes occurring during this sequence.

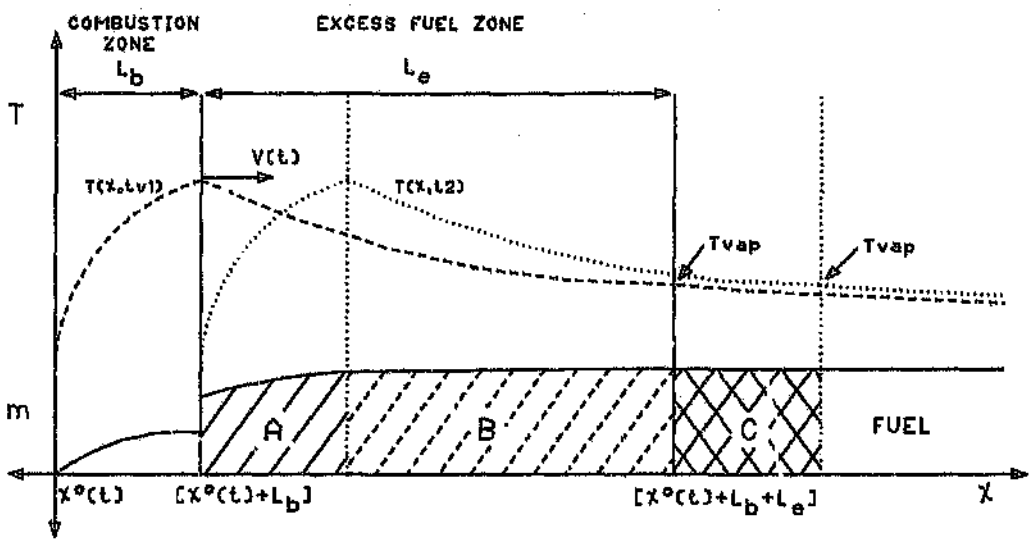


FIGURE 2.6. Effect of migrating fire zones on fuel loading.

Region A will experience vaporization from the moving excess fuel zone and consumption from the migrating fire-front. The resulting fuel loading in this region can be calculated from equation (2.20) in the following way:

$$m(x-X_{lbz},t_2) = m(x,t_{v1}) - \frac{U_f}{H_{vap}} \int_{t_{v1}}^{t'(x)} \left[T(x,t) - T_{vap}\right] dt - \gamma \left[t_2 - t'(x)\right],$$

and this is true only for $X_{lbz} \leq x \leq 2X_{lbz}$ i.e for $t_{v1} \leq t'(x) \leq t_2$. One limit of integration in the above equation is position x dependent and is also evaluated from equation (2.20) as

$$t'(x) = t_{v1} + m(x-X_{lbz},t_{v1})/\gamma$$

The value $t'(x)-t_{v1}$ is the time the excess fuel zone spent over the point x while the upstream end of the fire moved away from $\chi^\circ(t_{v1})$, and $t_2-t'(x)$ is the time the combustion zone spent over x until the upstream end of the fire moved up to $\chi^\circ(t_2)$. Region B experiences only vaporization from the moving excess fuel zone and the resulting fuel loading is evaluated from,

$$m(x-X_{lbz},t_2) = m(x,t_{v1}) - \frac{h_f}{H_{vap}} \int_{t_{v1}}^{t_2} \left[T(x,t) - T_{vap}\right] dt,$$

and this is true only for $2X_{lbz} \leq x \leq (2X_{lbz}+X_{efz})$.

Finally, region C will experience vaporization due to the moving vaporization temperature-front. In this region the fuel loading is calculated from,

$$m(x-X_{lbz},t_2) = m(x,t_{v1}) - \frac{h_f}{H_{vap}} \int_{t_{v1}}^{t'(x)} \left[T(x,t) - T_{vap}\right] dt.$$

This is for $(2X_{lbz}+X_{efz}) \leq x \leq (3X_{lbz}+X_{efz})$. The condition for this equation is that when T(x,t) is less than T_{vap} the integral

takes on a zero value. That is, condensation of fuel vapour is not considered. Downstream condensation is found to have a small effect on fire propagation especially if T_{vap} is not too large (de Ris, 1970).

In all the above equations the gas temperature is a function of time and distance in as much as the temperature profile maintains the same shape but moves along the tunnel at some speed V(t). Because χ^* vs t is always first calculated one can evaluate T(t) numerically in the algorithm. T(t) is purely dependent on T(x) and $\chi^*(t)$ which are both known.

After Step 6 the fire continues its progress along the passage from a sequence similar to that in figure 2.5(b). From this point onward both the fire process and the calculation procedure are repetitive. The calculation goes back to step 3 and the respective steps are repeated with the upgraded values of all the variables.

The above sequence of calculations displays stability. Depending on the system parameters a constant fire propagation speed may be achieved after sufficient iterations are performed. Inherently, the steady state speed is equal to the fire propagation rate $\bar{\nu}$. If the fuel volatility ahead of the fire is high the fire propagation speed converges rapidly to its steady state. The other extreme is if fuel volatility ahead of the fire is negligible, because of a high latent heat or poor heat transfer to the condensed phase. In such a case the fire propagation speed may settle down to some type of periodic form. Whatever the case the time dependent variables should converge to a steady form. Some of these features are illustrated in the next section with the aid of an example.

2.3.1 Typical model output

A systematic method of solving the solid-phase equations has been presented and analytic solutions or simple numerical techniques can be used to solve the gas-phase equations. Time

and position dependent model variables can be solved and displayed graphically. The variables to be analyzed in this section are

- Gas temperature profile T(x,t);

- Fuel loading distribution along the duct m(x,t);

- Fire position inside the duct $\chi^{*}(t)$.

Other time and distance dependent variables emerge from the model equations, such as heat fluxes from the hot gas stream to fuel ahead of the fire and heat losses from the duct walls. These fluxes are directly related to T(x,t) and $\chi^{*}(t)$ and can be calculated with relatively little effort. At this stage of the analysis there is no apparent need to display these variables mainly because they will not be independently measured from fire experiments and compared to the model.

Statement of duct fire problem

To illustrate the type of behaviour the model displays a typical duct fire will be presented and the model equations will be solved. The tables below show all of the ystem parameters that will be used in this case study.

Cross-Sectional Area for Gas Flow X_{ar}	1.556×10^{-3} m^2
Perimeter of square duct cross-section C_d	0.085 m
Perimeter of Fuel Cross-Section C_f	0.05 m

TABLE 2.2(a). Duct Geometry Parameters.

$\hat{\Delta H}_r$	-12.76×10^6 J/(kg O_2)
$\hat{H}_{vap}$	8.0×10^5 J/kg
T_{vap}	99.2 °C
β	0.947
γ	9.3×10^{-3} kg/m^{2}s

TABLE 2.2(b). Fuel Parameters.

Average Wind Speed V_∞	1.5 m/s
Ambient Temperature	25 °C
Duct Heat Transfer Coefficients U_d, U_{d2}	50 W/m^{2}K
Gas Stream to Fuel Surface Heat Transfer Coefficient h_f	2.8 W/m^{2}K

TABLE 2.2(c). Flow Stream Parameters.

The initial condition to this problem is that there is a uniform flat fuel profile inside the duct before the fire starts,

$$m(x,0) = m^* = 2 \text{ kg/m}^2.$$

Also a fully developed fuel-rich fire is established at t=0. That is, fire growth or spread is ignored in this case.

Solution to the duct fire problem

It is possible to solve the model equations for each of the

variables using techniques described in section 2.3. The gas temperature profile inside the duct is shown in figure 2.7.

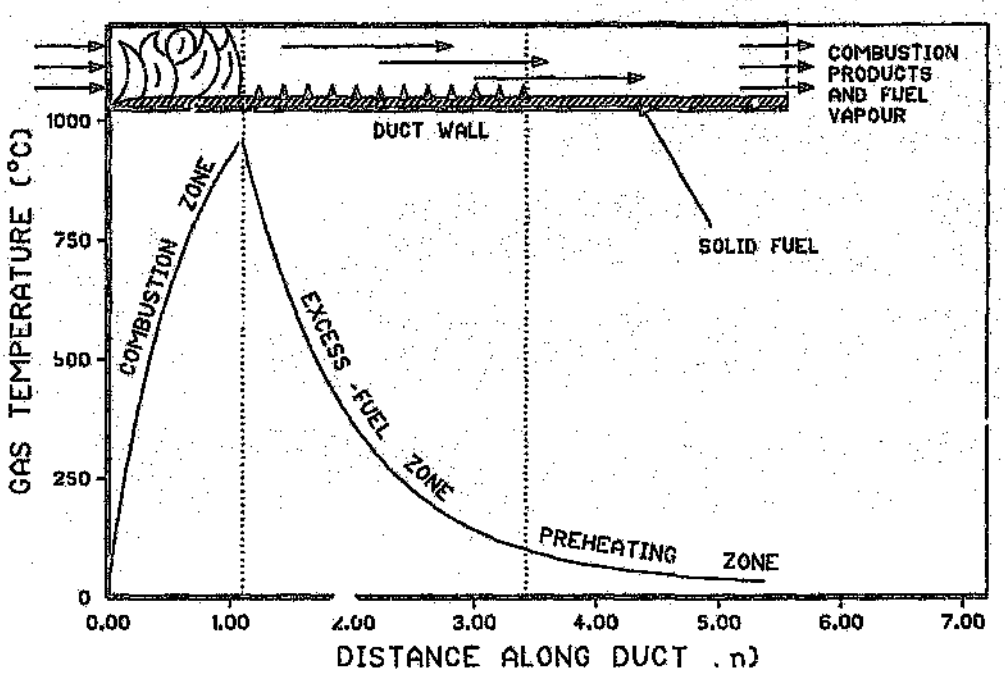


FIGURE 2.7. Gas temperature profile inside duct is shown in the lagrangian coordinate system.

The fire and hence the above shown gas temperature profile will migrate along the duct as fuel is progressively consumed. Throughout this time the solid fuel profile will change in shape and therefore influence the fire propagation speed. The fuel distribution m(x) inside the duct is shown in figure 2.8 at different moments in time throughout the propagation history.

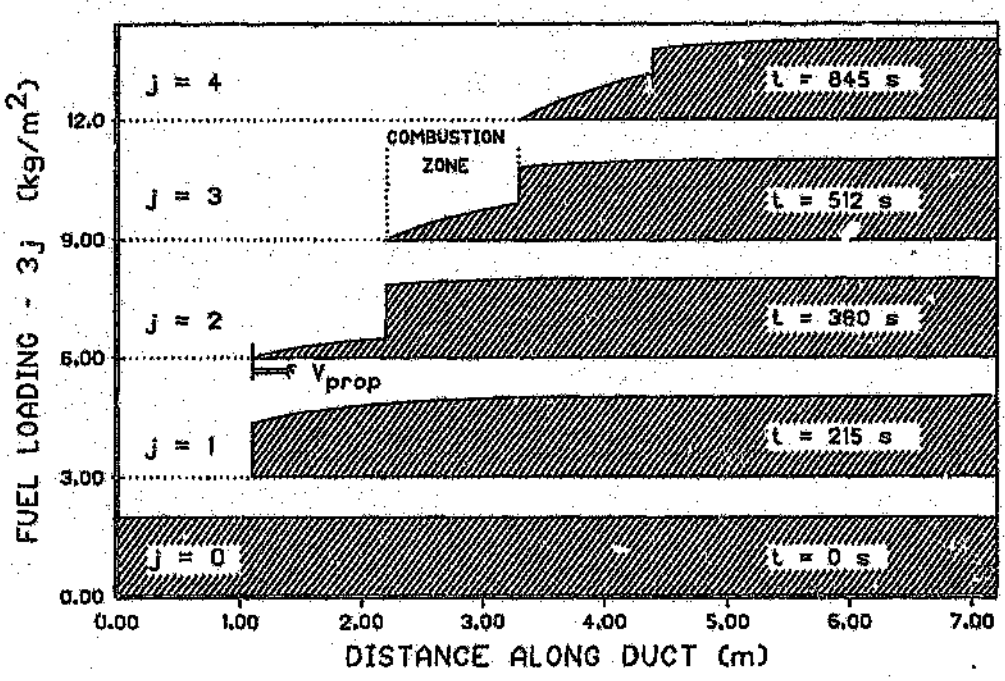


FIGURE 2.8. Transient model solution of fuel distribution along the duct length.

After enough time has evolved a constant fire propagation speed is achieved as a consequence of an invariant shape of fuel profile. This motion prior to reaching steady-state is clearly shown in figure 2.9.

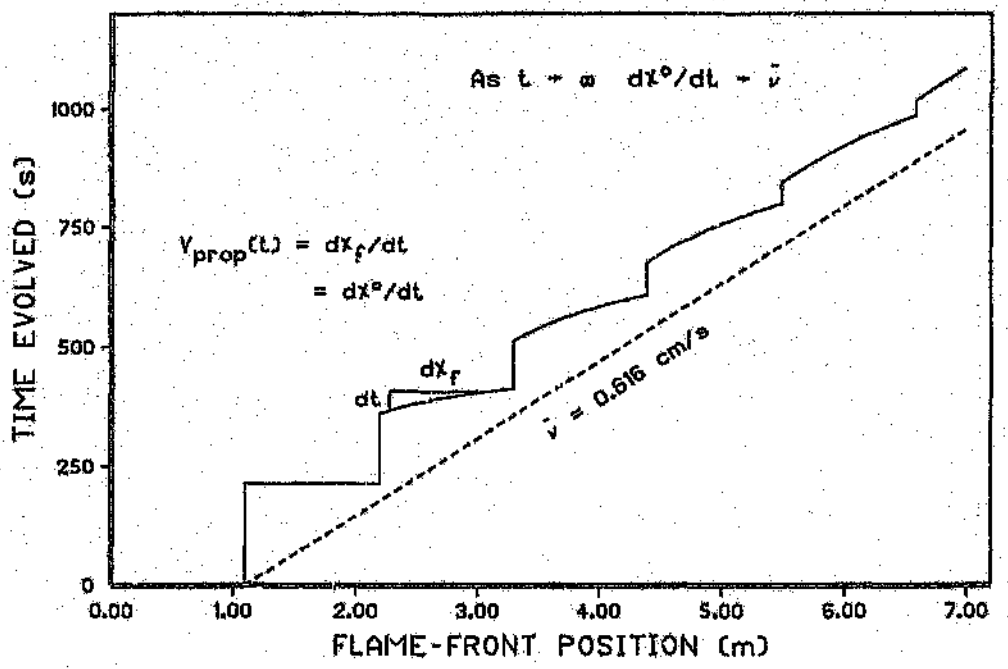


FIGURE 2.9. Fire-front history inside the duct.

The fuel profile inside the duct takes on the steady-state form shown in figure 2.10. A linear fuel profile emerges in the combustion zone which has an invariant slope with respect to time. The fuel profile in the excess fuel zone has a specific curvature so that when it passes into the combustion zone a linear profile with the same slope results. This condition is achieved at steady-state.

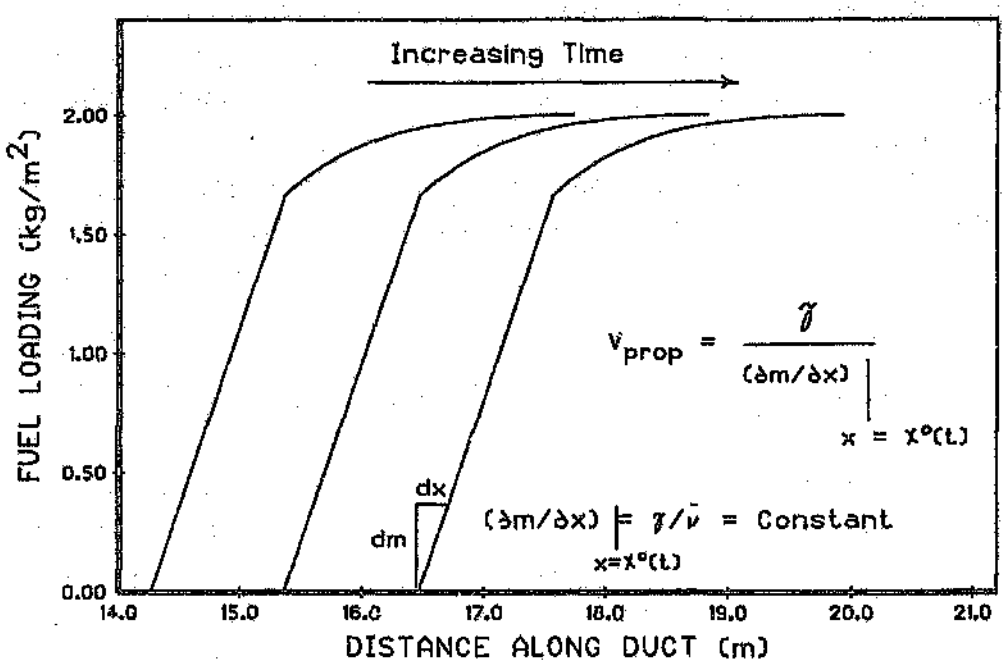


FIGURE 2.10. Steady-state fuel profile achieved after a long time. Shown in the eulerian coordinate system.

Discussion

Whether fires behave in the way this model suggests is something that can only be answered through experiment involving real fires. The model suggests the fire "jumps" along the duct moving incremental distances equivalent to the combustion zone length. This stepping or "jumping" motion comes as a result of the initial flat fuel distribution along the duct and because of the constant burning rate in the combustion zone. Each subsequent "jump" appears to be different on the χ° vs t plot because of the ever changing shape of the condensed fuel profile as time evolves. Eventually the fire propagation speed V(t) reaches a constant value which is equivalent to the fire propagation rate $\tilde{\nu}$.

It is also interesting to see the effect of increasing or

decreasing fuel volatility by choosing different values of $\hat{H}_{vap}$. Essentially, the same effect is achieved if h_f is adjusted. Figure 2.12 in section 2.4 shows this effect. In general, fires occurring under conditions where fuel volatilizes very easily should reach steady state very quickly (soon after the first "jump"). The other extreme occurs when fuel volatility is minimal or essentially zero and the fire continues to "jump" indefinitely.

2.4 Dimensional and Sensitivity Analysis of Model Equations

Since there are a number of parameters in this model it will be beneficial to perform a dimensional analysis in order to ascertain exactly how many parameters characterise the gas temperature T(x). To do this it is desirable to express $\dot{m}_{vf}$ (the fuel flowrate required to use all the oxygen) and $\dot{m}_o$ (the initial air flowrate) in terms of the pressure and wind velocity. This is done using the ideal gas law. The equations are as follows:

$$\dot{m}_{vf} = \frac{y\,\beta\,P_o\,V_\infty\,D^2\,M_{O_2}}{RT_o} \tag{2.23}$$

$$\dot{m}_o = \frac{P_o\,V_\infty\,D^2\,M_{air}}{RT_o} \tag{2.24}$$

The meaning of all the symbols in the above equations are explained in table 2.3 ($M_{O_2/air}$ are the oxygen or air molecular masses). It is possible to show that the gas temperature profile inside the duct depends on 14 dimensional parameters and two dimensionless numbers. Time t is not considered because the gas temperature profile is assumed to not vary with time in the lagrangian coordinate system. These parameters as well as their dimensions, using the mLθT (mass, length, time, temperature) system, are tabulated in table 2.3. In their dimensional analysis Young and Glasser (1990) did not consider T_{vap} and U_{d2}.

	PARAMETER	DIMENSION
y	mole fraction of oxygen in the air feed	-
β	stochiometric coefficient for combustion reaction	-
P_o	stream pressure	$m/L\theta^2$
V_∞	wind velocity	L/θ
D	duct width (assuming square cross-section)	L
T_o	ambient temperature	T
$\hat{C}_p$	gas mean specific heat capacity	$L^2/\theta^2 T$
$\Delta\hat{H}_r$	gaseous enthalpy of reaction	L^2/θ^2
$\hat{H}_{vap}$	enthalpy of vapourization	L^2/θ^2
T_{vap}	fuel vapourization temperature	T
γ	fuel burning rate	$m/L^2\theta$
U_d	duct overall heat transfer coefficient for the combustion zone	$m/\theta^3 T$
U_{d2}	duct overall heat transfer coefficient for the excess fuel and preheating zones	$m/\theta^3 T$
h_f	heat transfer coefficient between the gas and condensed fuel	$m/\theta^3 T$
x	distance coordinate	L
C_f	perimeter of fuel cross-section	L

TABLE 2.3. Gas-Phase Model Parameters

There are 15 parameters and one variable which is the distance coordinate x. Using the Rayleigh method the above system may be characterized by twelve dimensionless numbers. A set of dimensionless numbers produced by this technique is not a unique set since multiplying or dividing two dimensionless numbers produces another. One possible set of dimensionlesss numbers is:

$$\Pi_1 = \frac{P_o}{V_\infty \gamma} \qquad \Pi_5 = \frac{T_{vap}}{T_o} \qquad \Pi_9 = \frac{h_f T_o}{V_\infty^2 \gamma}$$

$$\Pi_2 = \frac{\hat{C}_p T_o}{V_\infty^2} \qquad \Pi_6 = \frac{C_f}{D} \qquad \Pi_{10} = y$$

$$\Pi_3 = \frac{\Delta\hat{H}_r}{V_\infty^2} \qquad \Pi_7 = \frac{U_d T_o}{V_\infty^2 \gamma} \qquad \Pi_{11} = \beta$$

$$\Pi_4 = \frac{\hat{H}_{vap}}{V_\infty^2} \qquad \Pi_8 = \frac{U_{d2} T_o}{V_\infty^2 \gamma} \qquad \Pi_{12} = \frac{x}{D}$$

The gas temperature in the duct now depends on the eleven dimensionless numbers listed here and on the dimensionless distance along the duct, x/D. This analysis clearly indicates that the model is complex. However, it is useful to examine these numbers. Π_{10} will usually be fixed for r at 0.21. Π_1, Π_3, Π_4, Π_5 and Π_{11} are essentially fuel properties. Π_6 is determined by the ratio of fuel circumference to the duct width.

For a given duct with a specified fuel type and geometry, and knowledge of the air flowrate the gas temperature profile depends on three free parameters (Π_7, Π_8 and Π_9). These unknown parameters are heat transfer coefficients. The problem may be further simplified in certain cases if a sensitivity analysis reveals that the equations are insensitive to one or more of these parameters. Section 2.4.1 deals with this.

2.4.1 Sensitivity analysis of model

A simple sensitivity analysis is performed on the model. All model parameters are set to values in the neighbourhood of those conditions experienced in the experimental studies appearing in later sections. This way sensitivity of model solutions to changes in each free parameter is determined around the region of interest in parameter space. Model sensitivity to each parameter may vary if other regions of parameter space are explored in this manner. Of interest to the present study is only that region where experimental studies of real fires are conducted. The significance of such an analysis will become

clearer in later sections where the same parameters will be estimated by fitting the model to experimental data. Those features of the model which are most affected by small changes in a parameter will be critical in determining the value of that parameter. Because of the large number of free parameters already identified in the dimensional analysis complicated non-linear least squares algorithms will be avoided when fitting the model to data.

A typical base case is considered with parameters set close to those in the experimental study of liquid fuels. Sensitivity is tested by varying the parameter of interest + and - 50% of its base case value. The effect is then observed in the model solution of $T(x)$ and $\chi^*(t)$. Base case values of all parameters are listed in table 2.4(a) and (b). Duct geometric parameters are the same as those in table 2.2(a).

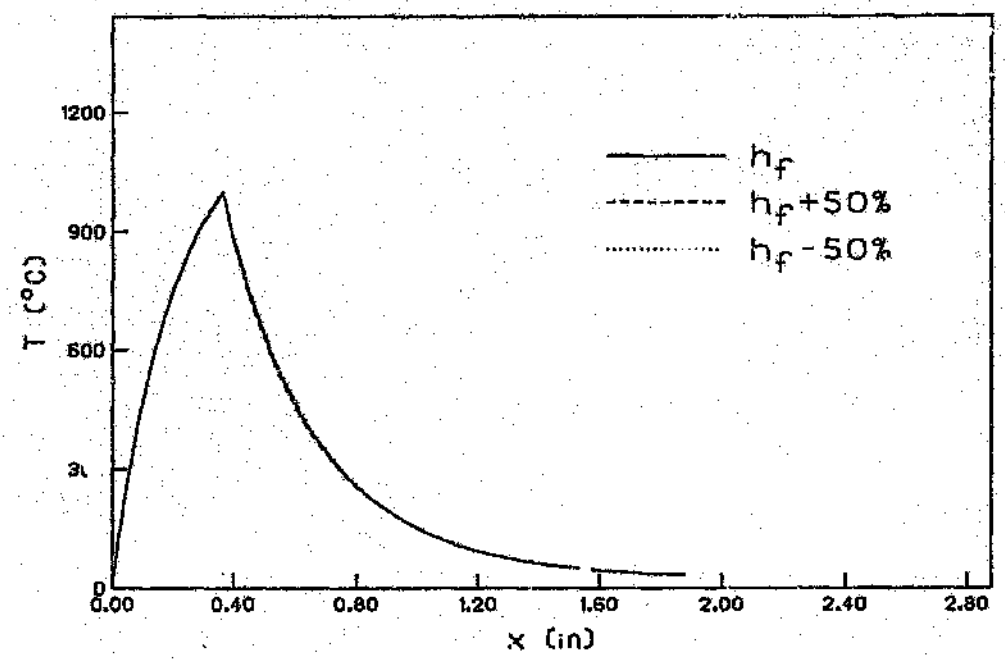
$\hat{\Delta H}_r$	-12.76×10^6 J/(kg O_2)
$\hat{H}_{vap}$	27.2×10^4 J/kg
T_{vap}	99.2 °C
β	0.947
γ	9.3×10^{-3} kg/m^{2}s

TABLE 2.4(a). Fuel Properties.

Average Wind Speed V_∞	0.5 m/s
Ambient Temperature	25 ^oC
Duct Heat Transfer Coefficients $U_d = U_{d2}$	50 W/m^2K
Gas Stream to Fuel Surface Heat Transfer Coefficient h_f	1.5 W/m^2K
Initial Fuel Loading	2 kg/m^2

TABLE 2.4(b). Fire conditions.

Sensitivity analyses are performed on those free parameters used to fit the model to data in later sections. Fuel burning rate γ, mass stoichiometric coefficient β, duct wall overall heat transfer coefficients U_d and U_{d2}, and gas-to-fuel surface film heat transfer coefficient h_f will be examined for sensitivity. Results of this analysis are shown below.



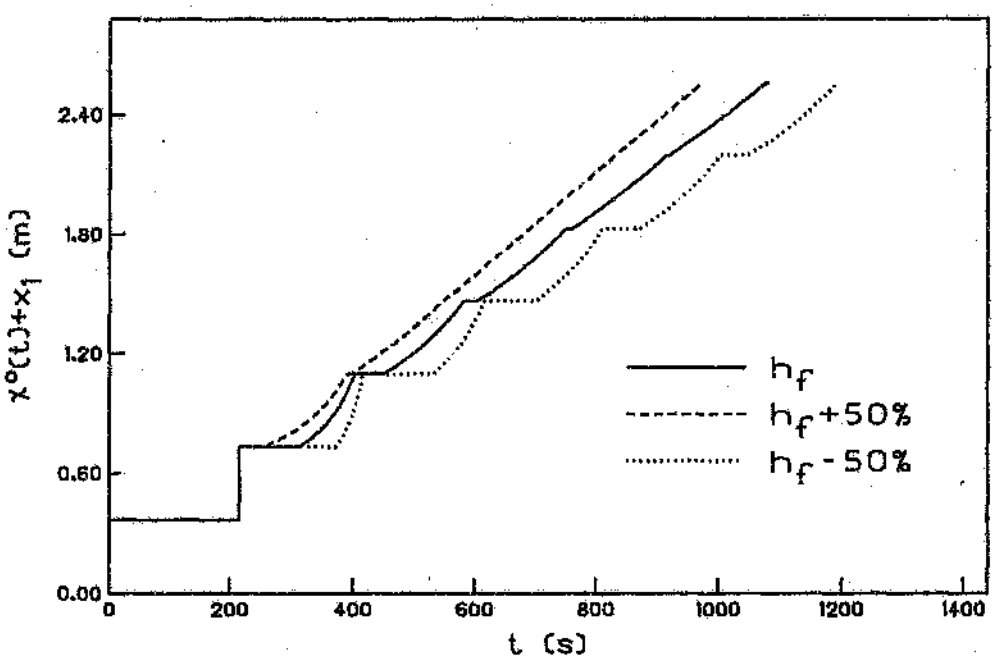


FIGURE 2.11. Effect of h_f.

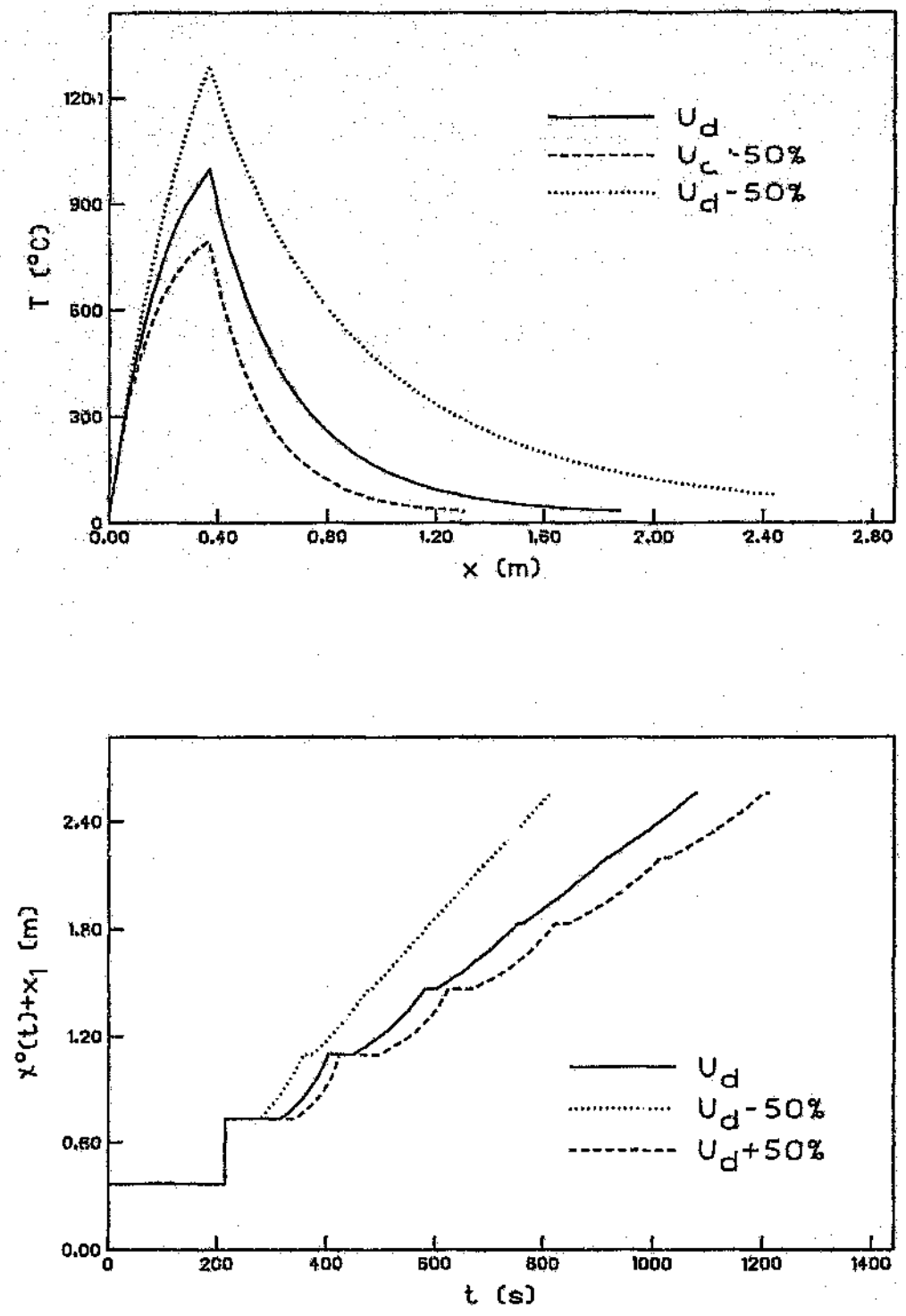
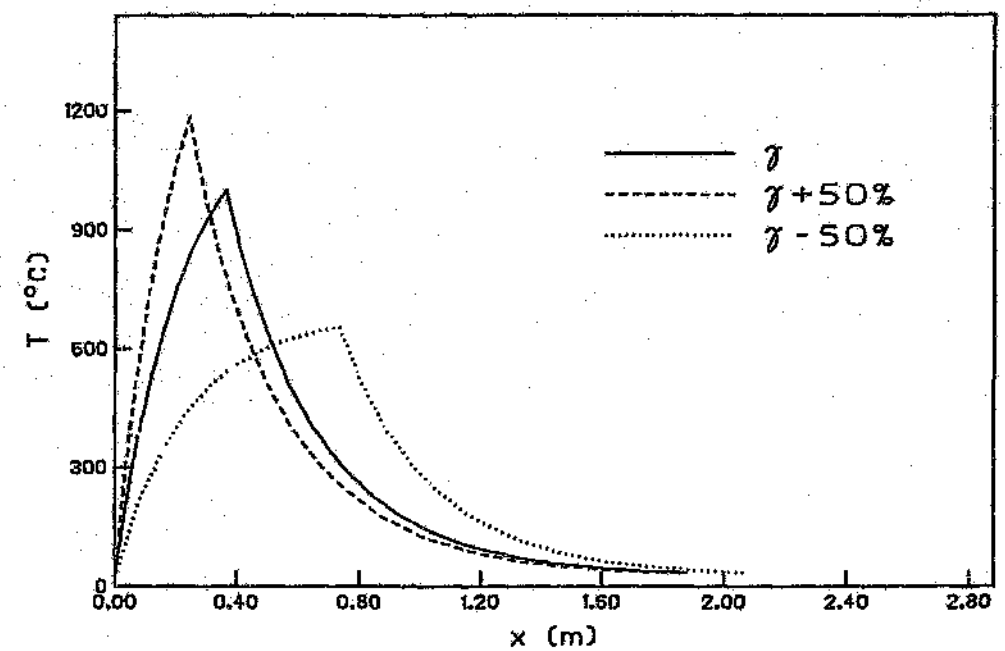


FIGURE 2.12. Effect of U_d.



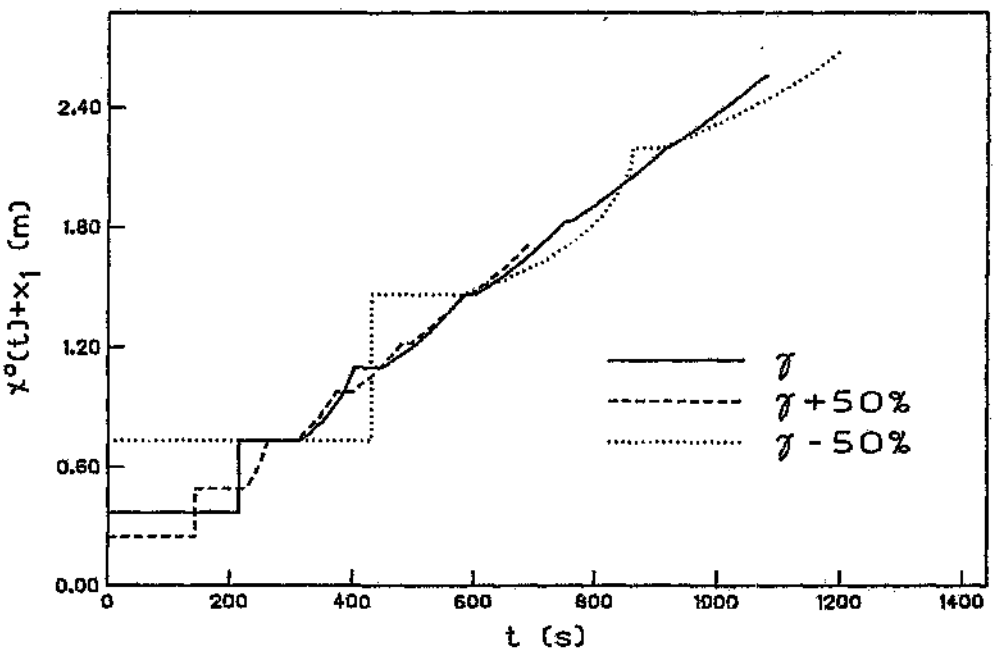


FIGURE 2.13. Effect of γ.

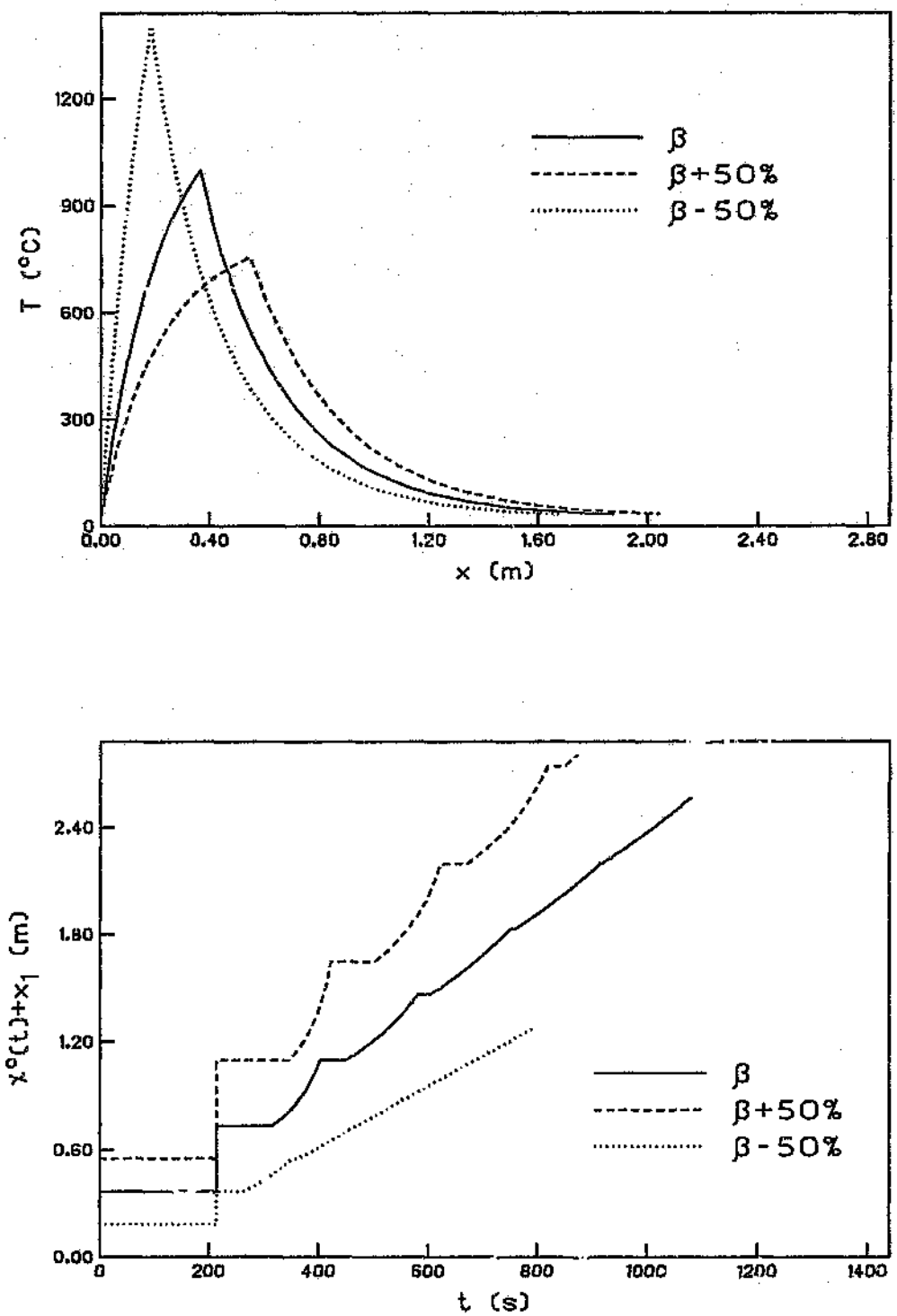


FIGURE 2.14. Effect of β.

Parameter	X_{lbz} m	X_{efz} m	$\bar{\nu}$ x10^{-2} m/s
Base Case	0.366	0.813	0.229
h_f + 50%	0.366	0.813	0.257
h_f - 50%	0.366	0.813	0.200
γ + 50%	0.244	0.867	0.243
γ - 50%	0.732	0.732	0.203
U_d + 50%	0.366	0.488	0.199
U_d - 50%	0.366	1.87	0.329
β + 50%	0.548	0.792	0.299
β - 50%	0.183	0.854	0.167

TABLE 2.5. Duct fire features from sensitivity analysis.

Model parameters, except h_f, are shown to have profound effects on the gas temperature profile and propagation history. h_f plays an insignificant role in the gas phase equations but has marked effects on propagation histories. The importance of this result is seen later when the model is fitted to experimental data. Compared to U_d and U_{d2}, h_f plays no role in the gas phase process. In the model $\hat{H}_{vap}$ has the inverse effect that h_f displays but with the exact same sensitivity on T(x) because it always appears in the term $(h_f/\hat{H}_{vap})$. Such small effects of $\hat{H}_{vap}$ on the gas-phase energy balance (eqn. 2.2) justifies neglecting the sensible heating of condensed fuel in equation (2.2) since sensible heating of solid fuel would have a similar if not smaller effect. Sensible heating of condensed fuel is often much smaller than the fuel latent heat.

γ is inversely proportional and β is directly proportional to the combustion zone length X_{lbz}. These are obvious consequences of the fuel-rich fire assumption. γ is also inversely proportional to the length of the first jump shown by propagation histories χ^* versus t in figure 2.13. Of course γ

and β will also affect the maximum gas temperature since they are reaction related properties. Long-term effects of γ, β, U_d, and h_f on propagation histories are also significant but not as obvious to predict without first solving the system of model equations. The effect of U_d on T(x) is significant. It is likely that these temperature profiles contain enough information to fit to experimental data and hence adequately determine U_d and U_{d2}.

Relationships shown between a parameter and those model features discussed so far will provide a useful basis for modelling real fire data in later sections of this thesis.

2.5 Effect of Heat Loss Due to Thermal Radiation

Exclusion of thermal radiation from the gas phase model equations may result in excessively large duct heat transfer coefficients. This is because the convective term will have to account for losses due to radiation as well as convection. It is possible to solve the combustion zone temperature profile if thermal radiation and convection are the two dominant modes of heat transfer from the duct walls. For the combustion zone, the heat loss can therefore be modelled as:

$$\frac{dq}{dx} = C_d U_d (T - T_o) + \sigma \epsilon C_d (T^4 - T_o^4) \qquad (2.25)$$

where ϵ is the duct wall emisivity;

σ is the Stefan-Boltzmann constant;

U_d is the duct convective heat transfer coefficient determined from correlations.

Equations (2.2), (2.3) and (2.25) may be manipulated into the following differential equation describing the gas stream temperature profile for the combustion zone:

$$\frac{dT}{dx} = \frac{AT^4 + BT + C}{D + Ex} \tag{2.26}$$

where $A = -C_d \epsilon \sigma T_o^4$; $B = \hat{C}_p C_f \gamma + C_d U_d$;

$$C = \left[\frac{(\hat{\Delta H}_r)}{\beta} - \hat{H}_{vap} + \hat{C}_p T_o\right] C_f \gamma + \left[\sigma \epsilon T_o^3 + U_d\right] C_d T_o;$$

$D = \dot{m}_o \hat{C}_p$; $E = \hat{C}_p C_f \gamma$

A fourth order Runge-Kutta routine was programed to solve (2.26). Appendix A contains the Turbo Pascal code for this routine. Equation (2.26) will be used to study data from fires in the following chapter.

3 LIQUID FUELLED FIRES IN NON-STRATIFIED FLOW

Duct fire problems are frequently addressed when trying to understand fire propagation in large scale tunnels. One of the most striking features of large-scale confined fires is the persistence of severely stratified flow patterns induced by rising hot combustion gases (Newman, 1984). Whether there are naturally induced or forced convective air currents entering the tunnel, stratified flow will occur depending on whether buoyancy forces are greater than cross flow forces. This phenomenon has been studied by Newman (1984), who presents correlations for determining the degree of fire induced stratification. Acquiring data from a fire propagating within the confines of a passage poses the problem that such stratification phenomena often intrude upon the effect of underlying fire spread and propagation mechanisms. It is therefore necessary to study, in isolation, such mechanisms prior to understanding the coupled effect of fluid dynamics.

In this section the study is therefore restricted to scenarios involving the horizontal ventilated fuel-lined duct where the gas flow stream is radially well mixed, or at least the use of a single average temperature is justified. A well mixed flow assumption is based on the premise that in some cases large Reynolds numbers (over 10000) are easily achieved in full scale mine tunnels with low ventilation currents (~ 0.3 m/s). The large duct diameter being an important parameter allowing turbulence to prevail. Moreover, the fuel source is considered to be in its condensed form where burning is the result of diffusion type flames burning over the fuel surface. Such a study will provide an examination of the proposed model and will lead to an improved understanding of fires occurring in the well mixed flow regime.

Two experimental tunnels have been constructed and used in studies for this thesis. The first is devoted to investigating fires without stratified flow, and the second is used to investigate fires when three dimensional aerodynamic effects are

inherent. This section deals with the former case.

3.1 Apparatus for Non-Stratified Conditions

Fire propagation experiments were carried out using a 5 metre long, 43 mm wide, and 42 mm high mild steel duct as shown in figure 3.1. A more detailed drawing appears in appendix D. With these dimensions and air velocities used in the experiments the degree of gas stream temperature stratification can be estimated from a Froude number calculated as (Newman, 1984)

$$Fr = \frac{V_{avg}}{\left[(\Delta T_{cf}/T_{avg})gH\right]^{1/2}} \qquad (3.1)$$

Here H is the tunnel height, V_{avg} is calculated as the average "hot" velocity through the duct calculated at T_{avg} the average gas temperature. ΔT_{cf} is the difference between the ceiling and floor gas temperatures, and g the acceleration of gravity. In this case T_{avg} was approximated to be equivalent to the measured gas stream temperature because it is measured approximately along the centre-line of the duct flow stream. This approximation is reasonable if stratification is not severe and the gas temperature rises from floor to ceiling. Using this information and a correlation developed by Newman (1984) which relates ΔT_{cf} to H, T_{avg} and V_{avg} it is then possible to calculate ΔT_{cf}. For these experiments Fr is found to lie within the range $1 \leq Fr \leq 10$, a regime dominated by strong interactions between cross flow and buoyancy forces (Newman, 1984). In this regime severe stratification does not prevail.

Thus it is likely that the present experimental flow conditions are not characteristic of two separate gas layers (one hot stream along the ceiling and a cold stream along the floor), as in severe stratification. Instead a single hot gas stream flows through the entire duct cross-section with a definite vertical temperature gradient. Since the Reynolds number for these experiments is either within the laminar or transitional regime

between fully developed turbulence and laminar flow (800 < Re < 4500) the above analysis suggests some radial temperature variation. Using Newman's (1984) correlation for these experiments the estimated order of magnitude of ΔT_{cf}, if T_{avg}=400°C, can range from 0 to 400°C, depending on air speed. However, the gas stream temperatures are measured midway between the duct floor and ceiling and are therefore taken to be approximately equal to the average gas temperature thus allowing for comparison with the model which assumes good mixing.

A narrow duct was used because of its economically desirable scale with the possibility of reducing stratification by virtue of a lower duct height. The limitation being that a very narrow duct cannot accommodate sufficient fuel mass for experimentation, and increasing air velocities in an attempt to increase the Reynolds number may result in blowing the fire out. The alternative is to work on a larger scale of duct diameter (also allowing for a larger exposed fuel surface area) where the Reynolds number can be increased well into the turbulent regime without having to operate at blow-out air velocities. For this reason the well mixed slug flow assumption may be realistic for full scale mine tunnel fires. The disadvantage of such large apparatus is that long duct lengths would be required in order to measure the entire gas stream temperature profile. That is, from the combustion zone up to a length where the gas stream has cooled to below T_{vap}. In this section of the study a compromise is made by using a duct with which one cannot guarantee good mixing although stratification will be absent. A subsequent section will deal with a study where stratification does indeed occur.

Also, a simple criterion (de Ris, 1970) based on a variation of the Froude number can be used to reduce the possibility of back-flow of hot combustion gases along the duct ceiling. For the present arrangement and the range of air velocities used the dimensionless group $\Delta\rho Hg/\rho V_a^2$ is found to lie between 0.12 and 3.5 when $\Delta\rho/\rho \approx 2/3$ and V_a is the ventilation air average velocity. Ideally this dimensionless group should be less than unity to ensure no backflow. This criterion for back-flow is

discussed by de Ris (1970). Again one is forced to accept a situation that is not quite ideal.

The first meter of length provides a calming section to smooth the air flow supplied from the mains. The next 3 meters is the actual fire test section at the end of which is one meter of duct to eliminate end effects. A three meter steel tray rests along the floor of the test section. Liquid fuels may be distributed along the tray length by soaking the required amount along an asbestos wick residing inside the tray. Flame spread over a porous solid soaked with combustible liquids has been investigated by Takeno and Hirano (1986). If the liquid level does not lie above the upper surface of the porous solid then flame spread behaviour is similar to that over solid fuels.

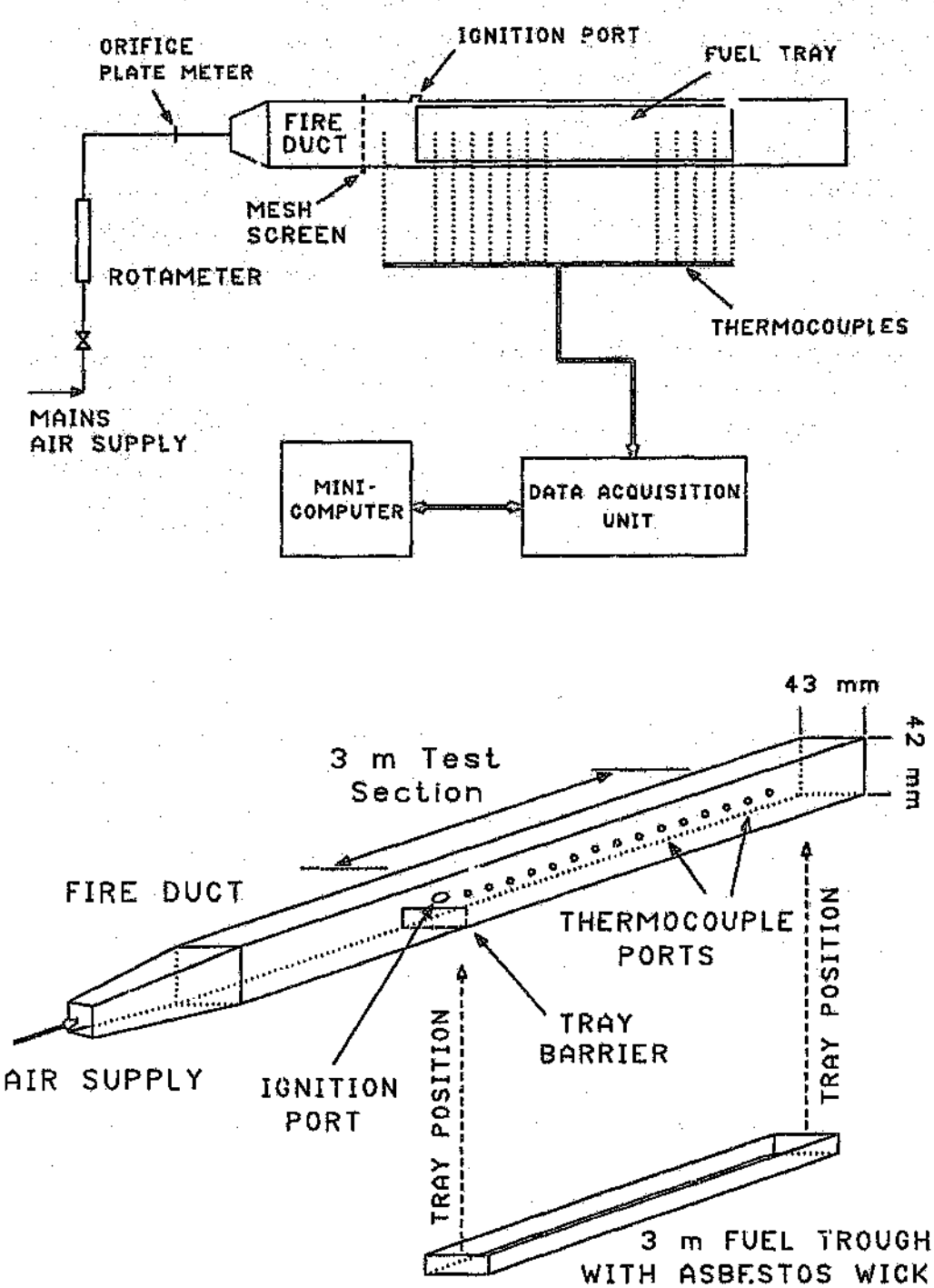


FIGURE 3.1. Schematic representation of equipment used for fire experiments.

Thirty-four chromel-alumel thermocouples (type K) are inserted half-way into the flowing stream, to measure the gas stream temperature distribution, at 91 mm intervals over the 3-m test section. Thermocouple emfs are recorded with an H-P data acquisition unit, controlled by a personal computer. Each measured temperature, accompanied with a distance and time is recorded and stored on disc. Details on gas temperature measurement, storage of data and a radiation shielding test are placed in appendix C.

Air is supplied to the duct entrance at atmospheric pressure and temperature. The flowrate is measured with a rotameter and an orifice plate meter inserted upstream from the duct. An ignition port is located at the start of the test section and is sealed with a threaded cap.

3.2 Experimental Procedure

The total mass of fuel is weighed and separated into 15 equal portions. Each portion is evenly distributed along 20 cm segments which constitute the tray length. This is done in order to achieve a uniform fuel distribution along the tray. The fuel tray is carefully loaded into the duct and the air supply set to the required flowrate. By inserting a burning torch into the ignition port the upstream end of the fuel tray is ignited and the data logging set-up initiated simultaneously. The ignition port is sealed immediately.

The data acquisition unit is programmed to take all 34 thermocouple readings every 30 seconds, the first set taken 30 seconds after ignition. It takes approximately 5 seconds to read one set of thirty-four thermocouples.

3.3 Results

Experiments were performed with a variety of fuels all of which are pure organic liquids. The advantage being that their

thermodynamic properties are well known so that the governing equations can be used to model the fires. Also, most liquid fuels support rapidly growing fires, so that the transient period of fire growth from an ignition source to a fully developed fuel-rich state is small. The three substances used are, isooctane (Iso), n-butanol (Butol), and ethylene glycol (Eg), chosen in order to have a range of fuels of decreasing volatility. Also these are substances with very simple molecules and should therefore vaporize cleanly into the gas phase without intermediate complications such as pyrolysis reactions.

For each experiment the gas temperature profile is measured as the fire propagates along the duct. Figure 3.2 shows temperature distributions measured at three different times for the same fire (run 5). The model was fitted to the first temperature profile when the fire is stationary at the start of the test section. The same fit is deliberately placed on the temperature distribution data of the fire when it has progressed roughly 1 and 2 metres along the duct.

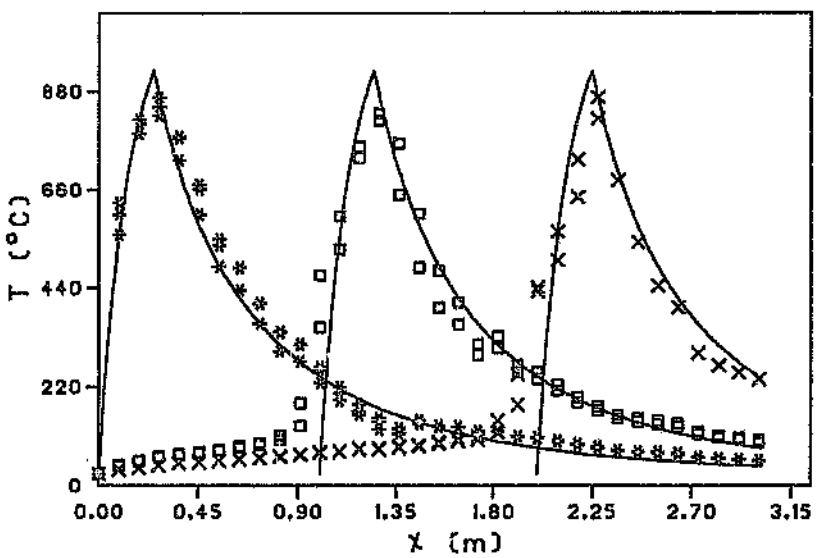


FIGURE 3.2. Gas temperature profiles from run 5 showing the stationary fire soon after ignition (*) and the moving fire 750 seconds (□) and 1200 seconds (x) after ignition. Proposed model fits (——) are also shown.

In order to monitor the motion of the fire along the duct it was assumed that the fire-front position can be determined as being the position of the maximum gas temperature. To estimate the position of this maximum, parabolic interpolation was used on each of the measured gas temperature profiles. Figure 3.3 shows fire-front position versus time data for three different fires (including one replicate).

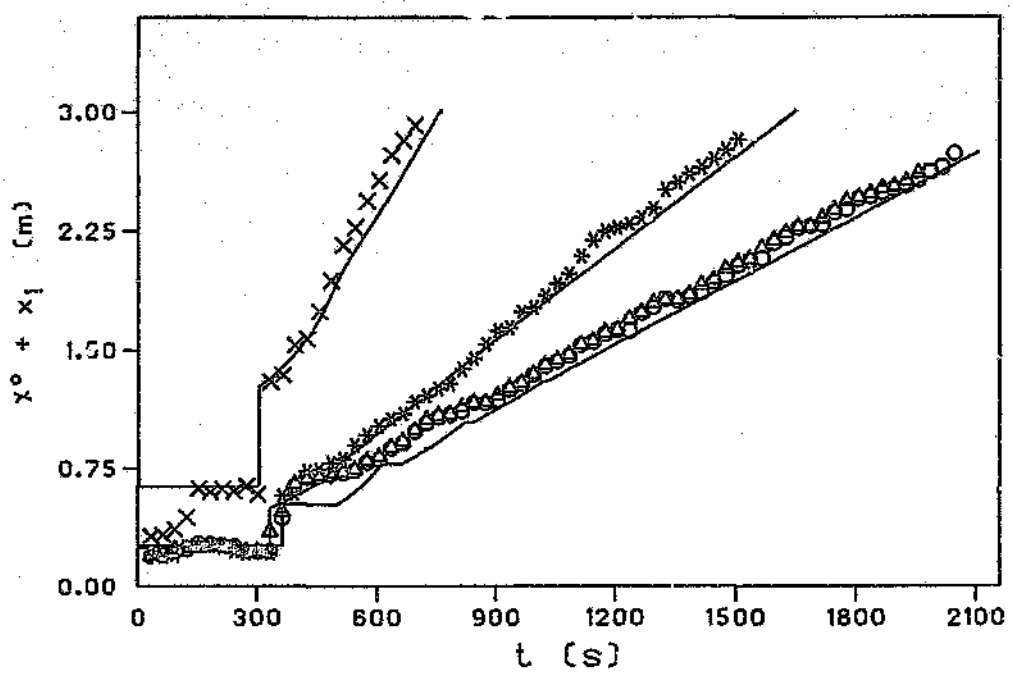


FIGURE 3.3. Fire-front history along the duct for run 4 (x), run 5 (*) and run 8 (Δ). Run 8 was repeated (o) to test for the quality of reproduction of the experiment. Proposed model fits (——) are also shown.

It is also helpful to see how this temperature profile changes as time progresses. Because the gas temperature is changing with time and distance the whole process may be viewed graphically in three dimensions. A three dimensional display of run 5 is shown in figure 3.4(a). The result is a clear picture of the time evolving gas temperature profile inside the duct. Figure 3.4(b) is the same surface "landscape" shown from above in the form of a contour plot. Although these graphic

representations are not necessarily useful in quantitative analyses they provide a means of viewing the entire fire propagation process at a glance.

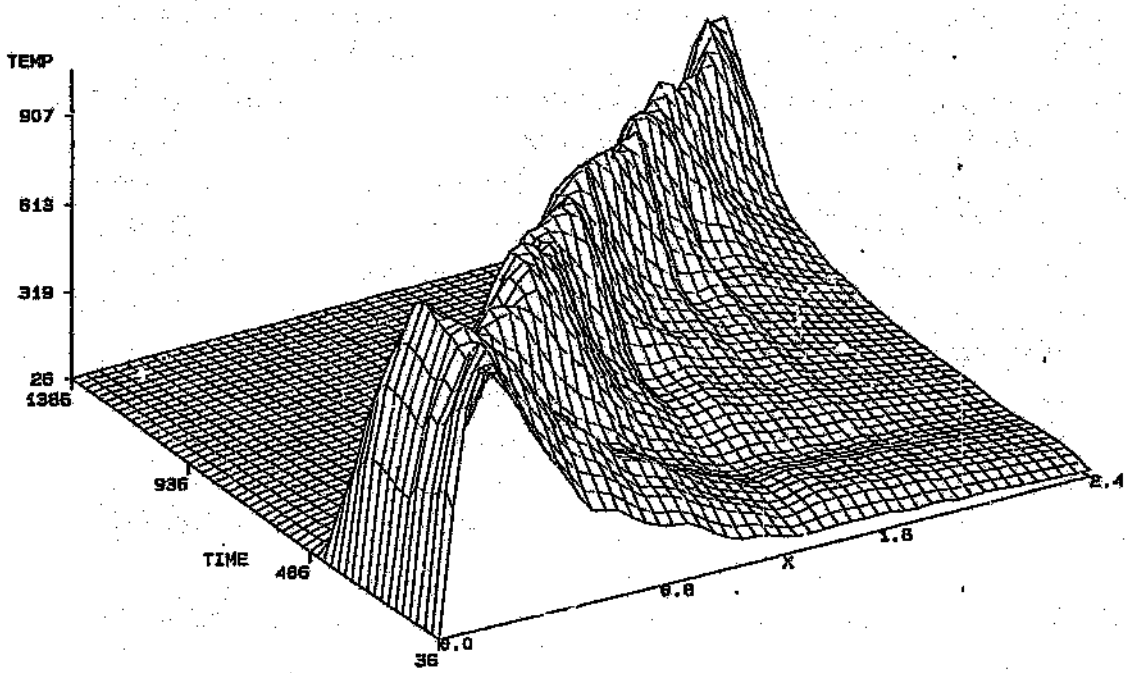


FIGURE 3.4(a). Graphic display of experimental data acquired from run 5. The surface shows the gas temperature profile evolving with time.

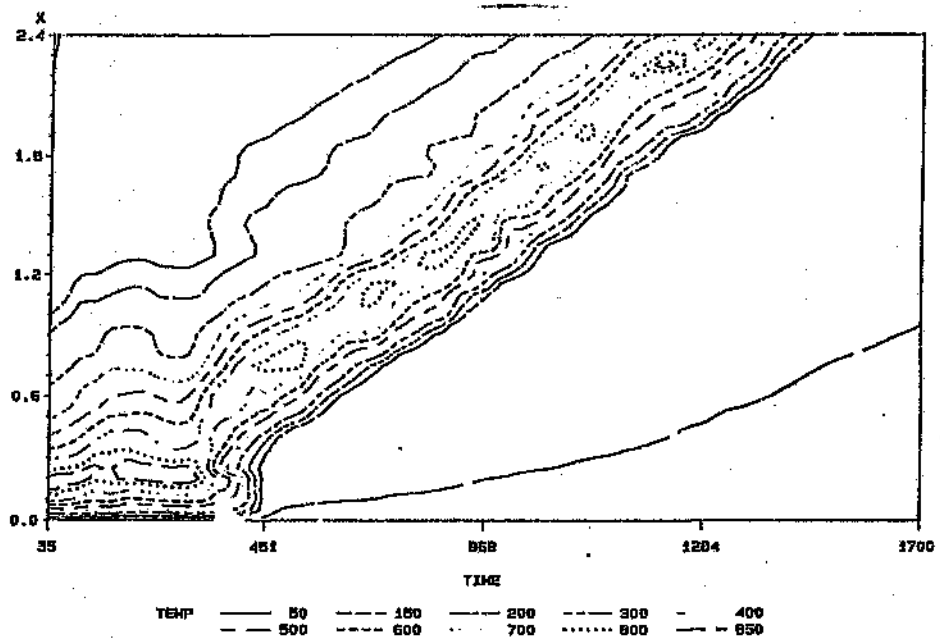


FIGURE 3.4(b). Contour plot of the time evolving temperature profile inside the duct for run 5.

Fitting the gas-phase model to gas temperature data provides values of all unknown model parameters except for h_f. This is because the temperature distribution is hardly influenced by significant changes in h_f. However, the fire propagation speed V(t) is a strong function of the gas stream-to-fuel heat transfer coefficient h_f. So it is this free parameter that is used to fit the condensed- hase equations to fire-front history data. Figure 3.3 shows the resulting model fit to three fire-front histories and table 3.1 reports all model parameters used in the model fitting procedure together with the fuel loading and air flowrates used. A listing of experiments performed with reference to data files stored (in the thesis) on disc appear in appendix B.

Run Number, Fuel	m'' kg/m^2	V_∞ x10^2 m/s	$\dot{m}''$ kg/m^{2}s	β -	U_d W/m^{2}K	U_{d2} W/m^{2}K	h_f W/m^{2}K	$\bar{\nu}$ x10^2 m/s	h_i W/m^{2}K
1 Iso	2.0	150	$9.30\text{x}10^{-3}$	0.947	50	35	2.8	0.972	3.9
2 Iso	2.0	31.0	$7.27\text{x}10^{-3}$	0.892	55	15	2.3	0.239	2.3
3 Iso	2.66	91.1	$10.3\text{x}10^{-3}$	1.69	31	31	3.4	0.676	3.3
4 Iso	3.66	65.3	$12.0\text{x}10^{-3}$	1.63	38	25	4.0	0.409	3.0
5 Iso	3.66	31..	$11.0\text{x}10^{-3}$	1.21	50	17	3.6	0.193	2.3
6 Iso	3.66	111	$15.9\text{x}10^{-3}$	2.20	26	40	5.0	0.806	3.3
7 Butol	3.34	64.4	$8.44\text{x}10^{-3}$	1.42	30	22	6.0	0.358	3.0
8 Butol	2.66	28.3	$7.31\text{x}10^{-3}$	0.962	51	15	3.5	0.134	2.2
9 Eg	3.34	27.9	$6.95\text{x}10^{-3}$	0.937	50	15	4.8	0.093	2.3
*10 Iso	3.66	31.4	$12.0\text{x}10^{-3}$	1.59	42	18	3.0	0.194	2.3
*11 Butol	2.66	27.7	$6.29\text{x}10^{-3}$	0.777	55	15	4.0	0.126	2.3

*Repeat runs.

TABLE 3.1. Model parameter listing for all experiments. Also shown is h_i the duct inside film heat transfer coefficient as estimated from correlations for air flowing in conduits.

The reported values represent the "best" fits. They were merely

determined by visual comparison of the model curve and experimental data of gas temperature versus χ or fire-front versus t. Exact methods used will be described later. It is very convenient that the parameters can be fitted individually because every free parameter affects a unique feature of the curves T(x) and $\chi^{\circ}(t)$. Table 3.1 also reports values of the duct inside heat transfer coefficient, h_i, estimated from literature correlations (Coulson and Richardson, 1986). The difference between h_f and h_i is that h_f is estimated from the model fit, whereas h_i is calculated from heat transfer correlations for hot air flowing through conduits.

Fuel burning rate

The fuel burning rate determines the time t_{res} the fire will take before it "jumps" from its initial position (the length of the horizontal part of the curves in Fig. 3.3). To calculate γ the initial fuel loading m° is divided by the measured time t_{res}.

Reaction stoichiometry

For the reaction stoichiometry there are a large number of possible combustion reactions. The stoichiometric coefficient β is therefore also calculated from data. Based on the fuel-rich fire assumption and using the measured combustion zone length X_{lbz}, β may be evaluated as

$$\beta = (\gamma C_f X_{lbz})/(\dot{m}_a Y_{ox}).$$

The value of β cannot be predetermined since the exact combination of combustion reactions occurring in fuel-rich fires is unknown. Oxygen is limited in fuel-rich fires and a variety of reaction mechanisms may contribute to incomplete combustion of fuel molecules. The expected combustion products are therefore CO, C, large sooty hydrocarbon molecules and H_2O. In some cases H_2 has also been observed as a combustion product (Kennedy and Roberts, 1964). A consequence of not knowing the exact chemical reactions in the combustion process is that the value of the heat of combustion will also remain unknown. For

the purpose of estimating an approximate value of the heat of reaction $\Delta\hat{H}_r$ complete combustion is assumed. That is when CO_2 and H_2O are the only products.

If complete combustion occurs the following β values are expected:

$$C_8H_{18} + \frac{25}{2} O_2 \longrightarrow 8\ CO_2 + 9\ H_2O \qquad \beta = 0.286$$

$$C_4H_{10}O + 6\ O_2 \longrightarrow 4\ CO_2 + 5\ H_2O \qquad \beta = 0.385$$

$$C_2H_6O_2 + \frac{5}{2} O_2 \longrightarrow 2\ CO_2 + 3\ H_2O \qquad \beta = 0.776$$

Incomplete combustion may result in very different β values depending on the reactions. For example consider the following possible reactions resulting in incomplete combustion of 2,2,4-Trimethylpentane (isooctane):

$$C_8H_{18} + \frac{17}{2} O_2 \longrightarrow 8\ CO + 9\ H_2O \qquad \beta = 0.420$$

$$C_8H_{18} + \frac{9}{2} O_2 \longrightarrow 8\ C + 9\ H_2O \qquad \beta = 0.793$$

$$\frac{n}{8} C_8H_{18} + \left(\frac{5n}{16} - \frac{1}{2}\right) O_2 \longrightarrow C_nH_{(n+2)} + \left(\frac{5n}{8} - 1\right) H_2O$$

For any large n, $\beta \geq 1.427$

If the hydrocarbons that are formed from incomplete combustion have an even higher H to C ratio than shown above, the value of β can be larger than 1.427. The same analysis can be applied to other fuels.

Duct heat transfer coefficients U_d and U_{d2}

U_d is estimated by adjusting its value until the combustion zone model produces a maximum gas temperature close to that of the data points on a T(x) plot. U_{d2} is adjusted until the excess fuel zone model produces a gas temperature decay that matches the data. The heat transfer coefficient for the combustion zone, U_d, is evaluated first because it is

independent of the excess fuel and preheating zone heat transfer coefficient U_{d2}.

Comparison of these heat transfer coefficients is possible with correlations from Coulson and Richardson (1986). Assuming a thin duct wall the duct overall heat transfer coefficient is written as

$$\frac{1}{U_{overall}} \approx \left(\frac{1}{h_i} + \frac{1}{h_c}\right),$$

where h_i is the film heat transfer coefficient inside the duct and h_c is the outside film heat transfer coefficient due to outside natural convection.

Coulson and Richardson (1986) is used to estimate h_i, and Burrows *et al* (1984) is used to estimate h_c as

$$h_c = 1.4 \left(T_{wall} - T_o\right)^{1/3}$$

Gas-to-fuel surface heat transfer coefficient h_f

According to the sensitivity analysis in section 2.4.1 h_f has a very weak influence on the gas temperature profile. Figure 2.11 shows h_f to have a strong effect on the fire propagation history and speed. This is purely because of its direct influence on the rate at which fuel is volatilized ahead of the fire. Therefore the value of h_f is best determined by varying until the fire propagation rate v, predicted by the model, matches the final slope suggested by fire-front versus time data.

Stationary gas temperature profiles for two fires are shown in figure 3.5, together with results from the gas-phase temperature model. Also shown are results from the combustion zone gas-phase temperature model where thermal radiation is included as a means of heat loss from the duct walls. That is, the solution to equation (2.26) is shown. In this case h_i and

h_c, the duct inside and outside heat transfer coefficients, are calculated from correlations (Burrows *et al*, 1984; Coulson and Richardson, 1986) and used to estimate U_o, the overall duct heat transfer coefficient. The duct wall emissivity ϵ is then used as the only model fitting free parameter. Table 3.2 shows these results. It is worth mentioning that the combustion zone model equation (2.26) for gas temperature was found to be very sensitive to ϵ compared to the much weaker effect of U_o. Emissivities for various types of steel surfaces can range from 0.3 for mild steel to 0.6 for oxidized steel (Perry, 1984).

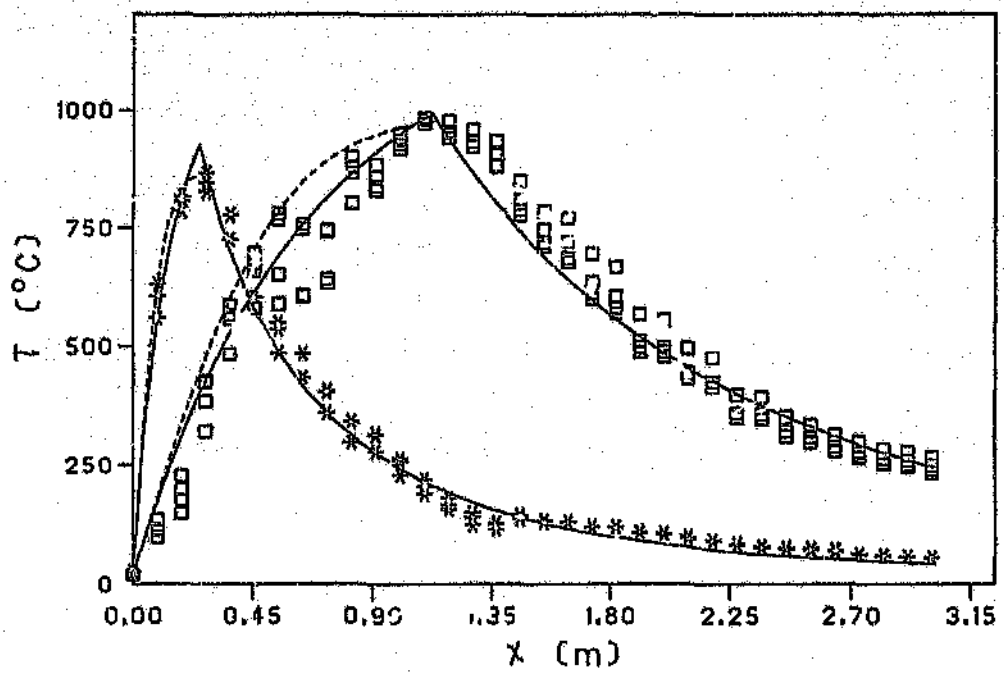


FIGURE 3.5. Comparison of gas temperature profiles from run 1 (□) and run 5 (*) with proposed model (——). Combustion zone model solved with the radiation term is also shown (----).

Run Number	1	2	3	4	5	6	7	8	9
U_o (W/m^2K)	2.6	1.8	2.3	2.1	1.8	2.4	2.1	1.7	1.7
ϵ	0.42	0.60	0.30	0.42	0.60	0.60	0.60	0.60	0.60
X_{lbz} (m)	1.12	0.27	1.09	0.64	0.25	1.10	0.80	0.26	0.28

TABLE 3.2. Combustion zone parameters where thermal radiation is included as an important pathway for heat losses.

Remaining model parameters are known *a priori* and are reported in tables 3.3(a) and 3.3(b) below.

$P_o = 0.84atm$	$C_d = 0.085m$	$\hat{C}_p = 1400J/kgK$ $X_{ar} = 1.556x10^{-3}m^2$
$C_f = 0.05$ m	$Y_{ox} = 0.21$	$T_o = 15\ ^oC$ to $30\ ^oC$

TABLE 3.3(a). Parameters known for each run.

FUEL MOLECULAR FORMULA	$\hat{\Delta H}_r$ [J/kg O_2] Complete Combustion	$\hat{H}_{vap}$ [J/kg]	T_{vap} [^oC]
C_8H_{18}	$-12.76x10^6$	$27.2x10^4$	99.2
$C_4H_{10}O$	$-13.07x10^6$	$58.3x10^4$	117.7
$C_2H_6O_2$	$-14.07x10^6$	$84.7x10^4$	197.2

TABLE 3.3(b). Fuel parameters.

3.4 Discussion

In the light of the present theory the self-similar form of the gas temperature profiles displayed by data in figure 3.2 provide conclusive evidence for a steady state gas phase process. Figures 3.4(a), 3.4(b) and 3.2 also show that the stationary fire (first temperature profile) is almost identical to the migrating fire (second and third profiles). The regular structure in figure 3.4(b) is a very clear indication of a steady-state gas-phase process. Therefore neglecting to correct for the air flowing into the control volume, as a result of adopting the lagrangian coordinate system, is a valid and useful simplification for modelling such systems. Figure 3.2 also shows that preheating of the air entering the burning zone is minimal and this justifies the thin wall assumption.

Although the gas-phase equations suggest a sudden change in temperature gradient at the end of the combustion zone this behaviour is only observed in small fires such as run 5 and not in fires with large air velocities. Run 1 in figure 3.5, for instance, shows a relatively smooth temperature transition from the combustion zone to the excess fuel zone. The discontinuity in the model equations comes from the assumption that the fuel burning rate is independent of position and that burning halts at x_1. Neglecting radiation also makes a more distinct discontinuity. Realistically, the gas-phase reaction rate is likely to slow down significantly as oxygen concentrations become smaller at regions near the end of the combustion zone. In this regime a constant γ assumption is likely to break down as reaction kinetics may control the rate of burning. The result is a more gradual temperature transition from the combustion to the excess fuel zone. Di Blasi *et al* (1989) show this concentration effect near the flame tip of a wind aided fire. In spite of this assumption the model fits the experimental data very well.

Duct heat transfer coefficients used in model fitting suggest that thermal radiation is a likely mechanism for heat losses from the duct walls. U_d and U_{d2} are clearly too large when

compared to literature values U_o. Excepting run 6, U_{d2} is smaller than U_d probably because of the lower gas temperatures, and hence less radiation, in the excess fuel and preheating zones. When the model includes thermal radiation duct surface emissivities correspond reasonably with literature values. One can in principle readily include radiation in the model but with an increased complexity in solving the equations.

U_o in table 3.2 is purely for convective heat transfer and does not include radiative effects. If comparison of U_d and U_{d2} is to be made with predicted values then radiative heat transfer effects must be added to U_o and only then compared. For example run 2 has its average gas temperature close to about 400°C, but the outer surface temperature of the duct would be somewhat cooler. If the surface temperature is about 300°C and $\epsilon \approx 0.6$ then one should add about 12.4 W/m^2K to U_o in order to account for radiation. This is estimated only for the decaying portion of T(x) for run 2. This radiation term is calculated from an expansion of the Stefan-Boltzmann equation in the form of the convection-type equation. See equation (E.3) appendix E. It is only approximate because it is based on the average surface temperature. The model estimated value of U_{d2}=15 W/m^2K is close to the predicted estimate of about 14.2 W/m^2K ($=U_o+12.4$ W/m^2K) which is quite reassuring.

It should be mentioned at this stage that the exact reactions occurring are unknown. Comparison of model estimates of β with those determined from complete combustion indicates that actual reaction stoichiometry is unknown. It was demonstrated in section 3.3 that there is a large range or combination of possible reactions that may contribute to these β values. Consequently, $\Delta\hat{H}_r$ is only a rough estimate of its true value. This will certainly affect estimates of U_d and ϵ, causing inaccurate estimates that do not display trends with V_∞. Also, runs 1 and 6 were performed with air velocities near to extinction (blow-out) conditions and in the case of run 6 the fire actually died out before reaching the end of the test section. It is probable that this reflected poor estimates of γ and β and would strongly influence fits of U_d since the model

is not formulated to account for blow-out effects or conditions.

Transient growth of fires from ignition to a state of maximum size is a problem that has received no attention in developing the mathematical model. Most experiments showed that such growth rates are rapid in comparison to fire propagation along the duct. Transient growth behaviour becomes important when larger air flowrates are used and the fire is allowed to expand over a long burning zone. The growth rate is slowed down even further if low volatility fuels are used. Under such conditions fire growth is slow enough to be observed in fire-front history data. The initial part of run 4 in figure 3.3 shows this transient growth phenomenon. This effect is not reflected in runs 5 and 8 probably because the burning zones are small and the ignition source is sufficiently large to cover this distance rapidly.

All results in figure 3.3 show the fires growing from ignition to a maximum size and thereafter remaining in their original location inside the duct. As soon as the fuel in this region is consumed the fire "jumps" displacing approximately one combustion zone length along the duct. Then the jumping attenuates rapidly to a relatively constant speed. All of these fire propagation characteristics are in complete agreement with the model. What is most reassuring is the value of h_f that would generate this model prediction. Although fitted h_f values do not follow a general trend with respect to V_∞ they are very close to literature correlations of internal film heat transfer coefficients for nonreactive flows in conduits. The use of liquid fuels results in large vaporization rates ahead of the fire consequently rapidly shaping the fuel profile to such an extent that $(\partial m/\partial \chi)|_{\chi=0}$ reaches its steady state value soon after the first "jump". Clearly then, if fuels are chosen to be less volatile, perhaps solid fuels, the model would suggest unsteady fire propagation for longer periods of time. This merits further experimentation and will be examined in later sections.

The effect of air flowrate on combustion zone length is seen in table 3.2. A graph representing this relationship is seen in figure 3.6. There seems to be a linear direct dependence between air flowrate and combustion zone length as expected from fuel-rich fires. Toward higher air velocities though, close to blow-out conditions prevail and γ may change, leading to the observed deviation from linear dependence as shown in figure 3.6.

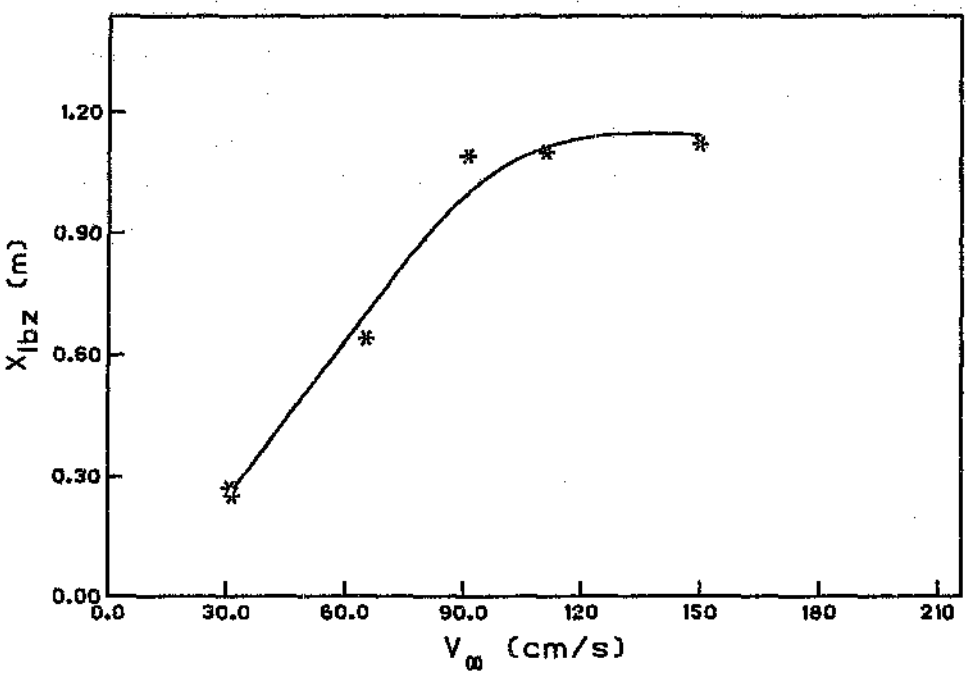


FIGURE 3.6. Air flow effect on combustion zone length for isooctane fuelled fires in non-stratified flow.

This analysis is devoted to fitting model equations to experimental data and thereafter examining the resulting parameter estimates with respect to their physical significance. For the most there is good agreement between model estimates of free parameters and literature values. The sensitivity of model predictions to the various free parameters is also critical in determining whether reliable *a priori* predictions are possible. Such predictions would also require good estimates of the

combustion reaction stoichiometry and burning rates. A simple but crude sensitivity analysis has been performed by setting all free parameters to typical values as estimated from such experiments (see section 2.4.1). Thereafter one may vary each parameter individually to obtain an indication of its effect on the gas temperature profile and fire-front history. Section 2.4.1 presents such a study and is adequate if predictions are required at similar conditions. The following chapter will present an experimental study of duct fires supported by solid fuels. Parameters will be estimated in the same manner presented here and the fuel mass profile m(x) of Polymethylmethacrylate (PMMA), measured at steady state, will be predicted without any further adjustments to the fitted model parameters. This analysis will reveal useful information about the predictive capabilities of the proposed model and help to interpret some of its assumptions.

3.5 Conclusion

A one dimensional theory with a pseudo-steady-state gas temperature profile for the propagation of fires in fuel-lined ducts has been derived. A set of experimental results on three fuels in a small duct have been obtained.

The model accurately describes the centre-line (average) gas temperature profiles inside the duct as well as fire propagation histories. This analysis has revealed that for the scale and class of fires studied convective heat transfer from the gas stream to the condensed fuel governs to a great degree the fire propagation history and average propagation speed. For the case of thin duct walls heat losses from the system to the surroundings is significantly dominated by radiative heat transfer especially from the flaming region of the duct. One might therefore speculate that radiative heat transfer from the fire-front to condensed fuel could become significantly important in larger scale fires where the fuel surface-to-fire front view factor is dramatically enhanced. Use of the present model for deterministic predictions of duct fire dynamics

requires further knowledge of fuel burning rates and reaction stoichiometry.

A fundamental concept arising in theory is illustrated by virtue of experiment, namely the important distinction between fire propagation rate $\dot{p}$ and fire propagation speed V(t) defined herein. Emerging from this study is the result that the condensed fuel profile $n(x,t)$ is the key to understanding how a fire traverses through the confines of a duct. The familiar assumption of constant fire propagation speed in typical duct fire scenarios can break down and the possibility of a periodic fire propagation motion is shown to exist. One may conclude from the observed "jump" phenomenon that the assumption of constant burning rate with respect to distance inside the combustion zone is realistic for the major part of this region.

Theoretical considerations and mechanisms which have been identified in this study suggest that if fuel volatility is increased steady-state is achieved sooner in the propagation history. The same effect is expected if heat transfer from fire to fuel is enhanced.

It is clear from a simplified Froude number analysis and the experimental and model comparison that although the reactive flow stream is not well mixed it is plausible, in this case, to work with the approximation of an average gas temperature. This approximation clearly simplifies the mathematical analysis from solving three-dimensional equations describing the gas phase processes to the much simpler one dimensional model presented here. It is likely that in the case of large scale mine tunnels, with moderate ventilation currents, the one dimensional approach may provide an adequate description of the process because of the larger Reynolds numbers. If more detail is required to describe duct fires with laminar flow conditions then clearly a more rigorous analysis with the inclusion of mixing would be necessary. The case where the flow is poorly mixed and severe stratification occurs will be considered in detail in chapter 5.

One can in conclusion say that the fundamental assumptions of the model (fuel-rich fires, steady-state gas profiles, heat transfer dominated process) seem to hold up well in practice. This leads to a reasonably simple model with good powers of prediction. Many of the parameters used in this model can be estimated from existing correlations.

At this stage it may also be of interest to note that much of the work presented in chapters 2 and 3 has also been published (Comitis *et al*, 1994a) as part I of a series of three papers This should provide a more concise presentation of the main features explored up to this stage in the thesis. A copy of this publication is provided in appendix F. Parts II and III (Comitis *et al*, 1994b; Comitis *et al*, 1994c) of this series of papers have been derived from work explored in chapters 4 and 5 of this thesis and shall be submitted to the same journal.

4 SOLID FUELLED FIRES

The topic of this chapter is to extend the analyses of chapters 2 and 3 to a case of fires in a ventilated duct lined with solid instead of liquid fuels. Most confined fires in self sustained or forced convective flows are supported by solid fuels such as plastics, fossil fuels or flammable liquids frequently soaked in porous media (e.g., carpet, wood). The proposed model has already been analyzed with experiments using liquid fuels soaked in a porous solid inert. The use of solid material as fuel lining provides a system where an independent measure of the fuel loading distribution m(x) is also practically possible. An experimental study of this variable aids to corroborate the phenomenology proposed in the model to a greater extent. m(x,t) is identified in the formulation as being directly related to transient fire propagation along the duct.

Inherent in most models (Roberts and Clough, 1967; Hunter and Favin, 1981; de Ris, 1970), including the present, is the assumption of a radially well mixed flow stream moving in the direction of fire propagation. A direct consequence is the assumption of maximised heat feedback to the solid fuel source resulting in rapid fire propagation. A condition of maximized heat feedback has already been studied with liquid fuels in chapter 3 and will now receive attention in a solid fuel analysis. This study may provide useful clues as to whether the discovered jump phenomenon is repeated if fuel volatility is decreased by using solid fuels.

In chapter 2 it was shown that fire motion at any moment in time is governed by the fuel distribution inside the combustion zone at that moment. Studies in chapter 3 verify the useful assumption that each model zone is constant in size as the fire propagates along the duct (pseudo-steady-state gas phase assumption). As the combustion zone progresses along the duct it encounters a fuel profile already shaped by the excess fuel zone. This fuel profile is consumed uniformly in the combustion zone (constant γ) and the fire moves in a manner described by

equation (2.22). In turn, this motion determines the way in which the excess fuel zone will shape the fuel lining ahead of the combustion zone. This provides a newly shaped fuel profile to be encountered by the combustion zone at a later stage. Clearly this is a manifestation of the familiar feedback cycle through which fires propagate. This same feedback mechanism therefore also has a profound influence on the fuel profile history and consequently fire motion along the duct.

It is worth noting that fire propagation in this context implies the forward migration of a fully developed fire along the duct and not fire spread or growth from an ignition source to a fully developed state. Although both these processes result in forward motion of the fire-front they are essentially different dynamics. It will also be shown in this section that fire spread is a more prominent feature when solid or less volatile fuels are in question. A brief analysis of fire spread will be conducted in this chapter because of its importance on the fire process. Specifically to assess the concept of vaporization temperature as a fire spread controlling mechanism. Of course flame spread over fuel surfaces has received much experimental and theoretical attention by various researchers (Fernandez-Pello, 1979; Fernandez-Pello and Mao, 1981; Loh and Fernandez-Pello, 1984; Apte *et al*, 1991; Di Blasi *et al*, 1989; Ishida, 1986; Ishida, 1988; Ishida, 1992).

4.1 Experimental

Solid strips and shavings of polymethylmethacrylate (PMMA) were used as solid fuel lining. PMMA is widely used in experimental studies of fire phenomena and is therefore a familiar substance with known burning properties. Such properties are often quoted in the literature. It is therefore desirable to work with PMMA from a modelling point of view. A trial run was also conducted using charcoal but this will be discussed later. A schematic of the equipment and fire duct arrangement are shown in figure 3.1 of chapter 3. Experiments were carried out in the same duct as that used for liquid fuel studies. The only difference is the

absence of the asbestos wick from the 3 meter long fuel tray.

Fuel strips were cut from sheets of clear PMMA, each strip being 20 cm long and laid down end to end in the fuel tray floor forming a continuous constant (flat) fuel mass distribution with respect to distance. Each strip is 1 cm thick and 1 or 1.3 cm wide, depending on the specific run performed. In the case of experiments with PMMA shavings the shavings were collected from machined sheets of clear PMMA. Fifteen portions of equal mass of shavings were then weighed. Each equal portion was distributed evenly over a 20 cm segment that constitutes the fuel tray length.

To examine the model it is necessary to conduct experiments in such a way that initial conditions are well known. Since the model is deterministic in nature and attempts to describe the system variables with respect to time, setting the desired initial condition is absolutely essential. This work will focus on a typical case where initially fuel is evenly distributed with a constant loading with respect to duct length. The model does not address the phenomenon of fire growth and assumes the fire to grow to its fully developed size almost immediately after ignition. In chapter 3 this was shown to be a good assumption for liquid fuels soaked in a porous solid. However, for solid fuels transient growth is more significant (see figure 4.1) and will therefore affect the initial fuel distribution in a way not accounted for by the model. For this reason it is necessary to avoid the growth pattern by igniting the fuel lining over a length equivalent to the combustion zone length. That is, instead of employing a point ignition source at $x=0$ and allowing the fire to grow as in the case of studies in chapter 3.

The fully developed combustion zone length was estimated from trial experiments on PMMA where the fire was allowed to grow to its fully developed size. This is achieved when the combustion zone reaches its maximum length, controlled by the rate of air supplied to the duct. An oxy-acetylene torch was used as the ignition source. As soon as the air supply to the duct is set

and a desired length of fuel lining is set alight, the fuel tray is inserted into the duct and the data logging arrangement initiated to record gas stream temperatures. This technique was adopted for both PMMA strip and shaving experiments.

In the case of PMMA strips it was possible to measure the solid fuel profile. This was done by cutting the air supply at any moment when the fire was propagating at a steady rate (steady-state). By doing this it is possible to examine the steady state fuel distribution in the light of the proposed theory. The fuel lining resulting from steady fire propagation is removed and cut into small segments of about 2 to 3 cm. Each segment is weighed and measured so that an independent measure of m(x) is calculated at the end of each experiment. This represents the measured steady state fuel profile for each fire.

A trial run was also conducted with small charcoal particles (~0.5 cm diameter) uniformly distributed along the fuel tray. Start-up procedure was similar to that of PMMA studies.

4.2 Results

4.2.1 Polymethylmethacrylate (PMMA)

Measurements of three system variables were acquired from each experiment, namely the gas stream temperature profile T(x,t), fire propagation history $\chi_0(t)$, and the steady-state solid fuel profile m(x,t). Most model parameters are known *a priori* to the analysis. The latent heat of pyrolysis for PMMA is taken to be 903.7 kJ/kg. This is taken from Kanury (1974) where the sensible heat raising the fuel from ambient to pyrolysis temperature has been subtracted. The vaporization temperature and heat of combustion for PMMA is taken from Fernandez-Pello (1979) to be 363 °C and -13.57×10^6 J/kg of O_2 respectively. Other parameters are known from the duct geometry or estimated by fitting the model equation to experimental data. Simplified techniques for estimating each free parameter have been discussed in chapter 3. Parameters estimated from the model-fit

are the fuel burning rate γ, reaction mass stoichiometric coefficient β, duct wall heat transfer coefficients U_d and U_{d2}, duct wall surface emissivity ϵ, and gas stream-to-fuel surface film heat transfer coefficient h_f. The value of h_f determines the rate of fuel vaporization in the excess fuel zone and therefore has a direct influence on the average fire propagation speed and propagation history.

Fire growth from a point ignition source to a fully developed fire over surfaces soaked in flammable liquids was found to be rapid and not significant in comparison to the remaining fire propagation process (chapter 3). In the case of PMMA transient fire growth shown in figures 4.1 and 4.2 is quite significant and would clearly affect the initial fuel profile. Among others Loh and Fernandez-Pello (1984) have studied fire growth or spread over PMMA surfaces in wind-aided environments. Figure 4.2 shows the fire-front history $\chi_f(t)$ of the same PMMA supported fire of figure 4.1. Figure 4.2 is a plot of the maximum temperature position χ_f versus time t. Maximum temperature positions are determined from parabolic interpolation of temperature data and are assumed equal to the fire-front position. The plot (figure 4.2) is used to determine the initial fire growth or spread rate. Initially $\chi_f(t)$ is horizontal during the ignition period when an external heat source (natural gas burner) is used. After sufficient heating the external heat source is removed and the fire spreads over the PMMA surface (sloped section of $\chi_f(t)$ data). An analysis referring to fire growth over PMMA will appear later in the discussion section.

As discussed in the experimental section fire growth is avoided in the main tests by intentionally setting the entire combustion zone alight at the start of each run. This study will focus more attention on propagation than spread or growth.

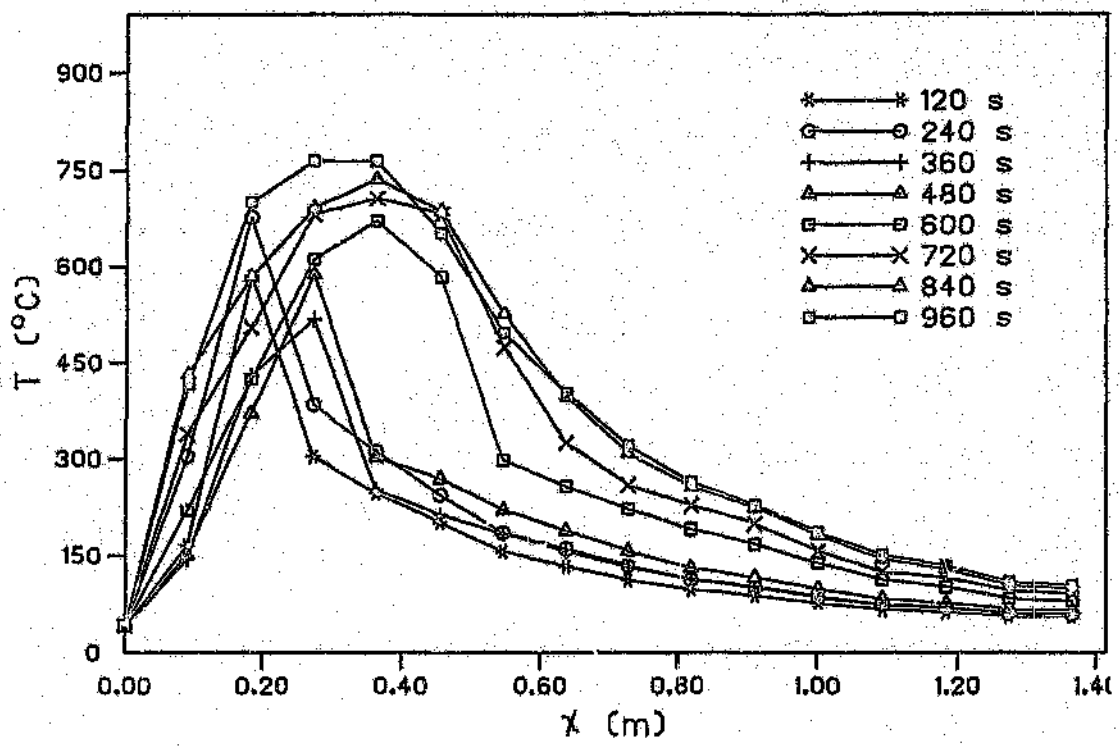


FIGURE 4.1. Fire growth from point ignition source to fully developed size over a PMMA sheet 6 mm thick, 30 mm wide, lying flat on fuel tray floor. Gas temperature profiles shown at 2 minute intervals.

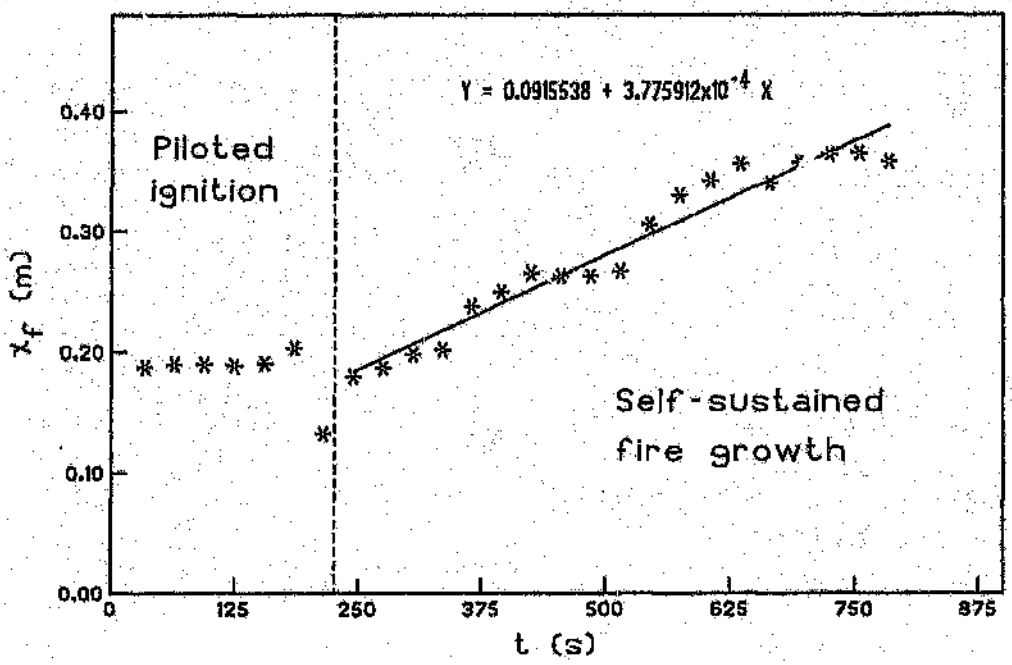


FIGURE 4.2. Fire growth data.

Steady state gas temperature profiles for two fully developed PMMA fires are shown in figure 4.3. The model-fit is shown in each case. Also shown are estimated gas temperature profiles in the combustion zone if thermal radiation is incorporated into the model equation as a mode of heat loss. That is, when $\varepsilon \neq 0$ in equation (2.25).

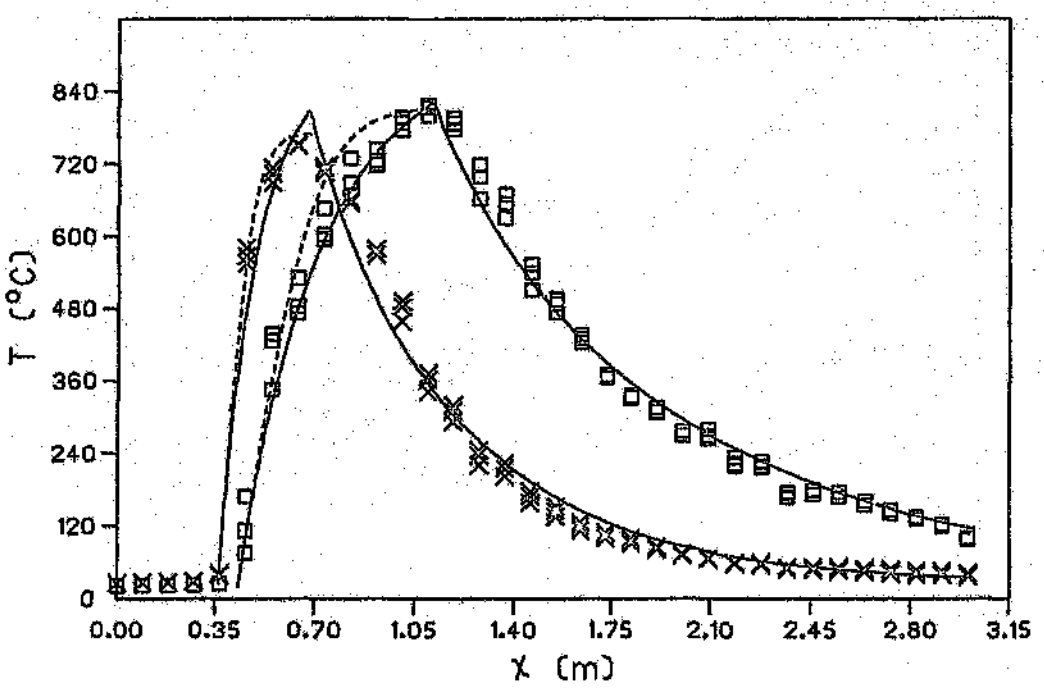


FIGURE 4.3. Gas stream temperature profiles for two typical fully developed duct fires supported by PMMA (run 3 (x) and 5 (□)). Proposed model fit is also shown in each case with radiative (----) or without (——) radiative model.

The profiles shown in figure 4.3 are for stationary fires at the start of the duct section when the motion of the combustion zone has not yet begun. By estimating the position of the maximum temperature for each measured temperature profile it is possible to follow the fire from position in the duct as a function of time. The maximum for each profile is again estimated using parabolic interpolation and taken to represent the end of the combustion zone. Fire propagation history data are shown in figure 4.4 for three typical PMMA fires. Figure 4.5 shows a contour diagram of the time evolving gas temperature profile for run 2 and may be compared to figure 3.4(b) in chapter 3. This comparison is discussed later.

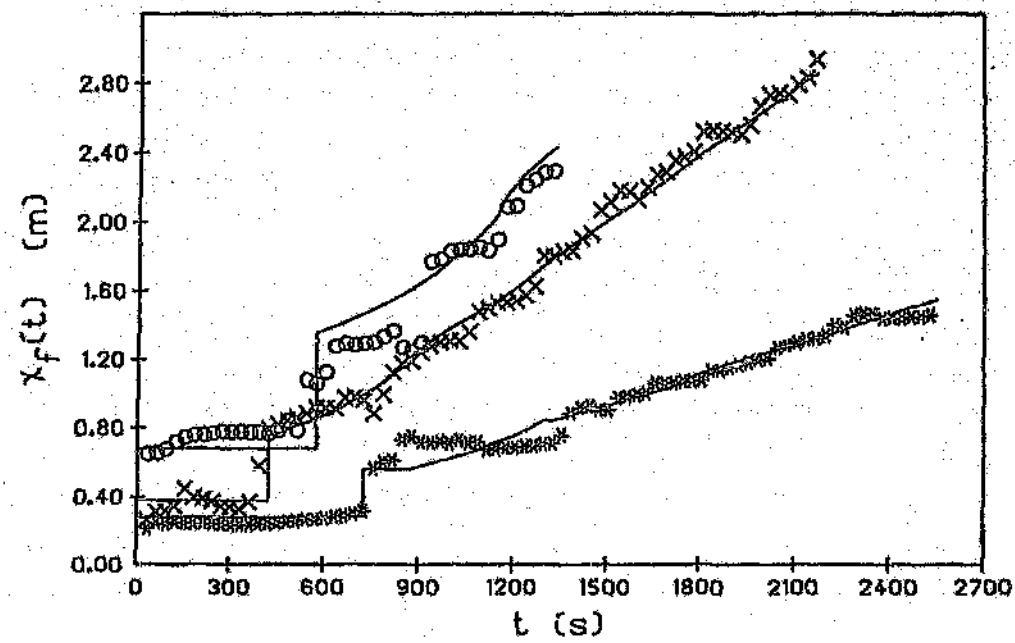


FIGURE 4.4 Progressive motion of the combustion zone represented as fire-front propagation $\chi_f(t)$ for three duct fires (run 2 (*), 5 (o) and 7 (x)). Proposed model is also shown (——).

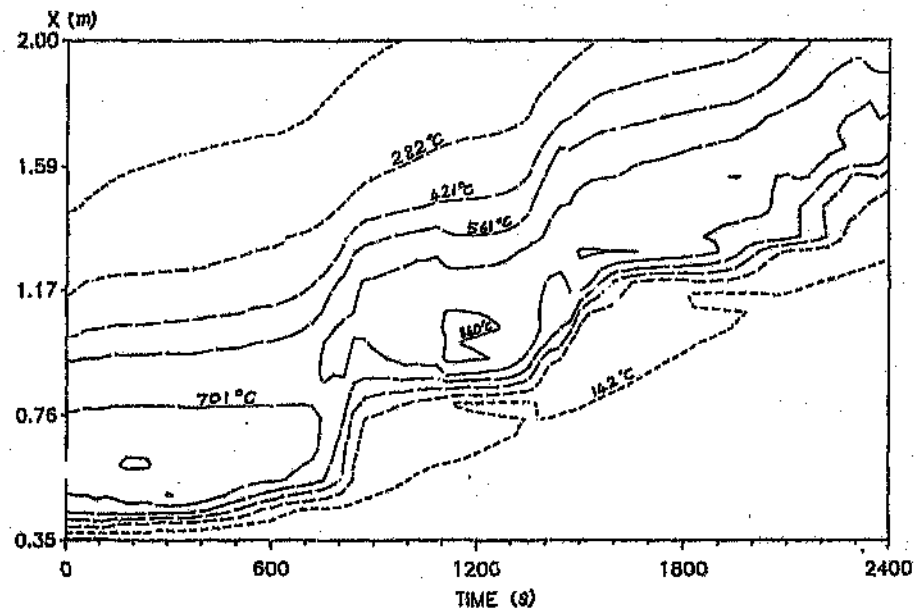


FIGURE 4.5. Contour diagram of time evolving gas temperature profile inside the duct for run 2 (PMMA).

The system variables and estimated parameters for all experiments are shown in table 4.1. In the case of fitting the combustion zone equation with $\epsilon \neq 0$ the overall duct wall heat transfer coefficient U_o is estimated from typical literature correlations (Burrow *et al*, 1982) and the value of ϵ is evaluated from the fit.

Run Number	$\dot{m}''$ kg/m^2	V_∞ cm/s	γ kg/m^{2}s	β -	U_d W/m^{2}K	U_{d2} W/m^{2}K	h_f W/m^{2}K	h_i W/m^{2}K
1 Strips	4.52	33.3	6.50×10^{-3}	0.59	50	17	9.5	1.9
2 Strips	4.79	29.8	6.60×10^{-3}	0.53	60	17	9.0	1.4
3 Strips	3.86	29.3	7.56×10^{-3}	0.63	60	18	9.5	1.4
4 Strips	3.82	29.1	6.97×10^{-3}	0.60	59	18	9.5	1.4
5 Flakes	1.74	36.3	3.03×10^{-3}	0.67	31	12	5.9	1.7
6 Flakes	1.74	32.3	4.11×10^{-3}	0.55	50	17	7.0	1.5
7 Flakes	1.74	32.0	4.11×10^{-3}	0.58	52	17	8.3	1.5

TABLE 4.1. Duct fire conditions and estimated model parameters for all experiments. Also shown is h_i the duct inside film heat transfer coefficient as estimated from correlations for air flowing in conduits.

Table 4.2 shows values of ϵ used to fit the combustion zone model for the case when radiative heat loss is incorporated. Also shown are some general fire characteristics, namely the length of each zone x_1 and $x_2 - x_1$, steady-state fire propagation speed V_{ss}, and percentage of heat generated by combustion that is fed back to the solid fuel up to the end of the combustion (α_1) and excess fuel (α_2) zones according to equation (2.2). These fire characteristics are determined using the model-fit.

Run Number	U_o W/m^2K	ϵ	x_1 m	$(x_2 - x_1)$ m	V_{ss} cm/s x10	α_1 %	α_2 %
1 trips	1.6	0.65	0.45	0.70	1.00	3.9	6.1
2 Strips	1.2	0.70	0.28	0.47	0.59	3.5	5.4
3 Strips	1.2	0.76	0.32	0.40	0.83	4.2	5.5
4 Strips	1.2	0.76	0.33	0.40	0.80	4.0	5.3
5 Flakes	1.5	0.33	0.68	0.72	1.66	4.5	6.3
6 Flakes	1.3	0.65	0.35	0.47	1.21	3.6	5.4
7 Flakes	1.3	0.70	0.38	0.42	1.27	3.9	5.5

TABLE 4.2. Duct wall emissivities estimated from model fit. Some fire characteristics determined from the model are also shown.

All model parameters are known after fitting the model to gas stream temperature data and fire propagation histories. It is now possible to solve the fuel loading profile m(x,t) using the model equations on the basis of the estimated model parameters. Figure 4.6 shows predicted fuel profiles for approximately steady state conditions together with measured profiles from four PMMA strip experiments. These are the profiles, measured and predicted, at a time when the fire is propagating at relatively constant speed. Constant fire propagation speeds are identified as straight lines from plots such as those in figure 4.4.

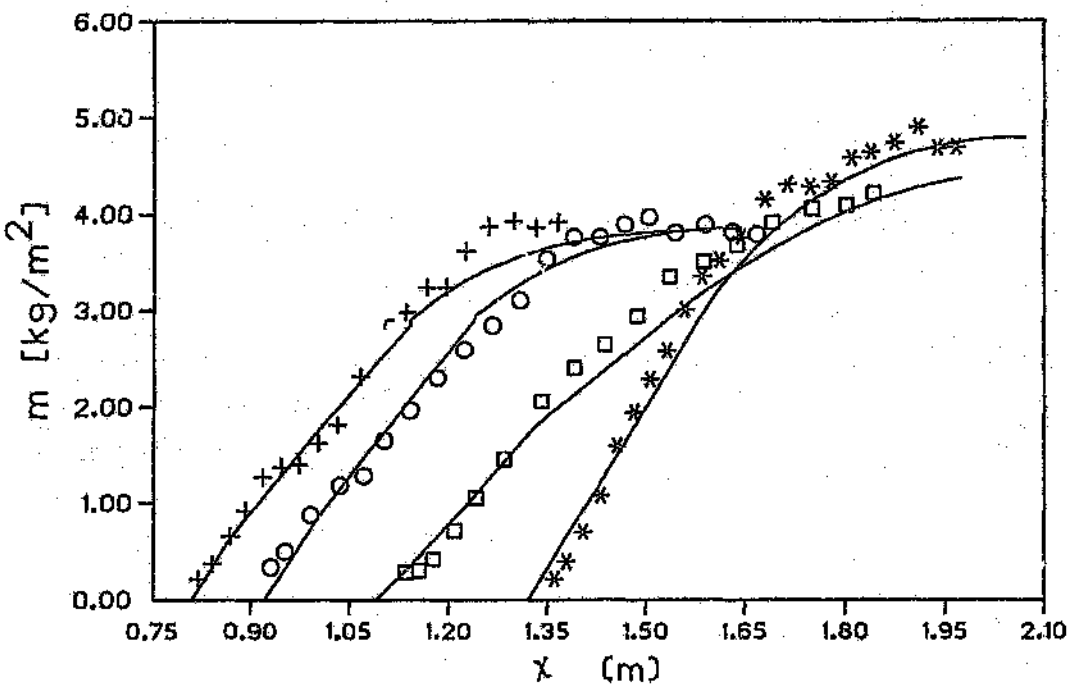


FIGURE 4.6. Measured fuel mass distributions for run 1 (□), 2 (*), 3 (o), and 4 (+) after sufficient time has evolved to allow relatively constant fire propagation speeds. Model prediction (———) is compared in each case.

A number of trial experiments were performed in order to establish combustion zone lengths for all of the runs. As described earlier this information was used when setting the desired initial condition for each run. Trial experiments with flakes together with run 5, 6 and 7 have also been used to examine the effect of air mass flow and fuel loading on the final steady fire propagation speed V_{ss} (figure 4.7). In this case V_{ss} is estimated from linear least squares fits on the straight line section of plots such as those in figure 4.6. Air flowrate and mass fuel loading vary from one data point to another in figure 4.7. For a list of data files from experiments in this chapter see appendix B which also contains stored files on a disc.

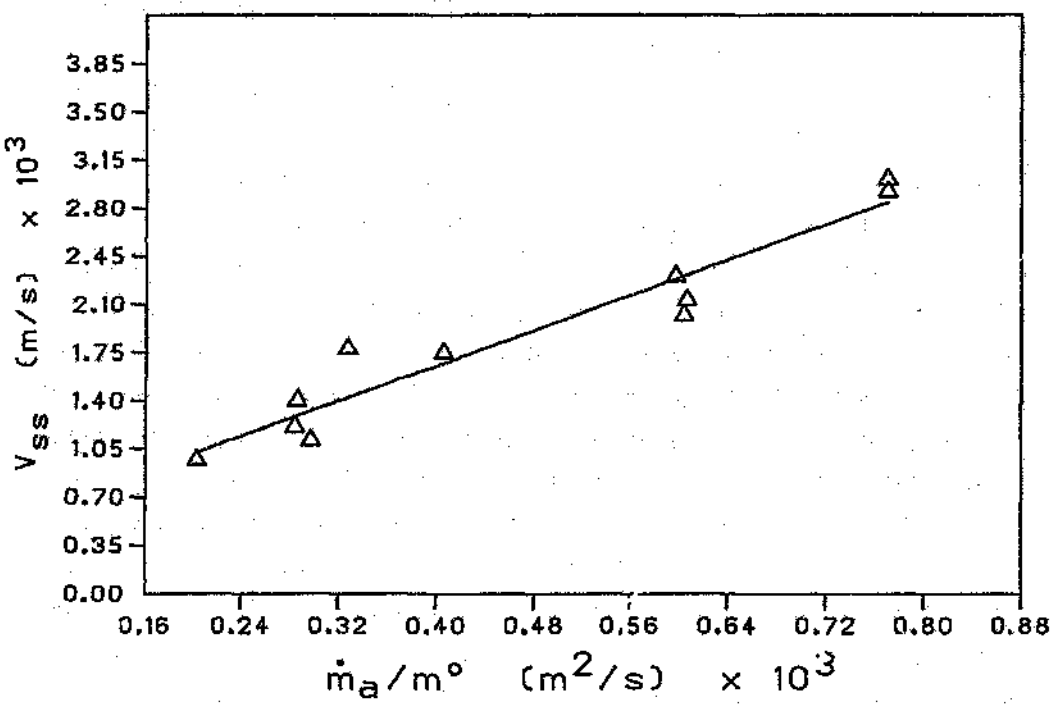


FIGURE 4.7. Effect of air mass flowrate supplied to the duct and solid fuel mass loading on steady fire propagation speed.

4.2.2 Char-Coal

A trial run showed that char-coal burnt over approximately 1.8 meters of lining for a significant period and then extinguished without progressing forward. Char-coal experiments in the present apparatus were very difficult to perform primarily because of ignition problems due to large heat losses that may have also resulted in the above observation. On inspection the coal bed lining the duct was mostly consumed in the combustion zone but ahead there was no evidence of burnt coal. From combustion zone to "excess" fuel zone there was a step in fuel mass loading from almost no coal up to the initial mass loading which appeared unaffected. This feature was clearly evident by observation. Implications of such findings will be discussed later in view of the proposed model.

4.3 Discussion

4.3.1 Fire propagation

Evident in model predictions of fuel profiles of runs 3 and 4 (figure 4.6) are small steps occurring at the end of the combustion zone. This is because the model solution has not quite reached steady state though the difference would be small. The model prediction of run 1 shows a discontinuous bend inside the combustion zone. This is because the mechanism for fuel vaporization in the combustion zone differs functionally from that in the excess fuel zone. As a consequence of these zones also not [illegible] in length the excess fuel zone affects a longer [illegible] the combustion zone eventually burns over as [illegible] es forward. This discontinuity is inherent in [illegible] tions but is more evident in the model output of [illegible] ue steady state the bend is no longer present. Be[illegible] ove described features are small and therefore not expected to appear in measured data. Despite this, model predictions of fuel distributions inside the duct for steady propagating fires are very close to measured data. Since none of the parameters are ever fitted by using the fuel profile data, close agreement between the model prediction and measured fuel mass distributions is further evidence to validate the model. These are therefore good *a priori* predictions of steady state fuel profiles.

The present study also confirms that energy feedback in small scale duct fires is dominated by convective heat transfer. Such a conclusion comes from consistently good predictions of steady state fuel distributions that are ultimately determined by a convective heat transfer model at the fuel surface This conclusion was also arrived at from liquid fuel studies in chapter 3. If a constant fire propagation speed is achieved at steady-state then fuel vaporization ahead of the fire must be position dependent. This is understood from explanations provided in chapter 2. If fuel loss rate ahead of the fire was constant with respect to position the fire would continue

jumping all the way. Because fuel loss ahead of the fire is slower than inside the fire the initially flat profile would merely be transformed into a series of steps and would never form a line of constant slope. That is, constant fire propagation speed would never be achieved. In this study and in the previous chapter convective heat transfer is found to control fuel loss rates which result in a position (temperature) dependence ahead of the fire. Constant fuel loss rates ahead of the fire were proposed by de Ris (1970) and Roberts and Clough (1967) but are clearly not justified by present findings.

When the fire reaches its fully-developed size the gas stream temperature profile is rapidly achieved and maintained while the fire migrates along the duct. Equation (2.2) makes this pseudo-steady-state assumption, shown to be valid for fires supported by liquid fuels soaked in a porous solid (chapter 3). PMMA results reflect similar behaviour excepting when the fire moves rapidly in a step-like motion indicated in figure 4.4 and figure 4.5. During this rapid motion the net flow of air into the moving combustion zone is significantly reduced thereby instantaneously adjusting the gas temperature profile. Also, the solid PMMA temperature profile may take longer to readjust to such rapid effects and momentarily affect the fuel burning rate since this is controlled by heating effects. If this motion is rapid enough the effect on the gas and solid temperature structure should not last long enough to influence the solid significantly.

A pseudo-steady-state assumption is therefore also valid for the solid fuel case but to a somewhat lesser extent. Figure 4.5 shows the time evolving gas temperature profile for run 2 and should be compared to the more regular structure in figure 3.4(b). The liquid fuelled fire has a steadier temperature profile with respect to time, whereas that of PMMA in figure 4.5 is less steady as it moves. This effect is small but evident and is probably dominated by an interplay between propagation mechanisms described in the model and growth-type dynamics as the fire shrinks and grows slightly while propagating.

Model gas temperature profiles and fire front histories correlate with the measured data very well. Estimated model parameters from fitting procedures result in values that correspond closely to literature or expected values. For example the estimated duct wall emissivities using the combustion zone model range from 0.65 to 0.76 (excepting run 5), which corresponds to literature values for mild steel in this temperature range. This result explains why the duct overall heat transfer coefficients U_d and U_{d2} are so much larger when radiation is excluded from the model formulation. Run 5 represents the highest air flow condition of the PMMA flakes experiments and is not as consistent with this conclusion and particular set of results. It is likely that estimates of β and $\Delta\hat{H}_r$ are inaccurate and do not represent the true combustion properties, ultimately resulting in a poor estimate of ϵ and U_d. Complete combustion would result in a value of β equal to 0.52. Table 4.1 shows that run 5 has β=0.67 and represents the largest deviation from the complete combustion assumption. Therefore $\Delta\hat{H}_r$, calculated for complete combustion conditions, is likely to be more inaccurate in this case than in any of the others, resulting in a poor model estimate of ϵ. Most of the other runs have resulted in β values that are closer to that of complete combustion, hence the assumed value of $\Delta\hat{H}_r$ (complete combustion) is closer to the true values prevailing in those fires. Good estimates of ϵ are therefore obtained from these runs. It may also be that at higher air flowrates (run 5) the constant γ approximation breaks down. Gas stream concentration profiles would begin to control the reaction rate to an extent that vaporization kinetics need not dominate alone.

If γ is measured independently it may be compared to fitted values of table 4.1. By burning in an open environment a known mass of PMMA strip with known surface area and measuring the time taken to burn completely a value of $6.84\times10^{-3}kg/m^2s$ is obtained. This is very similar to those estimated using the model (see table 4.1).

Gas stream-to-fuel surface film heat transfer coefficients are almost 5 times larger than the expected values. Because this

parameter represents the degree of heat feedback to the solid fuel its estimate is strongly influenced by the value of the fuel latent heat of pyrolysis used in the model equations. Evidently, consistent estimates of the latent heat of pyrolysis for PMMA seem to be lacking in the literature. This is evident from varying estimates quoted by Kanury (1974). Therefore no firm conclusion may be drawn from this result. However, model estimates of h_f compared very well with h_l in liquid fuel studies of chapter 3 where the latent heat was well known.

It is interesting to note that although these duct fire results represent the case where heat feedback is maximized, only about 6 percent of the total heat generated goes back into the vaporization process. Despite the low percentage this value represents an upper limit resulting in rapid achievement of a constant fire propagation speed soon after the first fire "jump" is observed (figure 4.4). Most of the heat generated is lost to the surroundings or used to heat the flow stream. Clearly, fire propagation dynamics of this type must be extremely sensitive to energy feedback since it was also shown in chapter 2 that the exact distribution of heat flux at the fuel surface is critical in determining the migration history of a fully developed fire. For the liquid fuelled fires of chapter 3, α_1=4 and α_2=7 percent on average for all the fires, which is similar to what is seen in PMMA fires. The 6 percent of energy feedback is also in good agreement with results obtained by Sibulkin and Lee (1974) who studied energy feedback in flames spreading over PMMA cylinders.

The exact dependence of each estimated model parameter on air flowrate is not clearly evident. To observe such trends one would probably have to explore a wider range of air flowrates. Also, the model fitting procedure is only approximate. That is, the sum of the squared errors is not exactly minimised in each case. In spite of this, estimated parameters are relatively consistent in relation to expected values. However, v_{ss} does indeed follow a definite trend with respect to mass flow of air and fuel loading as figure 4.7 illustrates. The observed close to linear behaviour is also in agreement with the model as

equation (2.16) suggests. This behaviour also comes from the fuel-rich fire assumption. More specifically the combustion zone length is directly proportional to air flowrate and the excess fuel zone length is also nearly directly proportional to air flowrate. Hence fuel mass loss rates are directly related to these zone lengths and therefore air flowrate. As in the combustion zone lengths of chapter 3, combustion and excess fuel zone lengths in this study also increase with air flowrate as table 4.2 suggests.

4.3.2 Fire growth

Fire growth has been avoided by setting the appropriate initial condition as described in the experimental section. However it does form part of the natural fire phenomenon and would otherwise dominate the initial stages of the fire process. According to Loh and Fernandez-Pello (1984) fire spread rate V_p is correlated well with a heat transfer based model. The spread rate is determined by conduction through the gas and solid phases and the following rel tionship was developed

$$V_p \sim \frac{\rho_g C_p \lambda_g (T_f - T_v)^2}{\rho C \lambda (T_v - T_i)^2} V_\infty, \qquad (4.1)$$

where ρ_g, C_p, λ_g, are the gas density, specific heat capacity and thermal conductivity respectively. ρ, C and λ are the solid PMMA density, specific heat capacity and thermal conductivity respectively. T_i, T_v, T_f and V_∞ are the initial temperature, PMMA pyrolysis temperature, adiabatic flame temperature and average wind speed respectively. The constant of proportionality can be calculated from their data to be approximately 0.29. If the flame spread rate of the fire in figure 4.2 is calculated using relationship (4.1) a value of 1.3×10^{-5} ms^{-1} is obtained. Compared to the measured spread rate of 3.8×10^{-4} ms^{-1}, equal to the slope of the data shown in figure 4.2, the prediction is significantly smaller. Equation (4.1) is formulated so that gas and solid thermal conductivities control

the rate of heat transfer and hence the spread rate. Apparently the controlling mechanism is not yet known for the present fire spread conditions.

According to Williams (1976) spread rates may be modelled with a simple but fundamental energy equation (eqn. 4.2). Also introduced is the concept that the flame-front progresses forward to regions where the solid fuel temperature reaches its ignition temperature. The ignition temperature T_{ig} is usually equated to the fuel pyrolysis or vaporization temperature T_{vap}.

$$\rho V_p \Delta h = \dot{q} \qquad (4.2)$$

Spread rate V_p is therefore expressed in terms of $\dot{q}$, the net heating rate per unit area into the solid fuel source from the fire. As described in section 1.2 this is the heat flow through the *surface of fire inception*. In equation (4.2) ρ is the solid fuel density, Δh is the difference in enthalpy (per unit mass) between the fuel at its ignition temperature and the virgin fuel at ambient temperature. That is

$$\Delta h = \hat{C}_p (T_{ig} - T_o) \qquad (4.3)$$

One may prescibe any heat transfer mechanism(s) for $\dot{q}$ and test its effect on spread rate predictions with equation (4.2). For convective heat transfer $\dot{q}=h_f(T_f-T_o)$ where T_f is the adiabatic flame temperature and T_o is ambient temperature. If radiative heat transfer is assumed to control the spread rate a value that is about half the measured value is predicted (1.78×10^{-4} ms^{-1}). And this is when view factor and emissivity are set at unity in the expression $\dot{q}=\sigma\epsilon(T_f^4-T_o^4)$. Clearly there is no other possible enhancement of heat transfer that will account for such a rapid spread rate as that measured in figure 4.2. One can only suspect that the ignition temperature responsible for fire-front progress is in this case significantly lower than T_{vap}. More precisely if V_p is set at the measured value T_{ig} is found to equal 197.2°C compared to T_{vap}=390°C. Of course convective/conductive heating would add to

the total heat transfer and T_{ig} is likely to be somewhere between 197.2 and 390°C. It is therefore suggested that the fire-front might spread onto fresh fuel even if its temperature is not as high as T_{vap}. Another observation from figure 4.2 is that the χ_f is linear with respect to t during the spread or growth period. From equation (4.2) this implies that fire-to-fuel surface heat flux is time independent for this scale of spread.

4.3.3 Char-coal

Char-coal has a very low volatility so that there is no fuel loss ahead of the fire. When the fuel was consumed in the combustion zone the fire would have jumped except that the post fire zone is not volatile enough due to insufficient preheating and low volatility. From the observations made this fuel has a low enough volatility for repeated jumping but not volatile enough for the fire to self ignite ahead of itself (propagate) during the jump period. Hence, the fire dies before it can jump forward onto fresh fuel. A 2 kW, 3 meter long heating coil was added in a second attempt to assist propagation but this too was not adequate. A careful choice of duct/fuel system is required for the anticipated repeated jumping to occur. Wood was also tested in the present duct in an attempt to study its behaviour but this too was unsuccessful since only charred wood was left inside the duct after each attempt.

Presently the fire does not jump because of insufficient heat feedback (preheating) ahead of the fire. Reducing heat losses by insulation (which was also attempted) and decreasing the ratio of exposed surface area to fuel bed thickness should enhance heat feedback. The present ratio of surface area to bed thickness is probably too large to sustain propagation of char-coal or wood fires. Only a mere 6 percent total heat feedback occurs (see table 4.2), which compares to open fire studies conducted by Sibulkin and Lee (1974). Improvements on this percentage may therefore be possible in larger and more insulated passages.

4.4 Conclusion

A one dimensional model describing fire propagation dynamics in fuel-lined ducts has been studied with solid fuels. These results show that a solid fuel such as PMMA can support fires in a manner that is essentially no different to liquid fuels soaked in a porous inert solid. Solid fuels were chosen because of their lower volatility relative to liquids. This was done in an attempt to study the possibility of different fire dynamics from that observed with liquid fuels. Repetitive fire-front "jumping", appearing only once in the propagation histories of PMMA runs, results from the model if high latent heats are used, or when very low values of h_f prevail. That is, low vaporization or pyrolysis rate ahead of the fire. Evidently the observed duct fire behavior places PMMA in the same general category as volatile liquids. Despite a mere 6 percent feedback of the heat generated in these fires steady state is rapidly achieved and, at most, one "jump" in the fire-front history is observed.

Fire growth resulting from a point ignition source would indeed adjust the fuel profile to an extent that even the first "jump" (a consequence requiring an initially flat fuel profile in the combustion zone) may not be observed. In this respect solid fuels can behave differently.

A trial test on char-coal, being less volatile than PMMA, shows that conditions for repeated fire jumping are possible but a new duct design is required to prevent extinction during the jump period.

The steady-state gas-phase assumption also works with PMMA fires but to a lesser extent than liquid fuels. Fire growth dynamics are likely to interfere with propagation during rapid motion such as jumping, as the fire needs to re-establish itself after it jumps onto fresh fuel. This assumption may therefore require further assessment for other typically less volatile solid fuels

such as carbon.

As in the case of liquid fuels the model accurately describes gas temperature profiles and fire-front histories. Contributing to the study of the originally proposed model, experiments with PMMA provide physical measurement of fuel mass distributions $m(x,t)$ inside the duct. This variable provides an independent check on the proposed fuel vaporization mechanisms. Close agreement between predicted and measured fuel distributions suggest that the proposed mechanism for fuel vaporization, namely convective heat transfer, provides an accurate description of the physical process. The fuel-rich duct fire assumption has also been further validated by this study. A linear dependence between steady-state propagation speed (or propagation rate $\bar{\nu}$) and air flow/fuel loading verifies the fuel-rich fire assumption.

Horizontal flame spread over a PMMA surface is controlled by a surface ignition temperature that is found to be considerably lower than previously measured fuel vaporization or pyrolysis temperatures. It might be a sufficiently high temperature such that sufficient fuel vapors will issue from the solid surface to sustain burning. Also for the present scale of fire, fire-to-fuel surface heat flux is time independent during the growth period.

5 FIRE-INDUCED STRATIFICATION EFFECTS

Fire induced stratification in passages implies layering or separation of a hot gas stream from a cooler stream that bypasses the fire and eventually runs along the tunnel floor. The result being in effect two almost immiscible layers of gas travelling along the duct in the direction of ventilation, which is either forced or naturally induced. Newman (1984) performed experimental evaluations of stratified flow where the degree of stratification is correlated with the Froude number. The present work concentrates on stratified flow ahead of and within the fire. The phenomenon of reverse stratified flow occurring as hot combustion gases travel along the tunnel ceiling in a direction opposing the direction of ventilation is not considered. A two dimensional analysis of reverse stratified phenomena was presented by Hwang *et al* (1977) but will not be considered here.

The purpose of this section is to present an analysis describing stratified gas flow during a typical tunnel fire and to study its effect on propagation. The analysis is aided with the one dimensional model that has been developed and will be used to describe the reactive flow stream inside a tunnel under stratified conditions. Propagation will be described by the same model. Although many simplifying assumptions are made, the present analysis should prove useful for interpreting results for this class of fires. Developing more sophisticated models and simulations would also be aided by findings in this study. In this chapter more attention is focused on the flow regime where stratification is severe. The case of close to well mixed or non-layered flow has been explored in chapters 3 and 4 and will also be considered here to some degree.

5.1 Experimental

A diagram of the tunnel used for studying duct fires with stratified flow is shown in figure 5.1. A detail drawing appears

in appendix D. The tunnel geometry is such that fire induced buoyancy forces can overcome ventilation crossflow forces. By allowing the fire plume to rise high enough a large vertical momentum can be achieved and a buoyancy dominated plume may develop if crossflow forces are small. This argument can be quantified in terms of a Froude number (Fr) analysis which has been presented by Newman (1984). The analysis is based on a correlation where Fr is written as

$$Fr = \frac{V_{avg}}{\left[(\Delta T_{cf}/T_{avg})gH\right]^{1/2}} . \qquad (5.1)$$

ΔT_{cf} is the gas temperature difference from floor to ceiling, V_{avg} is the average gas stream velocity evaluated at the average gas temperature T_{avg}, and g and H are the acceleration due to gravity and duct height respectively.

According to Newman (1984) three distinct regimes are identified, each associated with different degrees of gas temperature and composition stratification. The first region is associated with small Froude numbers ($Fr \leq 0.9$) resulting in severe stratification where hot combustion gases travel along the duct ceiling. The second region, with larger Froude numbers ($0.9 < Fr \leq 10$), is dominated by strong interactions between crossflow and buoyancy forces. This region, although not severely stratified or layered, involves vertical temperature gradients and is mixing dominated. The third region has insignificant vertical temperature gradients ($Fr > 10$). This does not necessarily imply that the flow is turbulent.

Work in this chapter involves duct fire conditions in the first two regions ($Fr \leq 10$). Gas stream temperatures are measured along the tunnel length at three different heights; 50 mm, 147 mm and 250 mm above the floor. This provides a two dimensional gas temperature grid which will aid analysis of the flow structure. Thermocouple positions and an ignition port are also shown in figure 5.1. The duct is constructed of mild steel and a three meter metal fuel tray rests along its floor. Liquid

fuels are distributed along the tray length by soaking the required amount along an asbestos wick residing inside the tray. Thirty four chromel-alumel thermocouples are used to measure stream temperatures. The tunnel also includes glass windows to allow visual inspection of the fire. To eliminate end effects two meters of tunnel length was added to the tunnel end. A one meter calming section is placed before the test section to straighten the air stream originating from the mains air supply.

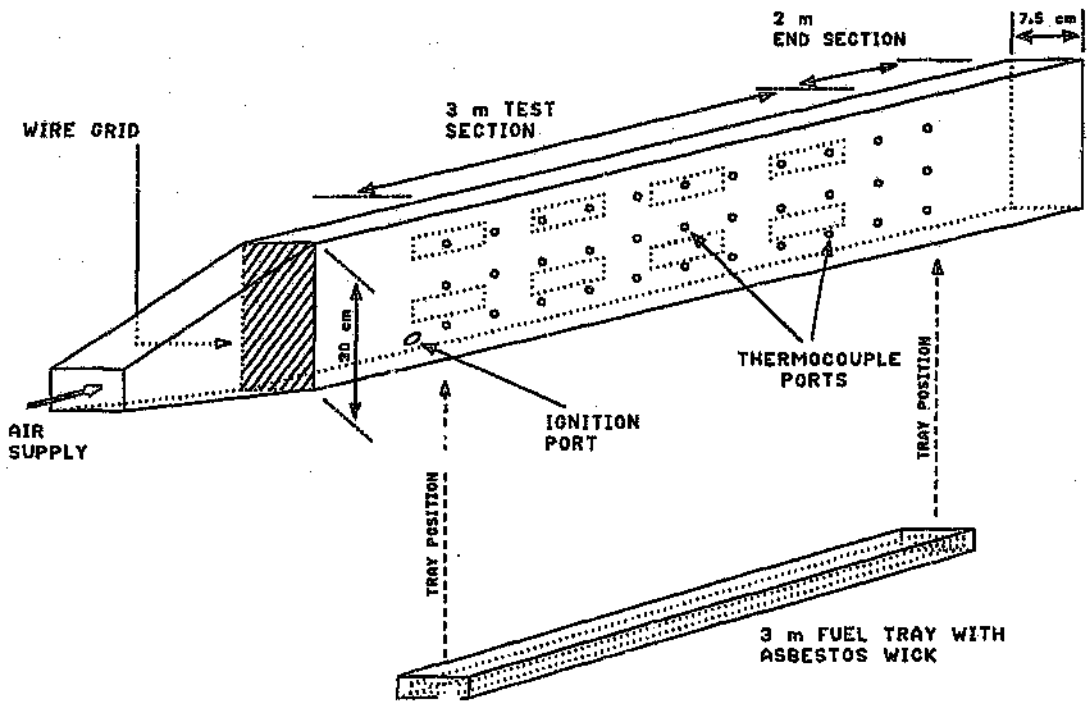


FIGURE 5.1. Fire tunnel apparatus used for stratified flow experiments. C_f=0.06 m, C_d=0.75 m.

Ethanol (Etoh), isooctane (Iso) and ethylene glycol (Eg) fires were studied. For each fuel, mass fuel loading and ventilation air flowrate are varied. One can therefore study the effect of air flowrate and fuel loading on the gas phase process as well as on fire propagation. Experimental procedure follows that of the non-stratified flow experiments when liquid fuels were used (chapter 3). All experiments are given in table 5.1 with their respective conditions.

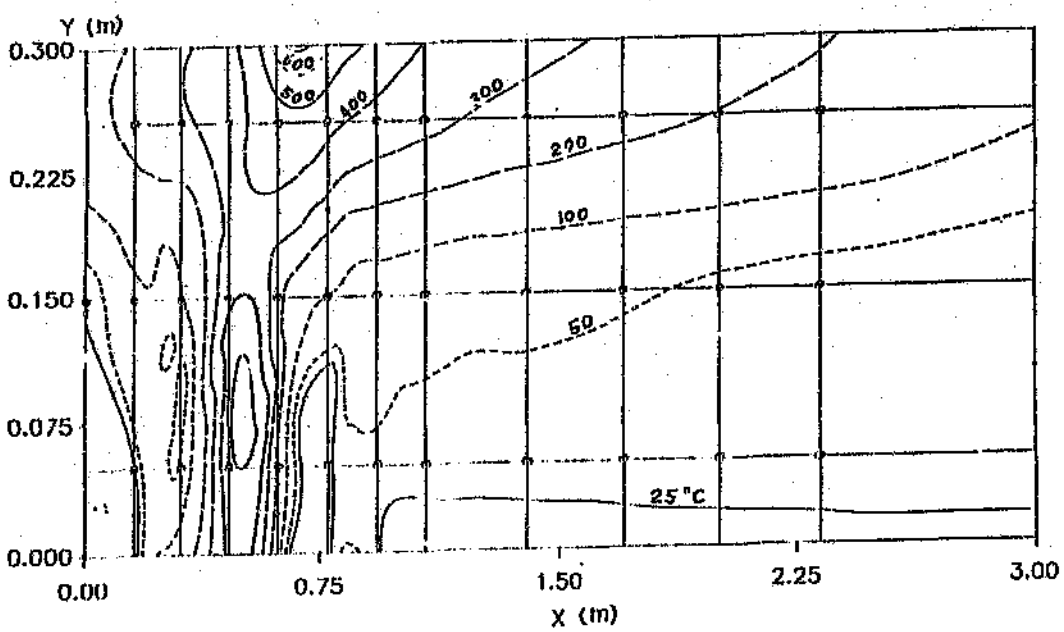
Run Number, Fuel	$\dot{m}''$ kg/m^2	V_∞ x10^2 m/s	γ kg/m^{2}s	$(1-B_{pl})$ mass fraction	α area fraction	$C_{d(est)}$ m	U_d° W/m^{2}K	U_o W/m^{2}K
1 Iso	1.11	9.11	4.51×10^{-3}	0.35	0.25	0.23	73	3.0
2 Iso	1.12	12.8	4.85×10^{-3}	0.32	0.32	0.26	62	3.1
3 Iso	1.25	10.8	4.17×10^{-3}	0.29	0.23	0.21	70	3.0
4 Iso	1.33	9.20	4.87×10^{-3}	0.38	0.29	0.25	81	3.0
5 Iso	1.33	12.7	5.56×10^{-3}	0.35	0.40	0.32	54	3.1
6 Etoh	1.11	9.00	4.54×10^{-3}	0.22	0.08	0.12	88	3.0
7 Etoh	1.11	17.0	5.70×10^{-3}	0.27	0.26	0.23	49	3.2
8 Etoh	1.25	12.9	5.10×10^{-3}	0.22	0.13	0.15	85	3.1
9 Etoh	1.33	9.10	4.87×10^{-3}	0.25	0.11	0.14	86	3.1
10 Etoh	1.33	17.0	6.82×10^{-3}	0.29	0.29	0.25	63	3.1
11 Eg*	0.560	17.2	4.47×10^{-3}	0.13	0.07	0.12	3	3.3
12 Eg*	0.569	25.2	4.47×10^{-3}	0.09	0.01	0.08	254	3.6
13 Eg*	0.570	50.0	4.47×10^{-3}	0.04	-0.09	0.02	940	3.8
14 Eg*	0.667	17.1	4.47×10^{-3}	0.12	0.06	0.11	171	3.3
15 Eg*	0.834	50.0	4.47×10^{-3}	0.04	-0.09	0.02	825	3.8

° U_d calculated using estimated $C_{d(est)}$ and not C_d=0.75m.
* γ estimated from asbestos tray open fire tests.

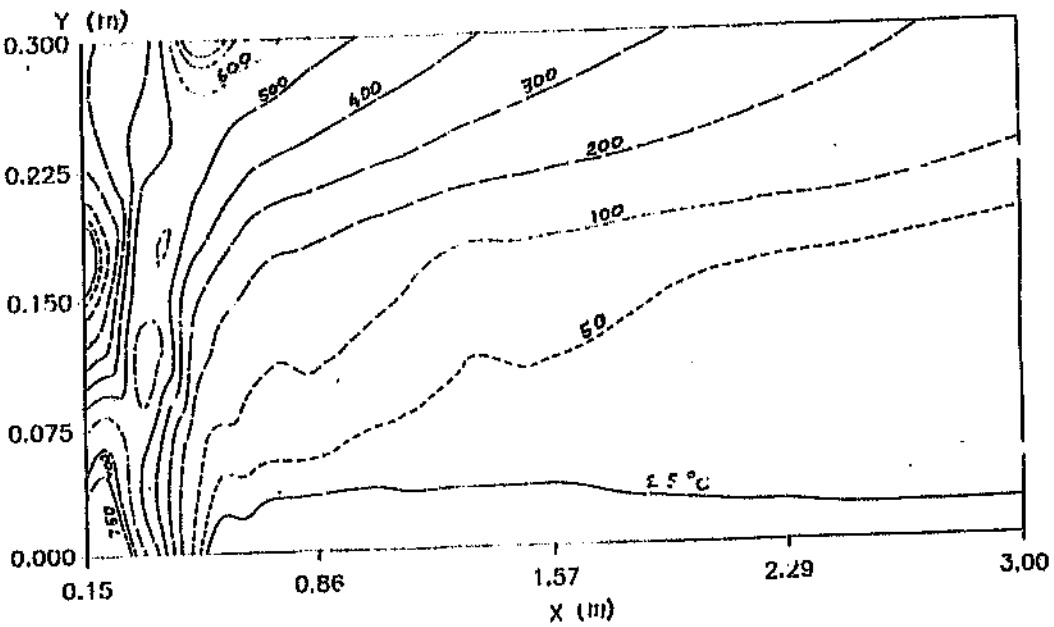
TABLE 5.1. Listing of experiments performed together with results obtained from flow analysis.

5.2 Results

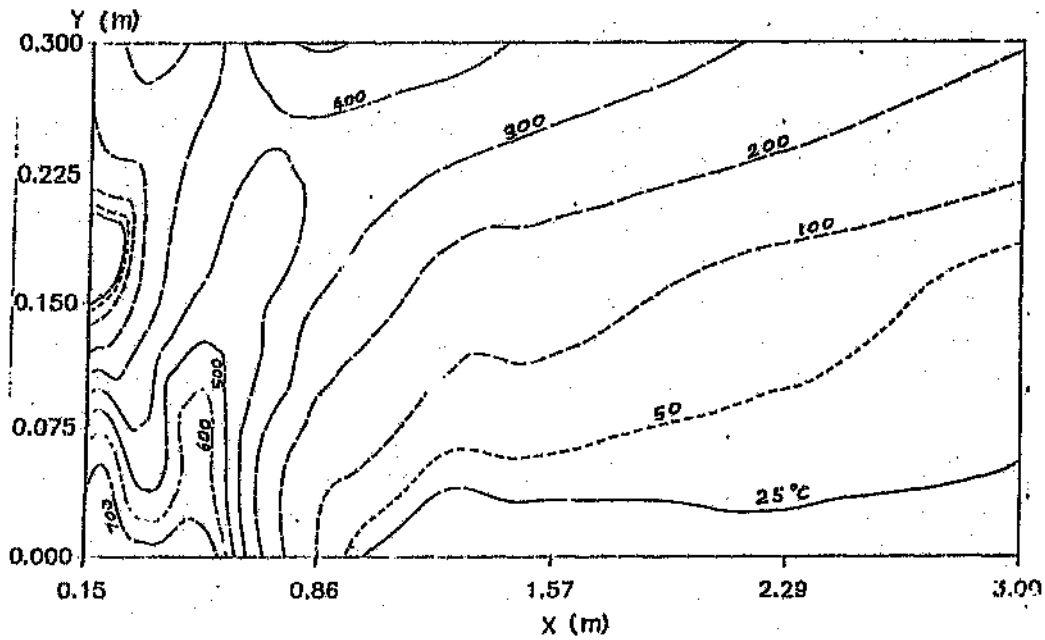
For each duct fire gas temperature distributions may be represented on an x-y grid. Measured grid temperatures are interpolated and a two dimensional gas temperature structure is constructed with contour isotherms. Figure 5.2 shows contour isotherms for runs 1, 2, 7 and 13. The first contour diagram shows the thermocouple grid. Runs 2, 7 and 13 in figure 5.2 are gas temperature distributions for stationary fires. Stationary because sufficient fuel remains at the beginning of the fuel tray and the fire therefore continues to burn for some time at its starting position. Run 1 (figure 5.2(a)) is shown when the fire has moved some distance along the tunnel. A degree of reverse stratification is evident on the x-y grid but this will not be discussed any further.


Y (m)
0.300
0.225
0.150
0.075
0.000
0.00
0.75
1.50
2.25
3.00
X (m)
600
500
400
300
200
100
50
25 °C

(a)


Y (m)
0.300
0.225
0.150
0.075
0.000
0.15
0.86
1.57
2.29
3.00
X (m)
600
500
400
300
200
100
50
25 °C

(b)



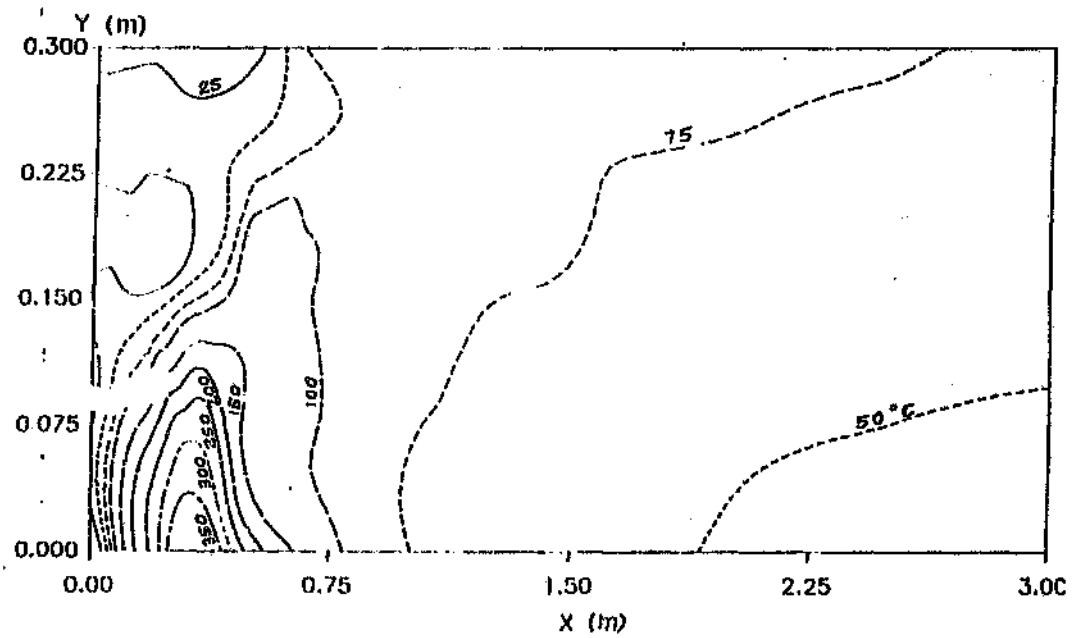


FIGURE 5.2. Contour plots of 2-D gas temperature profile inside duct for (a) run 1 (isooctane), (b) run 2 (isooctane), (c) run 7 (ethanol) and (d) run 13 (ethylene glycol).

Figures 5.2 (a), (b) and (c) display a striking feature consistent with the assumption that extreme stratification occurs and results in gas stream layering. This feature is seen if one follows the likely path of the hot fire plume, from floor to ceiling, along the maximum temperature ridge. The ridge starts at a high temperature near the floor and, as it rises toward the ceiling the temperature drops gradually. Further upward towards the ceiling, the temperature rises to a high value again. Clearly it is impossible for the hot fire plume to blend with the cold crossflow stream and then reappear at the ceiling as the contours suggest. It is more likely that the fire plume rises past the cold stream, but in so doing bypasses the thermocouples in that region of the tunnel. Hot plume gases would therefore avoid mixing and eventually collect at the ceiling where the measured peak ceiling temperature is located. See figures 5.2 (a) and (b). Such tendencies for two fluids of different transport properties to avoid mixing while flowing past each other are often observed in meteorological and oceanographic processes. As already suggested by de Ris (1970), similar mechanisms may control such stratification results.

The plume uses the third physical dimension of tunnel width as it avoids mixing with the bypass stream. Hot plume gases collect where a maximum ceiling temperature is recorded and travel along the ceiling in the direction of the ventilation current. This is not seen directly on the contour diagram which is just one 2-D planar cross-section of the 3-D temperature structure inside the tunnel. Together with the above discussion this explains the "saddle" feature appearing along the maximum temperature ridge somewhere between the floor and ceiling. It is likely that most of the interchange between the streams occurs in this region of the tunnel where the "saddle" appears.

Figure 5.3 provides a means of distinguishing severely stratified cases (such as run 1 and 2) from those dominated by strong interactions between crossflow and buoyancy forces (such as run 13). The plot is based on the correlation developed by Newman (1984) who estimated from tunnel fire tests that

$$(\Delta T_{cf}/\Delta T_h) = 0.67(\Delta T_{cf}/\Delta T_{avg})^{0.77} \qquad (5.2)$$

for the strong interaction regime ($0.9 < Fr \leq 10$), and $\Delta T_h \approx \Delta T_{cf}$ for the severely stratified regime ($Fr \leq 0.9$). Gas temperature rise, above ambient, along the ceiling is written as ΔT_h and the average gas temperature rise above ambient is ΔT_{avg}. It can be seen that present results follow the proposed correlation. Isooctane and ethanol supported duct fires resulted in extremely stratified flow, whereas ethylene glycol fires lie in the strong interaction region as well as in the buoyancy domirated region. This is expected as ethylene glycol is the least flammable fuel used and would support a smaller fire with weaker buoyancy forces. Also the air velocities used for ethylene glycol fires were on average much larger in order to achieve strong interaction between crossflow and buoyancy.

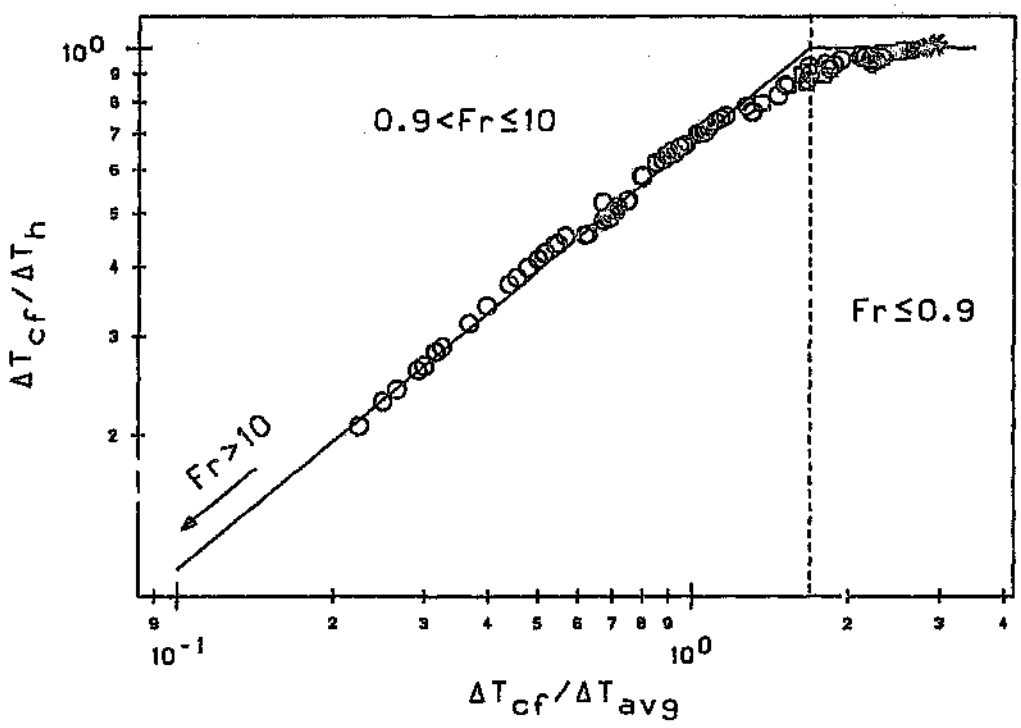


FIGURE 5.3. A comparison between the correlation (———) developed by Newman (1984) to predict fire induced stratification and present results. Isooctane (*), Ethanol (□), and Ethylene Glycol (o) results.

As previously mentioned extreme stratification as it is observed in these profiles is unavoidably a three dimensional phenomenon. As streamlines of fluid flow cannot intersect it is impossible for a rising plume, on its way to the ceiling, to pass by (or through) the bypass stream without using the third physical dimension of tunnel width. To model this fire system the complexity of the problem has been reduced to one schematically represented in figure 5.4. In this simplified analysis, cold air that flows over already vaporizing fuel is assumed to instantaneously react with the vapour as it is produced. Heat is generated locally and a significant increase in local gas temperature occurs. An upward plume develops which, on its way to the tunnel ceiling, passes the remaining unreacted air. Effectively the two gas layers, in order to achieve stable flow, undergo inversion. In doing so some mixing and heat transfer occurs between them. Also, as the hot plume rises it loses heat to the duct walls. Beyond this region the two gas layers are stable and lose heat to the tunnel walls as they travel with the ventilation current. Further evidence supporting this model is clearly seen in figure 5.5.

5.2.1. Modelling

Aided by the one dimensional model from chapter 2 the above description of the flow process provides the basis for analyzing fires in extremely stratified flow. The one dimensional burning region in figure 5.4 is made to follow the fire plume inside the tunnel for cases of severely stratified flow.

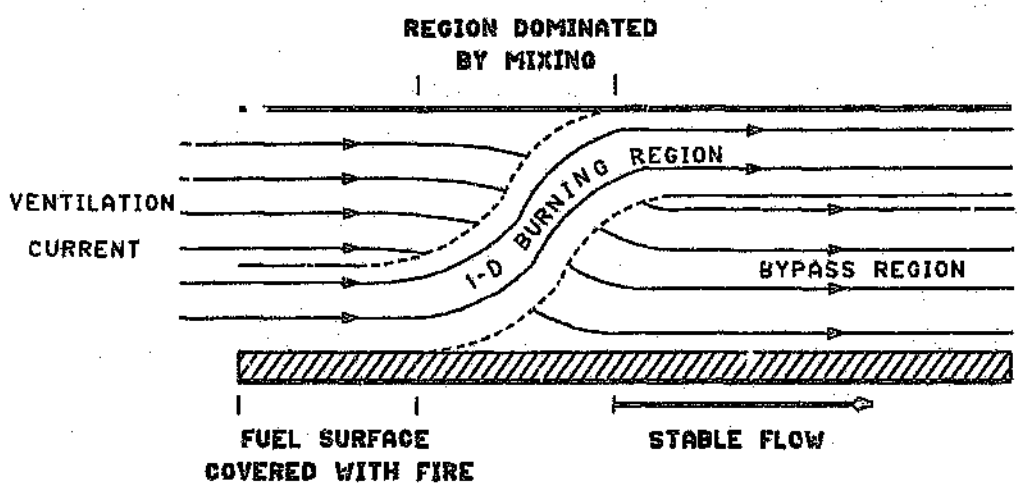


FIGURE 5.4. Flow pattern expected from severely stratified flow inside a flaming tunnel.

The one-dimensional model, as it is described in chapter 2, will be used to model the gas phase processes inside the one dimensional burning region shown in figure 5.4. In the severely stratified case the burning region starts along the tunnel floor and is assumed to rise virtually instantaneously at the end of the burning zone. It then continues its path along the tunnel ceiling. The analysis assumes the conservation equation of mass, as it is written in the original model, holds for the one dimensional burning region. It is assumed at the interchange point, where the fire plume rises, some plume mass is lost to the bypass stream, and the bypass in return loses some of its cooler mass to the plume. A net mass gain or loss, in either of these streams, due to this process would cause some deviation from the original model though this difference is assumed small. An attempt to quantify this mixing is in principle possible using simple mass and energy balances on the hot and cold

streams after reaction has occurred. Such calculations were done but were not revealing for reasons explained in Appendix E.

Exchange of hot and cold mass between the two streams will result in a mismatch in enthalpy from the end of the floor burning region to the start of the ceiling region. Because of this discontinuity, the energy balance, which is the gas-phase model equation, is first used from the entrance of the burning region up to the start of the mixing region. Another balance is used from the end of the mixing region up to any x in the ceiling layer. These calculations involve first fitting the gas-phase equations to floor temperature data up to the maximum floor temperature. Then the gas-phase equations are fitted to ceiling temperature data starting from a point ahead of the mixing zone. Floor temperatures therefore represent the combustion zone while ceiling temperatures represent the excess fuel and preheating zones of the original model. The difference between the floor and ceiling maximum temperatures at the end of the combustion zone is therefore related to mixing and heat loss occurring between the two streams.

Parameter estimation and plume model evaluation

Fuel burning rate

Except for ethylene glycol fires fuel burning rates γ are estimated in the same manner as non-stratified analyses in chapters 3 and 4. All ethylene glycol experiments resulted in slow initial fire growth. Initial fuel distributions were affected to an extent that fire-front history data displayed no stationary period at the start of the tunnel (t_{res} of γ could not be determined). For ethylene glycol γ was estimated by measuring the time taken for a flame to burn over a known platform area of wick soaked in a weighed quantity of fuel (outside the tunnel). This value of γ is then used in the model. To check this assumption γ for isooctane and ethanol was also measured in this manner. Comparison between values estimated from the model-fit (table 5.1) and independent tests are reported in table 5.2. The same comparison is done for γ

estimated from modelling non-stratified fires of chapters 3 and 4. It can be seen that estimated parameters from fits of large (stratified) tunnel fires agree well with those measured independently (outside duct) and those estimated from model fits of small duct fires are on average somewhat larger. This is because in the slim (non-stratified, chapters 3 and 4) duct heat feedback within the combustion zone is likely to be larger than in the stratified cases, hence more rapid vaporization or fuel burning occurs. Large tunnel results in table 5.2 therefore justify using $\gamma_{(measured)}$ for modelling ethylene glycol fires instead of fitting γ as it is done for isooctane and ethanol fires.

Fuel	Outside Duct $\gamma_{(measured)}$ kg/m^2s	Large Tunnel $\gamma_{(model)}$ kg/m^2s	Small Duct $\gamma_{(model)}$ kg/m^2s
Isooctane	$5.39x10^{-3}$	$4.80x10^{-3}$	$11.1x10^{-3}$
Ethanol	$5.40x10^{-3}$	$5.41x10^{-3}$	-
Ethylene Glycol	$4.47x10^{-3}$	-	$6.95x10^{-3}$
n-Butanol	$6.76x10^{-3}$	-	$7.35x10^{-3}$
PMMA (strip)	$6.84x10^{-3}$	-	$6.91x10^{-3}$

TABLE 5.2. Comparison between measured burning rates $\gamma_{(measured)}$ and averaged values ($\gamma_{(model)}$) from table 5.1 and non-stratified fires (table 3.2 and 4.2) in chapter 3 and 4.

Air bypass fraction

The reaction stoichiometric coefficient β is assumed as being that for complete combustion (production of CO_2 and H_2O). This may be a poor assumption and is not backed by experiment. Therefore, only trends will be considered from calculations which involve this assumption. Using the known air flowrate $\dot{m}_a$ entering the tunnel, γ, β, and the estimated combustion zone length X_{lbz}, one can calculate the fraction B_{pl} of air mass flowrate bypassing the reaction. Bypass fractions are calculated as

$$B_{pl} = (\dot{m}_a Y_{ox} - \gamma C_f X_{lbz}/\beta)/\dot{m}_a Y_{ox}. \qquad (5.3)$$

B_{pl} is based on the combustion zone lengths X_{lbz} estimated from floor temperature profiles. This the fraction of air that crosses the rising fire plume. The ..e dimensional model will be used with the fraction $(1-B_{pl})$ of air flowrate that reacts. Based on this fraction of air the combustion zone model is fitted to floor temperature data up to a point where the temperature is a maximum. The remaining model temperature profile is then fitted to measured ceiling temperatures (a temperature decay).

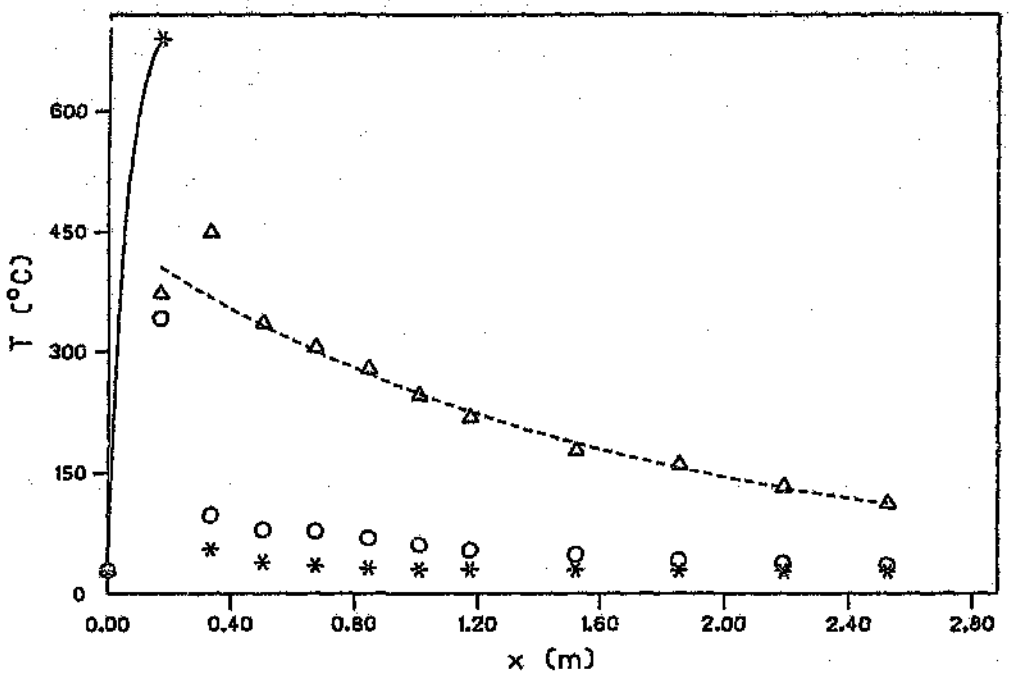


FIGURE 5.5. Model fit to plume of run 1. Temperature profiles at three different heights are shown (0.05m (*), 0.147m (o), and 0.25m (Δ) above floor). First the floor (——) and then the ceiling (----) section of the plume are followed with the one dimensional model.

Figure 5.5 shows a typical model fit to a severely stratified isooctane fire. The profile is measured while the fire is

stationary. A time averaged profile is shown because the fire remains stationary for enough time to measure the same profile several times. Table 5.1 shows results obtained after fitting model parameters.

Area fraction occupied by plume layer

Severe flow stratification takes the hot gas away from the fuel and thus effectively stops fuel vaporization ahead of the fire-front. In this case the value of h_f can be set to zero, where h_f is the heat transfer coefficient from the hot gas to the fuel in the "excess fuel" zone (along the ceiling). The model equation for this section then reduces to that of the preheating zone. A simple linear least squares fit is used to determine $_dU_{d2}$ for this section. C_d is the perimeter of duct cross-section (thin walls) and U_{d2} is the duct overall heat transfer coefficient along the "excess fuel" and "preheating zones". Slopes from a linear least squares fit of the temperature decay data along the tunnel ceiling give this information from

$$-C_dU_{d2} \;/\; [(\dot{m}_a(1-B_{pl}) + \dot{m}_{vu})C_p] = \text{slope},$$

where $(\dot{m}_a(1-B_{pl})+\dot{m}_{vu})$ is the mass flow of the hot layer and requires bypass fraction data. Note that B_{pl} depends on β which, as previously discussed, is assumed equal to that for complete combustion. Therefore C_dU_{d2} and any number derived from it will only be an estimate. Despite this the analysis may still prove useful and revealing if trends are considered with respect to $(1-B_{pl})$.

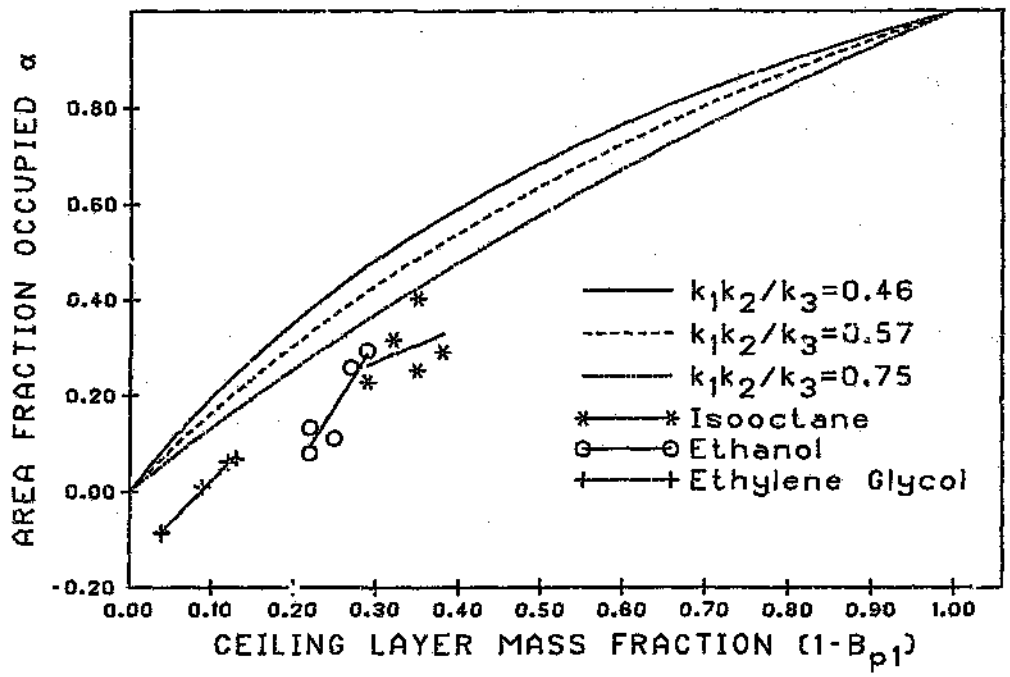


FIGURE 5.6. Fraction of cross-sectional area α occupied by hot gas layer as a function of bypass mass fraction B_{pl}.

Assuming the two layers are immiscible and of constant thickness throughout, the fraction α of tunnel cross-section occupied by the hot gas layer can be calculated. An estimate of the hot layer perimeter of cross-section $C_{d(est)}$ is used to calculate α. See appendix E for details of these calculations.

Values of α and $C_{d(est)}$ are shown in table 5.1. Figure 5.6 shows α increasing as $(1-B_{pl})$ increases. This relationship should be true if the relative average temperature and velocity of each layer does not vary much between runs. As B_{pl} decreases the hot plume layer gets thicker and hence α should increase as indicated in figure 5.6. A theoretical relationship between α and B_{pl} is derived in appendix E and possible cases for each fuel are compared in figure 5.6.

While there is some resemblance between the theoretical and the experimental results there is not much data so that figure 5.6

should be interpreted with some caution.

Heat transfer coefficient in combustion zone

$C_{d(est)}$ can also be used to estimate the combustion zone heat transfer coefficient U_d. The fitted value U_dC_d (fitted to floor temperature profiles in the same manner to fits of studies from chapters 3 and 4) is simply divided by $C_{d(est)}$ to get an estimate U_d. Values of U_d are listed in table 5.1.

Quenching of the hot plume layer by entrainment of cold air might explain why for ethylene glycol fires the estimated U_d in table 5.1 increases dramatically with increasing air velocity. This effect is more noticeable with ethylene glycol fires probably because a wider range of air velocities were examined. Also, these were the least buoyant of all fires studied, permitting more entrainment.

Fire propagation and averaging gas temperature profiles

Hot gases traveling along the duct ceiling do not significantly vaporise unburned fuel, and hence do not affect the fuel profile ahead of the fire. This was not found in chapters 3 and 4 where flow was non-stratified. Here, energy feedback to fuel is at a minimum. Fuel loss rates ahead of the fire are consequently reduced, even though volatile fuels are used. One might expect more jumping, a phenomenon already explored in chapters 2, 3 and 4. In earlier chapters it was shown that evaporation of fuel ahead of the fire attenuated fire jumping.

Figure 5.7 shows the fire propagation history of a severely stratified fire. In many of the experimental fires the fire length was shorter than the distance between thermocouples. Since parabolic interpolation is used to estimate the position of the maximum temperature the step-wise motion observed in those cases could be an artifact of over-spaced thermocouples. The propagation history shown in figure 5.7, however, is for a case when the fire length, as measured along the center-line thermocouples, is about twice the distance between each

thermocouple. Measurements of this kind are therefore more representative of the propagation history and clearly show jumping.

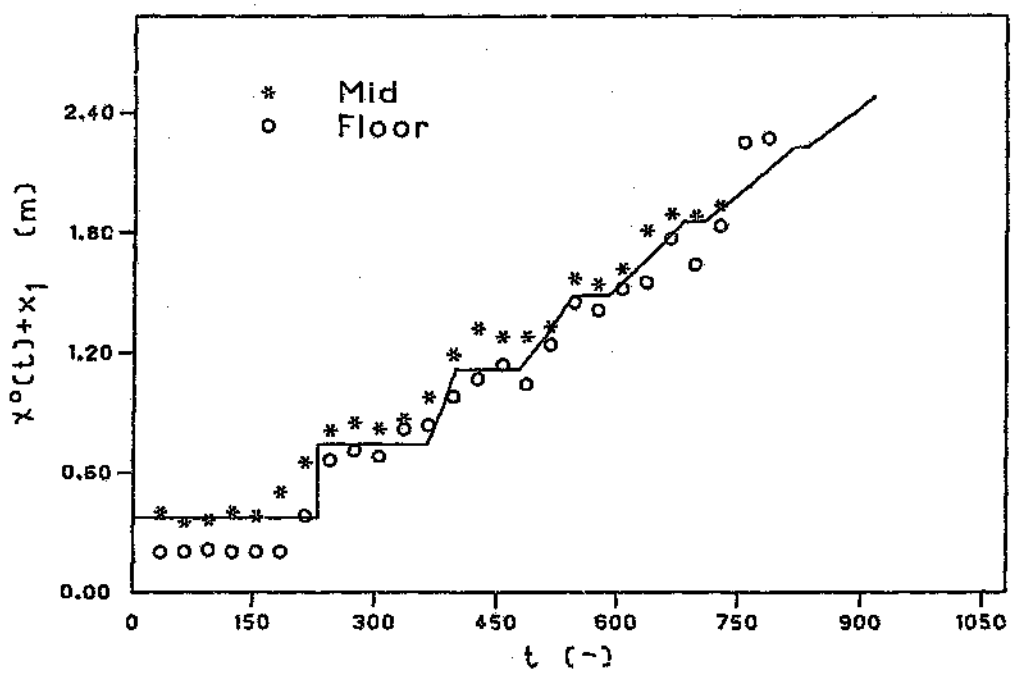


FIGURE 5.7. Fire-front history of an isooctane fire (run 2) measured from the floor and from the center-line gas temperature probes. Model fit is also shown.

Figure 5.7 also shows the fire propagation history measured with floor thermocouples. An observable difference between the two measurements is the combustion zone length. The reason for this becomes apparent if one examines figure 5.2(b). The length appears longer from the center-line because the plume is inclined, a consequence of flow forcing the fire plume forward. Also evident in figure 5.7 is a jump length longer than the combustion zone length measured from floor thermocouples. This would occur if the plume bends over and above the fuel surface and significantly heats and evaporates fuel ahead of the combustion zone length measured from the floor. Thus fuel will be depleted over a longer length than that measured from the floor thermocouples and so the measured length of the jump will be longer than the fire length as measured from the floor.

In order to describe fire propagation using the one dimensional model fuel vaporization profiles ahead of the fire must be known. This determines the propagation history. The gas temperature profile determines the heat transfer rate from gas to fuel which in turn determines fuel vaporization. If the average gas temperature profile is used to obtain a description of fuel loss rates (heat transfer rates) then the model is found to describe propagation histories quite well. The gas-phase model equation is first fitted to the measured averaged gas temperature profile (average profiles from 3 heights). Then the propagation history is fitted to χ° vs t data by adjusting h_f in the model. h_f determines heat transfer from the gas-phase to the fuel surface.

Propagation of severely stratified fires is then modelled in the same way as propagation in chapters 3 and 4 (i.e., $h_f \neq 0$) since some fuel will still vaporize ahead of the fire despite the hot layer being far above the floor. For the purpose of modelling gas temperature profiles in severe stratification h_f was set to zero as already described in the previous section. This is because the effect of h_f is almost negligible on the gas-phase energy balance (see figure 2.11) and this clearly simplifies model fitting. In dealing with propagation (fuel loss rates) one cannot ignore h_f since its effect is very significant as figure 2.11 indicates.

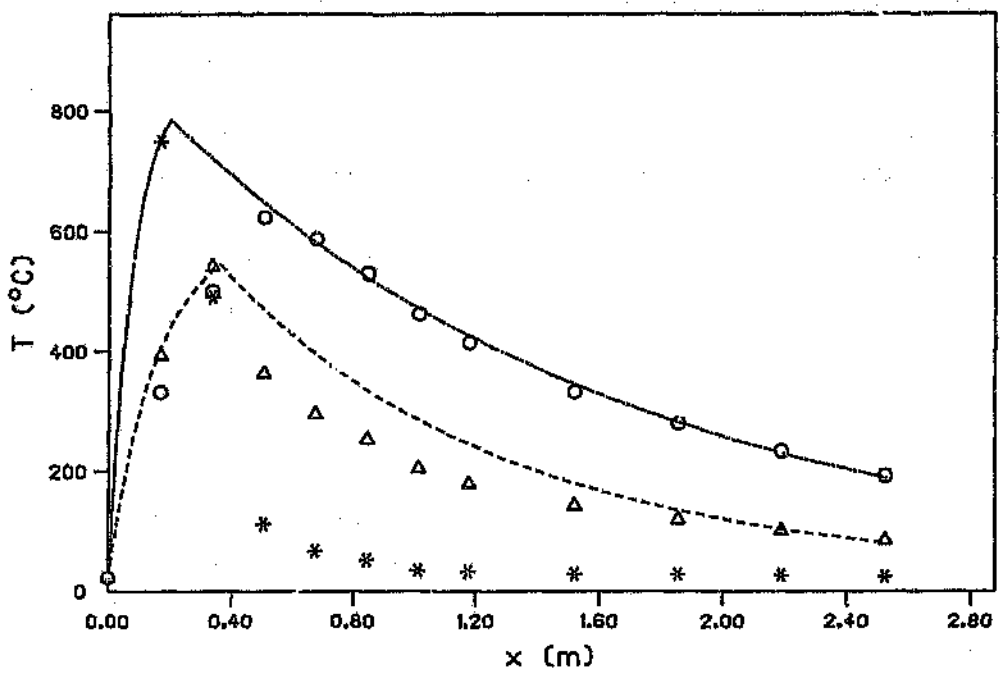


FIGURE 5.8. Floor temperature profile (*;——) and ceiling profile (o) of run 5 meet with no discontinuity. Average gas temperature profile (Δ) and model fit (-----) are also shown.

Results of propagation modelling are shown in table 5.3. This is identical to analyses from non-stratified flow experiments. The gas-phase energy balance involves the entire flow stream. Bypass fractions B_{p2} are now used to determine the amount of heat generated by combustion and not to split the flow into a hot and cold layer. X_{lbz} from average temperature profiles (not floor profiles) are used to calculate B_{p2} from equation (5.3). B_{p2} is determined from combustion zone lengths that are estimated from average gas temperature profiles as opposed to floor profiles used for B_{p1}. Average gas temperature profiles are used also in the fitting procedure. Figure 5.8 shows an average gas temperature profile for run 5 together with a model fit. Values of h_f fitted to propagation history data appear in table 5.3 and are compared to estimates h_i from a correlation (Coulson and Richardson, 1986). Table 5.3 also shows

correlation estimates of overall heat transfer coefficients U_o which include radiation effects. See Appendix E for radiative effects of U_o.

For the combustion zone U_i is fitted to average gas temperature profiles in exactly the same manner as was done in chapters 3 and 4 and values are reported in table 5.3. C_d=0.75m in this case and is not an estimate since all the flow is used in calculating the average gas temperature profile. U_d can therefore be compared to U_o in table 5.3.

For ethylene glycol fires average gas temperatures were always below or just above the fuel boiling point. Evaluation of h_f from the model is therefore not possible for these cases because h_f has little or no effect on propagation in the model. The value of h_f is therefore set to zero and the model equation for the excess fuel zone reduces to that of the preheating zone. Values of U_{d2} can therefore be determined from linear least squares fits of the gas temperature decay using a value of C_d=0.75 because the entire gas stream is involved with average gas temperatures. Model comparisons to data using fitted values of U_{d2} in the model, for some ethylene glycol fires, appear in figure 5.9. Figure 5.9 also shows the effect of increasing air velocity on the goodness of model-fit to measured average gas temperature profiles. Ethylene glycol runs represent the poorest of all fits obtained from all fuels studied but display an improvement at increased air velocities.

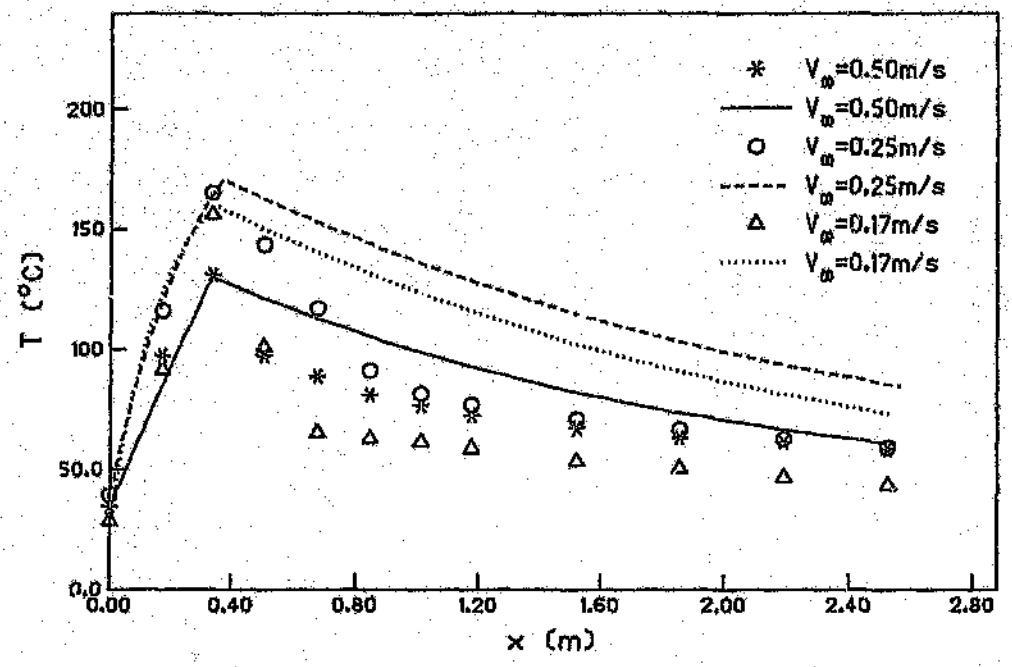


FIGURE 5.9. Effect of increasing air velocity on the model fit to data when the average gas temperature is used to describe the gas phase process.

Run Number, Fuel	$(1-B_{p2})$ mass fraction	U_d W/m^{2}K	U_{d2} W/m^{2}K	U_o^* W/m^{2}K	h_F W/m^{2}K	h_1^* W/m^{2}K	$\bar{\nu}^\circ$ x10^2 m/s
1 Iso	0.35	26.0	5.0	3.0	1.3	1.4	0.141
2 Iso	0.57	40.0	5.0	3.1	1.4	1.6	0.261
3 Iso	0.51	32.0	5.0	3.0	1.3	1.5	0.182
4 Iso	0.38	31.0	5.0	3.0	2.0	1.4	0.098
5 Iso	0.63	33.0	5.6	3.1	1.8	1.5	0.229
6 Etoh	0.30	17.0	5.0	3.0	3.5	1.4	0.165
7 Etoh	0.40	22.0	6.5	3.2	1.7	1.7	0.307
8 Etoh	0.31	20.0	4.5	3.1	3.2	1.6	0.210
9 Etoh	0.39	21.0	4.0	3.1	3.2	1.4	0.173
10 Etoh	0.48	33.0	7.0	3.1	0.5	1.7	0.245
11 EG	0.14	60.0	3.5	3.3	0.0	1.7	0.146
12 EG	0.10	33.0	5.0	3.6	0.0	1.9	0.235
13 EG	0.05	8.0	8.62	3.8	0.0	2.4	0.172
14 EG	0.14	40.0	3.58	3.3	0.0	1.7	0.139
15 EG	0.05	8.0	8.5	3.8	0.0	2.4	0.135

* Correlation estimates which include radiation effects.
° Average fire propagation speed $\bar{\nu}$ is estimated from linear least square fits of χ° vs t data.

Table 5.3. Parameters estimated from fire propagation analysis where the average gas temperature is used to describe the gas phase process.

It is also possible to examine the effect of air flowrate (total) and fuel mass loading on the average fire propagation speed $\bar{\nu}$. Figure 5.10 shows this for isooctane and ethanol fires. Because the daily ambient temperature T_o can vary, propagation rate data in figure 5.10 display some error. This effect was observable on χ° vs t plots of some reproducibility runs performed in the smaller scale duct of chapter 3.

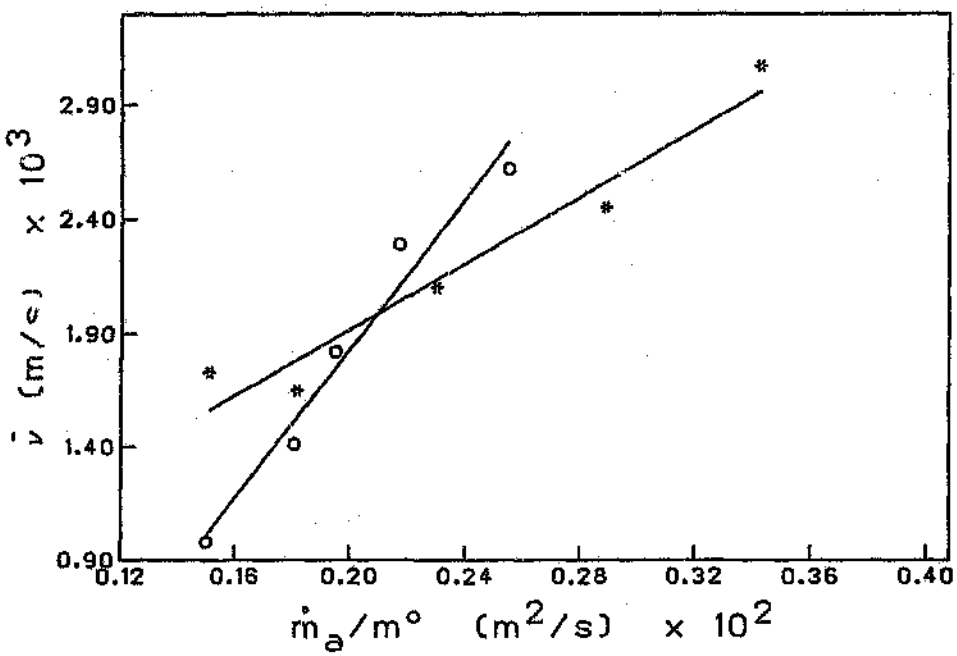


FIGURE 5.10. Observed effect of air ventilation rate (total) $\dot{m}_a$ and fuel mass loading on fire propagation speed for ethanol (*) and isooctane (o) fires.

Ethylene glycol fire propagation speeds show no trend with respect to ($\dot{m}_a/m^\circ$) and are omitted for clarity. Fire propagation data for ethylene glycol (χ° vs t) reflected a large degree of noise and the steady fire propagation speed for each run could not be determined accurately.

5.3. Discussion

Reaction stoichiometry was assumed as that for complete combustion. This fixes the value of $\Delta\hat{H}_r$ and consequently leaves U_d as the only free parameter in the combustion zone. Comparison of U_d in table 5.1 with U_o shows no agreement between fitted U_d and expected U_o which includes radiation effects. This discrepancy is attributed to poor estimates of β (B_{pl} and therefore $C_{d(est)}$) and $\Delta\hat{H}_r$, since complete combustion

conditions may not have been achieved in practice. The model is also very sensitive to β. See section 2.4.1.

For severely stratified flow, temperature profiles are well modelled if one follows the reactive stream, and therefore such an approximation is valid. If stratification is not severe, such as for some ethylene glycol fires (fig. 5.2(d)), then layers do not form and the plume cannot be followed. Large degrees of mixing with the bypass stream prevail. Runs 13 and 15 are examples of this and are identified in figure 5.3. In this regime flow is neither severely stratified nor well mixed ($0.9 < Fr \leq 10$). Average gas temperature profiles can describe the gas-phase process in this case. Figure 5.9 and work in previous chapters on non-stratified flow verify this result since fires in chapter 3 and 4 are either in well mixed conditions or lie in the strong interaction (mixing controlled) regime. Ethylene glycol fires are described by the model to a lesser extent but the average gas temperature approach works much better for less stratified cases ($0.9 < Fr \leq 10$) than for severely stratified ($Fr \leq 0.9$). See figure 5.9.

When the model is fitted to average gas temperature profiles values of h_f, used to fit propagation histories, correspond very well with literature estimates h_l (see table 5.3). This is true even for severely stratified cases. Not only is h_f close to h_l but the step-wise motion described by the model corresponds closely to what is measured (see figure 5.7).

When modelling average gas temperature profiles values of U_{d2} are somewhat larger than those from correlations (U_o). U_o is about 1.5 to 2 times smaller than U_{d2} in table 5.3. This is partly attributed to an imprecise average gas specific heat capacity used in the energy balance ($\hat{C}_p$=1400 kJ/kgK). Also, such low values of U_o are often obtained with some error since they come from correlations based on log scales. The difference between U_o and U_{d2} may be due to such error.

Figure 5.10 shows a linear relationship between average fire propagation speed and air flowrate/fuel loading. Such linear

dependence was also observed in non-stratified fires studied in chapter 4. This corresponds with the proposed one dimensional model which assumes fuel-rich fires in ideal plug-flow. Although results in this chapter are not for well mixed flows (quite the opposite) increasing air flowrate effectively supplies more oxygen into the reaction region (plume). This increases the rate of fuel consumption by enlarging the fire and effectively enhances heat transfer. Evidently the net effect is a close to linear dependence of propagation speed on air flowrate. Also, the slope of isooctane fires is somewhat larger than for ethanol in figure 5.10. This is expected because propagation is controlled by heat transfer and subsequent resistance to vaporization. As the model suggests, the fuel latent heat has an inverse effect on the propagation rate (eqn. 2.17). Of course not only latent heat affects the slope but also variables such as $\Delta\hat{H}_r$ and C_f. This is also seen from equation 2.17.

5.3.1. A proposed simple correlation for stratification.

In order to use the one dimensional model for predictive purposes the degree of stratification needs to be determined without prior experimentation. That is, to decide whether a fire system would be in the severely stratified or mixing controlled regime and therefore follow the plume or model with average gas temperature profiles. Newman's correlation could be used to do this, except that measurements of $\Delta T_{cf}/\Delta T_{avg}$ are required. The use of this correlation for prediction of stratification without experiment is thus not possible. It is therefore desirable to have a correlation, based on fuel/duct properties, which can be used to predict stratification in advance. Clearly g and $\Delta T_{cf}/\Delta T_{avg}$ form the buoyancy term in the Froude number and are essential for describing stratification.

It may be possible to relate buoyancy to those fuel properties that determine the fire intensity or heat generation rate since buoyancy is a consequence of local heat generation. A fire intensity number is therefore defined as $G \rightarrow \gamma(-\Delta\hat{H}_r/\beta)(1-B_{pl})$ W/m^2, and considered to be that fuel property contributing to

buoyancy inside the fire. This number may be understood as a heat generation rate per unit platform area of tunnel and will be incorporated into a proposed Froude-type number correlation for predicting stratification.

Because gas stream temperatures decay along the duct the Froude number is position dependent. Heat loss rates, causing this decay, depend on duct wall properties and film heat transfer coefficients. For simplicity the distance variable x will be used to correlate gas temperature decay along the duct. This analysis is therefore developed only for the present tunnel. Because stratification is determined by the balance between crossflow and buoyancy forces variables g, V_∞ and H must also be used. Acceleration due to gravity g is constant and common to all present tunnel fires and is combined into the stratification correlation's constant of proportionality. A dimensional analysis results in the following correlation for stratification

$$\frac{\Delta T_{cf}}{\Delta T_h} = k \left[\frac{Gx}{(T_o \rho_o \hat{C}_{pg}) V_\infty H} \right] \left[\frac{\hat{H}_{vap}(T_{vap} - T_o)}{T_o^2 \hat{C}_{pg}} \right]^{1.6} \qquad (5.4)$$

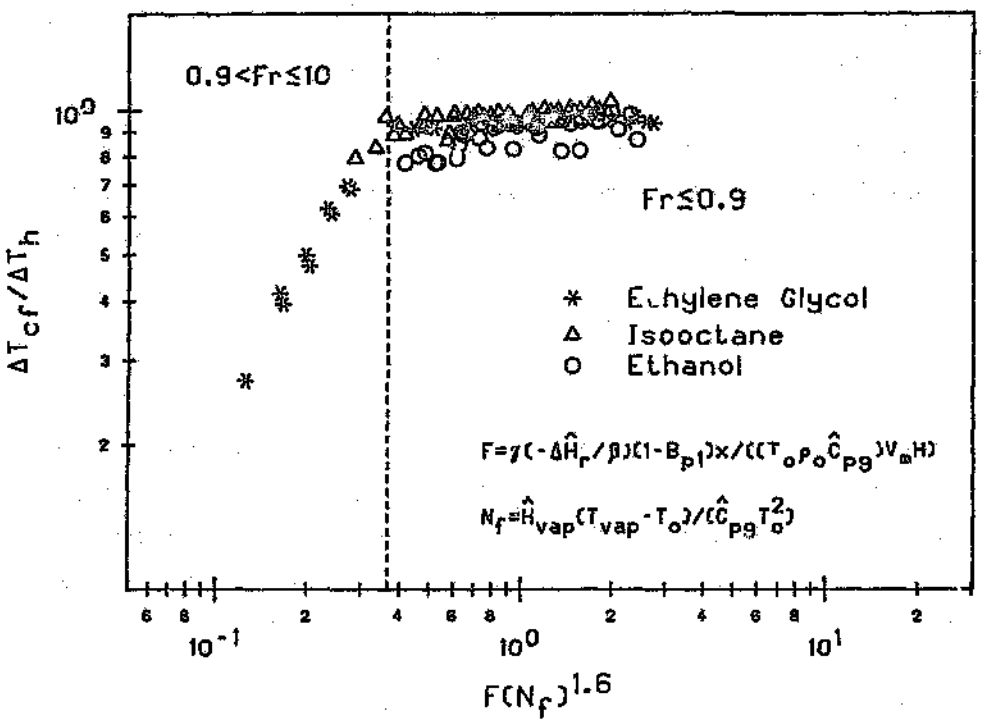


FIGURE 5.11. Stratification correlated with fuel properties.

The power of 1.6 was obtained by fitting the correlation to the data shown in figure 5.11.

Figure 5.11 shows present data correlated according to equation (5.4). The above correlation can be extended to include the tunnel overall heat transfer coefficient U_o and then could be applied to other tunnels. Of course this correlation is only estimated for three fuels and may require further manipulation if other fuels are examined. Also, B_{pl} is not known prior to a fire scenario. This variable contributes to the heat generation term and further experimentation is required to correlate B_{pl} and predict its value in advance. An interesting result seen in table 5.1 is that $(1-B_{pl})$ ranges from 0.29 to 0.38 for isooctane. 0.22 to 0.29 for ethanol, and 0.04 to 0.13 for ethylene glycol. Each fuel has its own limited range of B_{pl} which suggests this variable may be correlated with some simple flame characteristics of the fuel in question. Flame height and

temperature could be co. related with B_{pl} since these variables are directly associated with fire induced buoyancy forces inside a passage. B_{pl} is not only affected by the rate at which hot plume gases will rise but also by the average cross-wind speed V_∞, hence the observed range of B_{pl} for each fuel. Therefore a correlation for B_{pl} based on fuel properties and wind speed may be possible.

5.4 Conclusion

The present analysis has shown that a simple one dimensional model can be used to describe fires during typically severely stratified flow inside a passage. The assumption of immiscible layers occurs in practice if $Fr \leq 0.9$. Model temperature profiles follow closely the hot plume measured temperature profiles. The immediate separation and layering of hot and cold streams permits the use of a one dimensional approach. An expected discontinuity in enthalpy, reflected in hot plume stream temperature profiles, occurs between the rising floor stream and the hot ceiling layer. There is also evidence of increasing air entrainment from the cool bypass to the rising plume as air velocities are increased. Despite this the hot and cold gas layers will in all important aspects behave as two immiscible fluids in cases of severe stratification.

If the flow is non-layered ($0.9 < Fr \leq 10$) mixing between bypass and rising plume are extended to a degree where the layers blend or mix. The flow is then non-stratified and the original one dimensional approach of chapters 2, 3, and 4 applies if average gas temperature profiles are used. The model can describe the average gas temperatures of the entire stream as in previous chapters. Judging from figure 5.9 and work in chapters 3 and 4 the average temperature method works better if the flow is closer to well mixed, which is achieved at higher ventilation velocities.

The decision to choose between following the plume or to use the average temperature approach depends on the flow scenario;

extremely stratified or mixing controlled. This decision is aided by the Newman (1984) correlation which is in agreement with flow regimes studied in this work. A correlation of this kind is therefore indispensable.

It is suggested in this chapter that stratification may be correlated purely in terms of fuel and duct properties and a correlation based on this assumption is presented. More work is required to assess the accuracy of the correlation that has been proposed. Some parameters such as B_{pl} and β still need to be correlated with fuel properties and flow conditions. This correlation, based purely on fuel and duct properties, could be very useful in order to predict flow conditions for modelling purposes. Coupled with the one dimensional model this correlation could in principle be used to model fire behaviour in passages.

There may of course be some cases of fires with intermediate velocities where mixing mechanisms would dominate and a three dimensional model with the inclusion of mixing mechanisms may still be required. However, the two extreme cases, severe stratification and close to well mixed flow, are in all important aspects adequately described by the much simpler one dimensional approach presented in this thesis.

Extreme stratification is a case where fuel loss rates ahead of the fire are reduced to an extent where the transient jump-type phenomenon is more evident. Propagation histories are well described by the model suggesting correctly assumed mechanisms for the fuel loss rate. More jumping is therefore possible with passage fires in cases of severe stratification due to less heat feedback ahead of the fire. This is true if fuel is lined along the passage floor and not the ceiling.

The observed direct dependence between fire propagation rate $\bar{v}$ (steady-state propagation speed) and air flowrate, and inverse dependence with fuel mass loading is similar to that found in fuel-rich fires where stratification does not occur.

Finally the chemistry of these combustion reactions needs more attention. Although in the present analysis the problem of understanding combustion chemistry has been avoided, β and $\Delta\hat{H}_r$ must be known if accurate *a priori* duct fire predictions are to be made. Therefore more sophisticated models or simulations are not warranted until such information is available.

6 CONCLUSIONS AND RECOMMENDATIONS

6.1. Summary and Conclusion

6.1.1. Duct fires in well mixed flow.

A theoretical treatment of fire propagation along a fuel-lined duct with a radially well mixed axial flow has been presented. The gas phase is modelled as a steady state process whereas the condensed-phase (fuel source) is taken to be the cause of transient fire propagation along the duct. Experiments were performed, with liquid fuels soaked in a porous medium, in a small scale duct where fire propagation histories and gas temperature profiles were acquired. Experimental results confirm hypotheses of pseudo steady-state gas-phase processes. Theory and experiment display transient fire propagation for typical duct fire scenarios where initial fuel mass loading is constant with respect to duct length. The phenomenon observed, as predicted by theory, is an initial "jump" of the fully developed combustion process followed by attenuation to a steady state constant fire propagation speed. The theory is in all important aspects able to quantitatively model the experimental results.

Fire propagation supported by solid fuel lining in a small scale ventilated duct were studied in an attempt to extend the analysis from the case of liquid fuelled fires to that of solid fuels. Polymethylmethacrylate (PMMA) and char-coal were used. The use of a solid fuel has also provided the possibility of acquiring an independent measure of solid fuel mass distributions along the duct interior, an important transient variable involved propagation dynamics and in the model. Comparison of model predictions of fuel profiles and measured fuel mass distributions reveals good quantitative agreement between theory and experiment. This is a good test of the assumptions of the proposed model. By imposing the desired initial condition on PMMA duct fire experiments, in order to avoid fire growth phenomena, it was shown that the propagation of duct fires supported by a solid fuel behave in a similar

manner to fires supported by liquid fuels soaked in a porous solid. In accord with the model, a trial run with charcoal suggests that fuels with very low volatility might support repeated fire jumps if fuel preheating ahead of the fire is sufficient. A brief fire growth analysis on PMMA is used to assess the concept of an ignition temperature as a controlling mechanism. The model also gives good quantitative descriptions of gas stream temperature profiles and fire front histories when fitted to PMMA duct fire data.

From studies of non-stratified flow, liquid fuel supported fires the following major findings may be summarized:

1) The simple model accurately describes centre-line (average) gas temperature profiles inside the duct as well as fire propagation histories even if the flow is not perfectly mixed in the radial direction.

2) For the scale and class of fires studied, convective heat transfer from the gas stream to the condensed fuel governs the fire propagation history and average propagation speed.

3) For the case of thin duct walls heat losses from the system to the surroundings is dominated by radiative heat transfer, especially from the flaming region.

) . e : the present model for deterministic predictions of duct fire dynamics requires better knowledge of reaction stoichiometry.

5) An important fundamental difference is identified between fire propagation rate $\dot{\nu}$ and fire propagation speed V(t), a concept not addressed in duct fire literature.

6) Coupled with gas-phase dynamics mass fuel loading distributions m(x,t) control fire propagation histories and can be used to successfully predict these histories.

7) The assumption of constant fuel burning rate (γ) in the

combustion zone works very well in models for this class of fire and explains why a jump phenomenon does indeed occur.

8) Points 5, 6 and 7 explain why the familiar assumption of constant fire propagation speed can break down in typical tunnel fire scenarios. These findings are used in the model to determine the jump-type behaviour, propagation histories and conditions for possible periodic fire motion.

9) If fuel volatility is higher and/or heat transfer (feedback) from the fire to fuel is more effective then steady-state propagation is achieved sooner during the history.

10) For close to well mixed flow or in cases where use of center-line average temperatures are justified the following assumptions seem to work well in practice:

- fuel-rich fire.
- steady-state gas-phase process.
- heat transfer dominated fire process.

This leads to a reasonably simple model with good powers of prediction. Many of the parameters used in the model can be estimated from existing correlations.

From studies of non-stratified flow, solid fuel supported fires the following major findings are revealed.

1) Despite a mere 6 percent feedback of the heat generated in these fires, constant propagation speeds are rapidly achieved. This is also observed with fires supported by liquid fuels.

2) Prolonged fire growth resulting from a point ignition source is observed. This may adjust the solid fuel profile to such an extent that the first fire jump may not be observed. In this respect solid fuels can behave differently from liquid fuels.

3) The steady-state gas-phase assumption also works with fully developed solid fuelled fires, but to a somewhat lesser extent.

This is at least true for PMMA but may require reassessment for other solids, such as carbon.

4) The model accurately predicts measured fuel mass distributions at steady state. This justifies the convective heat transfer mechanism used in the excess fuel zone model to quantify fuel loss rates as well as the constant γ assumption.

5) The fuel-rich fire assumption is once again further verified for this flow regime (close to well mixed or non-stratified). The observed direct dependence between fire propagation rate $\dot{v}$ and air flowrate and inverse dependence with initial fuel mass loading is evidence for this.

6) Horizontal flame spread over a PMMA surface seems to be controlled by a surface ignition temperature that is considerably lower than the pyrolysis or vaporization temperature. Presumably this is a temperature at which sufficient fuel vapors can issue from the solid surface and sustain burning.

6.1.2. Duct fires with stratification.

A simplified approach to the study of fires in ventilated passages with fire induced stratification is presented. In conjunction with small scale experiments on liquid fuelled fires it is shown that a one dimensional model, requiring minimal computational effort, may be used to describe propagation as well as the dominant features of the flow process. Separation of the gas flow stream into a hot and cold layer is identified as being extreme stratification whereas flow systems with higher Froude and Reynolds numbers may result in no evident layering, although mixing may still control. Identification of the two types of flow scenario is found to be important in the application of the one dimensional model to such fire systems. A previously developed Froude number based correlation (Newman, 1984) is used to identify severely stratified cases from those where layering is not likely to occur. The present analysis is

in good agreement with flow regimes delineated by Newman's (1984) correlation. A new correlation for stratification using fuel/duct properties and air velocity is also presented as a means of *a priori* predictions of stratification. The 1-D model is found to operate well in the severely stratified regime and in a regime where the flow is neither well mixed nor layered. Fire propagation along the passage is also well described by the model under such flow conditions. In conjunction with a correlation for predicting stratification the one dimensional model can in principle be used to describe fires in well mixed, mixing controlled and severely stratified flow regimes.

Studies on stratified flow have resulted in the following main findings:

1) A simple one dimensional model can be used to describe the hot reactive plume stream during severely stratified flow inside a passage. A hot and cold gas layer develop and remain almost immiscible with the exception of some entrainment. Model temperature profiles seem to follow closely with hot plume temperature profiles.

2) If the Froude number falls into the non-layered regime ($0.9<Fr\leq10$) or flow is closer to well mixed the one dimensional approach may still apply. In this case average gas temperatures are used instead of following the "plume".

3) The exact method of application of the model is determined from a correlation that delineates various stratification regimes. That is, severe stratification requires following a plume stream whereas non-layered flow is better modelled with average temperatures. Such a correlation is therefore indispensable.

4) The observed direct dependence between fire propagation rate (steady-state propagation speed) and air flowrate and inverse dependence with fuel mass loading is similar to that found in fuel-rich fires.

5) Stratification can be correlated purely in terms of fuel/duct properties and flow velocity. Ultimately a correlation based purely on such properties would prove useful in *a priori* predictions of the flow condition. Point 3 justifies this need.

6.1.3. Concluding remarks.

Studies of liquid and solid fuelled fires in a passage with no severely stratified flow have provided a better understanding of duct fires in moderate Froude number conditions. Higher Froude and Reynolds numbers would result in closer approximations to the idealized situation that is already well described by the model. Well mixed flow scenarios are therefore not problematic from a modelling or simulation point of view. In contrast to the well mixed flow condition is that of severe stratification or layering. Evidently this flow scenario is also not problematic when described with a simple model despite its appearance as being in complete contrast to ideal plug flow. It is likely that the intermediate flow regime, neither close to well mixed nor severely stratified, could present a more formidable simulation problem. Such methods as computational fluid dynamics (CFD) may be required to simulate or model this intermediate flow regime. However, an average gas temperature approach has also proved to be adequate when modelling in this flow regime.

In conclusion the present study has explored a broad range of flow scenarios. From well mixed flow, where heat feedback to fuel ahead of the fire is maximized, to mixing controlled and all the way to severely stratified flow, representing conditions of minimum feedback. The study has explored the flow problem and its effect on propagation for this class of fires.

6.2. Recommendations for Future Work

It is of the course quite difficult to determine the relevance of present results to ducts of realistic dimensions. One could speculate with some confidence that these results are scalable

in terms of Froude and Reynolds numbers, but in the end verification with results from larger passages would be necessary. Work on pressure modelling would also be valuable because, as de Ris *et al* (1973) show, small scale experiments may be used to simulate large scale events if certain conditions are met. Radiation is likely to be very important in larger scale fires and would certainly require more attention. Full-scale experiments to study radiation effects might also be unavoidable since not even pressure modelling techniques can accurately simulate radiation in the fire process unless specific conditions are met. See last paragraph of section 1.2.2. Present results in which stratification occurs provides some bearing on what one might expect from modelling large scale fires. This is because sever stratification is an effect that tends to persist in full scale fires.

One could in principle try to use CFD to model these fires, but this task is many orders of magnitude more complex than the one undertaken in this thesis, particularly if one accurately allows for radiation, mixing and the actual reactions involved. It seems that there are other approximations in the one dimensional model, such as radiation and stoichiometry, to which one should first pay attention before delving into CFD calculations. On the face of the evidence of fits between the present formulation and results, such complex calculations are not really warranted at this stage. The present model is one which uses only the average (center-line) gas temperature profile along the duct or reactive plume stream and has proved to be quite precise.

From a dynamics view point the observed jumping phenomenon displayed by fully-developed fires in ducts is very interesting. The question of whether subsequent jumping is indeed possible throughout the course of propagation is still unanswered, at least by experiment. Conditions for this are that very little or no fuel should vaporize or pyrolyse ahead of the fire while the fire burns at a uniform rate in the combustion zone. Ironically this same condition could result in extinction just as the fire attempts to jump onto a hardly volatile fuel surface occupied by the "excess fuel zone". However if a fuel/duct

system is chosen to have appropriate properties there may be just enough fuel pyrolysis and preheating ahead of the fire to prevent extinction during the jump-transition period. In such a case several clear jumps might be observed before steady state is reached during propagation. Fires propagating in severely stratified flow conditions also show some promise with regard to prolonged jumping because of minimal heat feedback to fuel ahead of the rising fire plume.

One can only speculate that open bush fires in strong wind conditions propagating downwind might also burn in a similar manner when the plume rises above the fuel surface ahead of the fire. Strong winds create a boundary layer over the burning bushes and therefore restrict air supply primarily to the upstream end of the fire. Much like confined fires studied in this thesis pyrolysing fuel ahead of the fire is starved of oxygen, only entering the fire process from the upstream end, and therefore will only ignite when the fire progresses to that region. Coupled with fuel loading distributions and varying wind speeds these are the same mechanisms controlling duct fire propagation in its simplest form. In a sense, these fires are also fuel-rich if one considers an envelope that engulfs only the reactive plume stream and its combustion products. In most cases such a plume stream will rise over the fuel surface and ahead of the fire due to an interaction between buoyant and crossflow forces, this being the same physics explored in the stratified flow analysis. Of course there are some major differences when one considers that bush fire propagation is dominated by radiative and not only convective/conductive heat transfer. Also propagation may be aided through fire-brand spotting due to strong winds transporting fire brands to new regions far ahead of the original parent fire. An extensive review of such wind effects on mass fire phenomena has been presented by Pitts (1991).

A fuel property based correlation for determining stratification has been proposed and although present data are well correlated more experimentation will be necessary. Prediction of stratification would be most useful in practical situations, and

indispensable in the application of the present model, if only fuel/duct properties need be known. Of course a great deal of work is still needed to understand the reactions occur in these fires before the stoichiometry can be predicted and used in such a correlation. It is pleasing to see that a recent publication (Tewarson *et al*, 1993) addresses some of these issues. Prediction of temperature stratification may then also be used to predict combustion product species stratification because it was shown by Newman (1984) that temperature and species stratification follow closely. Knowledge of such effects in passages becomes critical in avoiding hazardous encounters with hot toxic gases typically produced in confined fires.

APPENDIX A: PROGRAMS TO SOLVE MODEL EQUATIONS

The first program solves the entire set of model equations and outputs to three separate files. The gas temperature profile, fire propagation history and fuel mass loading at various stages of the propagation history are output to the files TMPR5ST.DTA, TMPR5SX.DTA, and TMPR5SM.DTA respectively. It can also provide such information as the average fire propagation speed, fuel loss rates, and the fraction of heat generated that goes into various parts of the fire process. The program is written in TURBO PASCAL and appears under the file name DUCTFIR.PAS. Some parts of this code are adapted from Young and Glasser (1990).

```
{$M 32000,0,655360}
Program Firehop(input,output);

type
    vect1by100 = array [1..800] of real;
var
   i,j,kk,l,ie          :integer;
   xlbz,qbl,xmo,
   xmvf,xil,xmv,x,
   x2,dt2,di,dx,
   qvap,qtot,vprop,
   tl,tvl               :real;
   tc,xc,te,xe,tp,
   xp,dmodx,mo,m,
   me,mb,too            :vect1by100;
   outfile,outfile2,
   outfile3             :text;
const
                {* MODEL PARAMETERS ARE ENTERED HERE *}
{1 ENTHALPY OF REACTION OF FUEL (GASEOUS) WITH OXYGEN J/(KG OF OXYGEN)}
    dhr=12.76E6;
{2 DUCT CROSS SECTIONAL AREA (M2)}
    xar=1.556e-3;
{3 WIND SPEED (M/S)}
    vw=0.314;
{4 STOCHIOMETRIC COEFFICIENT FOR FUEL (KG FUEL/KG OXYGEN)}
```

```
    beta=1.5...,
{5 FUEL BURNING RATE (KG FUEL/M2 OF FUEL S)}
    fbr=0.0120;
{6 PERIMETER OF FUEL CROSS SECTION M}
    fprim=0.05;
{7 ENTHALPY OF VAPOURIZATION OF FUEL J/KG}
    hvap=27.2e4;
{8 MEAN SPECIFIC HEAT CAPACITY OF GAS J/KKG}
    cpg=1400.0;
{9 PERIMETER OF DUCT M}
    dprim=0.085;
{10 HEAT TRANSFER COEFF BETWEEN GAS AND DUCT WALLS (W/M2K)}
    ud=42.0; ud2=18.0;
{11 HEAT TRANSFER COEFF BETWEEN GAS AND FUEL, hf (W/M2K)}
    uf=3.0;
{12 FUEL VAPOURIZATION TEMP C}
    tvap=99.2;
{13 AMBIENT TEMP C}
    tamb=24.4;
{14 AMBIENT PRESSURE Pa}
    pamb=85113.0;
{15 FUEL LOADING IN DUCT (KG OF FUEL/M LENGTH OF DUCT)}
    xlmda=0.1833;
{16 FUEL LOADING PER UNIT AREA}
    ma=3.6667;
{17 1-bypass fraction}
    bypass=1.0;
k=10; {*increment*}
{=============================================================================}

function pr(base,power:real):real;
    begin
    pr:=exp(power*ln(base));
    end;
{=============================================================================}

procedure combustion_zone(var   xi1,xmvf,xmo,xlbz,qbl   :real;
                          var   tc,xc                   :vect1by100);
```

```
  var
     xntot,xmvx,tmax,
     htrcor,alpha,fhl,
     fhv,fhh,ftot          :real;


begin
{CALCULATE INITIAL GAS FLOWRATES USING I.G LAW}
  xntot:=vw*xar*pamb/(8.314*(tamb+273.0));
  xmo:=0.0288*xntot;
  xmvf:=0.032*0.21*xntot*beta*bypass;
{CALCULATION OF LENGTH OF BURNING ZONE}
  xmvx:=fbr*fprim;
  xlbz:=xmvf/xmvx;  {BURNING LENGTH}
  tmax:=((dhr*(1/beta)*xmvx-xmvx*hvap))/(xmvx*cpg+dprim*ud);
  htrcor:=dprim*ud/(xmvx*cpg);
  for i:=1 to k do
    begin
    xc[i]:=(i*xlbz)/(k-1)-xlbz/(k-1);
    tc[i]:=tamb+tmax*(1-pr(1+xmvx*xc[i]/xmo,-(1+htrcor)));
{    writeln(xc[i]:3:3,'  ',tc[i]:3:3);}
    end;
  alpha:=xmvx/xmo;
  if(htrcor > 0)then
    xil:=tmax*(xlbz+(1/(htrcor*alpha))*(pr(1+alpha*xlbz,-htrcor)-1))
    else
    xil:=tmax*xlbz-(1/alpha)*ln(1+alpha*xlbz);
  qbl:=dprim*ud*xil;
{ENERGY BALANCE CONSISTENCY CHECK}
  fhl:=qbl*beta/(xmvf*dhr);
  fhv:=xmvf*hvap*beta/(xmvf*dhr);
  fhh:=(xmvf+xmo)*cpg*(tc[k]-tamb)*beta/(xmvf*dhr);
  ftot:=(fhl+fhv+fhh);
{ftot SHOULD BE 1}
writeln('latent:',fhv:3:3,'  lost:',fhl:3:3,'  heated:',fhh:3:3);
end;
{=============================================================================}

function fn(c1,c2,c3,c4,c5,c6,x,y : real): real;
```

```
begin;
fn:=(c5*x-c4*y-c6)/(c2*y-c3*x+c1)
end;
{=============================================================================}

Procedure rk4(c1,c2,c3,c4,c5,c6,h,x0,y0 : real; var x1,y1 : real);
(This performs one step of the 4th order Runge Kutta Method)
Var
   xk1,xk2,xk3,xk4 : real;

Begin

   xk1:=h*fn(c1,c2,c3,c4,c5,c6,X0,Y0);
   xk2:=h*fn(c1,c2,c3,c4,c5,c6,x0+0.5*h,y0+0.5*xk1);
   xk3:=h*fn(c1,c2,c3,c4,c5,c6,x0+0.5*h,y0+0.5*xk2);
   xk4:=h*fn(c1,c2,c3,c4,c5,c6,x0+h,y0+xk3);
   x1:=x0+h;
   y1:=y0+(xk1+2.0*xk2+2.0*xk3+xk4)/6.0;

end;
{=============================================================================}

Procedure excessfuelzone(xmo,xmvf,xi1,xlbz          : real;
                         var xmv,x2,dt2,qbl,di,dx   : real;
                         var j                      :integer;
                         var te,xe                  : vectlby100);

Var
   c1,c2,c3,c4,c5,c6,
   dx0,di0,h,dxf,dte,
   xwr,test,dxh,qblex,
   dxmv,dt,fhl2,fhv2,
    hh2,ftot2          :real;
   i,num               :integer;

Begin

    c1:=(xmo+xmvf)*cpg;
    c2:=fprim*uf*cpg/hvap;
```

```
    c3:=(fprim*uf*cpg*(tvap-tamb))/hvap;
    c4:=dprim*ud2+fprim*uf;
    c5:=fprir*uf*(tvap-tamb);
    c6:=dprim*ud*xil+xmvf*hvap-dhr*xmvf/beta;

  dx0:=0.0;
  di0:=0.0;
  h:=xlbz/(k-1);
  dxf:=500;
  j:=1;
  test:=1.0;
    While test > 0 do begin
        rk4(c1,c2,c3,c4,c5,c6,h,dx0,di0,dx,di);
        dx0:=dx;              {*x-increment*}
        di0:=di;
           dte:=fn(c1,c2,c3,c4,c5,c6,dx,di);
           xwr:=dx+xlbz;
         {  writeln(dx:5:3,'':3,dte+tamb:5:2,'  ',j);}
           j:=j+1;
         te[j]:=dte+tamb;
         xe[j]:=dx+xlbz;
        { writeln(xe[j]:5:3,'':3,te[j]:5:2,'  ',j);}
         dt:=(c5*dx-c4*di-c6)/(c2*di-c3*dx+c1);
         test:=dt-(tvap-tamb);
       end;
       te[1]:=tc[k];    {*SET THIS CONDITION*}
       xe[1]:=xc[k];
    dt2:=dt;
    qblex:=dprim*ud2*di;
    qbl:=qbl+qblex;
    dxmv:=(fprim*uf/hvap)*(di-(tvap-tamb)*dx);
    xmv:=xmvf+dxmv;
    x2:=dx;

{Energy balance consistency check in the combustion and excess fuel zones}
{fhl2 is the fraction of energy liberated lost to the walls}
{fhv2 is the fraction of energy used to vaporize the fuel}
{fhh2 is the fraction of energy used to heat the gas}
```

```
      fhl2:=qbl*beta/(xmvf*dhr);
      fhv2:=xmv*beta*hvap/(xmvf*dhr);
      fhh2:=(xmv+xmo)*cpg*dt*beta/(xmvf*dhr);
      ftot2:=fhl2+fhv2+fhh2;
      writeln('latent:',fhv2:3:3,'  lost:',fhl2:3:3,'  heated:',fhh2:3:3);
end;
{=============================================================================}

Procedure preheatingzone(xi1,di,xmv,xmvf,
                         xm0,xlbz,x2,dt2,qbl          :real;
                         var   qvap,qtot,vprop        :real;
                         var   kk                     :integer;
                         var   tp,xp                  :vect1by100);
Var
   xi2,eta,xmu,dx,
   dt,x,increment,qpr   :real;

Begin;
increment:=0.05;
xi2:=xi1+di;
eta:=dhr*xmvf/(beta*dprim*ud2)-xi2-xmv*hvap/(dprim*ud2)-xi1*(ud/ud2-1);
xmu:=dprim*ud2/((xm0+xmv)*cpg);
dx:=0;
dt:=5000.0;
kk:=0;
   while dt > 10 do begin
      kk:=kk+1;
      dx:=dx+increment;
      dt:=eta*xmu*exp(-xmu*dx);
      x:=xlbz+x2+dx;
      tp[kk]:=dt+tamb;
      xp[kk]:=x;
     { writeln(outfile2,x:5:2,'':3,dt:5:2);}
   end;
{Heat loss in the preheating zone}
    Qpr:=(xm0+xmv)*cpg*dt2;
{Total heat loss}
    Qtot:=qpr+qbl;
    Qvap:=xmv*hvap;
```

```
{Fire Propogation velocity}
    vprop:=((dhr*xmvf/beta)-qtot)/(xlmda*hvap);
end;
{═══════════════════════════════════════════════════════════════════════}

procedure initial_mo(j,k  :integer;
                     var   mo    :vectlby100);
var
i   :integer;

   begin
   for i:= 1 to k+j-1 do
     mo[i]:=ma;
       {*INCLUDE COMBUSTION ZONE*}
     (*EQUATION FOR INITIAL FUEL LOADING*)
   end;
{═══════════════════════════════════════════════════════════════════════}

procedure excessloss(j,k  :integer; t :REAL;  mo,tm  :vectlby100;
                     var m       :vectlby100);
   var i:integer;

 begin
 tm[j]:=tvap;
 for i:=1 to j do
  begin
  m[i]:=mo[i+k-1] - t*uf*(tm[i]-tvap)/hvap;
{  writeln(m[i]:3:3,'  ',mo[i]:3:3,'  ',ta[i]:3:3,'  ',i);}
  end;
 for i:=j+1 to j+k-1 do
  m[i]:=ma;
 end;
{═══════════════════════════════════════════════════════════════════════}

procedure reinitial(m   :vectlby100; j,k   :integer;
                    var  mo   :vectlby100);

  var i   :integer;
```

```
  begin
  for i:=i to k-1 do
    mo[i]:=0;
  for i:=k to j+k-1 do
    begin
    mo[i]:=m[i];
    end;
  end;
{=============================================================================}

procedure burn(k :integer;  m  :vectlby100;
               var  mb  :vectlby100);

var  i  :integer;

   begin
   for i:=1 to k do
     mb[i]:=m[i]-m[1];
   end;
{=============================================================================}

procedure  dist_time(mo   :vectlby100; tv   :REAL;  k :integer;
                     var   too  :vectlby100);
   var   i  :integer;

    begin
    for i:=1 to k do
      too[i]:=mo[i]/fbr + tv;
    end;
{=============================================================================}

procedure velocburn(mo,tm  :vectlby100;too :vectlby100;k :integer;tv  :real;
                    var   m    :vectlby100);
   var
      trap    :REAL;
      i,kk,cc    :integer;
      int,burn,h   :vectlby100;
```

```
      begin
      if (k>j) then
       begin
       for cc:=j to k do
        tm[cc]:=tvap;
       end;
      tm[j]:=tvap;
      h[1]:=too[2]-tv;
      for i:=2 to k-1 do
       h[i]:=too[i+1]-too[i];
      burn[1]:=fbr*(too[k]-tv);
      iNT[1]:=0;
      for I:=2 to k do      {USING TRAPEZOIDAL RULE}
       begin
       trap:=0;
       for kk:=1 to i-1 do
         begin
         trap:=h[i-kk]*uf*((tm[kk]-tvap)+(tm[kk+1]-tvap))/(hvap*2) + trap;
         end;
       int[i]:=trap;
       burn[i]:=fbr*(too[k]-too[i]);
       end;
      for i:=1 to k do
       m[i]:= mo[i]-int[i]-burn[i];
      end;
{=============================================================================}

procedure velocexcess(mo,tm :vect1by100;too:vect1by100;tv :REAL;j,k:integer;
                      var m  :vect1by100);
   var
      trap    :REAL;
      i,kk    :integer;
      int   :vect1by100;
      h  :vect1by100;

     begin
     tm[j]:=tvap;
     h[1]:=too[2]-tv;
     for i:=2 to k-1 do
```

```
      h[i]:=too[i+1]-too[i];
     for i:=0 to j-k do      {USING TRAPEZOIDAL RULE}
      begin
      trap:=0;
      for kk:=2 to k do
        begin
        trap:=h[k+1-kk]*uf*((tm[kk+i-1]-tvap)+(tm[kk+i]-tvap))/(hvap*2) + trap;
        end;
      int[i+1]:=trap;
      end;
     for i:=1 to j-(k-1) do
      m[i+(k-1)]:= mo[i+(k-1)]-int[i];
     end;
{=============================================================================}

procedure velocfresh(mo,tm :vect1by100;too :vect1by100;tv  :real;j,k :integer;
                     var   m    :vect1by100);
   var
      trap    :REAl;
      i,kk,cc    :integer;
      int,burn,h   :vect1by100;


     begin
     if (k>j) then
      begin
      for cc:=j to k do
       tm[cc]:=tvap;
      end;
     tm[j]:=tvap;
     h[1]:=too[2]-tv;
     for i:=2 to k-1 do
      h[i]:=too[i+1]-too[i];
     for i:=1 to k-1 do      {USING TRAPEZOIDAL RULE}
      begin
      trap:=0;
      for kk:=1 to i do
        begin
     trap:=h[k-kk]*uf*((te[j+kk-i-1]-tvap)+(te[j+kk-i]-tvap))/(hvap*2) + trap;
```

```
        end;
       int[k-i]:=trap;
       end;
       int[k]:=0;
      for i:=1 to k do
       m[i+j-1]:= mo[i+j-1]-int[i];
      end;
{=============================================================================}

procedure velocfresh2(mo,tm :vect1by100;too :vect1by100;tv :real;j,k :integer;
                      var   m    :vect1by100);
   var
      trap    :REAL;
      i,kk,cc    :integer;
      int,burn,h   :vect1by100;


     begin
     if (k>j) then
      begin
      for cc:=j to k do
       tm[cc]:=tvap;
      end;
     tm[j]:=tvap;
     h[1]:=too[2]-tv;
     for i:=2 to k-1 do
      h[i]:=too[i+1]-too[i];
     for i:=1 to j-1 do      (USING TRAPEZOIDAL RULE)
      begin
      trap:=0;
      for kk:=1 to i do
        begin
      trap:=h[k-kk]*uf*((te[j+kk-i-1]-tvap)+(te[j+kk-i]-tvap))/(hvap*2) + trap;
        end;
      int[j-i]:=trap;
      end;
      int[j]:=0;
     for i:=1 to j do
      begin
```

```
      m[i+k-1]:= mo[i+k-1]-int[i];
      end;
     end;
{=============================================================================}
                          {* MAIN CODE BEGINS *}
begin
assign(outfile,'c:\tmpr5sx.Dta');  {* Propagation History *}
rewrite(outfile);
assign(outfile2,'c:\tmpr5st.dta'); {* Gas Temperature Profile *}
rewrite(outfile2);
assign(outfile3,'c:\tmpr5sm.dta'); {* Fuel Mass Loading Distribution *}
rewrite(outfile3);
for l:=1 to k do
  too[l]:=0;
                  {* Solving the Gas Temperature Profile *}
combustion_zone(xil,xmvf,xmo,xlbz,qbl,tc,xc);
excessfuelzone(xmo,xmvf,xil,xlbz,xmv,x2,dt2,qbl,di,dx,j,te,xe);
preheatingzone(xil,di,xmv,xmvf,xm0,xlbz,x2,dt2,qbl,qvap,qtot,vprop,kk,tp,xp);
for l:=1 to k do
  writeln(outfi 2,xc[l]:3:3,'   ',tc[l]:3:3);
for l:=1 to j do
  writeln(outfile2,xe[l]:3:3,'   ',te[l]:3:3);
for l:=1 to kk do
  writeln(outfile2,xp[l]:3:3,'   ',tp[l]:3:3);

writeln('Combustion zone length:',xlbz:3:3,'        vprop: ',vprop:3:9);
writeln('Excess fuel zone length:',dx:3:3,'     ',j);
  writeln(outfile,0,'  ',xlbz:3:3);
   initial_mo(j,k,mo);
      tl:=mo[1]/fbr; X:=2*xlbz;
   writeln(outfile,tl:3:3,'  ',xlbz:3:3);
   excessloss(j,k,tl,mo,te,m);
   for ie := 1 to j do
writeln(outfile3,xe[ie]:3:3,'  ',m[ie]:3:3);
      {tl:=tl + xlbz/Vw;}  {* Must put an if statement for other fuel loadings}
        {*initialize*}
{      initial_mo(j,k,m);}   {*Initail if mo is not flat*}
      tvl:=m[1]/fbr + tl;
       writeln(outfile,tl:3:4,'  ',x:3:3);
```

```
      writeln(outfile,tv1:3:4,'  ',x:3:3);

If (k<j) Then   (* IF COMBUSTION ZONE IS LARGER THAN EXCESSFUEL ZONE *)
  begin

   for l:=1 to 10 do   (* REPEAT  AS MANY TIMES AS REQUIRED *)
    begin
    burn(k,m,mb);
     writeln(outfile3);
      for ie := 1 to k do
        writeln(outfile3,xc[ie]+x-xlbz:3:3,'  ',mb[ie]:3:3);
        reinitial(m,j,k,mo);
        dist_time(mb,tv1,k,too);
        for i:= 2 to k do
           begin
           x:=x+xlbz/(k-1);
          { if (too[i]<(x-xlbz)/Vw) then
             begin
             too[i]:=(x-xlbz)/Vw;
             end;}
     writeln(outfile,too[i]:3:3,'  ',x:3:3);
          end;
       excessloss(j,k,tv1-t1,mo,te,me);
    for ie := 1 to j do
       writeln(outfile3,xe[ie]+x-2*xlbz:3:3,'  ',me[ie]:3:3);
       velocburn(me,te,too,k,tv1,m);
       velocexcess(me,te,too,tv1,j,k,m);
       velocfresh(me,te,too,tv1,j,k,m);
         tv1:=m[1]/fbr+too[k];
         t1:=too[k];
       writeln(outfile,tv1:3:3,'  ',x:3:3);
    end;          (* UNTIL AS MANY TIMES AS REQUIRED *)

  end
 else          (* IF COMBUSTION ZONE   IS SHORTER THAN EXCESSFUEL ZONE *)
  begin

for l:=1 to 5 do           (* REPEAT  AS MANY TIMES AS REQUIRED *)
    begin
```

```
    burn(k,m,mb);
     writeln(outfile3);
      for ie := 1 to k do
        writeln(outfile3,xc[ie]+x:3:3,'  ',mb[ie]:3:3);
        reinitial(m,j,k,mo);
      for ie := 1 to j do
        writeln(outfile3,xe[ie]+x:3:3,'  ',mo[ie+k-1]:3:3);
        dist_time(mb,tv1,k,too);
        for i:= 2 to k do
           begin
           x:=x+xlbz/(k-1);
          ( if (too[i]<(x-xlbz)/Vw) then
             begin
             too''']:=(x-xlbz)/Vw;
             end;)
      writeln(outfile,too[i]:3:3,'  ',x:3:3);
           end;
       excessloss(j,k,tv1-t1,mo,te,me);
       velocburn(me,te,too,k,tv1,m);
       velocfresh2(me,te,too,tv1,j,k,m);
         tv1:=x[1]/fbr+too[k];
         t1:=too[k];
       writeln(outfile,tv1:3:3,'  ',x:3:3);
    end;          (* UNTIL AS MANY TIMES AS REQUIRED *)
  end;

close(outfile);
close(outfile2);
close(outfile3);
end.              (* END OF MAIN CODE *)
```

```
    burn(k,m,mb);
     writeln(outfile3);
      for ie := 1 to k do
        writeln(outfile3,xc[ie]+x:3:3,'  ',mb[ie]:3:3);
        reinitial(m,j,k,mo);
      for ie := 1 to j do
        writeln(outfile3,xc[ie]+x:3:3,'  ',mo[ie+k-1]:3:3);
        dist_time(mb,tv1,k,too);
        for i:= 2 to k do
           begin
           x:=x+xlbz/(k-1);
          ( if (too[i]<(x-xlbz)/Vw) then
             begin
             too[i]:=(x-xlbz)/Vw;
             end;)
      writeln(outfile,too[i]:3:3,'  ',x:3:3);
           end;
       excessloss(j,k,tv1-t1,mo,te,m);
       velocburn(me,te,too,k,tv1,m);
       velocfresh2(me,te,too,tv1,j,k,m);
         tv1:=m[1]/fbr+too[k];
         t1:=too[k];
       writeln(outfile,tv1:3:3,'  ',x:3:3);
    end;          (* UNTIL AS MANY TIMES AS REQUIRED *)
  end;

close(outfile);
close(outfile2);
close(outfile3);
end.              (* END OF MAIN CODE *)
```

The following TURBO PASCAL program solves the combustion zone equation with the effect of thermal radiation heat losses using the Stefan-Boltzmann expression.

```
Program Radiation (input,output);

var
     outfile  :text;

const
                (* MODEL PARAMETERS ARE ENTERED HERE *)
{1 ENTHALPY OF REACTION OF FUEL (GASEOUS) WITH OXYGEN J/(KG OF OXYGEN)}
    dhr=13.07E6;
{2 DUCT CROSS SECTIONAL AREA (M2)}
    xar=1.556e-3;
{3 WIND SPEED (M/S)}
    vw=0.283;
{4 STOCHIOMETRIC COEFFICIENT FOR FUEL (KG FUEL/KG OXYGEN)}
    beta=0.962;
{5 FUEL BURNING RATE (KG FUEL/M2 OF FUEL S)}
    fbr=7.31e-3;
{6 PERIMETER OF FUEL CROSS SECTION M}
    fprim=0.05;
{7 ENTHALPY OF VAPOURIZATION OF FUEL J/KG}
    hvap=272000.00;
{8 MEAN SPECIFIC HEAT CAPACITY OF GAS J/KKG}
    cpg=1400.0;
{9 PERIMETER OF DUCT M}
    dprim=0.085;
{10 HEAT TRANSFER COEFF BETWEEN GAS AND DUCT WALLS (W/M2K)}
    ud=2.0;
{11 FUEL VAPOURIZATION TEMP C}
    tvap=99.2;
{12 AMBIENT TEMP C}
    tamb=33.0;
{13 AMBIENT PRESSURE Pa}
    pamb=85113.0;
{14 1-bypass fraction}
```

```
    bypass=1.0;
    xlbz=0.26;
    em=0.60;          {* Emissivity *}
    stef=5.6697e-8;   {* Stefan-Boltzmann const. *}
    mo=4.26e 4;       {* Mass of air flowrate *}
{=============================================================================}

function fn(x:  real; T:  real):  real;  (* COMBUSTION ZONE EQUATION *)
 var
 a,b,c,d,e,aa  :real;

 begin
 a:=(dhr/beta)*fprim*fbr-hvap*fprim*fbr;
 b:=cpg*fprim*fbr+dprim*ud;
 c:=dprim*em*stef;
 d:=mo*cpg;
 e:=cpg*fprim*fbr;
 fn:=(a-b*(T-Tamb)-c*(sqr(sqr(T+273))-sqr(sqr(Tamb+273))))/(d+e*x);
 end;
{=============================================================================}

procedure rungek4;      {4th ORDER RUNGE-KUTTA ALGORITH *}

  var
     xnew,Tnew,xn,Tn,ko,
     k1,k2,k3,xn1,xn2,xn3,
     Tn1,Tn2,Tn3,h          :real;

begin
 h:=0.005;
 xnew:=0.0;
 Tnew:=Tamb;
 repeat
  xn:=xnew;
  Tn:=Tnew;
  ko:=h*fn(xn,Tn);
  xn1:=xn+h/2; Tn1:=Tn+ko/2;
  k1:=h*fn(xn1,Tn1);
  xn2:=xn+h/2; Tn2:=Tn+k1/2;
```

```
  k2:=h*fn(xn2,Tn2);
  xn3:=xn+h; Tn3:=Tn+k2;
  k3:=h*fn(xn3,Tn3);
  Tnew:=Tn+(ko+2*k1+2*k2+k3)/6;
  xnew:=xn+h;
  writeln(outfile,xnew:3:3,'      ',Tnew:3:3);
 until(xnew > xlbc);
end;
{=============================================================================}

begin                          (* MAIN CODE *)
assign(outfile,'c:\butol4br.dat');
rewrite(outfile);
Rungek4;
close(outfile);
end.                           (* MAIN CODE *)
```

APPENDIX B: DATA AND FILE LISTING FOR RETRIEVAL

Run	Air Flowrate l/min	File Name T(x,t)
1 Iso	140	TMP1S.DAT
2 Iso	29.0	TMP2S.DAT
3 Iso	85.0	TMP3S.DAT
4 Iso	61.0	TMP4S.DAT
5 Iso	29.4	TMP5S.DAT
6 Iso	104	TMP6S.DAT
7 Butol	60.1	BUTOL2.DAT
8 Butol	26.4	BUTOL4R.DAT
9 Eg	26.0	EG1S.DAT
*10 Iso	29.3	TMPR5S.DAT
*11 Butol	25.9	BUTOL4.DAT

*Repeat runs.

TABLE B.1. Data files of liquid fuelled fires in small duct.

Run	Air Flowrate l/min	File Name T(x,t)
1 Strips	43.6	PMMA19.DAT
2 Strips	30.0	PMMA15.DAT
3 Strips	30.0	PMMA20.DAT
4 Strips	29.8	PMMA17.DAT
5 Flakes	33.9	PMMA26.DAT
6 Flakes	30.1	PMMA22.DAT
7 Flakes	29.9	PMMA27.DAT
GROWTH OVER SHEET EXPERIMENT	21.3	PMMA.DAT

TABLE B.2. Data files of PMMA fuelled fires in small duct, including the fire growth run of chapter 4.

Run	Air Flowrate l/min	File Name T(x,y,t)
1 Iso	123	TMP2.WKQ
2 Iso	173	TMP3.WKQ
3 Iso	146	TMP4.WKQ
4 Iso	124	TMP5.WKQ
5 Iso	172	TMP6.WKQ
6 Etoh	122	ETOH1.WKQ
7 Etoh	229	ETOH2.WKQ
8 Etoh	174	ETOH3.WKQ
9 Etoh	123	ETOH4.WKQ
10 Etoh	229	ETOH5.WKQ
11 Eg	232	EG1.WKQ
12 Eg	340	EG2.WKQ
13 Eg	675	EG3.WKQ
14 Eg	231	EG5.WKQ
15 Eg	675	EG6.WKQ

TABLE B.3. Data files of liquid fuelled fires in stratified flow (chapter 5).

m'' kg/m^2	Air Flowrate l/min	File Name T(x,t)
1.16	21.3	PMMAF.DAT
2.33	29.6	PMMA1.DAT
1.16	43.4	PMMA2.DAT
1.74	83.9	PMMA3.DAT
1.74	83.8	PMMA5.DAT
1.16	43.4	PMMA7.DAT
1.74	43.3	PMMA8.DAT
1.16	43.9	PMMA9.DAT

TABLE B.4. PMMA flake experiment data files for V_{ss} versus $(\dot{m}_a/\lambda)$ for ta.

PMMA15		PMMA17		PMMA19		PMMA20	
x m	m'' kg/m^2	x m	m'' kg/m^2	x m	m'' kg/m^2	x m	m'' kg/m^2
1.360	0.21	0.820	0.21	1.135	0.28	0.930	0.33
1.379	0.39	0.842	0.37	1.155	0.30	0.952	0.49
1.404	0.70	0.869	0.65	1.177	0.42	0.991	0.87
1.430	1.08	0.892	0.92	1.209	0.71	1.035	1.18
1.456	1.59	0.917	1.27	1.241	1.05	1.071	1.28
1.481	1.94	0.946	1.37	1.283	1.45	1.102	1.65
1.506	2.28	0.973	1.40	1.339	2.06	1.141	1.96
1.532	2.58	1.002	1.62	1.390	2.40	1.182	2.30
1.558	3.00	1.032	1.82	1.437	2.65	1.223	2.59
1.584	3.35	1.066	2.32	1.486	2.94	1.265	2.84
1.611	3.52	1.102	2.90	1.536	3.35	1.306	3.10
1.643	3.76	1.134	2.98	1.587	3.50	1.348	3.54
1.679	4.15	1.166	3.24	1.637	3.67	1.389	3.76
1.713	4.30	1.196	3.24	1.691	3.91	1.429	3.76
1.746	4.28	1.225	3.62	1.749	4.05	1.467	3.89
1.779	4.33	1.260	3.87	1.800	4.09	1.504	3.96
1.809	4.58	1.297	3.92	1.842	4.21	1.544	3.80
1.838	4.64	1.331	3.89	1.590	3.89		
1.873	4.73	1.365	3.91	1.631	3.81		
1.909	4.90			1.668	3.79		
1.938	4.68						
1.966	4.69						

TABLE B.5. Fuel mass loading data from PMMA strips experiments (steady-state).

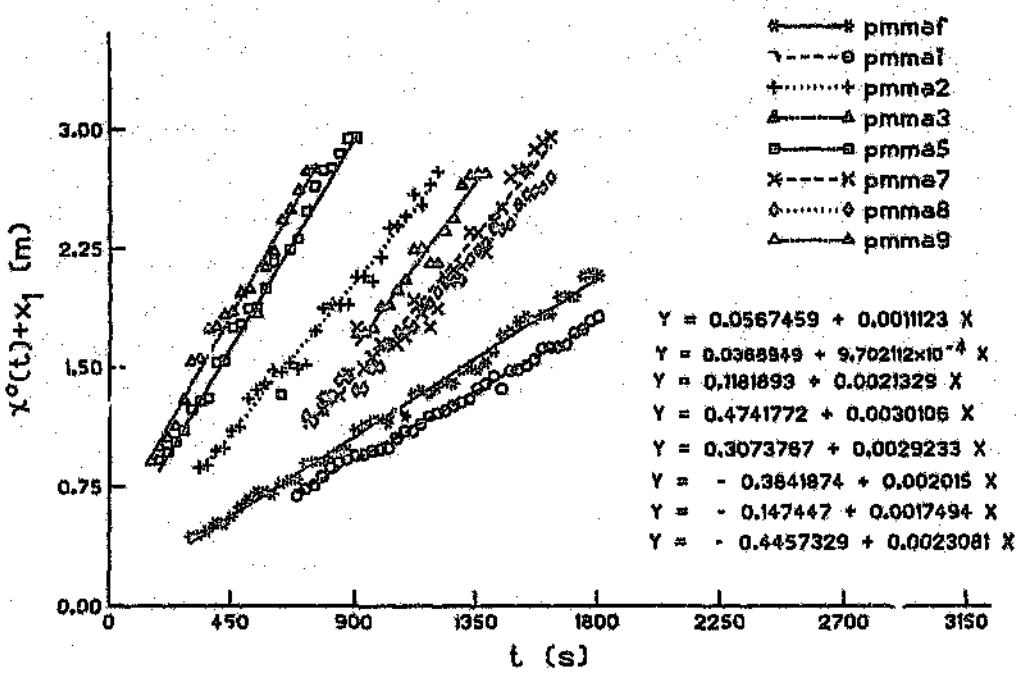


FIGURE B.1. Steady-state propagation rate data from PMMA flakes experiments.

DATA RETRIEVAL

All computer programs and data files referred to in this appendix are stored on a disc which is included in this appendix.

All data files have been compressed to save disc space. Compressed versions are in four files namely B1.ARJ, B2.ARJ, B3.ARJ and B4.ARJ, each representing data files found in tables B.1, B.2, B.3, and B.4 respectively. To de-compress, for example, files in B1.ARJ (files listed in table B.1) and send data files to a disc on drive b type as follow at the DOS prompt when the original parent disc is in the current drive

ARJ e B1 b:\

For help on ARJ (the back-up utility), type "arj" and ENTER.

The TURBO PASCAL program below reads-in data from the source data file (e.g., PMMA20.DAT) and arranges the data in DISTANCE, TEMPERATURE and TIME columns into another file (e.g., PMMA20C.DAT). It is written only for the small duct data (non-stratified analyses). It appears under the filename "DATSORT.PAS". The source files contain no distances, only thermocouple numbers for each temperature measured. Stratified flow (large duct) data, however, are already in this type of format and are in the form of QUATRO spreadsheet files and do not require sorting (files in table B.3). Data files from tables B.1, B.2 and B.4 WILL require this program to sort the data.

```
Program datsort(input,output);     {FOR SMALL DUCT}
    VAR
        INFILE,OUTFILE,INFL          :TEXT;
        I,ii                         :INTEGER;
        TITLE                        :STRING[30];
        TEMP,TIME,DIST,DIS,TEM,TIM   :ARRAY[1..34]OF REAL;
BEGIN
DIS[1]:=0.0;DIS[2]:=0.091;DIS[3]:=0.182;DIS[4]:=0.273;DIS[5]:=0.364;
DIS[6]:=0.455;DIS[7]:=0.546;DIS[8]:=0.637;DIS[9]:=0.728;DIS[10]:=0.819;
DIS[11]:=0.91;DIS[12]:=1.001;DIS[13]:=1.092;DIS[14]:=1.183;DIS[15]:=1.274;
DIS[16]:=1.365;DIS[17]:=1.456;DIS[18]:=1.547;DIS[19]:=1.638;DIS[20]:=1.729;
DIS[21]:=1.82;DIS[22]:=1.911;DIS[23]:=2.002;DIS[24]:=2.093;DIS[25]:=2.184;
DIS[26]:=2.275;DIS[27]:=2.366;DIS[28]:=2.457;DIS[29]:=2.548;DIS[30]:=2.639;
DIS[31]:=2.73;DIS[32]:=2.821;DIS[33]:=2.912;DIS[34]:=3.003;
ASSIGN(INFILE,'a:\pmma20.dat');
RESET(INFILE);
ASSIGN(OUTFILE,'a:\pmma20c.dat');
REWRITE(OUTFILE);
  READ(INFILE,TITLE);
  I:=0;
  WHILE NOT EOF(INFILE) DO
      BEGIN
        I:=I+1;
        READ(INFILE,DIST[I]);READ(INFILE,TEMP[I]);READ(INFILE,TIME[I]);
        IF (I=34) THEN
```

```
        BEGIN
        for ii:=1 to 34 do
        begin
        writeln(outfile,dis[ii]:3:3,' ',temp[ii]:3:2,' ',time[ii]:3:2);
        end;
        writeln(outfile);
        i:=0;
        END;
      END;
CLOSE(INFILE);
CLOSE(OUTFILE);
END.
```

The TURBO PASCAL program below reads a source data file (e.g., PMMA20.DAT) and calculates the position of the maximum temperature for each measured temperature profile and stores in another file (e.g., PMMA20X.DAT) this position versus time data (fire-front versus time data). As the program is shown it is only for small duct data and appears under the filename "FLAMFRON.PAS". For large duct data the set of numbers shown in the program code must be replaced with those appearing at the end of this program. In this case the program can be used on any one set of thermocouples (floor, middle or ceiling). Calculations of fire-front versus time data are based on parabolic interpolations.

```
Program FlameFront(input,output);

   VAR
        INFILE,OUTFILE,INFL        :TEXT;
        I,Imax,J,N,K,L,point1,point2,count    :INTEGER;
        NUM,TMAX,Q1,Q2,y1,y2,y3,x1,x2.
        x3,xmax,ymax               :REAL;
        TITLE                      :STRING[30];
        TN                         :ARRAY[1..34] OF INTEGER;
        TEMP,TIME,DIST             :ARRAY[1..34]OF REAL;
        DIS                        :ARRAY[1..34]OF REAL;
```

```
        tim,x                   :ARRAY[1..200]OF REAL;
        LASTELEMENT             :BOOLEAN;

Procedure Quadratic(x1,x2,x3,y1,y2,y3 :Real;
                    Var  xmax,ymax    :Real);
  Var a,b,c :Real;

 Begin
 a:=((x1-x2)*(y2-y3)-(x2-x3)*(y1-y2))/((sqr(x2)-sqr(x3))*(x1-x2)-(x2-x3)*
                                                    (s  (x1)-sqr(x2)));
 b:=((y1-y2)-a*(sqr(x1)-sqr(x2)))/(x1-x2);
 c:=y1-a*sqr(x1)-b*x1;
 xmax:=-b/(2*a);
 ymax:=a*sqr(xmax)+b*xmax+c;
 End;

 BEGIN
      {*This set of numbers is used to convert thermocouple numbers}
      {to actual distances (meters). For the large duct they must be}
      {replaced with the set of numbers appearing at   nd of this}
      {program.*}
 DIS[1]:=0.0;DIS[2]:=0.091;DIS[3]:=0.182;DIS[4]:=0.273;DIS[5]:=0.364;
 DIS[6]:=0.455;DIS[7]:=0.546;DIS[8]:=0.637;DIS[9]:=0.728;DIS[10]:=0.819;
 DIS[11]:=0.91;DIS[12]:=1.001;DIS[13]:=1.092;DIS[14]:=1.183;DIS[15]:=1.274;
 DIS[16]:=1.365;DIS[17]:=1.456;DIS[18]:=1.547;DIS[19]:=1.638;DIS[20]:=1.729;
 DIS[21]:=1.82;DIS[22]:=1.911;DIS[23]:=2.002;DIS[24]:=2.093;DIS[25]:=2.184;
 DIS[26]:=2.275;DIS[27]:=2.366;DIS[28]:=2.457;DIS[29]:=2.548;DIS[30]:=2.639;
 DIS[31]:=2.73;DIS[32]:=2.821;DIS[33]:=2.912;DIS[34]:=3.003;

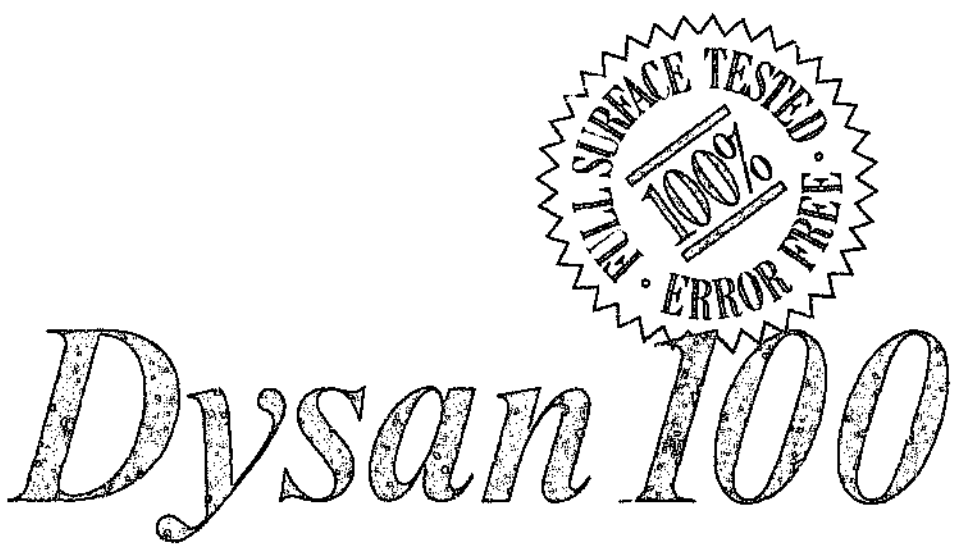
 ASSIGN(INFILE,'a:\PMMA20C.DAT');
 RESET(INFILE);
 ASSIGN(OUTFILE,'a:\PMMA20x.DAT');
 REWRITE(OUTFILE);
{   READ(INFILE,TITLE);}
   I:=0;j:=0;
   WHILE j<50 DO  (* Depends on length of data file*)
       BEGIN
         I:=I+1;
         READ(INFILE,DIST[I]);READ(INFILE,TEMP[I]);READ(INFILE,TIME[I]);
```

```
        IF (I=34) THEN   (I=12 For Large Tunnel; I=34 For Small Duct)
         BEGIN
         Q1:=0;
         FOR i:=1 TO 34 DO
           BEGIN
           If (temp[i]>Q1) Then Begin
            y1:=temp[i];x1:=dis[i];
            Q1:=temp[i];
            point1:=i End;
           END;
         Q2:=0;
         FOR i:=1 to 34 do
           BEGIN
           If ((temp[i]>Q2)AND(temp[i]<Q1)) Then Begin
            y2:=temp[i];x2:=dis[i];
            Q2:=temp[i];
            point2:=i End;
           END;
         IF (point1<point2) THEN
          BEGIN
          y3:=temp[point1-1];x3:=dis[point1-1]
          END
         ELSE
          BEGIN
          y3:=temp[point1+1];x3:=dis[point1+1]
          END;
         I:=0;
         j:=j+1;
         Quadratic(x1,x2,x3,y1,y2,y3,xmax,ymax);
         tim[j]:=time[point1];  x[j]:=xmax;
         writeln(outfi e,time[point1]:3:2,'  ',xmax:3:2);
   {writeln(temp[point1]:3:3,' ',xmax:3:3,' ',point1,' ',time[point1];}
         END;
       END;
CLOSE(INFILE);
CLOSE(OUTFILE);
END.
```

These numbers are to be used with large duct data files where only one of either row of thermocouple readings are used, i.e., floor, middle or ceiling. The following are large duct thermocouple positions (in meters) along the x-direction (horizontal axis):

```
DIS[1]:=0.0;DIS[2]:=0.17;DIS[3]:=0.335;DIS[4]:=0.505;DIS[5]:=0.675;
DIS[6]:=0.845;DIS[7]:=1.01;DIS[8]:=1.175;DIS[9]:=1.52;DIS[10]:=1.855;
DIS[11]:=2.19;DIS[12]:=2.525;
```

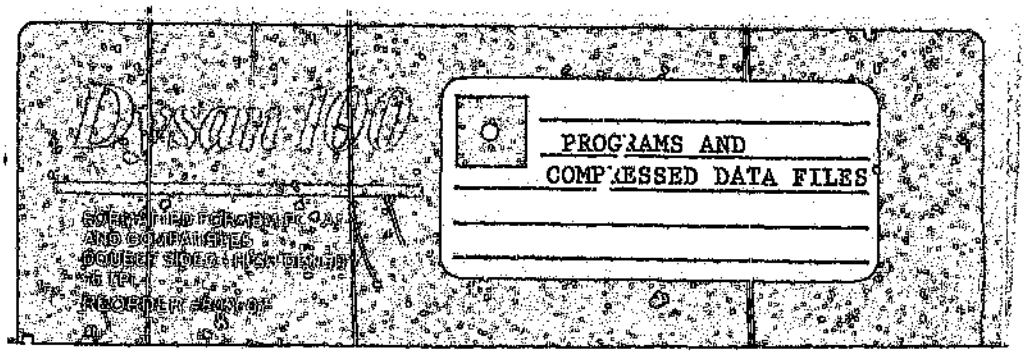
NOTE: In the above program I=34 in the IF statement. This is for the small duct data. For large tunnel data replace with I=12.

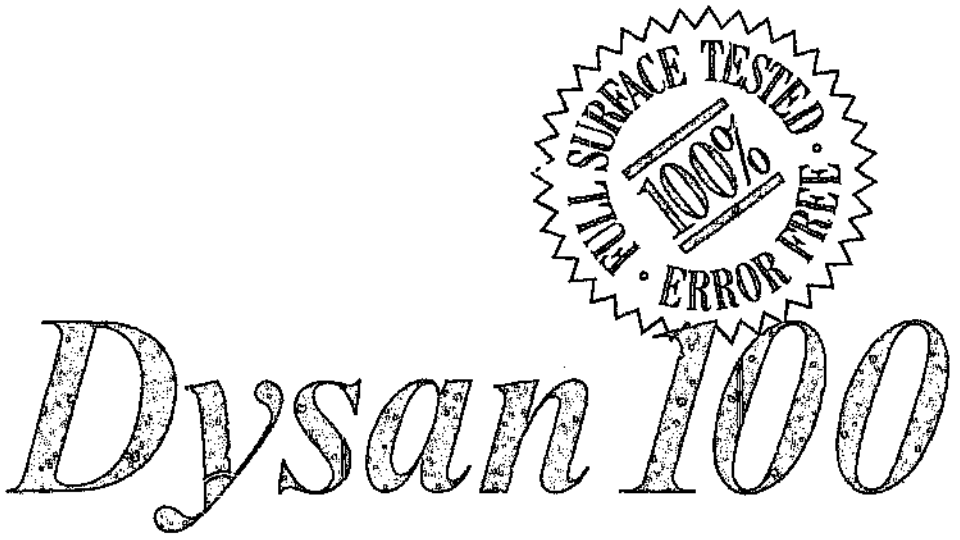


These numbers are to be used with large duct data files where only one of either row of thermocouple readings are used, i.e., floor, middle or ceiling. The following are large duct thermocouple positions (in meters) along the x-direction (horizontal axis):

```
DIS[1]:=0.0;DIS[2]:=0.17;DIS[3]:=0.335;DIS[4]:=0.505;DIS[5]:=0.675;
DIS[6]:=0.845;DIS[7]:=1.01;DIS[8]:=1.175;DIS[9]:=1.52;DIS[10]:=1.855;
DIS[11]:=2.19;DIS[12]:=2.525;
```

NOTE: In the above program I=34 in the IF statement. This is for the small duct data. For large tunnel data replace with I=12.





APPENDIX C: GAS TEMPERATURE MEASUREMENT

Gas temperatures along the duct length are measured using 34 chromel-alumel (type K) thermocouples. Each chromel-alumel junction node is protected inside a 1.6 mm diameter stainless steel cylinder containing a silicate packing to electrically insulate the terminals. These thermocouple probes are half a meter in length and are inserted into the duct so as to measure the flowing stream temperature. The electromotive force (emf) generated by each thermocouple is recorded using a data acquisition unit (HP 3497 A) which is controlled by an HP16 personal computer. A simple computer program was written in order to actuate the appropriate switches for measuring the millivolt readings of each thermocouple. The circuit constructed to connect the thermocouples to the voltmeter appears in Figure C.1. Thermocouples are connected to a 20-Channel thermocouple card (one channel reads the cold junction reference temperature from a thermistor) and a 16-Channel actuator card (a series of double-throw switches). These cards are slotted into the back of the acquisition unit.

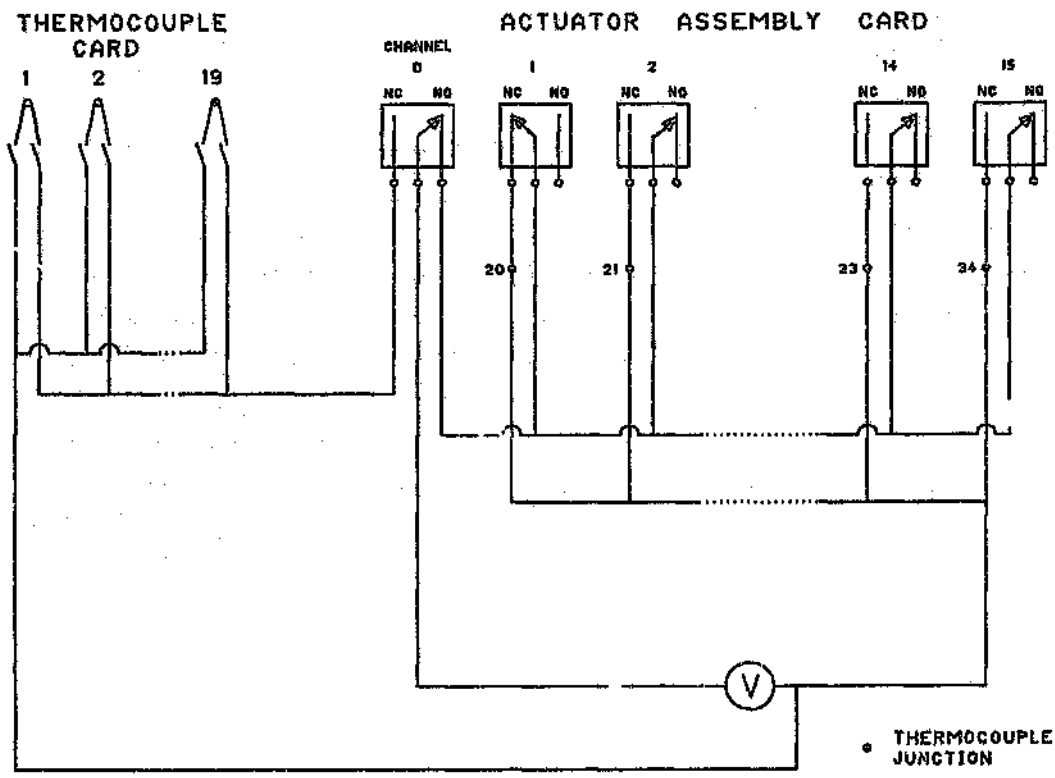


FIGURE C.1. Circuit diagram of thermocouple connections showing how the switches are multiplexed to read the emf of 34 thermocouples individually. At this instant thermocouple 20 is connected to the voltmeter.

The computer program used to measure and record temperatures is written in HP-BASIC and appears at the end of this appendix. Two versions of this program exist, one for the small duct experiments and the other for the larger duct. The program uses the cold junction reference temperature and a thermocouple calibration function to convert the millivolt readings into temperatures and subsequently store them on disc.

Altogether 34 thermocouples could be used and individually actuated to record their millivolt readings. Individual thermocouples connected to the thermocouple card can be closed into a circuit with the voltmeter using the appropriate command, so long as the actuator channel number 0 is set to NC (Normally Closed). If this switch is set to NO (Normally Open) only those thermocouples connected to the actuator card may be part of the

...tmeter circuit.

The Case for Radiation Shielding

For the simple case of a hot gas stream having a true gas temperature T_g and flowing through a duct of a diameter large compared with that of the thermocouple probe, the measured temperature T_m may be significantly lower. This is due to the probe receiving thermal radiation from the hot gas and losing heat by radiation to the cooler duct walls which may be at a temperature T_s. An energy balance on the thermocouple probe gives the equation:

$$\dot{q}_{gr} + h_c A_p (T_g - T_p) = (0.171)(\epsilon_p A_p)(T_p^4 - T_s^4) + \dot{q}_k \qquad (C.1)$$

where h_c is the convective heat transfer coefficient;

$\dot{q}_{gr}$ is the radiative heat transfered from the gas stream to the probe;

A_p is the probe surface area;

ϵ_p is the probe emissivity;

$\dot{q}_k$ is the heat loss due to probe conduction;

T_m is the probe temperature.

McAdams (1954) discusses the use of equation (C.1). Methods of reducing the difference between T_m and T_g are discussed in King (1943). In the special case where a luminous flame is present within the gas stream the value of $\dot{q}_{gr}$ (radiation coming from the flame and hot gas) may be large enough to result in T_m being larger than the true gas stream temperature. The extent to which this occurs will depend on the probe-to-flame view factor, the gas absorptive or emissive property, and various other gas and flame radiative characteristics.

An effective recourse is to interpose a number of radiation screens or shields, in the form of concentric cylinders, between the thermocouple tip and the duct walls. An extensive study

concerned with determining an optimum size and arrangement of these shields was carried out by King (1943).

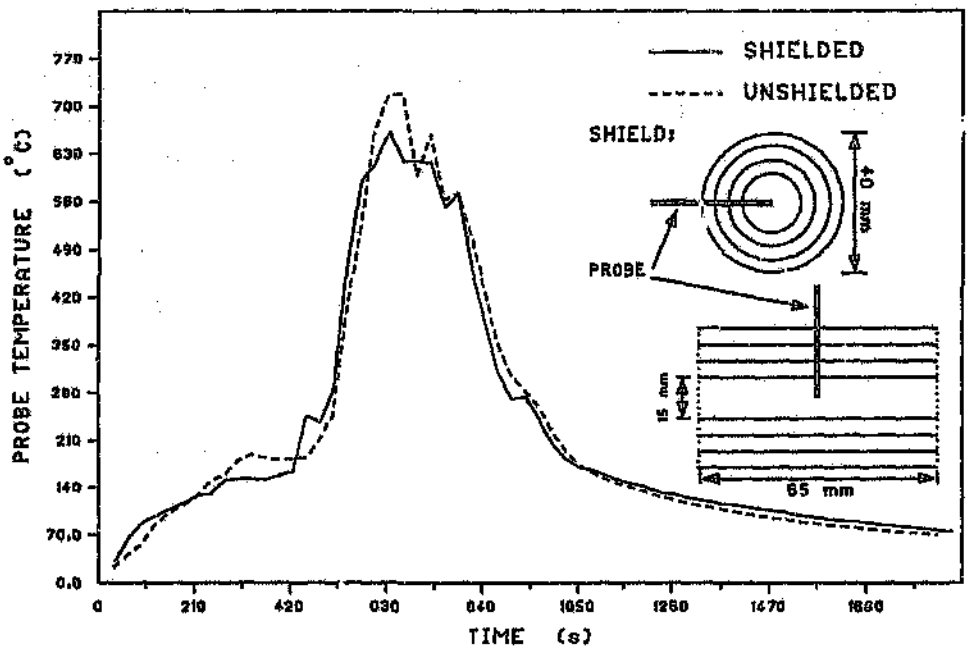


FIGURE C.2. Effect of radiation on a thermocouple probe 1.018 m along the larger tunnel during fire propagation using paraffin lamp oil as the fuel.

In order to determine whether radiation shielding of thermocouples is necessary the effect of a brass radiation shield of the form shown in Figure C.2 was studied. Two identical experiments were performed, one with no shielding of the thermocouples, and the other where one of the thermocouples half-way along the tunnel length is protected from radiation using the shield. The two temperature versus time results for that specific thermocouple are compared in Figure C.2.

Clearly there is no significant difference in temperature between the shielded and unshielded probe, except for a small difference in peak temperatures. This effect may not even be due to radiation (because it is so small). The radiation shield's added specific heat capacity may cause this. A number

of experiments were repeated to verify this result.

The fact that thermal radiation does not distort gas temperature measurements may be attributed to a small view factor inherent in the wind tunnel and to the use of thin probes. Equation (C.1) could also be used to show that the effect of thermal radiation leaving the probe may be roughly equal to radiation striking the probe from the hot gas and luminous flame. This will result in a small difference between T_g and T_m.

TEMPERATURE MEASUREMENT PROGRAM FOR HP COMPUTER

```
10   CLEAR 701
11   ! PROGRAM FOR LARGE TUNNEL
13   GRAPHICS ON
20   DIM Volt_av(48)
30   DIM Volt(48)
32   DIM Voltint(48)
33   DIM T2int(48)
40   DIM Tint(48)
50   DIM T2(48)
51   DIM Tn(15)
60   R0=8.2E-7
70   R1=3.964E-5
80   R2=1.6E-8
90   MASS STORAGE IS ":HP9121,700,1"
100  INPUT "ENTER FILENAME FOR DATA STORAGE: ",Filename$
110  DISP "DOES ";Filename$;" EXIST (Y/N) :";
120  LINPUT Option$
130  IF Option$="Y" THEN
140    DISP "DO YOU WANT TO OVERWRITE THIS FILE (Y/N) :";
150    LINPUT Overwrite$
160    IF Overwrite$="N" THEN STOP
170  ELSE
180    CREATE ASCII Filename$&":HP9121,700,1",500
190  END IF
200  SET TIME TIME("00:00:00")
210  T1=TIMEDATE
211  ! SET-UP AXES FOR GRAPHIC DISPLAY
213  GCLEAR
214  GINIT
215  WINDOW -0.5,3,-250,1000
216  AXES 1,100
217  LORG 6
218  FOR I=0 TO 3 STEP 1
219    MOVE I,0
220    LABEL I
221  NEXT I
222  LORG 8
223  FOR I=0 TO 1000 STEP 100
224    MOVE 0,I
225    LABEL I
226  NEXT I
227  ! OPEN FILE PATH FOR DATA STORAGE ON DISC
229  ASSIGN @Path_1 TO Filename$
230  OUTPUT @Path_1;"THERMO NO     TEMP       TIME"
240  ! PRINT "THERMO NO       TEMP         TIME"
241  ! INITIALIZE DATA LOGGER
250  OUTPUT 709;"SI"
251  OUTPUT 709;"VC0"
260  OUTPUT 709;"AR"
270  OUTPUT 709;"VT1"
280  OUTPUT 709;"VN1"
290  OUTPUT 709;"VR5"
300  ! THERMOCOUPLE MEASUREMENT AND STORAGE LOOP STARTS HERE
310  ON CYCLE 30 GOSUB Twenty
320  ON DELAY 2400 GOTO Quit
321 T:DISP TIME$(TIMEDATE)
322  GOTO T
331 Twenty:!
```

```
332  ! SWITCHING TO ACTUATOR CARD IN SLOT 1
334  OUTPUT 709;"DV1"
336  OUTPUT 709;"DO1,0"
338  FOR M=1 TO 15
339    OUTPUT 709;"DC1,";M
340  NEXT M
341  ! MEASUREMENT OF THERMOCOUPLE EMF's THROUGH ACTUATOR CARD
343  FOR M=1 TO 15
344    OUTPUT 709;"DO1,";M
345    ENTER 709;Voltint(M)
346    T2int(M)=TIMEDATE
347    OUTPUT 709;"DC1,";M
348  NEXT M
349  ! SWITCHING TO THERMOCOUPLE CARD IN SLOT 0
351  OUTPUT 709;"DC1,0"
367  OUTPUT 709;"DV0"
369  OUTPUT 709;"AFOAL19"
370  ! MEASURE THERMOCOUPLE EMF's THROUGH THERMOCOUPLE CARD
372  FOR N=0 TO 19
373    OUTPUT 709;"AI";N
374    ENTER 709;Voltint(N+16)
375    T2int(N+16)=TIMEDATE
384    OUTPUT 709;"AS"
390  NEXT N
400  OUTPUT 709;"AR"
410  !    CONVERT REFERENCE JUNCTION TEMPERATURE TO THERMOCOUPLE
     !    EMF EQUIVALENT
413  Volt_av(35)=R0+(Voltint(35)*10)*(R1+R2*(Voltint(35)*10))
420  PRINT ""
421  ! STORAGE OF DATA ON DISC
430  FOR I=1 TO 34
440    Volt_av(I)=Voltint(I)+Volt_av(35)
450    Caltemp(Volt_av(I),Tint(I))
460    OUTPUT @Path_1;(I-1),Tint(I),(T2int(I)-T1)
470   !PRINT (I-1),Tint(I),(T2int(I)-T1)
480  NEXT I
481  !  AVERAGING  GAS  TEMPERATURES FOR GRAPHIC DISPLAY OF AVG.
     !  TEMP. PROFILE
483  FOR I=1 TO 11
484    Tint(I+1)=(Tint(3*I-1)+Tint(3*I)+Tint(3*I+1))/3
485  NEXT I
486  FOR I=1 TO 12
487    Look(I,Dist)
488    DRAW Dist,Tint(I)
489  NEXT I
498  PEN -1
499  MOVE 0,0
500  PEN 1
501  ON KEY 0 GOTO Quit
502  RETURN
503  ! END OF MAIN LOOP
505 Quit:PRINT""
510  ASSIGN @Path_1 TO *
511  PRINT "DATA IS STORED, I/O PATH IS CLOSED"
513  END
514  ! SUBROUTINE FOR TYPE-K T/C CALIBRATION OF TEMP. VERSUS EMF
520  SUB Caltemp(V,Temp)
530    P0=-5.1E-2
540    P1=2.48503E+4
550    P2=-3.82662E+5
560    P3=9.9661057E+7
570    P4=-1.0820624E+10
```

```
580     P5=6.0392855E+11
590     P6=-1.9109E+13
600     P7=3.4782347E+14
610     P8=-3.3991028E+15
620     P9=1.3828514E+16
630     T1=P0+P1*V+P2V^2+P3*V^3+P4*V^4+P5*V^5+P6*V^6+P7*V^7+
           P8*V^8+P9*V^9
640     Temp=INT(T1*1000+0.5)/1000
650   SUBEND
651   !  SUBROUTINE  WITH  THERMOCOUPLE DISTANCES USED IN GRAPHIC
      !  DISPL^Y
660   SUB Look(I,Dist)
661     DIM Tn(19)
662     Tn(1)=0
670     Tn(2)=0.035
680     Tn(3)=0.135
690     Tn(4)=0.335
700     Tn(5)=0.505
710     Tn(6)=0.675
720     Tn(7)=0.845
730     Tn(8)=1.01
740     Tn(9)=1.353
750     Tn(10)=1.686
760     Tn(11)=2.019
770     Tn(12)=2.354
790     Dist=Tn(I)
800   SUBEND
```

APPENDIX D: DRAWINGS OF APPARATUS

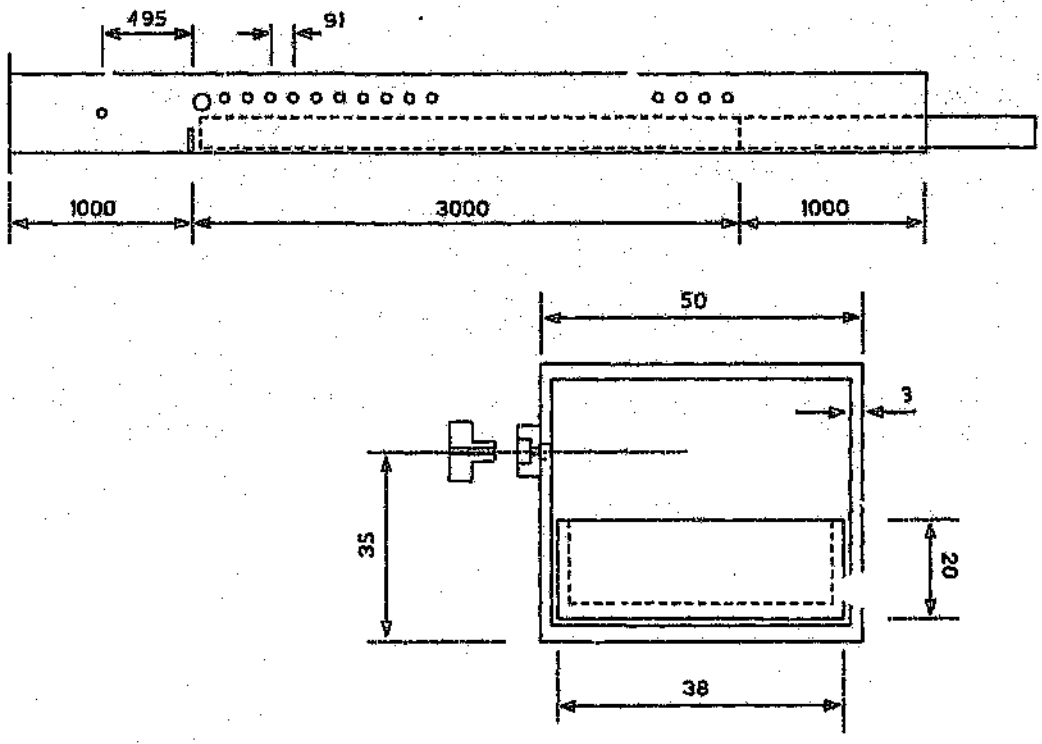


FIGURE D.1. Details of small tunnel construction (non-stratified).

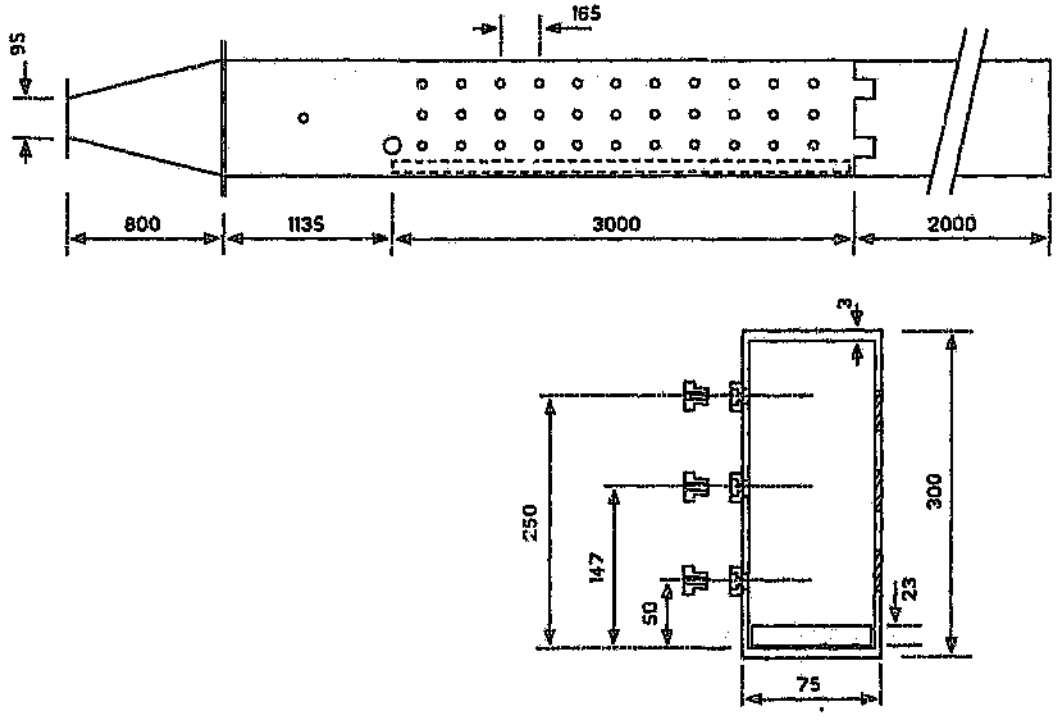


FIGURE D.2. Details of large tunnel construction (stratified).

APPENDIX E: HOT AND COLD LAYER ANALYSIS (STRATIFICATION)

Hot and cold layer mixing

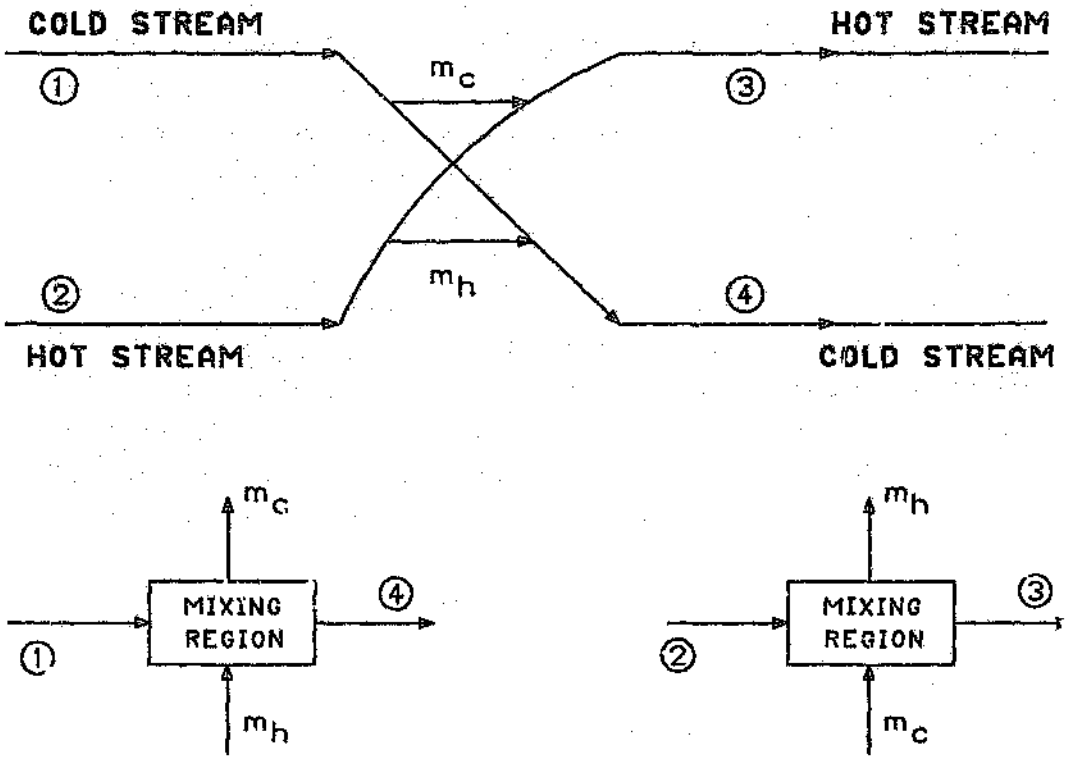


FIGURE E.1. Simplification of mixing zone showing hot plume stream exchanging mass with cold bypass.

Simultaneous mass and energy balance on both streams, assuming $\hat{C}_p$ is constant and same for all streams, shows that

$$m_c = m_1(T_4-T_1)(T_2-T_3)/[(T_4-T_3)(T_2-T_1)] - m_2(T_2-T_3)(T_2-T_4)/[(T_4-T_3)(T_2-T_1)], \quad (E.1)$$

and

$$m_h = (m_1-m_c)(T_4-T_1)/(T_2-T_4). \quad (E.2)$$

In this study it was not possible to obtain any meaningfull information from such calculations for two reasons.

i) Values of m_1 and m_2 depend on B_{p1} which requires knowledge

of stoichiometric coefficient β. β is not known and one cannot assume complete combustion. However, trends may still be explored with this assumption.

ii) More serious is temperatures i equations (E.1) and (E.2) are not easily determined. m_c and m_h depend critically on choosing the end of the mixing region. Temperatures vary dramatically around this vicinity.

Calculating α from data

The value of U_{d2} is equated to predicted U_o. U_o is calculated using a heat transfer correlation (Coulson and Richardson, 1986) wit' the added effect of radiation. The radiative component of U_o is estimated by factorising the radiation equation $C_d\sigma\epsilon(T^4-T_o^4)$ into a convective type equation

$$C_d(T-T_o)[\sigma\epsilon(T+T_o)(T^2+T_o^2)]. \qquad (E.3)$$

The radiative component of U_o (term inside the square brackets) is evaluated at $T=T_o$ for chapter 5 as outer surface temperatures are closer to T_o especially in stratified fires, because, in these cases, heated gases are cooler than for non-stratified fires. An estimated value of C_d used by the hot gas layer ($=C_{d(est)}$ in table 5.1) is calculated using the fitted value C_dU_{d2} and dividing by U_o. The result is $C_{d(est)}$.

$C_{d(est)}$ is equated to the perimeter of cross-section occupied by the hot gas layer. A hot ceiling gas layer runs along the ceiling of width W. The hot gas layer is channeled by the two side walls up to a depth Y, measured from the ceiling down. Therefore $C_{d(est)}=2Y+W$ and $\alpha=Y/H$, where H is the total tunnel height. This is an averaged area fraction through which the hot stream flows. The actual area probably varies along the tunnel length.

Evaluating $\alpha(B_{pl})$ theoretically

A relationship between B_{pl} and α can be derived if the ideal gas

law is used with the assumption of immiscible layers. One can show that

$$1/\alpha = 1 - k_1k_2/k_3 + k_1k_2/((1-B_{p1})k_3), \qquad (E.4)$$

where k_1 is the ratio of hot to cold stream molar masses, k_2 the ratio of hot to cold stream velocities and k_3 the ratio of hot to cold stream temperatures. Because individual layer velocities and molar masses are not known precisely it is not possible to determine an expected relationship between α and B_{p1}. Instead equation (E.4) is plotted in figure 5.6 using estimates of k_1k_2/k_3 and is compared to measured data.

Possible combustion reactions are considered, namely the formation of CO, CO_2, C and H_2O. If the reaction forming C is considered the hot ceiling layer would have an average molar mass of about 26 and therefore $k_1 \approx 0.9$. Measured ceiling and floor temperatures show that $k_3 \approx 1.96$ for isooctane, 1.58 for ethanol and 1.2 for ethylene glycol. If k_2 is close to unity comparison of theoretical and measured data of α versus $(1-B_{p1})$ is possible.

APPENDIX F: COPY OF JOURNAL PUBLICATION ON LIQUID FUELLED FIRES

428 COMBUSTION AND FLAME 96: 428–442 (1994)

An Experimental and Modeling Study of Fires in Ventilated Ducts. Part I: Liquid Fuels

S. C. COMITIS, D. GLASSER,* and B. D. YOUNG
Department of Chemical Engineering, University of the Witwatersrand, Private Bag X3, WITS 2050, Johannesburg, South Africa

A theoretical model for fire propagation through a fuel-lined duct with a radially well-mixed axial flow is presented. The gas-phase is modeled as a steady-state process whereas the condensed-phase (fuel source) is taken to be the cause of transient fire propagation along the duct. Experiments were performed in a small-scale duct where fire propagation and gas temperature histories were acquired. Experimental results confirm hypotheses of pseudo-steady-state gas-phase processes. Theory and experiment display transient fire propagation for typical duct fire scenarios where initial fuel mass loading is constant with respect to duct length. The phenomenon observed, as predicted by theory, is an initial "jump" of the fully developed combustion process followed by convergence to a steady-state constant fire propagation speed. The theory is in all important aspects able to quantitatively model the experimental results.

NOMENCLATURE

A, B, C, D, E, p, q	constants
C_d	perimeter of duct wall cross-section (m)
C_f	exposed perimeter of fuel-lining cross-section (m)
$\hat{C}_p$	mean specific heat capacity of flow stream (J/kgK)
Fr	Froude number
h_f	gas stream-to-fuel surface film heat transfer coefficient (W/m^{2}K)
$\Delta\hat{H}_r$	gaseous enthalpy of combustion per unit mass of oxygen reacted at ambient temperature (J/kg oxygen)
$\hat{H}_{vap}$	latent heat of vaporization or sublimation of fuel (J/kg)
$I(x)$	temperature integral variable (m.K)
$\dot{m}_a$	mass flowrate of air (kg/s)
$\dot{m}_v$	mass flowrate of fuel vapor (kg/s)
$m(x,t)$	transient fuel loading profile inside duct (kg/m^2)
$m^o(x)$	initial fuel loading profile inside duct (kg/m^2)
$\dot{q}$	rate of heat loss through the duct walls (J/s)
t	time variable (s)
t_{res}	fire residing time before "jump" (s)
$T(x)$	gas stream temperature in the lagrangian coordinate system (°C)
$T(\chi,t)$	transient gas temperature in the eulerian coordinate system (°C)
T_0	ambient gas temperature (°C)
T_{vap}	fuel vaporization or sublimation temperature (°C)
U_d	overall heat transfer coefficient of combustion zone duct walls (W/m^{2}K)
U_{d2}	overall heat transfer coefficient of excess fuel and preheating zone duct walls (W/m^{2}K)
U_0	overall heat transfer coefficient for duct calculated from correlations (W/m^{2}K)
V_a	air ventilation average velocity (m/s)
$V(t)$	fire propagation speed using the passage walls as the frame of reference (m/s)

*Corresponding author.

0010-2180/94/$7.00

Copyright © 1994 by The Combustion Institute
Published by Elsevier Science Inc.

x lagrangian distance coordinate (m)
$X_{lbz} = x_1$ length of combustion zone (m)
Y_{ox} oxygen mass fraction in air

$$C_1 = (\dot{m}_a + \dot{m}_{wf})\hat{C}_p;$$

$$C_2 = \frac{C_f h_f \hat{C}_p}{\hat{H}_{vap}};$$

$$C_3 = \frac{C_f h_f \hat{C}_p \theta_{vap}}{\hat{H}_{vap}};$$

$$C_4 = C_d U_d \Gamma + C_f h_f;$$

$$C_5 = C_f h_f \theta_{vap};$$

$$C_6 = C_d U_d \Gamma(x_1) + \dot{m}_{wf}\hat{H}_{vap} + (\Delta \hat{H}_r)\dot{m}_{wf}/\beta;$$

Greek Symbols

β combustion stoichiometric coefficient, mass of fuel reacted per unit mass of oxygen
γ fuel burning rate (kg/m^{2}s)
δ incremental change
ϵ duct wall emissivity
θ gas temperature above ambient, $T - T_0$ (°C)
λ constant fuel loading (kg/m^2)
σ Stefan-Boltzmann constant (W/m^{2}K^4)
$\bar{v}$ fire propagation rate (m/s)
ν_f molar fuel stoichiometric coefficient for combustion reaction
χ eulerian distance coordinate (m)
$\chi^o(t)$ start of combustion zone (m)

INTRODUCTION

Duct fire problems are frequently addressed when trying to understand fire propagation in large tunnels. One of the most striking features of large-scale confined fires is the persistence of severely stratified flow patterns induced by rising hot combustion gases [1]. Whether there are naturally induced or forced convective air currents entering the tunnel, stratified flow will occur depending on whether buoyancy forces are greater than cross flow forces. This phenomenon has been studied by Newman [1], who presents correlations for predicting the degree of fire induced stratification. Acquiring data from a fire spreading within the confines of a passage poses the problem that such stratification phenomena often intrude upon the effect of underlying fundamental flame spread mechanisms. It is therefore necessary to study, in isolation, such mechanisms prior to understanding the coupled effect of fluid dynamics.

This study is restricted to discussions involving the horizontal ventilated fuel-lined duct where the gas flow stream is radially well mixed, or at least the use of a single average temperature is justified. A well-mixed flow assumption is based on the premise that large Reynolds numbers (over 10000) are easily achieved in full-scale mine tunnels with low ventilation currents (~ 0.3 m/s) flowing through large cross-sectional areas, the large duct diameter being an important parameter that allows turbulence to prevail. Here, the fuel source is considered to be in its condensed form (solid or liquid) where burning is the result of diffusion type flames burning over the solid fuel surface. The aim of this work is to obtain a quantitative description of the fire dynamics inside the duct. Attention is focused on ducts with thermally thin walls, where heat transfer is important only in the outward direction, and there is assumed to be no accumulation in the walls. The assumption of thin walls should not affect the general form of the fire process inside the duct.

Ultimately the use of good mathematical descriptions of such fire processes may be incorporated into designs of fire control strategies for potentially hazardous environments such as mine roadways or tunnels. Accurate estimates of certain fire characteristics such as propagation rates and combustion gas production rates become critical variables in the design of optimally sized life support systems for mine tunnel occupants. Also, duct fire models can be used to interpret results from small-scale tests, revealing important information relating geometrical, chemical and physical properties of materials to their fire safety value [4]. These aspects are of immediate concern from a fire hazard point of view.

Most duct fire models to date are developed for fuel-rich fires and follow the same line as introduced by Roberts and Clough [2], who also performed small scale experiments. A simple duct fire model for ducts with thin walls has been developed by Hunter and Favin [3], where the case of an insulated duct is also analyzed. On the other hand, de Ris [4] performed a rigorous analysis of duct fires where heat transfer through the surrounding rock of a mine duct or tunnel is considered.

A SIMPLE MATHEMATICAL MODEL

Although part of this analysis is an adaptation of that presented by de Ris [4], a fundamental difference will emerge when the concept of fire propagation speed is in question. Moreover, the model presented by de Ris [4] is a steady state one, whereas this work will extend the model to include the nonsteady motion of the fire in the duct. The conceptual understanding provided here should prove helpful in interpreting results from duct fire experiments.

Three distinct zones, the lengths of which remain unknown prior to solving the model equations, are identified in the formulation of this fire model. Figure 1 depicts the relative position of each zone on a system of axes that moves along the duct at the fire propagation speed V. The value of V remains to be solved. Because no steady-state restriction is placed on V this variable will be written as time dependent $V(t)$.

As the ventilation air stream crosses the boundary $x = 0$ it encounters a combustion zone where the oxygen is consumed by the combustion reactions. In this zone the fuel volatilizes and is then assumed to instantaneously react with the inflowing oxygen. By the time the gas stream crosses $x = x_1$ the entire oxygen inventory is depleted and the heated gas stream enters the second of these zones, namely the excess fuel zone. Here the gas temperature is above the fuel vaporization or pyrolysis temperature. The fluid stream cools down as a consequence of heat losses to the duct walls and to vaporization of condensed fuel lining the duct. It is assumed that the condensed fuel will vaporize at a fixed temperature termed the vaporization temperature. This will be valid for single component stable liquid fuels. Vaporization continues up to $x = x_2$ where the flowing gas stream has cooled down to the fuel vaporization temperature. This marks the start of the preheating zone. Beyond this region the gas stream cools down to ambient temperature as it loses heat to the duct walls. Recondensation of fuel vapor will be ignored in this zone. de Ris [4] shows this

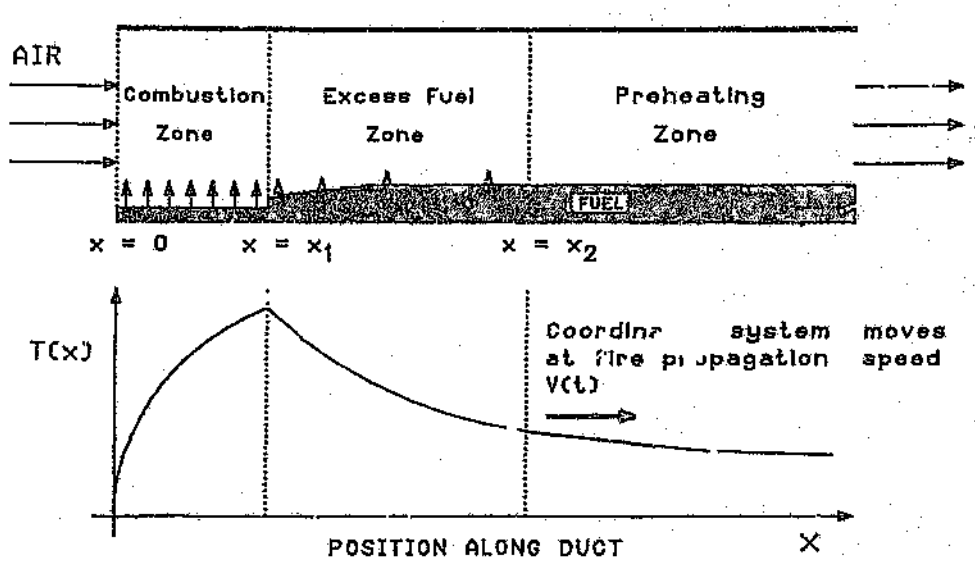


Fig. 1. Schematic representation of proposed duct fire model.

effect to be small. In any case this would only be relevant to fuels that do not pyrolyze to noncondensable materials.

It is worth mentioning that care should be taken when considering the rate of air supply into the combustion zone. The air flow crossing the boundary at $x = 0$ is moving past this boundary at a velocity equivalent to the induced air velocity V_∞ minus the fire propagation speed V. In most fires of this type, because of the large difference in molar density between the condensed fuel phase and the oxygen in the air (about a thousand times), V is small in comparison with V_∞, and is therefore neglected in this analysis. This same logic implies that, relative to the axial speed of the flame-front, the gas-phase temperature is rapidly achieved. This allows us to assume a pseudo-steady-state in the gas-phase energy balance.

Gas-Phase Equations

An energy balance is considered over a control volume which starts at $x = 0$ and extends to an arbitrary value x. This control volume envelopes only the gas phase inside the duct. An energy conservation equation can be written using the lagrangian coordinate system where $x = 0$ is always at the start of the combustion zone. The overall energy equation can be written

$$\begin{aligned}\left(-\Delta\hat{H}_c/\beta\right)(d\dot{m}_v/dx) &= \theta\hat{C}_p(d\dot{m}_v/dx) \\ &\quad + \hat{C}_p(\dot{m}_a + \dot{m}_v)(d\theta/dx) \\ &\quad + d\dot{q}/dx + \hat{H}_{vap}(d\dot{m}_v/dx). \qquad (1)\end{aligned}$$

The mass flowrate of fuel $\dot{m}_v$ that vaporizes into the gas flow stream, the rate of heat loss $\dot{q}$ to the duct walls, and the gas stream temperature θ above ambient all vary with respect to x. Equation 1 simply states that all the heat generated through combustion goes into heating the gas stream, vaporizing fuel, and losses through the duct walls. Inherent in this equation is the assumption that the gas-phase process is operating at steady state even though the fire is propagating down the duct at some speed $V(t)$. That is, the length of each zone and the flow streams involved are time independent. Hence, only total derivatives with respect to x need be used.

Combustion Zone. A single equation is used to account for all possible combustion reactions occurring inside the combustion zone. The fuel vapor is presumed to react as

$$\nu_f F + O_2 \rightarrow \text{Products}.$$

One mole of oxygen molecules reacts with ν_f moles of fuel F and forms products. A perfectly mixed flow stream is considered, where the above reaction occurs as fuel vaporizes from the condensed state into the reactive gas stream. Because of the strong temperature dependence of the Arrhenius expression, near flame temperature reaction rates are much faster than vaporization rates and fuel burning is assumed to be controlled by the rate of fuel vaporization. This leads to the assumption of a fuel-rich fire. It is also assumed that the fuel vaporization rate γ per unit platform area of fuel lining is constant with respect to distance along the combustion zone. This is surmised to be due to the existence of a flame over the entire length of fuel in this zone so that the heat flux at the fuel surface is approximately the same everywhere in this zone. This results in the same combustion zone model developed by de Ris [4]. Fuel vaporization in the combustion zone will therefore be described as

$$d\dot{m}_v/dx = C_f\gamma, \qquad \text{for } 0 \le x \le x_1. \qquad (2)$$

Because of the thin duct wall assumption heat losses will be modeled by an overall heat transfer coefficient. The heat transfer coefficient U_d represents the overall resistance to heat flux, by conduction and convection, from the inside gas stream to the surrounding atmosphere. Also, thermal radiation may be an important pathway for duct heat losses. Heat losses can therefore be modeled as

$$d\dot{q}/dx = C_d U_d(T - T_0) + C_d\sigma\epsilon\left(T^4 - T_0^4\right), \qquad \text{for } x \ge 0, \quad (3)$$

where C_d is the perimeter of the duct wall cross-section, T_0 the surrounding ambient ter-

perature, ϵ the duct surface emissivity, and σ the Stefan–Boltzmann constant. Substituting Eqs. 2 and 3 into Eq. 1 gives

$$\frac{dT}{dx} = \frac{AT^4 - BT + C}{D + Ex}, \qquad \text{for } 0 \le x \le x_1, \tag{4}$$

where $A = -C_d \epsilon \sigma T_0^4$, $B = \hat{C}_p C_f \gamma + C_d U_d$;

$$C = \left(\frac{(-\Delta \hat{H}_r)}{\beta} - \hat{H}_{vap} + \hat{C}_p T_0\right) C_f \gamma + \left(\sigma \epsilon T_0^3 + U_d\right) C_d T_0;$$

$$D = \dot{m}_0 \hat{C}_f; \qquad E = \hat{C}_p C_f \gamma.$$

The boundary condition is at $x = 0$, $T = T_0$. Equation 4 can be solved also for the case where radiation is not important ($\epsilon = 0$). The remaining two zones will be modeled without thermal radiative heat losses ($\epsilon = 0$) since these zones on average tend to be cooler.

Excess Fuel Zone. In the excess fuel zone there is no more oxygen left for reaction. Fuel is presumed to vaporize at a rate that is controlled by convective heat transfer from the hot flow stream to condensed fuel in this zone. This is a more sophisticated mechanism than that proposed by de Ris [4], who assumed a constant vaporization rate throughout the excess fuel zone. The rate of loss of fuel lining can therefore be written as

$$d\dot{m}_v/dx = \frac{C_f h_f}{\hat{H}_{vap}}(T - T_{vap}), \qquad \text{for } x_1 \le x \le x_2. \tag{5}$$

In this region the condensed fuel is assumed to be at its vaporization temperature T_{vap}. The fuel is assumed to be a pure substance that vaporizes cleanly at its boiling or sublimation point. The convective film heat transfer coefficient between the flowing gas stream and the condensed fuel is assigned to the variable h_f.

Substituting Eqs. 3 and 5 into Eq. 1 and introducing a new variable I defined as

$$I(x) = \int_0^x \theta \, dx'$$

or

$$dI/dx = \theta = (T - T_0) \tag{6}$$

yields the following differential equation describing the gas temperature profile inside the excess fuel zone:

$$(C_1 + C_2 \Delta I - C_3 \Delta x) d\Delta I/d\Delta x + C_4 \Delta I - C_5 \Delta x + C_6 = 0, \qquad \text{for } 0 \le \Delta x \le (x_2 - x_1); \tag{7}$$

where

$$\Delta I = I - I(x_1),$$

$$\Delta x = x - x_1.$$

The constant $\dot{m}_{vf}$ appearing in C_1 and C_6 is the total mass of fuel flowing into the control volume up to $x = x_1$, and can be easily calculated from Eq. 2; $\theta_{vap} = (T_{vap} - T_0)$; and U_{d2} is the overall heat transfer coefficient for the duct wall of the excess fuel zone. The boundary condition for Eq. 7 is simply $\Delta I = 0$ when $\Delta x = 0$.

Preheating Zone. In the preheating zone the gas has cooled to below the fuel vaporization or pyrolysis temperature and no more fuel can vaporize. Furthermore, as suggested by de Ris [4], no recondensation of fuel from the cooling gas stream is considered. The only process occurring here is heat transfer to the duct walls. The same heat transfer coefficient used in the excess fuel zone is used for the preheating zone. Using Eq. 3 in Eq. 1 and the fact that $d\dot{m}_v/dx = 0$ for $x \ge x_2$ the following equation describing the gas temperature profile in the preheating zone is obtained:

$$d\Delta I''/d\Delta x'' = (p - \Delta I'')/q \qquad \text{for } 0 \le \Delta x'' < \infty, \tag{8}$$

where

$$p = \left(\left(-\Delta\hat{H}_r\right)\dot{m}_{vf}/\beta - \dot{m}_{vu}\hat{H}_{vap}\right)/(C_dU_{d2}) - I(x_1)[U_d/U_{d2} - 1] - I(x_2),$$

$$q = \hat{C}_p(\dot{m}_a + \dot{m}_{vu})/(C_dU_{d2}).$$

The boundary condition for Eq. 8 is $\Delta I'' = 0$ when $\Delta x'' = 0$. Again, the variable I is used where $\Delta I'' = I - I(x_2)$ and $\Delta x'' = x - x_2$. The new constant $\dot{m}_{vu}$ is equivalent to the total mass of fuel flowing into the control volume up to $x = x_2$. This is the total rate of fuel entering the entire control volume and can be calculated from Eqs. 2 and 5 to give

$$\dot{m}_{vu} = \dot{m}_{vf} + C_f h_f/\hat{H}_{vap}\int_{x_1}^{x_2}(T - T_{vap})\,dx. \quad (9)$$

From the boundary condition, a very simple analytic solution to Eq. 8 can be found.

Defining a Fire Propagation Rate. If an energy balance is performed between $x = 0$ and $x \to \infty$, over the gas phase only, a very simple relationship results:

$$\left(-\Delta\hat{H}_r\right)\dot{m}_{vf}/\beta = \dot{q} + \dot{m}_{vu}\hat{H}_{vap}. \quad (10)$$

Since all the solid fuel is either burnt or vaporized it is possible to deduce a relationship between Eq. 10 and the condensed fuel lining inside the duct. If, for simplicity, it is assumed that the duct is uniformly lined with fuel, so that the duct fuel loading λ (mass of fuel per unit platform area of lining) is constant with respect to x, then

$$\dot{m}_{vu} = \lambda C_f \bar{v}, \quad (11)$$

The number $\bar{v}$ has the units of speed and is defined as the fire propagation rate (sometimes referred to as the average surface regression rate). Substituting into Eq. 10 results in an expression relating $\bar{v}$ to the thermophysical properties of the fuel-lined duct system.

$$\bar{v} = \frac{\left(-\Delta\hat{H}_r\right)\dot{m}_{vf}/\beta - \dot{q}}{\lambda C_f \hat{H}_{vap}}. \quad (12)$$

It is easy to mistake $\bar{v}$, the fire propagation rate, for the fire propagation speed V. The distinction between these two terms is crucial to the development of an accurate description of fire motion through a tunnel. Whereas V is the speed at which the combustion zone is moving along the duct, $\bar{v}$ is a measure of how rapidly the solid fuel lining is disappearing from the duct. In order to evaluate $V(t)$, the time-dependent fuel loading profile $m(x, t)$ (mass of fuel per unit platform area of lining) must be known. Such information is not used in formulating Eq. 12, which therefore does not possess the information necessary to describe the form of $V(t)$. The following section deals with the solid phase analysis, where the exact relationship between the fire propagation speed $V(t)$ and the fuel loading profile $m(x, t)$ is shown to be quite simple.

Condensed-Phase Equations

So far the governing equations inherently assume the gas phase process to be steady state. The only source of transient behavior comes from changes occurring in the solid or condensed phase. Also, any changes that the solid phase experiences will come as a consequence of the gas-phase dynamics.

Equations of Change. Consider a tunnel lined with a condensed fuel that reacts with a well-mixed gas phase that flows at a constant velocity V_∞. The combustion reaction takes place in the gas phase and is assumed to be infinitely fast in comparison with the fuel vaporization rate. Suppose that the duct houses a continuous distribution of fuel described by the continuous function $m(x, t)$ (mass of fuel per unit platform area of fuel surface), which is initially $m^o(x)$. A schematic representation of this system is shown in Fig. 2.

When considering the gas phase a reaction can occur only when the condensed phase is present in that region of the duct. Hence, the position along the duct that represents the point where the fuel loading begins (i.e., where $m = 0$) is the start of the combustion zone and therefore the origin ($x = 0$) of the lagrangian coordinate system. At some point x a time

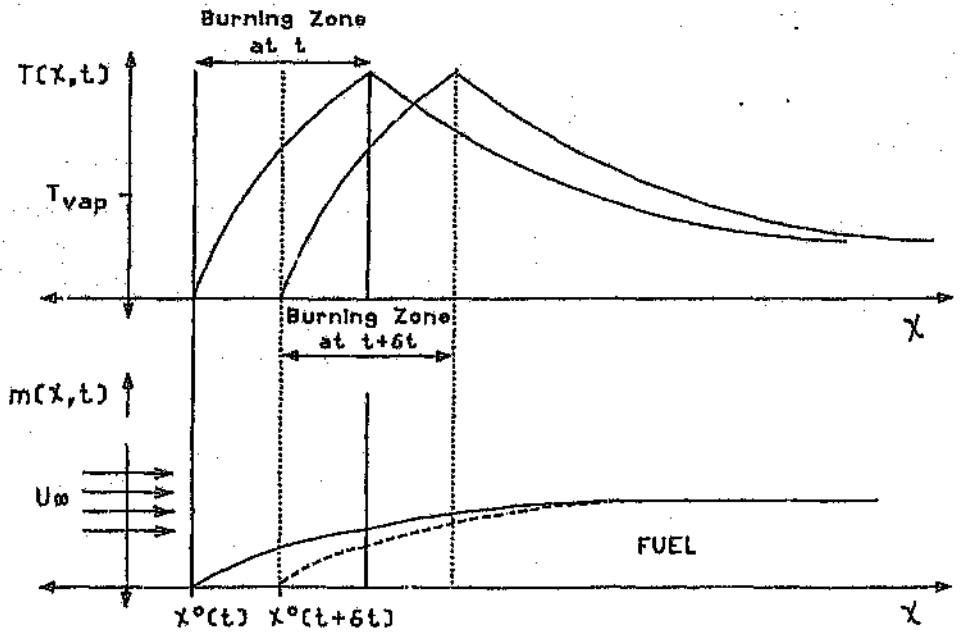


Fig. 2. Fire propagation along duct.

evolving material balance on the condensed fuel shows

$$\partial m(x,t)/\partial t = \begin{cases} -\gamma & \text{if } 0 \le x \le x_1, \\ \dfrac{-h_f}{\hat{H}_{vap}}(T - T_{vap}) & \text{if } x_1 \le x \le x_2, \\ 0 & \text{if } x > x_2. \end{cases} \tag{13}$$

Now consider the eulerian coordinate system that has the fire propagating away from its origin in the positive χ direction, χ being the eulerian distance coordinate. Relating the motion of the lagrangian coordinate system to the eulerian is one way of establishing a relationship for $V(t)$. Fuel loading in the duct changes as time progresses. It also varies with respect to distance. In differential form this can be written as

$$dm = \left(\frac{\partial m}{\partial t}\right)^{t\chi} dt + \left(\frac{\partial m}{\partial \chi}\right)^{t\chi} d\chi. \tag{14}$$

Equation 14 only applies to regions inside the duct where fuel exists, that is, for $x \ge 0$. Consider a moving point $\chi^\circ(t)$ in the eulerian system, which lies on top of and follows the point $x = 0$ (Fig. 2). The mass of fuel is always zero at this point so that $dm = 0$. Bearing in mind that $\chi = x + V(t)t$ one can show that $(d\chi/dt)|_{x=0} = V(t)$. Equation 14 can be written for the condition where $x = 0$ (which is the point $\chi = \chi^\circ(t)$). This results in an expression for the fire propagation speed $V(t)$ where the frame of reference is the duct wall.

$$(d\chi/dt)|_{x=0} = V(t) = \left.\frac{-(\partial m/\partial t)^{t\chi}}{(\partial m/\partial \chi)^{t\chi}}\right|_{\chi^\circ(t)} = \gamma/(\partial m/\partial \chi)|_{\chi^\circ(t)}. \tag{15}$$

Clearly, if the fire is to propagate at a constant velocity, the fuel profile inside the duct must be in a specific form so that $(\partial m/\partial \chi)|_{\chi^\circ(t)}$ remains constant as time evolves. If a solid homogeneous fuel is used then $V(t)$ is inversely proportional to the physical slope of the fuel surface at $x = 0$ (or $\chi^\circ(t)$), in which case $(\partial m/\partial \chi)|_{\chi^\circ(t)}$ can take on a large range of values (from infinity to zero) throughout the fire propagation history. Of course, the govern-

ing equations have been derived only for cases where $V(t) \ll V_\infty$. The situation where $V(t)$ is close to V_∞ is not considered in the gas-phase analysis.

Model Output

The above analysis completes the formulation of the governing equations. The equations describing the gas temperature profile can be solved analytically to give temperature as an explicit function of distance, except for Eq. 7 which can only be expressed as an implicit function of T and x. To find a value of T for any x ($x_1 \le x \le x_2$) a root searching technique must be employed which leads to problems of selecting the nontrivial root. In this case it is convenient to use a standard fourth-order Runge-Kutta algorithm to solve Eq. 7. The analytic solutions of Eqs. 4 and 8 together with the numerical solution of Eq. ' gives the complete gas temperature profile prior to any knowledge of the condensed-phase equations. The gas temperature profile is then used to solve the condensed-phase equations. The condensed-phase equation 13 is solved numerically for $\chi^\circ(t)$, since this system of equations depends on the numerical solution of Eq. 7.

To illustrate the basic method that is used to calculate $\chi^\circ(t)$ (or χ° versus t) consider the fire moving a distance equivalent to the combustion zone length X_{lbz} along the duct. Assume that the upstream end of the fire is at the point $\chi^\circ(t_1)$ and moves the distance X_{lbz} to a point $\chi^\circ(t_2)$. The values t_1 and t_2 are the associated times. We wish to know how χ° varies with time as it progresses from $\chi^\circ(t_1)$ to $\chi^\circ(t_2)$. The distance X_{lbz} is divided into discrete points and the time taken for the fuel loading to reach zero at each of these points is calculated from Eq. 13 to be

$$t(\chi^\circ) = m(\chi^\circ, t_1)/\gamma + t_1,$$

where χ° in this equation is the point of interest within the interval $\chi^\circ(t_1) \le \chi^\circ \le \chi^\circ(t_2)$. This procedure gives χ° versus t information that describes the fire motion up to the point $\chi^\circ(t_2)$. This calculation can be repeated for the next distance interval that would take the upstream end of the fire to a point $\chi^\circ(t_2) + X_{lbz}$ along the duct, except that $m(x, t_2)$ must first be evaluated. While the fire was migrating from $\chi^\circ(t_1)$ to $\chi^\circ(t_2)$ the region ahead of $\chi^\circ(t_2)$ was exposed to the migrating excess fuel and combustion zones. The new fuel profile achieved at time t_2 can therefore be calculated from Eq. 13 as

$$m(x, t_2) = m(x, t_1) - \left(h_f/\hat{H}_{vap}\right) \times \int_{t_1}^{t'(x)} \left(T(x, t) - T_{vap}\right) dt - \gamma[t_2 - t'(x)].$$

The one limit of integration is position x dependent and is evaluated from

$$t'(x) = t_1 + m(x - X_{lbz}, t_1)/\gamma.$$

The value $t'(x) - t_1$ is the time that the excess fuel zone spent over the point x while the upstream end of the fire moved from $\chi^\circ(t_1)$, and $t_2 - t'(x)$ is the time the combustion zone spent over x until the upstream end of the fire moved to $\chi^\circ(t_2)$. The computation of the new fuel loading $m(x, t_2)$ shown above is specifically for the region $0 \le x \le X_{lbz}$. Similar expressions can be written to evaluate the fuel loading downstream of X_{lbz}. When this is done one can obtain the new fuel loading $m(x, t_2)$ for the entire length up to the preheating zone where recondensation of fuel vapor is neglected. Clearly, the above procedure can be repeated.

The above sequence of calculations displays stability. Depending on the system parameters a constant fire propagation speed may be achieved after sufficient iterations. Inherently, the steady-state speed is proportional to the fire propagation rate $\bar{v}$. If the fuel volatility ahead of the fire is high the fire propagation speed converges rapidly to its steady state. The other extreme is when fuel volatility ahead of the fire is negligible, because of a high latent heat or poor heat transfer to the condensed phase. In such a case the fire propagation speed may settle down to some type of periodic form. Whatever the case the time-dependent variables should converge to a steady form.

Whether fires behave in this way can only be answered by experiments. The model suggests

that the fire will initially "jump" along the duct length, moving incremental distances equivalent to the combustion zone length. This stepping or "jumping" motion comes as a result of the initially flat fuel distribution inside the duct and because of the way fuel is consumed evenly in the combustion zone, that is, constant burning rate γ.

EXPERIMENTAL

Apparatus

Fire propagation experiments were in a 5-m long, 43-mm wide, and 42-mm high mild steel duct, as shown in Fig. 3. For these dimensions and the air velocities employed the degree of gas stream temperature stratification can be estimated (1) from a Froude number calculated as

$$\mathrm{Fr} = \frac{V_{avg}}{\left((\Delta T_{cf}/T_{avg})gH\right)^{1/2}}.$$

Here H is the tunnel height, V_{avg} is calculated as the average "hot" velocity through the duct, calculated at T_{avg} the average gas temperature. ΔT_{cf} is the difference between the ceiling and floor gas temperatures, and g the acceleration of gravity. In the present work T_{avg} was approximated as equivalent to the measured gas stream temperature, because it is measured approximately at the center of the duct flow stream. This approximation is reasonable if stratification is not severe and the gas temperature rises from floor to ceiling. Using this information and a correlation developed by Newman [1] that relates ΔT_{cf} to H, T_{avg}, and V_{avg} it is possible to calculate ΔT_{cf}. For these experiments Fr is found to lie within the range $1 \leq \mathrm{Fr} \leq 10$, a regime dominated by strong interactions between cross flow and buoyancy forces (1) where severe stratification does not prevail.

It is thus likely that for the present experiments flow conditions are not characteristic of two separate gas layers (one hot stream along the ceiling and a cold stream along the floor) as in the case of severe stratification but rather of a single hot gas stream flowing across the entire duct cross-section with a definite vertical temperature gradient. Since the Reynolds number for these experiments is either within the laminar or transitional regime between fully developed turbulence and laminar flow ($800 < \mathrm{Re} < 4500$) the above analysis suggests some radial temperature variation. Using Newman's [1] correlation the estimated order of magnitude of ΔT_{cf}, if $T_{avg} = 400°C$, can range from 0° to 400°C, depending on air speed. However, the gas stream temperatures are measured midway between the duct floor and ceiling and are therefore taken to be approximately equal to the average gas temperature, thus allowing comparison with the model which assumes good mixing.

A narrow duct was used because of its economically desirable scale with the possibility of reducing stratification by virtue of a lower duct height. The limitation is that a very narrow duct cannot accommodate sufficient fuel mass for experimentation, and increasing air velocities in any attempt to increase the Reynolds number may blow the fire out. The alternative is to work on a larger scale of duct diameter (also allowing for a larger exposed fuel surface area) where the Reynolds number can be in-

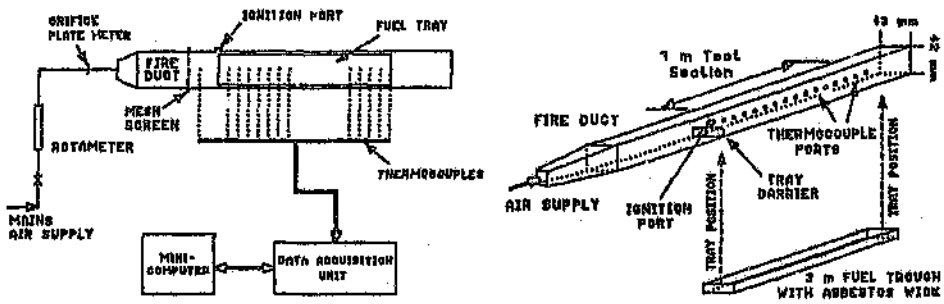


Fig. 3. Schematic representation of equipment used in fire experiments.

creased well into the turbulent regime without having to operate at blow out air velocities. For this reason the well mixed slug flow assumption may be realistic for a full scale mine tunnel fire. The disadvantage of such large apparatus is that long duct lengths would be required (from the combustion zone up to a length where the gas stream has cooled to below T_{vap}) in order to measure the gas stream temperature profile. In the present work a compromise used a duct which could not ensure good mixing, although stratification was absent. A subsequent article will examine cases where stratification occurs.

Also, a simple criteric ' based on a variation of the Froude nu. r can be used to reduce the possibility of back flow of hot combustion gases along the duct ceiling. For the present arrangement and range of air velocities the dimensionless group $\Delta\rho Hg/\rho V_a^2$ lies between 0.12 and 3.5 when $\Delta\rho/\rho \approx 2/3$ and V_a is the ventilation air average velocity. Ideally this dimensionless group should be less than unity to ensure no backflow. This criterion for backflow is discussed by de Ris [4]. Again the necessary situati n was not ideal.

The first meter of length provides a calming section. The next 3 m comprises the fire test section, at the end of which is 1 m of duct to eliminate end effects. A 3-m steel tray rests along the floor of the test section. Liquid fuels could be distributed along the tray length by soaking the required amount along an asbestos wick residing inside the tray. Flame spread over a porous solid soaked with combustible liquids has been investigated by Takeno and Hirano [5]. If the liquid level does not lie above the upper surface of the porous solid, then flame spread behavior is similar to that over solid fuels.

Thirty-four chromel–alumel thermocouples are inserted half-way into the flowing stream, to measure the gas stream temperature distribution, at 91 mm intervals over the 3-m test section. The thermocouple emf is recorded by an H-P data acquisition unit, controlled by a personal computer.

Air is supplied to atmospheric pressure and temperature. The flowrate is measured with a rotameter and an orifice plate meter inserted upstream from the duct. An ignition port is located at the start of the test section and is sealed with a threaded cap.

Procedure

The total mass of fuel is weighed and separated into 15 equal portions. Each portion is evenly distributed along 20-cm segments which constitute the tray length. This is in order to achieve a uniform fuel distribution along the tray. The fuel tray is carefully loaded into the duct and the air supply set to the required flowrate. By inserting a burning torch into the ignition port the upstream end of the fuel tray is ignited and the data logging setup initiated simultaneously. The ignition port is sealed immediately.

The data acquisition unit is programmed to take all 34 thermocouple readings every 30 s, the first set 30 s after ignition.

RESULTS

Experiments were with a variety of fuels all of which are pure organic liquids. Their thermodynamic properties are well known so that the governing equations can be used to model the fires. Also, most liquid fuels support rapidly growing fires, so that the transient period for the fire growing from an ignition source to its fully developed fuel-rich state is small. The three substances used are, isooctane (Iso), *n*-butanol (Butol), and ethylene glycol (Eg), chosen in order to have a range of fuels of increasing fuel volatility. Also these are substances with simple molecules and will therefore vaporize cleanly into the gas phase without intermediate complications such as pyrolysis reactions.

For each experiment the gas temperature profile is measured as the fire propagates along the duct. Figure 4 shows temperature distributions measured at three different times for the same fire (run 5). The model was fitted to the first temperature profile when the fire is stationary at the start of the test section. The same fit is deliberately placed on the temperature distribution data of the fire when it has progressed roughly 1 and 2 m along the duct.

In order to monitor the motion of the fire along the duct it was assumed that the flame-

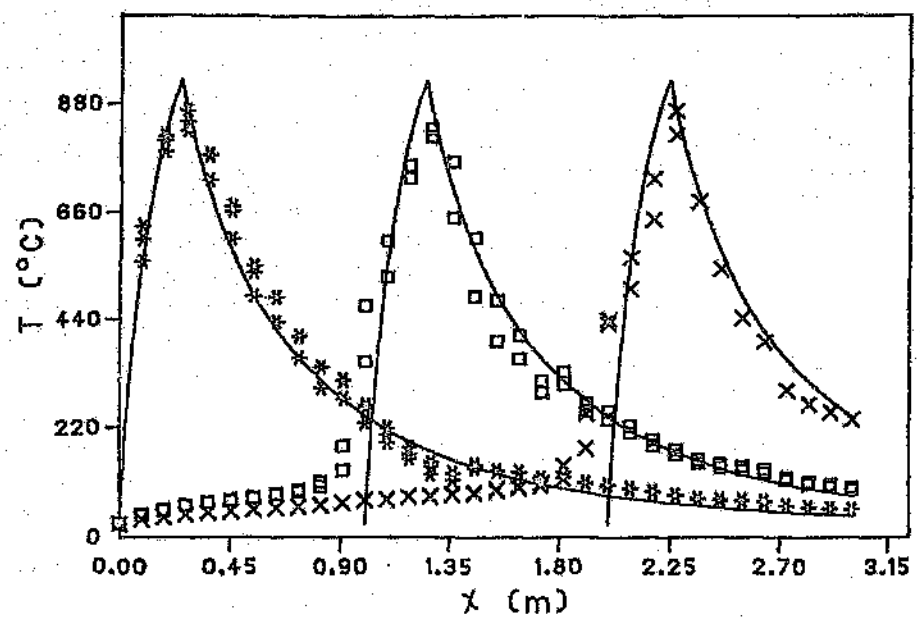


Fig. 4. Gas temperature profiles from run 5 showing stationary fire soon after ignition (•) and moving fire 750 seconds (□) and 1200 s (×) after ignition. Proposed model fits (—) are also shown.

front position is the position of the maximum gas temperature. To estimate the position of this maximum, parabolic interpolation was used on each of the measured gas temperature profiles. Figure 5 shows flame-front position versus time data for three different fires (including one replicate).

Fitting the gas-phase model to gas temperature data provided values of all unknown model parameters except h_f. This is because the tem-

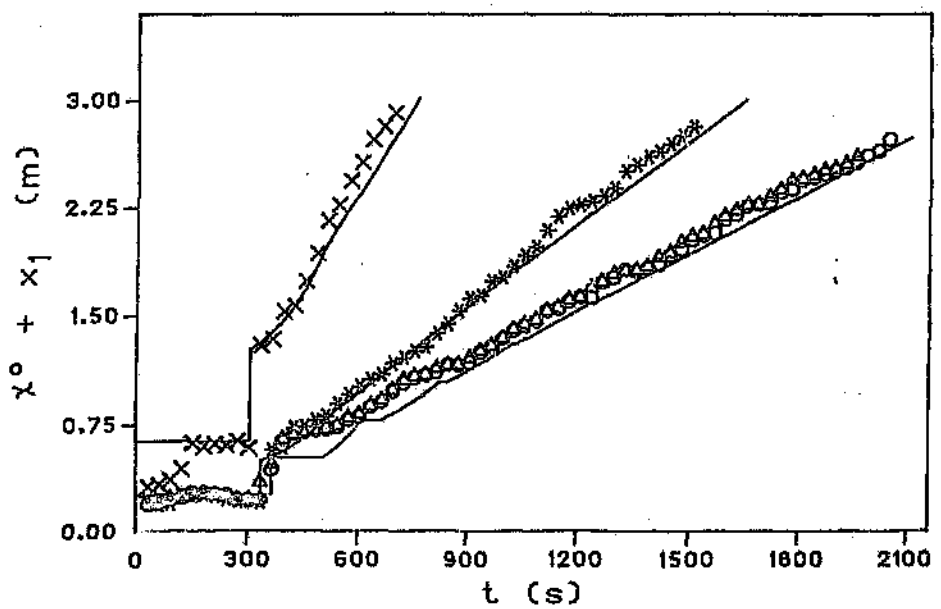


Fig. 5. Flame-front history along duct for run 4 (×), run 5 (+), and run 8 (△). Run 8 was repeated (○) to test for the quality of reproduction of the experiment. Proposed model fits (—) are also shown.

perature distribution is hardly influenced by significant changes in h_f. However, the fire propagation speed V is a strong function of the gas stream-to-fuel heat transfer coefficient h_f. It is this free parameter that is used to fit the condensed-phase equations to flame-front history data. Figure 5 shows the resulting fit of three fires and Table 1 reports all model parameters used in the model fitting procedure, together with the fuel loading and air flowrates.

The reported values represent the "best" fits. They were determined by visual comparison of the model curve and experimental data of gas temperature versus χ or flame-front versus t. It is very convenient that the parameters can be fitted individually because every free parameter affects a different feature of the curves $T(x)$ and $\chi^*(t)$. Table 1 also reports values of the duct inside forced convective heat transfer coefficient, h_i, as estimated from literature correlations [6]. The difference between h_f and h_i is that h_f is estimated from the model fit, whereas h_i is calculated from heat transfer correlations for hot air flowing through conduits.

Fuel Burning Rate

The fuel burning rate determines the time t_{res} the fire will take before it "jumps" from its initial position (the length of the horizontal part of the curves in Fig. 5). To calculate γ the initial fuel loading m° is divided by the measured time t_{res}.

Reaction Stoichiometry

For the reaction stoichiometry there are a large number of possible reactions. The stoichiometric coefficient β is therefore also calculated from the data. Based on the fuel-rich fire assumption and the measured combustion zone length X_{lbz}, β may be evaluated as

$$\beta = (\gamma C_f X_{lbz})/(\dot{m}_a Y_{ox}).$$

If complete combustion occurs the β values will be 0.286 for isooctane, 0.385 for butanol, and 0.776 for ethylene glycol. Incomplete combustion reactions result in very different values. Consider isooctane, for instance, which may react to produce H_2O and CO, C, or even a cocktail of unsaturated hydrocarbons. In which case β will be 0.420, 0.793, up to values greater than 1.4, respectively.

Duct Heat Transfer Coefficients U_d and U_{d2}

U_d was estimated by adjusting its value until the combustion zone model produced a maximum gas temperature close to that of the data points. U_{d2} was adjusted until the excess fuel zone model produced a gas temperature decay that matched the data.

Stream-to-Fuel Heat Transfer Coefficient h_f

This value is varied until the fire propagation rate $\bar{v}$, predicted by the model, matches the final slope suggested by the flame-front versus time data.

TABLE 1

Model Parameter Listing for All Experiments[a]

Run Number, Fuel	m° (kg/m²)	$V_\infty \times 10^2$ (m/s)	γ (kg/m²s)	β —	U_d (W/m²K)	U_{d2} (W/m²K)	h_f (W/m²K)	$\bar{v} \times 10^2$ (m/s)	h_i (W/m²K)
1 Iso	2.0	150	9.30×10^{-3}	0.947	50	35	2.8	0.972	3.9
2 Iso	2.0	31.0	7.27×10^{-3}	0.892	55	15	2.3	0.239	2.3
3 Iso	2.66	91.1	10.3×10^{-3}	1.69	31	31	3.4	0.676	3.3
4 Iso	3.66	65.3	12.0×10^{-3}	1.63	38	25	4.0	0.409	3.0
5 Iso	3.66	31.5	11.0×10^{-3}	1.21	50	17	3.6	0.193	2.3
6 Iso	3.66	111	15.9×10^{-3}	2.20	26	40	5.0	0.806	3.5
7 Butol	3.34	64.4	8.44×10^{-3}	1.42	30	22	6.0	0.358	3.0
8 Butol	2.66	28.3	7.31×10^{-3}	0.962	51	15	3.5	0.134	2.2
9 Eg	3.34	27.9	6.95×10^{-3}	0.937	50	15	4.8	0.093	2.3

[a] Also shown is h_i the duct inside film heat transfer coefficient as estimated from correlations for air flowing in conduits.

Stationary gas temperature profiles for two fires are shown in Fig. 6, together with the proposed model. Also shown is the combustion zone gas temperature model prediction where thermal radiation is included as a heat loss. In this case h_i and h_0, the duct inside and outside heat transfer coefficients, were calculated from correlations [6] and used to estimate U_0, the overall duct heat transfer coefficient. The duct wall emissivity ϵ was then used as the only model fitting parameter. Table 2 shows these results. The model equation for gas temperature was found to be very sensitive to ϵ compared to the much weaker effect of U_0. Emissivities for various types of steel surfaces can range from 0.3 for mild steel to 0.6 for oxidized steel [7].

DISCUSSION

In the light of the present theory the self-similar form of the gas-temperature profiles displayed by data in Fig. 4 provide conclusive evidence for a steady-state gas-phase process. Figure 4 also shows that the stationary fire (first temperature profile) is almost identical to the migrating fire (second and third profiles). Therefore neglect of the air flowing into the control volume, as a result of adopting the lagrangian coordinate system, is a valid and useful simplification. Figure 4 also shows that the preheating of the air entering the burning zone is minimal and this justifies the thin wall assumption.

Although the gas-phase equations suggest a sudden change in temperature gradient at the end of the combustion zone this behavior is only observed in small fires such as run 5 and not in fires with large air velocities. Run 1 in Figure 6 shows a relatively smooth temperature transition from the combustion zone to the excess fuel zone. The discontinuity in the model equations comes from the assumption that the fuel burning rate is independent of position (or gas-phase concentration) and that burning halts at x_f, and is also aggravated by neglecting radiation. Realistically, the gas-phase reaction rate slows down significantly as oxygen concentrations become smaller at regions near the end of the combustion zone. In this regime the constant γ assumption is likely to break down as reaction kinetics may control the rate of burning. The result is a more gradual temperature transition from the combustion to the excess fuel zone. Di Blasi et al. [8] show this concentration effect near the flame

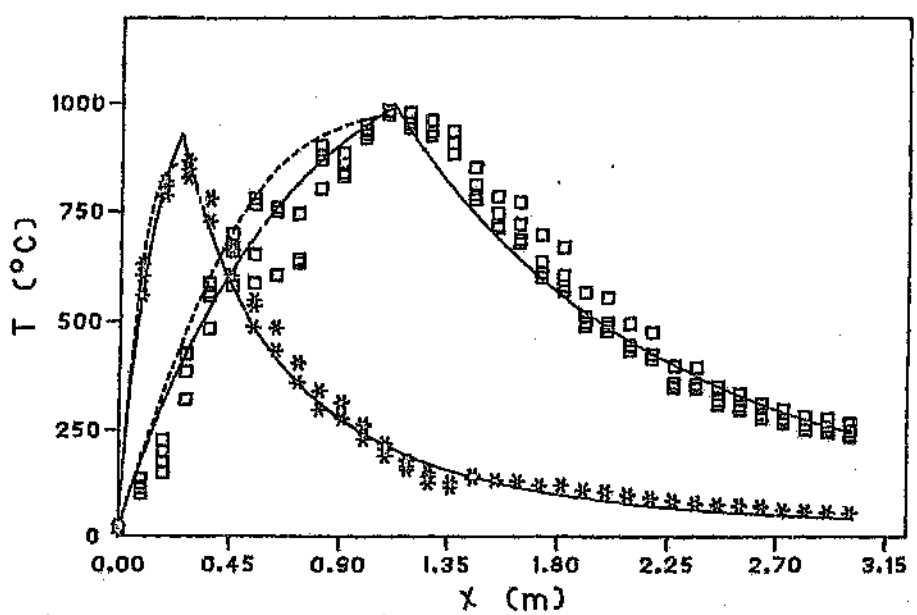


Fig. 6. Comparison of gas temperature profiles from run 1 (□) and run 5 (+) with proposed model (—). Combustion zone model solved with the radiation term is also shown (- - - -).

TABLE 2

Combustion Zone Parameters Where Thermal Radiation Is Included as an Important Pathway for Heat Losses

Run Number	1	2	3	4	5	6	7	8	9
U_0 (W/m^{2}K)	2.6	1.8	2.3	2.1	[illegible]	2.4	2.1	1.7	1.7
ϵ	0.42	0.60	0.30	0.42	[illegible]	0.60	0.60	0.60	0.60

tip of a wind-aided fire. In spite of this assumption the model fits the experimental data very well.

Duct heat transfer coefficients used in model fitting suggest that thermal radiation is a likely candidate for heat losses from the duct walls. U_d and U_{d2} are clearly too large when compared to literature values, U_0. Excepting run 6, U_{d2} is smaller than U_d, probably because of the lower gas temperatures, and hence less radiation, in the excess fuel and preheating zone. When the model includes thermal radiation duct surface emissivities correspond reasonably with the literature values. One can readily include radiation in the model but with an increased complexity in solving the equations.

It should be mentioned that the exact reactions occurring are unknown. Consequently, $\Delta \hat{H}_r$ is only approximate. This will certainly affect the fitting of U_d, U_{d2}, and ϵ, causing inaccurate estimates that do not display trends with V_∞. Runs 1 and 6 were performed with air velocities near to extinction conditions and, in the case of run 6 the fire actually died out before reaching the end of the test section.

Transient growth of fires from ignition to a state of maximum size is a problem that has received no attention in developing the mathematical model. Most of these experiments showed that such growth rates are rapid in comparison with fire propagation along the duct. Transient growth behavior becomes important when larger air flowrates are used and the fire is allowed to expand over a long burning zone. The growth rate is slowed down even further if low volatility fuels are used. Under such conditions fire growth is slow enough to be observed in the flame-front history data. The initial part of run 4 in Fig. 5 shows this transient growth phenomenon.

All results in Fig. 5 show the fires to grow from ignition to a maximum size and thereafter remain in their original location inside the duct. As soon as the fuel in this region is consumed the fire "jumps," displacing approximately one combustion zone length along the duct. Then it migrates along the duct at a relatively constant velocity. All of these characteristics are in complete agreement with the model. What is most reassuring is the value of h_f that would generate this model prediction. Although fitted h_f values do not follow a general trend with respect to V_∞ they come close to literature correlations of inside film heat transfer coefficients for nonreactive flows in conduits. The use of liquid fuels results in large vaporization rates ahead of the fire, consequently rapidly shaping the fuel profile to such an extent that $(\partial m/\partial \chi)|_{\chi=0}$ reaches its steady-state value soon after the first "jump." Clearly then, if fuels are chosen to be less volatile, perhaps solid fuels, the model would suggest unsteady fire propagation for longer periods of time. This merits further experiment.

This analysis is devoted to fitting model equations to experimental data and thereafter examining the resulting parameter estimates with respect to their physical significance. For the most part there is good agreement between model estimates of free parameters and literature values. The sensitivity of model predictions to the various free parameters is also critical in determining whether reliable a priori predictions are possible. Such predictions would also require good estimates of the combustion reaction stoichiometry and burning rates. A simple but crude sensitivity analysis may be performed by setting all free parameters to typical values as estimated from such experiments and thereafter varying each parameter individually to obtain an indication of its effect on the gas temperature profile and fire front history. This is adequate if predic-

tions are required for similar conditions. Current experimental studies of duct fires supported by (solid) polymethylmethacrylate (PMMA) are underway. Parameters are being estimated in the same manner presented here and the fuel mass profile $m(x)$, measured at steady state, can in principle be predicted without any further adjustments to the fitted model parameters. This analysis should reveal useful information about the predictive capabilities of the present model.

CONCLUSION

A one-dimensional theory with a pseudo-steady-state gas temperature profile for the propagation rate of fires in fuel-lined ducts has been derived. A set of experimental results on three fuels in a small duct have been obtained.

The model accurately describes the centerline (average) gas temperature profile inside the duct as well as the fire propagation history. This analysis has revealed that for the scale and class of fires studied convective heat transfer from the gas stream to the condensed fuel governs to a great degree the fire propagation history and average propagation speed. For the case of thin duct walls heat losses from the system to the surroundings is significantly dominated by radiative heat transfer especially from the flaming region of the duct. The radiative heat transfer from the fire front to condensed fuel might become significantly important in larger scale fires where the fuel surface to fire front view factor is dramatically enhanced. Use of the present model for predictions of duct fire dynamics requires further knowledge of fuel burning rates and reaction stoichiometry.

A fundamental concept arising in the theory is illustrated by virtue of the experiment, namely the important distinction between the fire propagation rate $\bar{v}$ and the fire propagation speed $V(t)$ defined herein. The condensed fuel profile $m(x,t)$ is the key to understanding how a fire traverses through the confines of a duct. The familiar assumption of constant fire propagation speed in typical duct fire scenarios can break down and the possibility of a periodic fire propagation motion is shown to exist. One may conclude from the observed "jump" phenomenon that the simplifying assumption of a constant burning rate with respect to distance inside the fire region has proved to be realistic for the major part of this region.

It is clear from a simplified Froude number analysis and the experimental and model comparison that although the reactive flow stream is not well mixed it is plausible, in this case, to work with the approximation of an average gas temperature. This approximation simplifies the mathematical analysis from solving the three-dimensional equations describing the gas-phase processes to the much simpler one-dimensional model. It is likely that in the case of large-scale mine tunnels, with moderate ventilation currents, the one-dimensional approach may provide an adequate description of the process because of the larger Reynolds numbers. If more detail is required to describe duct fires with laminar flow conditions then clearly a more rigorous analysis with the inclusion of mixing would be necessary.

In conclusion, the fundamental assumptions of the model (fuel-rich fires, steady-state gas profiles, heat transfer dominated process) seem valid in practice and lead to a reasonably simple model with good powers of prediction. Many of the parameters used in this model can be estimated from existing correlations.

REFERENCES

1. Newman, J. S., *Combust. Flame* 57:33–39 (1984).
2. Roberts, A. F., and Clough, G., *Combust. Flame* 11:365–376 (1967).
3. Hunter, L. W., and Favin, S., *Combust. Flame* 42:7–18 (1981).
4. de Ris, J., *Combust. Sci. Technol.* 2:239–258 (1970).
5. Takeno, K., and Hirano, T., *Twenty-First Symposium (International) on Combustion*, The Combustion Institute, Pittsburgh, 1986, p. 75.
6. Coulson, J. M., and Richardson, J. F., in *Chemical Engineering* (R. K. Sinnott, Ed.), Pergamon, 1986, Vol. 6, p. 537.
7. Perry, R. H., and Green, D. W., *Chemical Engineers Handbook*, McGraw-Hill, Singapore, 1984.
8. Di Blasi, C., Crescitelli, S., and Russo, G., *Computer Methods Appl. Mech. Eng.* 75:481–492 (1989).

Received 7 April 1993; revised 4 September 1993

REFERENCES

Apte, V.B., Bilger, R.W., Green, A.R., and Quintiere, J.G. (1991). Wind-aided turbulent flame spread and burning over large-scale horizontal PMMA surfaces. *Combustion and Flame* 85, 169.

Burrows, J., Hemp, R., Holding, W., and Stroh, R.M. (1982). Environmental engineering in South African mines. *The Mine Ventilation Society of South Africa.*

Carrier, G.F., Fendell, F.E., and Wolff, M.F. (1991). Wind-aided firespread across arrays of discrete fuel elements. I. Theory. *Combustion Science and Technology* 75, 31.

Comitis, S.C., Glasser, D., and Young, B.D. (1994a). An experimental and modeling study of fires in ventilated ducts. Part I: Liquid fuels. *Combustion and Flame* 96, 428.

Comitis, S.C., Glasser, D., and Young, B.D. (1994b). An experimental and modeling study of fires in ventilated ducts. Part II: Solid fuels. (To be submitted to *Combustion and Flame*).

Comitis, S.C., Glasser, D., and Young, B.D. (1994c). An experimental and modeling study of fires in ventilated ducts. Part III: Stratification. (To be submitted to *Combustion and Flame*).

Coulson, J.M., and Richardson, J.F. (1986). *in Chemical Engineering* (R.K. Sinnot, Ed), Pergamon, Vol. 6, p. 537.

de Ris, J.N. (1969). Spread of a laminar diffusion flame. *Twelfth Symposium (International) on Combustion*, The Combustion Institute, Pittsburgh, PA, 241.

de Ris, J. (1970). Duct fires. *Combustion Science and Technology* 2, 239.

de Ris, J., Kanury, A.M., and Yuen, M.C. (1973). Pressure modeling of fires. *Fourteenth Symposium (International) on Combustion*, The Combustion Institute, Pittsburgh, PA, 1033.

Di Blasi, C., Crescitelli, S., and Russo, G. (1989). Numerical modelling of flow assisted flame spread. *Computer Methods in Applied Mechanics and Engineering* 75, 481.

Fernandez-Pello, A.C. (1979). Flame spread in a forward forced flow. *Combustion and Flame* 36, 63.

Fernandez-Pello, A.C. and Mao, C.-P. (1981). A unified analysis of concurrent modes of flame spread. *Combustion Science and Technology* 26, 147.

Fernandez-Pello, A.C. and Hirano, T. (1983). Controlling mechanisms of flame spread. *Combustion Science and Technology* 32, 1.

Fernandez-Pello, A.C. (1984). Flame spread modelling. *Combustion Science and Technology* 39, 119.

Fleeter, R.D., Fendell, F.E., Cohen, L.M., Gat, N., and Witte, A.B. (1984). Laboratory facility for wind-aided firespread along a fuel matrix. *Combustion and Flame* 57, 2[illegible].

Hottel, H.C., Williams, G.C., and Steward, F.R. (1965). The modeling of firespread through a fuel bed. *Tenth Symposium (International) on Combustion*, The Combustion Institute, Pittsburgh, PA, 997.

Hottel, H.C., Williams, G.C., and Kwentus, G.K. (1971). Fuel preheating in free-burning fires. *Thirteenth Symposium (International) on Combustion*, The Combustion Institute, Pittsburgh, PA, 963.

Hunter, L.W., and Favin, S. (1981). Fire propagation in a thermally thin fuel-lined duct with a parallel well-mixed

forced flow. *Combustion and Flame* 42, 7.

Hwang, C.C., Chaiken, R.F., Singer, J.M., and Chi, D.N.H. (1977). Reverse stratified flow in duct fires: A two dimensional approach. *Sixteenth Symposium (International) on Combustion*, The Combustion Institute, Pittsburgh, PA, 1385.

Ishida, H. (1986). Flame spread over fuel-soaked ground. *Fire Safety Journal* 10, 163.

Ishida, H. (1988). Flame spread over ground soaked with highly volatile liquid fuel. *Fire Safety Journal* 13, 115.

Ishida, H. (1992). Initiation of fire growth on fuel-soaked ground. *Fire Safety Journal* 18, 213.

Kanury, A.M. (1974). Modeling of pool fires with a variety of polymers. *Fifteenth Symposium (International) on Combustion*, The Combustion Institute, Pittsburgh, PA, 193.

Kennedy, M., and Roberts, A.F. (1964). Modeling fires in mine roadways. 2nd International Fire Protection Seminar, Karlsruhe.

King, W.J. (1943). Measurement of high temperatures in high-velocity gas streams. Trans. A.S.M.E., vol. 38, pp. 421-431.

Loh, H.-T., and Fernandez-Pello, A.C. (1984). A study of the controlling mechanisms of flow assisted flame spread. *Twentieth Symposium (International) on Combustion*, The Combustion Institute, Pittsburgh, PA, 1575.

McAdams, W.H. (1954). *Heat Transmission*, McGraw-Hill, New York.

Newman, J.S., and Tewarson, A. (1983). Flame propagation in ducts. *Combustion and Flame* 51, 347.

Newman, J.S. (1984). Experimental evaluation of fire-induced

stratification. *Combustion and Flame* 57, 33.

Orloff, L., de Ris, J.N., and Markstein, G.H. (1975). Upward turbulent fire spread and burning of fuel surfaces. *Fifteenth Symposium (International) on Combustion*, The Combustion Institute, Pittsburgh, PA, 183.

Perry, R.H., and Green, D.W. (1984). *Chemical Engineers Handbook*, McGraw-Hill, Singapore.

Pitts, W.M. (1991). Wind effects on fires. *Prog. Energy Combust. Sci.* 17, 83-134.

Quintiere, J.G. (1988). *J. Res. Natl. Bur. Stand.* 93, 61-70.

Roberts, A.F., Clough, G., and Blackwell, J.R. (1966). A model duct for mine fire research. Research Report No. 243, Safety in Mines Research Establishment, Buxton, England.

Roberts, A.F., and Clough, G. (1967). The propagation of fires in passages lined with flammable material. *Combustion and Flame* 11, 365.

Sibulkin, M., and Lee, C.K. (1974). Flame propagation measurements and energy feedback analysis for burning cylinders. *Combustion Science and Technology* 9, 137.

Takeno, K., and Hirano, T. (1986). Flame spread over porous solids soaked with a combustible liquid. *Twenty-first Symposium (International) on Combustion*, The Combustion Institute, Pittsburgh, PA, 75.

Tewarson, A., Jiang, F.H., and Morikawa, T. (1993). Ventilation-controlled combustion of polymers. *Combustion and Flame* 95, 151.

Weber, R.O. (1989). Analytical models for fire spread due to radiation. *Combustion and Flame* 78, 398.

Williams, F.A. (1976). Mechanisms of fire spread. *Sixteenth Symposium (International) on Combustion*, The Combustion Institute, Pittsburgh, PA, 1281.

Wolff, M.F., Carrier, G.F., and Fendell, F.E. (1991). Wind-aided firespread across arrays of discrete fuel elements. II. Experiment. *Combustion Science and Technology* 77, 261.

Young, B.D., and Glasser, D. (1990). A simple steady state mathematical model for a mine fire. Report from the department of Chemical Engineering, University of the Witwatersrand.

Author: Comitis Spiros Costas.
Name of thesis: An experimental and modelling study of fires in ventilated passages.

PUBLISHER:
University of the Witwatersrand, Johannesburg
©2015

LEGALNOTICES:

Copyright Notice: All materials on the University of the Witwatersrand, Johannesburg Library website are protected by South African copyright law and may not be distributed, transmitted, displayed or otherwise published in any format, without the prior written permission of the copyright owner.

Disclaimer and Terms of Use: Provided that you maintain all copyright and other notices contained therein, you may download material (one machine readable copy and one print copy per page)for your personal and/or educational non-commercial use only.

The University of the Witwatersrand, Johannesburg, is not responsible for any errors or omissions and excludes any and all liability for any errors in or omissions from the information on the Library website.